UNIVERSIDADE ESTADUAL PAULISTA
"JÚLIO DE MESQUITA FILHO"
INSTITUTO DE BIOCIÊNCIAS – RIO CLARO

PROGRAMA DE PÓS-GRADUAÇÃO EM CIÊNCIAS BIOLÓGICAS (ZOOLOGIA)

Polimorfismo de cor no gênero *Brachycephalus* (Anura: Brachycephalidae): abordagens genéticas e evolução

JULIANE PETRY DE CARLI MONTEIRO

Rio Claro – SP
2024

UNIVERSIDADE ESTADUAL PAULISTA
"JÚLIO DE MESQUITA FILHO"
INSTITUTO DE BIOCIÊNCIAS – RIO CLARO

PROGRAMA DE PÓS-GRADUAÇÃO EM CIÊNCIAS BIOLÓGICAS (ZOOLOGIA)

Polimorfismo de cor no gênero *Brachycephalus* (Anura: Brachycephalidae): abordagens genéticas e evolução

JULIANE PETRY DE CARLI MONTEIRO

Tese apresentada ao Instituto de Biociências do Câmpus de Rio Claro, Universidade Estadual Paulista, como parte dos requisitos para obtenção do título de Doutora em Ciências Biológicas (Zoologia).

Orientador: Dr. Célio Fernando Baptista Haddad

Coorientadoras: Dra. Mariana Lúcio Lyra

Dra. Thais Helena Condez

Rio Claro – SP
2024

M775p

Monteiro, Juliane Petry de Carli
Polimorfismo de cor no gênero *Brachycephalus* (Anura: Brachycephalidae): abordagens genéticas e evolução / Juliane Petry de Carli Monteiro. -- Rio Claro, 2024
227 p. : il., tabs., mapas

Tese (doutorado) - Universidade Estadual Paulista (UNESP), Instituto de Biociências, Rio Claro
Orientador: Célio Fernando Baptista Haddad
Coorientadora: Mariana Lúcio Lyra, Thais Helena Condez

1. Anfíbios. 2. Aposematismo. 3. Mata Atlântica. 4. Polimorfismo de cor. 5. Variação intraespecífica. I. Título.

Sistema de geração automática de fichas catalográficas da Unesp. Biblioteca da Universidade Estadual Paulista (UNESP), Instituto de Biociências, Rio Claro.
Dados fornecidos pelo autor(a).

Essa ficha não pode ser modificada.

UNIVERSIDADE ESTADUAL PAULISTA

Câmpus de Rio Claro

CERTIFICADO DE APROVAÇÃO

TÍTULO DA TESE: Polimorfismo de cor no gênero Brachycephalus (Anura: Brachycephalidae): abordagens genéticas e evolução

AUTORA: JULIANE PETRY DE CARLI MONTEIRO
ORIENTADOR: CELIO FERNANDO BAPTISTA HADDAD
COORIENTADORA: THAIS HELENA CONDEZ
COORIENTADORA: MARIANA LUCIO LYRA

Aprovada como parte das exigências para obtenção do Título de Doutora em Ciências Biológicas (Zoologia), pela Comissão Examinadora:

Prof. Dr. CELIO FERNANDO BAPTISTA HADDAD (Participaçao Presencial)
Departamento de Biodiversidade / Unesp - IB Rio Claro

Profa. Dra. CARLA MARTINS LOPES (Participaçao Presencial)
USP

Prof. Dr. EVAN TWOMEY (Participaçao Virtual)
Departamento de Vida Selvagem, Biologia e Sistemática de Animais de Zoológico / Universidade Goethe de Frankfurt

Prof. Dr. TARAN GRANT (Participaçao Presencial)
Instituto de Biociências / USP

Profa. Dra. MARIANA MIRA VASCONCELLOS (Participaçao Presencial)
Instituto de Biociências / USP

Rio Claro, 31 de janeiro de 2024

Ela me disse que
Eu estudo para "melhorar o mundo".

Ela sempre quis estudar,
E me deu todo o apoio para voar.

À minha preciosa ancestral,
À toda sua luta e fé,
Ao nosso amor, amizade e partilha.

À Edithe de Carli Monteiro

AGRADECIMENTOS

Há nove anos meu orientador Célio Haddad abriu as portas do laboratório para a minha imersão na herpetologia. Esta oportunidade acadêmica conduziu-me para um mundo desconhecido da minha realidade até então, o que me proporcionou conhecimento em diversos níveis. Os sapos sempre me despertaram interesse e poder estudá-los é uma honra. Obrigada Célio. Uma única oportunidade muda a vida de muitas pessoas. Mudou a minha.

Nos desdobramentos das vivencias acadêmicas pessoas entram sutilmente nas nossas vidas e nas nossas pesquisas também! Sou muito grata à Mariana Lyra por me dar a mão em momentos difíceis pessoais e profissionais. Sua ajuda foi um gatilho para meu despertar e meu crescer refletindo em muito do que foi feito nesta tese. Obrigada Mari por sua amizade e partilha de intelecto. Ao longo dos anos dividimos muitas histórias de *Brachycephalus*, muitos conhecimentos e ideias. Um pontapé inicial nessa jornada foi dado pela Thais Condez que muito me apoiou. Prospectamos muitos objetivos e os transformamos em realidade. Obrigada Thata, pelos anos de aprendizado e crescimento. Não poderia esquecer de agradecer, também, ao Andrés Brunetti, pelos ensinamentos e por toda ajuda nos últimos anos. Também, agradeço a minha banca de defesa fantástica que muito contribuiu para a melhoria desse trabalho e me concedeu o título de doutora: Carla Lopes, Evan Twomey, Mariana Vasconcellos e Taran Grant.

Aos órgãos financiadores do Brasil que possibilitam a formação de pesquisadores.

O presente trabalho foi realizado com apoio da Coordenação de Aperfeiçoamento de Pessoal de Nível Superior - Brasil (CAPES) - Código de Financiamento 001.

Além disso, o presente trabalho foi financiado e desenvolvido pelo processo n° 2018/09691-0 e pelo processo n° 2021/08799-4, Fundação de Amparo à Pesquisa do Estado de São Paulo (FAPESP).

A pandemia trouxe muitas tristezas e inseguranças. Uma época que ficamos perdidos dentro de nós. Durante esse tempo só posso agradecer aos amigos e colegas de laboratório Ariadne Sabbag, Andrés Brunetti, Carla Lopes, Délio Baêta, Mariana Lyra e Tereza Thomé que compartilharam esse momento. Além disso, essas figuras muito fazem parte da minha construção pessoal e profissional. Obrigada Ari, Carla e Délio pelo conforto no fim de tese.

Dinâmica, a vida nos traz e nos leva pessoas incríveis com quem compartilhamos aprendizados e moldamos nossas ideias e até ideais. Assim, para os amigos e colegas que já foram ou permanecem por aqui enriquecendo conversas eu agradeço pelo prazer da companhia: Aline Aguiar, Anyelet Valencia Aguilar, Boris Blotto, Diego Bueno, Kaleb Pretto Gatto (agora docente da UFPR, orgulho desse guri!), Katyucia Araújo Vieira, Leo Malagoli, Marcus Thadeu

Santos, Nadya Pupin, Pedro Marinho, Pedro Taucce, Thiago Carvalho. Um destaque ao querido amigoThiago, pois dividimos sala por um bom tempo e conversamos muito!

Dentre as várias conversas de laboratório criamos o Projeto Cururu (@procururu), com foco em divulgação científica. Obrigada ao grupo que gira a roda atualmente: Ariadne, Mariana Vaini, Pedro Marinho, Lucas Almeida, Isabela Reis, Larah Campos, Letícia Lisboa e Eric Krüger. No entanto, não há como deixar de agradecer a quem tanto trilhou conosco e fez diferença para chegarmos até aqui: Aline, Anyelet, Nadya e Pedro Taucce.

Aos meus amigos dinossauros Anna Kelly Krassota, Pedro Balieiro e Renan Paitach, agradeço pelas conversas esparsas que enchem o coração. Obrigada pela ajuda na logística de alguns campos em São Chico, principalmente ao Pedro e ao Renan. Nós descobrimos o mundo fora de casa e crescemos juntos, muitas histórias especiais! A saudade sempre fica.

Durante minha bolsa sanduíche na Alemanha (obrigada FAPESP!), eu não poderia ter sido melhor recebida, acolhida e orientada como fui pelo Ariel Rodríguez e pela Heike Pröhl. O intensivo aprendizado que recebi a Universidade de Medicina Veterinária de Hannover (TiHo) é sem precedentes. Sou grata a maravilhosa Johanna Kroll, do escritório internacional de TiHo, que me auxiliou durante toda minha estadia na *Guest house*. Agradeço também aos colegas com quem compartilhei o ano em Hannover e também algumas taças de vinho: Alina Zacher, Amina Javodova, Christina Pätz, Kathrin Wicke, Laura Console Meyer, Lorna Jubran, Nikolaos Kladisios, Tristan e Vasiliki Mantzana Oikonomaki. Obrigada também ao Felix Felmy que como chefe do Instituto foi sempre solicito.

Aos meus pais, Jaime e Nidia, pelo apoio às cegas, pois descobriram comigo como é a carreira acadêmica. Aqui, posso dizer que três pessoas foram essenciais. Meu avô, Celso Monteiro, um trabalhador nato de humor sagaz. Quando nos deixou eu estava longe demais e não pude voltar. Nos despedimos na distância de um amor que sempre foi perto. Minha avó, Edithe (ela de novo!). Nela vigora o desejo de aprender e por isso uma grande incentivadora do saber. E, ao Eli de Nardin. Ele se aventurou comigo em Rio Claro, onde crescemos e evoluímos nosso ser. Ele fez parte direta dessa jornada me apoiando em amplo espectro em todos os momentos. Eli, sou muito grata pelo privilégio de seguir a vida contigo e pela base que construímos. Nossa história compartilhamos com nossos queridos gatos, Chica, Jimi Hendrix, Lina e Gandalf que nos preenchem de afeto.

Por fim, eu agradeço pelas caminhadas que tive a oportunidade de fazer com o Eli, cruzando as belas montanhas da Mata Atlântica, em busca das espécies de *Brachycephalus*. Há um aprendizado que não se traduz em palavras quando se presencia e percebe a biodiversidade pulsante que existe onde o homem não destruiu.

‘An extensive survey of the organic world thus leads us to the conclusion that colour is by no means so unimportant or inconstant a character as at first sight it appears to be; and the more we examine it the more convinced we shall become that it must serve some purpose in nature, and that besides charming us by its diversity and beauty it must be well worthy of our attentive study, and have many secrets to unfold to us.’

(A. R. Wallace, 1877, p. 643)

‘A poesia está guardada nas palavras — é tudo que eu sei.
Meu fado é o de não saber quase tudo.
Sobre o nada eu tenho profundidades.
Não tenho conexões com a realidade.
Poderoso para mim não é aquele que descobre ouro.
Para mim poderoso é aquele que descobre as
insignificâncias (do mundo e as nossas).
Por essa pequena sentença me elogiaram de imbecil.
Fiquei emocionado e chorei.
Sou fraco para elogios.’

(M. Barros, 2010, p. 403)

RESUMO

Os sinais de cor nos animais desempenham papéis cruciais em diversos sistemas de comunicação, sendo influenciados pela seleção natural e sexual. Desde as bases da produção de cor na pele até sua percepção pelos organismos, os sinais de cor resultam da interação de complexos mecanismos bióticos e abióticos que contribuem para a dinâmica evolutiva entre emissores e receptores. Espécies com coloração aposemática utilizam tons conspícuos como sinal de advertência para indicar a presença de defesas químicas, enquanto cores crípticas beneficiam-se da camuflagem com o ambiente. O aposematismo em anfíbios evoluiu independentemente em clados distantemente relacionados, muitas vezes associado ao hábito diurno e resultando em polimorfismo de cor intraespecífico. Os miniaturizados e aposemáticos sapinhos-pingo-de-ouro do gênero *Brachycephalus*, endêmicos da Mata Atlântica brasileira, também exibem cores vivas (laranja/amarelo), defesas químicas e atividade diurna. Contudo, a diferença de coloração entre as espécies tem sido utilizada como caractere diagnóstico para o reconhecimento de novas espécies. Neste estudo, focamos pela primeira vez na compreensão das relações genótipo-fenótipo em *Brachycephalus*. No primeiro capítulo, recuperamos a homoplasia do fenótipo dos sapinhos-pingo-de-ouro (coloração aposemática, provável presença de defesa química e corpo bufoniforme) utilizando uma análise filotranscriptômica. Também fornecemos evidências do polimorfismo de cor na espécie *B. actaeus*. No segundo capítulo, exploramos as bases genéticas da variação de cor em *B. actaeus* utilizando transcriptoma da pele para acessar genes diferentemente expressos. A coloração dos morfos, avaliada de uma perspectiva não humana, demonstrou a percepção do verde críptico ao laranja conspícuo. A histologia da pele caracterizou melanóforos e xantóforos, proporcionais à cor, ou seja, maior abundância de melanóforos foi encontrada no morfo verde. Nossos resultados indicam o papel poligênico, principalmente de genes relacionados à melanina, na regulação de cor em *B. actaeus*. No terceiro capítulo, investigamos a variação intraespecífica em *B. actaeus*, utilizando dados genômicos, fenotípicos e acústicos coletados ao longo de sua distribuição geográfica. Os resultados indicam fortes evidências de alta variação intraespecífica, possivelmente influenciada pelo aposematismo e miniaturização. Em conjunto, essas descobertas estabelecem uma base abrangente para explorar a diversidade de sinais de cor em *Brachycephalus*, demonstrando desafios significativos para compreender sua função e evolução.

PALAVRAS CHAVE: Anfíbios, aposematismo, Mata Atlântica, polimorfismo de cor, sapinhos-pingo-de-ouro, variação intraespecífica

ABSTRACT

Animal color signals play crucial roles in diverse communication systems influenced by natural and sexual selection. From integumentary color production to the visual color perception, a complex interplay of biotic and abiotic mechanisms contributes to the evolutionary dynamics between signal senders and receivers. Aposematic species employ warning bright colors to signal the presence of chemical defences, while cryptic colors aid in environmental blending. Aposematism in amphibians has independently evolved across unrelated taxa, often associated with diurnal activity, and resulting in color polymorphism within a species. The miniaturized and aposematic pumpkin toadlets of the genus *Brachycephalus*, endemic of the Brazilian Atlantic Forest, also display bright colors (orange/yellow), chemical defences, and diurnal activity. However, color differences have been used as evolutionary divergence to describe new species. In this study, we focused for the first time to understand the genotype-phenotype relationships in *Brachycephalus*. In the first chapter, we recovered the homoplasy of pumpkin toadlet phenotype (aposematic coloration, likely presence of chemical defences, and body shape morphology) in the genus throughout phylotranscriptomic analysis. Also, we provided evidence of color polymorphism in *B. actaeus* by inclusion of different morphs. The second chapter explores the genetic basis of color variation in *B. actaeus* through skin transcription. Morph coloration, assessed from a non-human perspective, demonstrated cryptic green to conspicuous orange perception. Skin histology characterized melanophores and xanthophores, which were proportional related with the color i.e. a higher density of melanophores in the green morph. Our results shown that melanin-related genes were predominately associated with color variation in *B. actaeus* underlining the role of polygenic and diversity regulation of color in frogs. In the third chapter, we investigated intraspecific variation in *B. actaeus* using genomic, phenotypic, and acoustic data across its geographic distribution. The results strongly support high intraspecific variation, likely influenced by aposematism and miniaturization. Altogether, these findings establish a comprehensive foundation for exploring color signal diversity in *Brachycephalus*. The research carries challenging implications understanding the color function and evolution within this genus.

KEYWORDS: Amphibians, aposematism, Atlantic Forest, color polymorphism, intraspecific variation, pumpkin toadlets

SUMÁRIO

APRESENTAÇÃO E ORGANIZAÇÃO DA TESE 13
1 INTRODUÇÃO GERAL 15
1.1 Escolha do sistema modelo 23
1.2 Observações naturalísticas sobre *Brachycephalus actaeus* 25
2 OBJETIVOS 27
CAPÍTULO I 33
Initial phylotranscriptomic confirmation of homoplastic evolution of the conspicuous coloration and bufoniform morphology of pumpkin-toadlets in the genus *Brachycephalus*. 33
Abstract 34
1 Introduction 35
2 Results 37
2.1 Phylogenetic Relationships 37
2.2 Reconstruction of Phenotype Evolution 39
2.3 Mitogenome Gene Order 39
3 Discussion 40
3.1 Evolution and Biogeography of *Brachycephalus* 40
3.2 Mitogenome Evolution and Cyto-Nuclear Discordance 41
3.3 Challenges and Perspectives for Future Taxonomic and Evolutionary Studies 42
4 Materials and Methods 43
4.1 Genetic Sampling 43
4.2 Phylotranscriptomic Analyses 43
4.3 Mitocondrial Genome Analyses 45
4.4 Reconstruction of Phenotype Evolution 45
References 47
Supplementary materials 50
CAPÍTULO II 62
Expression patterns of melanin-related genes are linked to crypsis and conspicuousness in a pumpkin toadlet 63
Abstract 64
1 Introduction 64
2 Material and methods 67
2.1 Field sampling and procedures 67
2.2 Color morph classification and bird visual modeling 67
2.3 Structural and ultrastructural analyses of the skin 69

2.4 RNA sequencing, reference transcriptome assembly, and annotation 70
2.5 Population structure 71
2.6 Differential gene expression analyses 72
2.7 Transcriptome-wide association analysis 73
2.8 Gene co-expression network analyses 73
3 Results 74
3.1 Color classification and bird visual modeling 74
3.2 Skin characterization 75
3.3 Reference transcriptome assembly and annotation 76
3.4 Genetic structure 79
3.5 Differential expression analyses 80
3.6 Gene expression association with continuous coloration traits 83
3.7 Gene co-expression network analyses 84
4 Discussion 85
4.1 Ecological and evolutionary implications of polytypism in *B. actaeus* 85
4.2 Population analyses and phylogenetic relationships 86
4.3 Insights of skin structural and ultrastructural 87
4.4 Gene expression differences between color morphs 88
4.4.1 Melanin synthesis and pigment associated genes 89
4.4.2 Genes involved in carotenoid metabolism and purine synthesis 92
4.4.3 Other genes associated with pigmentation 93
4.4.4 Transcriptome-wide association analysis between gene expression and predator perceptual space 93
4.5 General perspectives 94
5 Conclusions 95
References 97
Supporting information 108
1 Supplementary Methods 108
1.1 Color morph classification and bird visual modeling 108
1.2 Structural and ultrastructural skin preparation 110
References 111
2 Supplementary Tables & Figures 112
CAPÍTULO III 134
Aposematism and miniaturization: The evolutionary miscellany in *Brachycephalus* taxonomy 136
Abstract 136

1 Introduction 137
2 Material and methods 139
2.1 Species studied 139
2.2 Field sampling 140
2.3 Genomic data and analyses 142
2.3.1 DNA extraction and ddRADseq data generation 142
2.3.2 ddRADseq alignment 143
2.3.3 Population structure and genetic diversity 143
2.3.4 Mitochondrial genetic comparisons and phylogenetic inference 144
2.4 Phenotypic and acoustic traits 145
2.4.1 Morphometric measurements and analyses 145
2.4.2 Micro-CT scanning and osteology characterization 146
2.4.3 Advertisement call recordings and acoustic analyses 147
3 Results 149
3.1 Color variation in *B. actaeus* 149
3.2 Population analyses 149
3.2.1 Populations genetic structure 149
3.2.2 Genetic divergence and gene flow 152
3.3 Haplotype network and pairwise distance based on mtDNA 153
3.4 Variation in phenotypic and acoustic traits 157
3.4.1 Morphometry 157
3.4.2 Osteology 158
3.4.3 Advertisement call 159
4 Discussion 161
References 166
Supplementary information 181
CONCLUSÕES GERAIS 200
APÊNDICE I 202
Genetic diversity of *Oophaga vicentei* (Anura: Dendrobatidae) and taxonomic position of a remarkable color morph from Panama 202
APÊNDICE II 208
Notes on the hyperossified pumpkin toadlets of the genus *Brachycephalus* (Anura: Brachycephalidae) with the description of a new species 208

APRESENTAÇÃO E ORGANIZAÇÃO DA TESE

A presente tese está fundamentada na caracterização do polimorfismo de cor nas espécies de sapinhos-pingo-de-ouro do gênero *Brachycephalus*, utilizando a espécie *B*. *actaeus* como modelo. O objetivo principal é compreender a relação genótipo-fenótipo nesses organismos. Os desdobramentos aqui evidenciados visam esclarecer os intrincados mecanismos subjacentes à variação de coloração no gênero.

Este é o primeiro estudo a abordar a coloração conspícua como uma estratégia intraespecífica de sinal envolvida no polimorfismo de cor. Embora o enfoque principal tenha sido nas espécies do grupo de *B*. *pernix*, é crucial considerar essa perspectiva no contexto evolutivo bem como o potencial uso de estratégia aposemática, pouco estudada no gênero. O estudo incorpora métodos abrangentes que integraram abordagens genéticas, desde marcadores do DNA mitocondrial até RNAs transcritos, e diversas linhas de evidência dentro da taxonomia, proporcionando uma caracterização em nível genótipo-fenótipo.

Os resultados fornecem uma perspectiva inédita do ponto de vista evolutivo, deixando questões em aberto sobre as pressões adaptativas que moldam a diversificação no uso dos sinais de cor nessas espécies conspícuas e miniaturizadas, bem como a provável presença de defesa química e putativo aposematismo. Além disso, *Brachycephalus actaeus* emerge como um potencial exemplo evolutivo onde o surgimento da coloração conspícua pode estar envolvida no aposematismo que vem sendo atrelado a espécies diurnas, quimicamente defendidas e polimórficas de anfíbios.

O texto está estruturado da seguinte forma:

i) A introdução geral contextualiza a coloração animal, fornecendo embasamento para a compreensão da evolução de espécies de anfíbios aposemáticas, diurnas e tóxicas. Em seguida, são brevemente apresentadas as razões que motivaram o estudo dos sinais de cor em *Brachycephalus*, direcionando aos objetivos principais desta tese.

ii) O capítulo I, artigo já publicado (Lyra, Monteiro, et al. 2021), oferece uma visão das relações evolutivas entre as espécies dos principais clados de *Brachycephalus* spp. Além disso, fornece suporte para o polimorfismo de cor em *B*. *actaeus* por meio de uma abordagem filotranscriptômica.

iii) O capítulo II, artigo submetido para publicação (Monteiro, et al. submetido para "Molecular Ecology: Special Issue Ecology of Gene Expression"), investiga as

bases genéticas envolvidas na variação de cor em *B*. *actaeus* por meio da análise da transcrição da pele.

iv) O capítulo III, artigo em preparação, caracteriza a variação intraespecífica em *B*. *actaeus* utilizando sequenciamento de SNPs, bioacústica, osteologia e morfologia.

v) Ao final, o texto inclui dois apêndices que representam trabalhos já publicados que contribuíram para a construção deste processo de doutoramento. Um dos trabalhos reconhece um novo morfo de cor para a espécie de dendrobatídeo *Oophaga vicentei* (Monteiro et al., 2023). O outro descreve uma nova espécie de *Brachycephalus* que ocorre na região metropolitana de São Paulo e arredores (Condez et al., 2021).

1 INTRODUÇÃO GERAL

A função da coloração da pele nos animais está envolvida em diferentes processos evolutivos que podem estar relacionados à proteção física (termorregulação e proteção UV), sinalização inter e intraespecífica (seleção sexual e social) e/ou como estratégia para evitar a predação (camuflagem, mimetismo ou aposematismo) (Cuthill et al., 2017; Mappes et al., 2005; Poulton, 1890). A cor não é apenas um fenômeno físico produzido pela luz. A natureza da cor representa um sistema complexo de percepção da imagem que envolve a interação entre o ambiente, os filtros sensoriais e a arquitetura cognitiva do indivíduo (Bowmaker, 1998; Hubbard et al., 2010; Maia & White, 2018). Ao passo que a coloração é percebida e traduzida por um organismo, esta poderá implicar em uma resposta comportamental dentro de um sistema dinâmico de experiência, o qual influenciará na expressão e na evolução de exibições de quem envia e de quem recebe os sinais de cor (Hutton et al., 2015; Renoult et al., 2017).

Os fenótipos de cor são, portanto, características evolutivas que definem a detecção e o reconhecimento dos organismos, consequentes da aptidão de certos padrões e tons que aumentam a sobrevivência e o sucesso reprodutivo favorecidos pela seleção natural e sexual (Briolat et al., 2019; Endler, 1980). Espécies com polimorfismo de cor são interessantes sistemas modelos, pois fornecem informações evolutivas valiosas sobre o significado adaptativo da coloração (Briolat et al., 2019; Caro, 2017). O polimorfismo em espécies é definido pela ocorrência de múltiplos morfos de cor dentro de uma população (Ford, 1940, 1945; Meyer, 1963). É interessante notar que espécies polimórficas evoluíram independentemente e repetidamente em vários grupos taxonômicos, inclusive nos vertebrados, tais como peixes, anfíbios, répteis, aves e mamíferos (Briolat et al., 2019; Manceau et al., 2010; Stuart-Fox et al., 2021).

Um exemplo clássico de pesquisa sobre polimorfismo de cor foi desenvolvido com os peixes *guppies* (*Poecilia reticulata*) na América Central. Este foi o primeiro estudo em populações naturais destacando as pressões da seleção sexual e de predação em um sistema de cor. Nesta espécie, machos com colorações chamativas são preferidos pelas fêmeas, mas são facilmente detectados pelos predadores (Endler, 1980). Por outro lado, se os machos apresentarem cores muito discretas, as fêmeas optam por outro parceiro. Portanto, a coloração dos machos é resultado de um equilíbrio entre a efetividade para atrair fêmeas e evitar a predação (Endler, 1987).

Recentemente, o reconhecimento de espécies polimórficas tem sido ampliado pelo aumento de estudos nessa área, contribuindo para a interpretação da dinâmica da diversidade

de sinais de cor nos diferentes modelos evolutivos. Muitas espécies de lagartos, por exemplo, têm sido documentadas com polimorfismo de cor, principalmente na região da garganta (Stuart-Fox et al., 2021). Em algumas espécies, o sinal de cor pode indicar o modo de vida do indivíduo, como se a cor fosse atrelada a um "pacote genético" que pré-define suas características. Esse interessante sistema é observado no lagarto-com-manchas-laterais (*Uta stansburiana*). Nessa espécie, os machos de garganta laranja garantem mais fêmeas por apresentarem incremento corporal, agressividade e níveis de testosterona elevados; os machos de garganta azul trabalham em conjunto com as fêmeas para a defesa de território; e os machos de garganta amarela se assemelham às fêmeas possibilitando a invasão de territórios de outros machos para busca de parceiras. Por outro lado, nas fêmeas as cores indicam o modo reprodutivo. Assim, fêmeas de garganta laranja são r-estrategistas (grande número de descendentes), enquanto as fêmeas de garganta amarela são k-estrategistas (menor número de descendentes com melhor *fitness*) (Corl et al., 2010; Stuart-Fox et al., 2021).

Dentre as estratégias dos sinais de cor, a coloração críptica exibe cores que fazem referência ao ambiente, minimizando a detecção do indivíduo pelos potenciais predadores visualmente orientados. Inversamente, a coloração aposemática consiste em uma defesa primária na qual o predador é alertado pela exibição de uma cor conspícua, seguido de uma defesa secundária frequentemente associada à presença de defesas químicas, tornando a experiência do ataque desagradável para o predador (Rojas et al., 2015; Ruxton et al., 2018; Winters et al., 2021). Assim, a repetição de experiências negativas por parte dos predadores intensifica as pressões seletivas sobre os sinais de cor, de maneira geral, melhorando a aptidão individual da presa (Caro & Ruxton, 2019; Speed et al., 2010).

Num contexto evolutivo, é interessante pensar sobre o surgimento do aposematismo. Uma vez que a coloração conspícua torna o indivíduo mais atrativo para os predadores, como os predadores evitariam esse sinal sem o conhecer? Há quase dois séculos cientistas tentam endereçar alternativas para esclarecer esse paradoxo (Briolat et al., 2019; Caro, 2023). Recentemente, Loeffler-Henry e colaboradores (2023) mapearam as relações evolutivas do aposematismo em anfíbios, oferecendo uma alternativa inovadora para esse fenômeno. Os resultados encontrados sugerem que os primeiros sinais aposemáticos surgiram na região ventral de espécies com dorso críptico. As espécies com manchas conspícuas no ventre, sejam elas quimicamente defendidas ou não, ou que apresentavam o ventre inteiramente conspícuo sem defesa química, foram precursoras do surgimento de um estado dorsal críptico e ventre completamente conspícuo, com defesa química. Ao longo da evolução, os predadores

aprenderam a evitar tais sinais, levando ao surgimento de formas completamente conspícuas. O aposematismo em anfíbios mostrou-se evolutivamente flexível, com transições de ida e volta das espécies entre estados crípticos e polimórficos (Loeffler-Henry et al., 2023).

Quando a variação de cor é caracterizada pela presença de diferentes morfos de uma espécie selecionados localmente, ou seja, em cada localidade haverá um morfo distinto, é chamada de politipismo (Briolat et al., 2019; Mayr, 1963). Ambos, polimorfismo e politipismo de cor em espécies podem ser impulsionados pela presença de predadores heterogêneos, bem como a preferência de escolha de parceiros pelas fêmeas, promovendo uma rápida diversificação de estratégias de cores e padrões dentro de uma espécie ou grupo (Dreher et al., 2015; Dreher & Pröhl, 2014; Noonan & Comeault, 2009). Além disso, alguns estudos sugerem que em algumas espécies a fixação de fenótipos pode ocorrer de modo randômico através de deriva genética (Chouteau & Angers, 2012). O politipismo vem sendo bastante estudado na biologia evolutiva porque oferece a oportunidade de comparar as pressões de seleção de uma perspectiva local sobre os distintos morfos de cor.

Em anfíbios, as espécies aposemáticas evoluíram de forma independente diversas vezes em clados distantemente relacionados, implicando, geralmente, na coincidente relação com atividade diurna, presença de defesa química e simultânea ocorrência de polimorfismo e/ou politipismo (Emberts & Wiens, 2022; Wollenberg et al., 2008). Nesse sentido, as espécies do gênero *Mantella* na região de Madagascar, bem como os diversos sapos-venenosos da família Dendrobatidae na região Neotropical exemplificam a diversificação de sinais de cor nesse grupo (Wollenberg et al., 2008). Algumas espécies politípicas de dendrobatídeos, inclusive, são exemplos do uso múltiplo de estratégias de sinais de cor, apresentando um contínuo do críptico ao aposemático (Pröhl & Ostrowski, 2011; Willink et al., 2013).

Embora os aspectos ecológicos envolvidos na variação de cor sejam relativamente conhecidos em anfíbios, as bases genéticas que influenciam a regulação das células tegumentares que conferem cor ainda são pouco compreendidas. As cores observadas na pele dos anfíbios são produzidas especialmente, mas não exclusivamente, por pigmentos ou nanoestruturas existentes em três tipos de células conhecidas como cromatóforos: xantóforos, iridóforos e melanóforos (Hashimoto et al., 2021). Esses cromatóforos estão organizados em camadas que interagem entre si na derme, formando a unidade de cromatóforos dérmicos (Bagnara et al., 1968).

A composição de cada cromatóforo influencia a sensibilidade de absorção ou reflexão dos comprimentos de onda da luz, resultando na coloração da pele (Shawkey & D'Alba, 2017).

A camada de células próxima à epiderme é composta pelos xantóforos, que contêm pigmentos de carotenoides e pteridinas, produzindo cores que variam do amarelo ao vermelho (Andrade & Carneiro, 2021). Esses pigmentos são adquiridos a partir de fontes exógenas pela dieta. Na parte intermediária, os iridóforos possuem plaquetas de cristais de guanina que refletem a luz, e a variação em seu tamanho, forma, orientação e quantidade contribui para a coloração estrutural (Shawkey & D'Alba, 2017). Por fim, a camada mais profunda é formada pelos melanóforos, que contêm melanossomas com o pigmento melanina, esta responsável pelas cores escuras como marrom e preto (McNamara et al., 2021).

As variações genéticas abrangem genes que desempenham papéis nas vias dos pigmentos e na coloração estrutural, contribuindo para a diversidade da cor da pele (Hoekstra & Nachman 2003; Hashimoto et al. 2021). Além do fator genético, os genes podem ser ativados ou desativados por estímulos ambientais – área conhecida como epigenética – acarretando também em mudanças fenotípicas (Angers et al., 2020). Portanto, compreender como a expressão gênica promove o polimorfismo nas diferentes espécies é fundamental para entender as vias metabólicas envolvidas na determinação da cor.

O desenvolvimento de técnicas moleculares proporcionou avanços significativos em estudos genômicos e transcriptômicos relacionados aos mecanismos evolutivos associados à interação genótipo-fenótipo em anfíbios, especialmente nos dendrobatídeos (Kosch et al., 2023). Nas espécies estudadas, um sistema poligênico complexo controla a variação de cor na pele (Rodríguez et al., 2020; Twomey et al., 2023). Por exemplo, na espécie polimórfica *Ranitomeya sirensis*, a variação entre os morfos vermelho e amarelo parece estar relacionada à expressão de um gene que codifica enzimas de carotenoides, além de uma possível mutação de perda de função no gene β-caroteno oxigenase 2 (*bco2*) (Twomey et al., 2020). Em contraste, Rodríguez et al. (2020) realizaram uma comparação entre morfos de cores azul, verde e vermelho na espécie *Oophaga pumilio*, destacando a influência de diversos genes, sobretudo aqueles relacionados à síntese de pteridinas, ao metabolismo de carotenoides e ao metabolismo das purinas (guanina). Evidências para a plasticidade da regulação gênica foram destacadas ao comparar espécies no modelo de mimetismo Mülleriano (veja explicação abaixo), onde *R. imitator* simula morfos de *R. fantastica* e *R. variablilis* (Stuckert et al., 2021). O estudo revelou que os padrões e colorações miméticas em *R. imitator* possuem um perfil de expressão gênica completamente diferentes das duas espécies modelo.

Apesar de extensivos estudos disponíveis sobre a diversificação das espécies e dos múltiplos usos dos sinais de cor em dendrobatídeos, o status taxonômico de várias espécies é

um desafio devido ao elevado polimorfismo/politipismo somados a falta de caracteres morfológicos comumente usados na diagnose (Grant et al., 2017; Rojas, 2017; Stuckert & Summers, 2022). Por este motivo, existem muitas sinonímias de espécies que foram descritas com base na coloração e diagnoses falhas; novas espécies crípticas; e complexos de espécies (Brown et al. 2011; Grant et al. 2017; Pröhl e Ostrowski 2011). Portanto, uma taxonomia integrativa que una dados morfológicos, osteológicos, acústicos, moleculares e comportamentais é crucial para apoiar a determinação específica em espécies aposemáticas e polimórficas (Grant et al., 2017).

Por exemplo, como citado anteriormente, em *Ranitomeya*, além da variação inter e intraespecífica, existe a espécie mimética *R. imitator*. O mimetismo Mülleriano é visto como uma forma de reforçar o sinal antipredatório, onde os mímicos vivem em sintopia com os modelos (Stuckert et al., 2021). Nessas espécies, muitas vezes os caracteres diagnósticos usados comumente na taxonomia (e.g. morfologia, osteologia) não variam abaixo do nível de gênero, ou são plásticos (e.g. coloração, morfologia), sendo necessários dados acústicos e genéticos para determinar as espécies (Brown et al., 2011; Grant et al., 2017). Por outro lado, no gênero *Oophaga* espécies diferentes podem apresentar coloração similar apesar de viverem em alopatria, como é o caso de *O. arborea* e *O. vicentei*, o que pode gerar identificação equivocada (Apêndice I; Monteiro et al., 2023). De fato, a variação na coloração e a carência de variação morfológica em diversos táxons implicam em ausência de resolução taxonômica, até mesmo em uma das espécies de anfíbios mais bem conhecidas como *O. pumilio*, que há anos tem sido recuperada como parafilética (Grant et al., 2017; Hagemann & Pröhl, 2007; Monteiro et al., 2023).

Endêmico da Mata Atlântica brasileira, o gênero *Brachycephalus* Fitzinger, 1826 tem despertado a atenção de pesquisadores devido a notável diversidade de cores conspícuas presentes nas espécies. Atualmente, são reconhecidas 41 espécies, popularmente nomeadas com base em suas características morfológicas distintas, das quais cinco são chamadas de sapo-pulga (*B. didactylus*, *B. hermogenesi*, *B. pulex*, *B. puri* e *B. sulfuratus*) e as demais 35 espécies são conhecidas como sapinhos-pingo-de-ouro (Frost, 2023). As espécies de *Brachycephalus* são diurnas, com raros registros de atividade noturna (Dorigo et al., 2012). A distribuição do gênero abrange desde o sul do estado da Bahia até o centro-leste de Santa Catarina. Todas as espécies são miniaturizadas (< 20 mm) e habitam a serrapilheira de florestas em estágio médio a avançado de regeneração, onde se reproduzem por desenvolvimento direto. Assim, os ovos

dependem da umidade da serrapilheira de onde eclodem sapinhos miniaturas de seus, já diminutos, progenitores (Hedges et al., 2008; Condez et al., 2020).

Os sapos-pulga apresentam coloração geral do corpo marrom, com o formato do corpo leptodactiliforme e pernas longas (dos Reis et al., 2020), proporcionando agilidade para o salto. Essas espécies são encontradas em uma ampla variação altitudinal, desde o nível do mar até 950 m acima do nível do mar [a.n.m.]. Já os sapinhos-pingo-de-ouro, possuem coloração inteiramente aposemática laranja/amarela, ou parcialmente aposemática, na qual a região dorsal é críptica e a ventral apresenta as cores laranja/amarela em manchas ou cobrindo todo o ventre (J. Monteiro, observação pessoal). O formato do corpo bufoniforme e as pernas curtas auxiliam na locomoção sob as folhas, mas resultam numa menor aptidão para saltos (dos Reis et al., 2020). Os sapinhos-pingo-de-ouro são predominantemente encontrados em regiões elevadas das montanhas nas formações de Floresta Ombrófila Densa Sub-Montana, Montana, Alto-Montana e nos enclaves de vegetação dos Campos de Altitude, entre 450 – 1800 m a.n.m.) (Bornschein et al., 2019; Condez et al., 2020), com exceção de *B. actaeus* que é encontrado também próximo ao nível do mar (Monteiro et al., 2018). Além disso, é notável destacar que os sapinhos-pingo-de-ouro são aposemáticos, diurnos e tóxicos (Chimetto Tonon et al., 2021; Lyra, Monteiro et al., 2021; Rebouças et al., 2019).

As relações filogenéticas das espécies não apresentam correspondência com os nomes populares, uma vez que os sapinhos-pingo-de-ouro estão agrupados em dois grandes clados, cada um clado-irmão de diferentes espécies de sapos-pulga. Em outras palavras, não há monofiletismo nas denominações populares (Figura 1) (dos Reis et al. 2020; Lyra et al. 2021; Folly et al. 2021). A recente descoberta da espécie *B. clarissae* trouxe uma contribuição significativa para o gênero, pois a espécie possui características compartilhadas entre sapos-pulga e sapinhos-pingo-de-ouro (Folly et al., 2022).

O clado de sapinhos-pingo-de-ouro recuperado como irmão de *B. clarissae* agrupa espécies caracterizadas pela presença de hiperossificações no crânio e esqueleto, denominado de grupo de *B. ephippium* (14 espécies: *B. alipioi*, *B. bufonoides*, *B. crispus*, *B. darkside*, *B. ephippium*, *B. garbeanus*, *B. guarani*, *B. ibitinga*, *B. margaritatus*, *B. nodoterga*, *B. pitanga*, *B. rotenbergae*, *B. toby* e *B. vertebralis*), distribuídas desde o Espírito Santo até o sul de São Paulo (Folly et al., 2021; Lyra, Monteiro et al., 2021). Já no clado de sapinhos-pingo-de-ouro recuperado como irmão de *B. sulfuratus*, as espécies são caracterizadas pela ausência de hiperossificação e estão alocadas no grupo de *B. pernix* (20 espécies; *B. actaeus*, *B. albolineatus*, *B. auroguttatus*, *B. boticario*, *B. brunneus*, *B. coloratus*, *B. curupira*, *B.*

ferruginus, *B. fuscolineatus*, *B. izecksohni*, *B. leopardus*, *B. mariaterezae*, *B. mirissimus*, *B. olivaceus*, *B. pernix*, *B. pombali*, *B. quiririensis*, *B. tabuleiro*, *B. tridactylus* e *B. verrucosus*), distribuídas desde o sul de São Paulo até o centro-leste de Santa Catarina (Lyra, Monteiro et al., 2021). Devido ao parafiletismo, é inadequado o uso de grupos de espécies para denominar os sapos-pulga e *B. clarissae*, esta última espécie irmã do grupo de *B. ephippium* (Folly et al., 2022; Lyra, Monteiro et al., 2021; Monteiro et al., 2018).

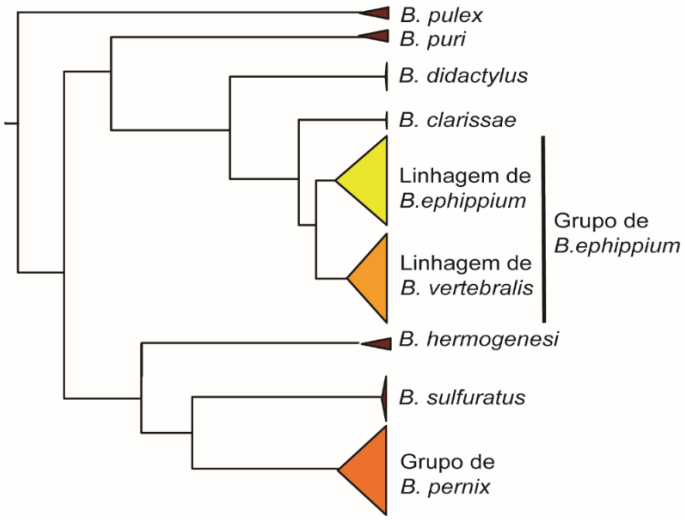


Figura 1. Esquema das relações filogenéticas para as espécies de *Brachycephalus*. Em amarelo e laranja, estão destacados os clados de sapinhos-pingo-de-ouro.

A diversidade de coloração das espécies do grupo de *B. pernix* tem sido apontada como um caráter diagnóstico para o reconhecimento de novas espécies resultante de uma evolução rápida, influenciada pela natureza biogeográfica das espécies, geralmente restritas às encostas e aos topos de montanhas (Pie et al. 2018a, 2013). Na última década, 14 das 20 espécies desse grupo foram descritas na região sul (Frost, 2023; Figura 2). No entanto, a delimitação das espécies tornou-se complexa devido à carência de caracteres distintivos para identificação em nível taxonômico inferior ao grupo e posição filogenética variável em diferentes análises (Condez et al., 2017; Monteiro et al., 2018). Consequentemente, a base taxonômica frágil gera impacto negativo para o desenvolvimento de novos estudos e implica diretamente nas políticas de conservação desses organismos.

Como exemplo, a espécie *B. coloratus*, é diferenciada das demais do grupo de *B. pernix* por apresentar três cores principais (vermelho pálido da cabeça até a região pélvica, verde amarelado na região lateral do corpo e coxas, e amarelo na parte ventral do corpo), enquanto as demais espécies apresentam uma ou duas cores (Ribeiro et al. 2017). Contudo, outras espécies como *B. actaeus*, *B. auroguttatus*, *B. fuscolineatus*, *B. mariaterezae*, *B. pernix* e *B. tabuleiro* apresentam três cores principais (veja Figura 2 e Mângia et al., 2023). Ou seja, a presença de

uma determinada quantidade de cores se tornou uma diagnose, mesmo estas não sendo comparáveis. Também, a semelhança de coloração em preservativo com *B*. *pernix* é destacada, mas a cor marrom escuro na lateral do corpo em *B*. *coloratus* comparada ao marrom claro em *B*. *pernix* foi utilizada exclusivamente como caráter diagnóstico entre as duas espécies (Ribeiro et al. 2017).



Figura 2. Diversidade de espécies no grupo de *Brachycephalus pernix*. A) *B*. *actaeus*, B) *B*. *albolineatus*, C) *B*. *auroguttatus*, D) *B*. *boticario*, E) *B*. *brunneus*, F) *B*. *curupira*, G) *B*. *ferruginus*, H) *B*. *fuscolineatus*, I) *B*. *izecksohni*, J) *B*. *leopardus*, K) *B*. *mariaterezae*, L) *B*. *mirissimus*, M) *B*. *olivaceus*, N) *B*. *pernix*, O) *B*. *pombali*, P) *B*. *quiririensis*, Q) *B*. *tridactylus* e R) *B*. *verrucosus*. Créditos: Juliane Monteiro (A, D – O), Miguel Vences (B), Thais Condez (C, P – R).

Um exemplo adicional relevante refere-se à espécie *B*. *mirissimus*, cujas relações filogenéticas, conforme apresentadas em sua descrição, não sustentam as espécies do clado de *B*. *albolineatus* (*B*. *albolineatus* + *B*. *boticario* + *B*. *fuscolineatus* + *B*. *mirissimus*), que inclui a nova espécie (Pie et al., 2018b). Os autores não fornecem comentários específicos sobre essa observação, mas ressaltam a indistinção entre os cantos de *B*. *mirissimus* e *B*. *albolineatu*s (Pie et al., 2018b). A ênfase na coloração como caráter distintivo foi empregada de maneira singular para separar essa espécie de todas as outras do grupo de *B*. *pernix* (Pie et al., 2018b). Assim, os exemplos supracitados ilustram a complexidade taxonômica e as lacunas na compreensão das relações entre as espécies do grupo de *B*. *pernix*.

Uma nova perspectiva surgiu com a descoberta da espécie *B*. *actaeus* na região da Baia Babitonga, litoral nordeste de Santa Catarina. Sua ocorrência é conhecida em uma área relativamente pequena (~80 km^2) entre os municípios de Garuva, Itapoá e São Francisco do Sul, em região continental e na ilha de São Francisco do Sul (Monteiro et al., 2018). Para delinear a área de ocorrência da espécie, foram realizadas amostragens em diversas localidades da região, principalmente na Serra do Saí, localizada na parte continental. O resultado foi o surpreendente encontro de distintos morfos de coloração, cada um em uma localidade específica, proporcionando uma oportunidade única para entender esse fenômeno em um contexto evolutivo (Monteiro, 2017).

Ao avaliar o embasamento teórico acima, a hipótese da diversidade de espécies recentemente descritas no grupo de *B*. *pernix* sustentada pela diferença de coloração do corpo revela-se frágil. Além disso, a falta de clareza nas relações filogenéticas interespecíficas, conduzida pela inclusão de um terminal por espécie e, até mesmo, pela edição manual das sequências (exclusão de zonas hipervariáveis) (Firkowski, et al. 2016; Pie et al., 2018a, 2013), deixa em aberto as variações genéticas em nível de espécie. Por outro lado, o conhecimento empírico e teórico documentado sobre a evolução da coloração aposemática sugere amplamente a falta de estudos em *Brachycephalus* nessa temática. Nesse sentido, um trabalho que considere o pressuposto evolutivo, onde a coloração conspícua (aposemática?) em espécies diurnas e quimicamente defendidas pode resultar no polimorfismo de cor, é necessário para esclarecer o entendimento da função e evolução dos sinais de cor no gênero.

1.1 Escolha do sistema modelo

Nos últimos dez anos, a espécie *B*. *actaeus* tem sido objeto de estudo em sua área de ocorrência conhecida, emergindo como um modelo para as hipóteses testadas nos capítulos

subsequentes aqui tratados. A espécie exibe uma notável variação de cores, desde o verde críptico ao laranja aposemático. Ao longo da distribuição, foram encontrados quatro morfos caracterizados como: i) verde, predominante na região dorsal e lateral do corpo, com manchas em tom laranja na região ventral; ii) marrom, dominante na região dorsal, com variação entre marrom e laranja na lateral, e região ventral totalmente laranja; iii) laranja, dominante em todo corpo com uma faixa vertebral branca na região dorsal; e iv) cinza, (tons acinzentados branco, marrom e verde variáveis) nas regiões dorsal e lateral, e totalmente laranja na região ventral. Notavelmente, o morfo verde é o único com ampla distribuição (Figura 3).

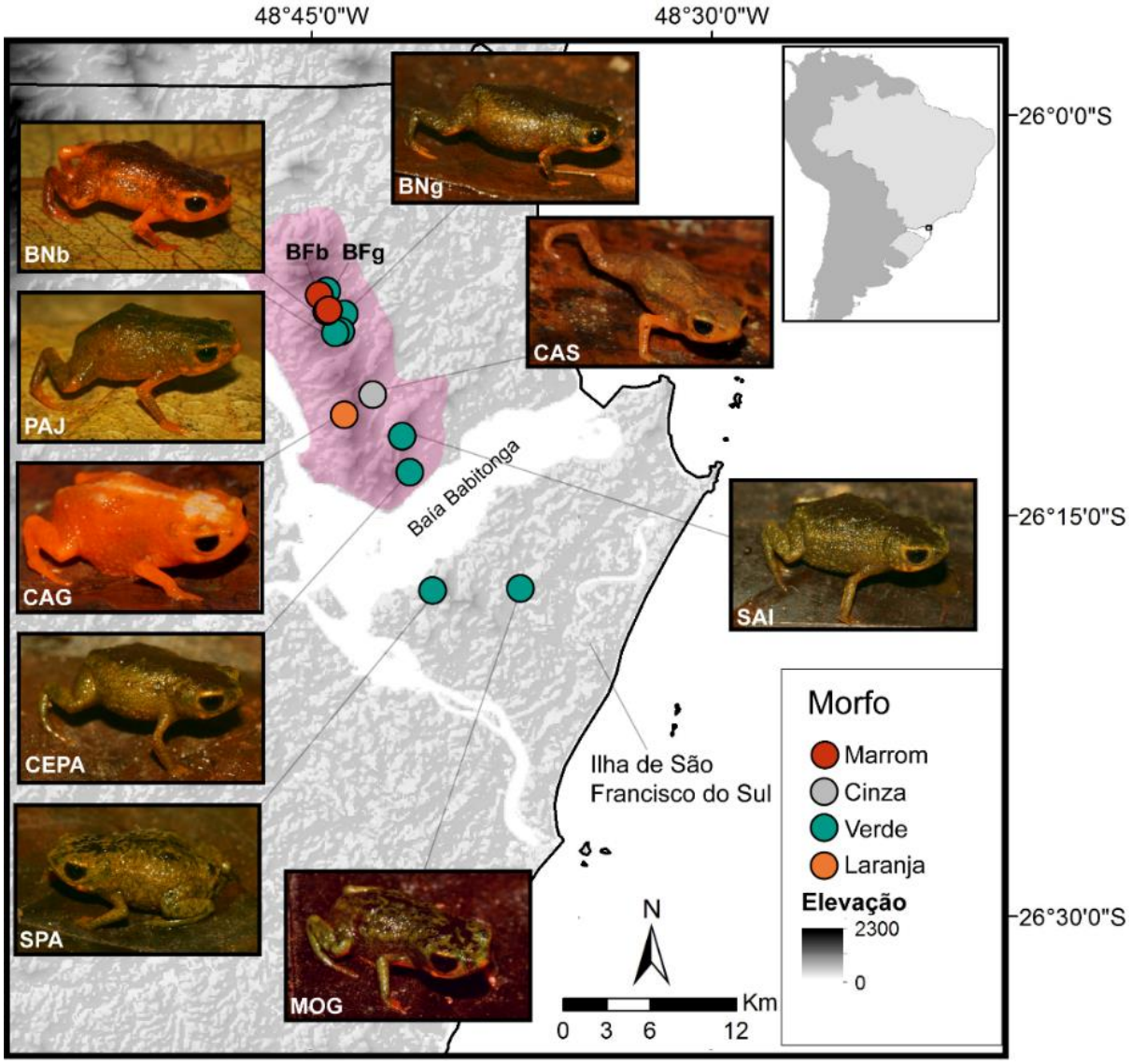


Figura 3. Mapa de distribuição da espécie *Brachycephalus actaeus* na região nordeste de Santa Catarina. Na região continental está situada a Serra do Saí (área esquemática em rosa). A coloração dorsal de cada morfo está referenciada na legenda. Abreviações: BFb, Bom Futuro marrom; BFg, Bom Futuro verde; BNb, Braço do Norte marrom; BNg, Braço do Norte verde; CAG, Morro Cantagalo; CAS, Casarão Backmeyer; CEPA, Centro de Estudos e Pesquisas Ambientais Vila da Glória da Universidade da Região de Joinville; MOG, Fazenda Morro Grande; SAI, Estrada do Saí; e SPA, Morro da Palha.

1.2 Observações naturalísticas sobre *Brachycephalus actaeus*

Ao longo dos anos de coleta, foram realizadas observações naturalísticas intrínsecas tanto sobre a espécies em questão quanto em relação as espécies correlatas. Assim como as demais espécies do grupo de *B*. *pernix*, a coleta de espécimes de *B*. *actaeus* apresenta certo grau de dificuldade devido ao hábito de vida sob a serrapilheira, sendo raramente avistado sobre o folhiço. Além disso, o acesso aos locais de coleta, em sua maioria, requer deslocamentos por trilhas a pé. Portanto, estes fatores dificultam a aplicação de estudos ecológicos e comportamentais das espécies.

A atividade acústica é sempre diurna, sendo mais intensa no início da manhã e no final do dia, cessando durante a noite. Nas horas mais quentes do dia, não há atividade. Em condições ideais, o canto de anúncio é emitido em sequência por cerca de um minuto; o macho cessa e retorna a cantar cerca de cinco minutos depois. Em dias muito quentes (> 28°C), os machos diminuem a atividade, emitindo poucos cantos em intervalos esporádicos. Contudo, em dias chuvosos e com clima ameno (18 – 22°C), é possível observar atividade ao longo do dia, embora com menor intensidade durante o meio-dia. Devido a influência da temperatura e umidade na taxa de emissão do canto de anúncio, quando analisado como um conjunto de notas sequenciais a cada intervalo de emissão, os resultados podem enviesar a interpretação da variação interespecífica. Logo, justifica-se considerar como uma sequência de cantos ao longo da emissão, acrescendo assim maior acesso à variação intraespecífica (e. g., Monteiro et al., 2018).

O canto de anúncio de *B*. *actaeus*, semelhante ao estridular de um inseto, integra a paisagem sonora, sendo necessário possuir ouvidos experientes para guiar-se pelo som, pois é a maneira mais eficaz de localizar os indivíduos. Ao ser direcionado ao local do canto, é preciso vasculhar a biodiversidade do folhiço, removendo folha a folha. O morfo verde críptico faz jus a sua estratégia de coloração, sendo o de mais difícil encontro. Já o morfo laranja, aposemático, não apresenta tal grau de dificuldade, sendo avistado mais facilmente. Os indivíduos foram observados, em algumas ocasiões, encolhendo-se e rolando por entre as folhas, assemelhando-se a uma semente. Essa estratégia é particularmente eficaz para indivíduos com colorações crípticas. Indivíduos juvenis não apresentam a cor dos adultos, sendo predominantemente marrons. Os distintos morfos de cor não foram observados em sintopia e não houve variação temporal de cor nas localidades.

Dentre os ambientes amostrados, *B*. *actaeus* não foi encontrado em áreas alteradas ou próximo às bordas de mata, demonstrando a sensibilidade da espécie à fragmentação e perda de habitat. Cabe aqui deixar documentada uma curiosa observação. Para acessar o Morro

Cantagalo, área de ocorrência do morfo laranja na região continental de São Francisco do Sul, era necessário atravessar um antigo plantio de *Pinus* sp. até alcançar o início da trilha na floresta nativa. Os indivíduos eram encontrados cerca de 1 km trilha adentro. Nos anos de 2015 e 2016, o plantio foi removido, permitindo uma rápida regeneração natural devido à proximidade da mata preservada circundante. Nos anos de 2020 e 2021, os indivíduos foram encontrados em menos de 100 m a partir do início da trilha na floresta nativa. Embora essa informação anedótica não tenha critério científico, ela destaca a potencial capacidade de dispersão/ocupação da espécie em condições microclimáticas favoráveis, sugerindo uma questão a ser investigada em futuras pesquisas.

2 OBJETIVOS

O objetivo geral desse trabalho foi aprofundar o conhecimento sobre a variação intraespecífica em nível genótipo-fenotípico utilizando a espécie *Brachycephalus actaeus* como modelo. Buscamos, assim, construir um cenário mais claro para o entendimento da evolução da coloração em espécies com coloração conspícua e miniaturizadas do gênero *Brachycephalus*.

Os objetivos específicos do projeto incluem:

(i) Avaliar a evolução da coloração no gênero *Brachycephalus* em um contexto filogenético.

Hipótese: *As colorações aposemáticas são homoplásticas no gênero e podem ser utilizadas para diferenciar as espécies*.

(ii) Explorar os mecanismos genéticos que poderiam explicar a variação da diversidade de cores em *Brachycephalus actaeus*.

Hipótese: *Genes relacionados à síntese de melanina regulam cores escuras, enquanto genes envolvidos nos pigmentos de carotenoides e pteridinas estão associados à cor laranja*.

(iii) Testar possíveis implicações ecológicas para a variação de cor intraespecífica.

Hipótese: *Se o contínuo de coloração, do críptico ao aposemático, em* Brachycephalus actaeus *define estratégias de sinais, estas devem ser percebidas por potenciais predadores*.

(iv) Analisar e caracterizar a diversidade genética e a estrutura de populações de *Brachycephalus actaeus* ao longo da atual distribuição geográfica.

Hipótese: *Os diferentes morfos de cor são populações geneticamente estruturadas*.

(v) Avaliar o uso de caracteres padrões em descrição de espécies em *Brachycephalus actaeus*.

Hipótese: *Caracteres morfológicos, bioacústicos e moleculares serão conservados em* Brachycephalus actaeus *ao longo de sua distribuição*.

REFERÊNCIAS

Andrade, P., & Carneiro, M. (2021). Pterin-based pigmentation in animals. *Biology Letters*, *17*(20210221), 1–12. https://doi.org/10.1098/rsbl.2021.0221

Angers, B., Perez, M., Menicucci, T., & Leung, C. (2020). Sources of epigenetic variation and their applications in natural populations. *Evolutionary Applications*, *13*(6), 1262–1278. https://doi.org/10.1111/eva.12946

Bagnara, J. T., Taylor, J. D., & Hadley, M. E. (1968). The dermal chromatophore unit. *Journal of Cell Biology*, *38*(1), 67–79.

Bornschein, M. R., Pie, M. R., & Teixeira, L. (2019). Conservation status of *Brachycephalus* toadlets (Anura: Brachycephalidae) from the Brazilian Atlantic Rainforest. *Diversity*, *11*(9), 9–11. https://doi.org/10.3390/d11090150

Bowmaker, J. K. (1998). Evolution of colour vision in vertebrates. *Eye*, *12*, 541–547.

Briolat, E. S., Burdfield-Steel, E. R., Paul, S. C., Rönkä, K. H., Seymoure, B. M., Stankowich, T., & Stuckert, A. M. M. (2019). Diversity in warning coloration: Selective paradox or the norm? *Biological Reviews*, *94*(2), 388–414. https://doi.org/10.1111/brv.12460

Caro, T. (2017). Wallace on coloration: Contemporary perspective and unresolved insights. *Trends in Ecology and Evolution*, *32*(1), 23–30. https://doi.org/10.1016/j.tree.2016.10.003

Caro, T. (2023). An evolutionary route to warning coloration. *Nature*, *618*, 34–35.

Caro, T., & Ruxton, G. (2019). Aposematism: Unpacking the defences. *Trends in Ecology and Evolution*, *34*(7), 595–604. https://doi.org/10.1016/j.tree.2019.02.015

Chimetto Tonon, L. A., Rua, C., Crnkovic, C. M., Bernardi, D. I., Pires Junior, O. R., Haddad, C. F. B., Pedrosa, C. S. G., Souza, L. R. Q., Rehen, S. K., de Azevedo, G. P. R., Thompson, C. C., Thompson, F. L., & Berlinck, R. G. S. (2021). Microbiome associated with the tetrodotoxin-bearing anuran *Brachycephalus pitanga*. *Toxicon*, *203*, 139–146. https://doi.org/10.1016/j.toxicon.2021.10.002

Condez, T. H., Haddad, C. F. B., & Zamudio, K. R. (2020). Historical biogeography and multi-trait evolution in miniature toadlets of the genus *Brachycephalus* (Anura: Brachycephalidae). *Biological Journal of the Linnean Society*, *129*(3), 664–686. https://doi.org/10.1093/biolinnean/blz200

Corl, A., Davis, A. R., Kuchta, S. R., & Sinervo, B. (2010). Selective loss of polymorphic mating types is associated with rapid phenotypic evolution during morphic speciation. *Proceedings of the National Academy of Sciences of the United States of America*, *107*(9), 4254–4259. https://doi.org/10.1073/pnas.0909480107

Cuthill, I. C., Allen, W. L., Arbuckle, K., Caspers, B., Chaplin, G., Hauber, M. E., Hill, G. E., Jablonski, N. G., Jiggins, C. D., Kelber, A., Mappes, J., Marshall, J., Merrill, R., Osorio, D., Prum, R., Roberts, N. W., Roulin, A., Rowland, H. M., Sherratt, T. N., … Caro, T. (2017). The biology of color. *Science*, *357*(6350). https://doi.org/10.1126/science.aan0221

Dorigo, T. A., Siqueira, C. C., Vrcibradic, D., Maia-Carneiro, T., Almeida-Santos, M., & Rocha, C. F. D. (2012). Ecological aspects of the pumpkin toadlet, *Brachycephalus garbeanus* Miranda-Ribeiro, 1920 (Anura: Neobatrachia: Brachycephalidae), in a highland forest of Southeastern Brazil. *Journal of Natural History*, *46*(39–40), 2497–2507. https://doi.org/10.1080/00222933.2012.713525

dos Reis, S. F., Clemente-Carvalho, R. B. G., dos Santos, C. M. S. F. F., Lopes, R. T., Von Zuben, F. J., Laborda, P. R., & Perez, S. I. (2020). Skull diversity and evolution in miniaturized amphibians, genus *Brachycephalus* (Anura: Brachycephalidae). *Anatomical Record*, *304*(6), 1–15. https://doi.org/10.1002/ar.24554

Dreher, C. E., Cummings, M. E., & Pröhl, H. (2015). An analysis of predator selection to affect aposematic coloration in a poison frog species. *PLoS ONE*, *10*(6). https://doi.org/10.1371/journal.pone.0130571

Dreher, C. E., & Pröhl, H. (2014). Multiple sexual signals: Calls over colors for mate attraction in an aposematic, color-diverse poison frog. *Frontiers in Ecology and Evolution*, *2*(22), 1–10. https://doi.org/10.3389/fevo.2014.00022

Emberts, Z., & Wiens, J. J. (2022). Why are animals conspicuously colored? Evolution of sexual versus warning signals in land vertebrates. *Evolution*, *76*(12), 2879–2892. https://doi.org/10.1111/evo.14636

Endler, J. A. (1980). Natural selection on color patterns in *Poecilia reticulata*. *Evolution*, *34*(1), 76–91. https://doi.org/10.1111/j.1558-5646.1980.tb04790.x

Endler, J. A. (1987). Predation, light intensity and courtship behaviour in *Poecilia reticulata* (Pisces: Poeciliidae). *Animal Behaviour*, *35*, 1376–1385.

Ford, E. B. (1945) Polymorphism. *Biological Reviews of the Cambridge Philosophical Society*, *20*, 73–88.

Ford, E. B. (1940) Polymorphism and taxonomy. In: Huxley, J. S., ed. *The new systematics*. Clarendon Press, 493–513.

Folly, M., de Luna-Dias, C., Miguel, I. R., Ferreira, J. C., Machado, A., Tadeu Lopes, R., & Pombal, J. P. (2021). Tiny steps towards greater knowledge: An osteological review with novel data on the Atlantic Forest toadlets of the *Brachycephalus ephippium* species group. *Acta Zoologica*, *December 2020*, 1–35. https://doi.org/10.1111/azo.12398

Folly, M., Vrcibradic, D., Siqueira, C. C., Rocha, C. F. D., Machado, A. S., Lopes, R. T., & Pombal, J. P. (2022). A new species of *Brachycephalus* (Anura, Brachycephalidae) from a montane Atlantic Rainforest of Southeastern Brazil, with a reappraisal of the species groups in the genus. *Ichthyology and Herpetology*, *110*(3), 585–601. https://doi.org/10.1643/h2020144

Grant, T., Rada, M., Anganoy-Criollo, M., Batista, A., Dias, P. H., Jeckel, A. M., MacHado, D. J., & Rueda-Almonacid, J. V. (2017). Phylogenetic systematics of dart-poison frogs and their relatives revisited (Anura: Dendrobatoidea). *South American Journal of Herpetology*, *12*(s1), S1–S90. https://doi.org/10.2994/SAJH-D-17-00017.1

Hagemann, S., & Pröhl, H. (2007). Mitochondrial paraphyly in a polymorphic poison frog species (Dendrobatidae; *D. pumilio*). *Molecular Phylogenetics and Evolution*, *45*, 740–747. https://doi.org/10.1016/j.ympev.2007.06.010

Hashimoto, H., Goda, M., Futahashi, R., Kelsh, R., & Akiyama, T. (2021). *Pigments, Pigment Cells and Pigment Patterns* (1st ed.). Springer International Publishing. https://doi.org/10.1007/978-981-16-1490-3

Hubbard, J. K., Uy, J. A. C., Hauber, M. E., Hoekstra, H. E., & Safran, R. J. (2010). Vertebrate pigmentation: From underlying genes to adaptive function. *Trends in Genetics*, *26*(5), 231–239. https://doi.org/10.1016/j.tig.2010.02.002

Hutton, P., Seymoure, B. M., McGraw, K. J., Ligon, R. A., & Simpson, R. K. (2015). Dynamic color communication. *Current Opinion in Behavioral Sciences*, *6*, 41–49. https://doi.org/10.1016/j.cobeha.2015.08.007

Kosch, T. A., Crawford, A. J., Mueller, R. L., Wollenberg Valero, K. C., Rodríguez, A., O'connell, L. A., Young, N. D., & Skerratt, L. F. (2023). Comparative analysis of amphibian genomes: An emerging resource for basic and applied research. *bioRxiv*. https://doi.org/10.1101/2023.02.27.530355

Loeffler-Henry, K., Kang, C., & Sherratt, T. (2023) Evolutionary transitions from camouflage to aposematism: Hidden signals play a pivotal role. *Science*, *379*(6637), 1136–1140.

Lyra, M. L., Monteiro, J. P. C., Rancilhac, L., Irisarri, I., Künzel, S., Sanchez, E., Condez, T. H., Rojas-Padilla, O., Solé, M., Toledo, L. F., Haddad, C. F. B., & Vences, M. (2021). Initial phylotranscriptomic confirmation of homoplastic evolution of the conspicuous coloration and bufoniform morphology of pumpkin-toadlets in the genus *Brachycephalus*. *Toxins*, *13*(816), 1–16. https://doi.org/10.3390/toxins13110816

Maia, R., & White, T. E. (2018). Comparing colors using visual models. *Behavioral Ecology*, *29*(3), 649–659. https://doi.org/10.1093/beheco/ary017

Manceau, M., Domingues, V. S., Linnen, C. R., Rosenblum, E. B., & Hoekstra, H. E. (2010). Convergence in pigmentation at multiple levels: Mutations, genes and function. *Philosophical Transactions of the Royal Society B: Biological Sciences*, *365*, 2439–2450. https://doi.org/10.1098/rstb.2010.0104

Mappes, J., Marples, N., & Endler, J. A. (2005). The complex business of survival by aposematism. *Trends in Ecology and Evolution*, *20*(11), 598–603. https://doi.org/10.1016/j.tree.2005.07.011

Mayr, E. (1963). *Animal species and evolution* (3rd ed.). Harvard University Press.

McNamara, M. E., Rossi, V., Slater, T. S., Rogers, C. S., Ducrest, A. L., Dubey, S., & Roulin, A. (2021). Decoding the evolution of melanin in vertebrates. *Trends in Ecology and Evolution*, *36*(5), 430–443. https://doi.org/10.1016/j.tree.2020.12.012

Monteiro, J. P. C. (2017). *Distribuição e taxonomia de* Brachycephalus *sp. (*aff. pernix*) (Anura: Brachycephalidae* [Dissertação de mestrado]. Universidade Estadual Paulista.

Monteiro, J. P. C., Condez, T. H., Garcia, P. C. D. A., Comitti, E. J., Amaral, I. B., & Haddad, C. F. B. (2018). A new species of *Brachycephalus* (Anura, Brachycephalidae) from the coast of Santa Catarina State, Southern Atlantic Forest, Brazil. *Zootaxa*, *4407*(4), 483–505. https://doi.org/10.11646/zootaxa.4407.4.2

Monteiro, J. P. C., Ibáñez, R., Mantzana-Oikonomaki, V., Pröhl, H., & Rodríguez, A. (2023). Genetic diversity of *Oophaga vicentei* (Anura: Dendrobatidae) and taxonomic position of a remarkable color morph from Panama. *Salamandra*, *59*(4), 347–351. https://www.salamandra-journal.com

Noonan, B. P., & Comeault, A. A. (2009). The role of predator selection on polymorphic aposematic poison frogs. *Biology Letters*, *5*(1), 51–54. https://doi.org/10.1098/rsbl.2008.0586

Pie, M. R., Faircloth, B. C., Ribeiro, L. F., Bornschein, M. R., & Mccormack, J. E. (2018a). Phylogenomics of montane frogs of the Brazilian Atlantic Forest is consistent with

isolation in sky islands followed by climatic stability. *Biological Journal of the Linnean Society*, *125*, 72–82. https://doi.org/10.1093/biolinnean/bly093

Pie, M. R., Ribeiro, L. F., Confetti, A. E., Nadaline, M. J., & Bornschein, M. R. (2018b). A new species of *Brachycephalus* (Anura: Brachycephalidae) from Southern Brazil. *PeerJ*, *6*(e5683), 1–27. https://doi.org/10.7717/peerj.5683

Pie, M. R., Meyer, A. L. S., Firkowski, C. R., Ribeiro, L. F., & Bornschein, M. R. (2013). Understanding the mechanisms underlying the distribution of microendemic montane frogs (*Brachycephalus* spp., Terrarana: Brachycephalidae) in the Brazilian Atlantic Rainforest. *Ecological Modelling*, *250*, 165–176. https://doi.org/10.1016/j.ecolmodel.2012.10.019

Poulton, E. B. (1890). *The colours of animals: Vol. LXVII* (1st ed.). The International Scientific Series.

Pröhl, H., & Ostrowski, T. (2011). Behavioural elements reflect phenotypic colour divergence in a poison frog. *Evolutionary Ecology*, *25*(5), 993–1015. https://doi.org/10.1007/s10682-010-9455-5

Rebouças, R., Carollo, A. B., Freitas, M. de O., Lambertini, C., Dos Santos, R. M. N., & Toledo, L. F. (2019). Is the conspicuous dorsal coloration of the Atlantic Forest pumpkin toadlets aposematic? *Salamandra*, *55*(1), 39–47.

Renoult, J. P., Kelber, A., & Schaefer, H. M. (2017). Colour spaces in ecology and evolutionary biology. *Biological Reviews*, *92*(1), 292–315. https://doi.org/10.1111/brv.12230

Ribeiro, L. F., Blackburn, D. C., Stanley, E. L., Pie, M. R., & Bornschein, M. R. (2017). Two new species of the *Brachycephalus pernix* group (Anura: Brachycephalidae) from the State of Paraná, Southern Brazil. *PeerJ*, *PeerJ* *5*(e3603), 1–28. https://doi.org/10.7717/peerj.3603

Rodríguez, A., Mundy, N. I., Ibáñez, R., & Pröhl, H. (2020). Being red, blue and green: The genetic basis of coloration differences in the strawberry poison frog (*Oophaga pumilio*). *BMC Genomics*, *21*(1), 1–16. https://doi.org/10.1186/s12864-020-6719-5

Rojas, B. (2017). Behavioural, ecological, and evolutionary aspects of diversity in frog colour patterns. *Biological Reviews*, *92*(2), 1059–1080. https://doi.org/10.1111/brv.12269

Rojas, B., Valkonen, J., & Nokelainen, O. (2015). Aposematism. *Current Biology*, *25*(9), R350–R351. https://doi.org/10.1016/j.cub.2015.02.015

Ruxton, G. D., Allen, W. L., Sherratt, T. N. & Speed, M. P. (2018). *Avoiding attack: The evolutionary ecology of crypsis, warning signals and mimicry*. 2nd ed., Oxford University Press.

Shawkey, M. D., & D'Alba, L. (2017). Interactions between colour-producing mechanisms and their effects on the integumentary colour palette. *Philosophical Transactions of the Royal Society B: Biological Sciences*, 372, 1–9. https://doi.org/10.1098/rstb.2016.0536

Speed, M. P., Brockhurst, M. A., & Ruxton, G. D. (2010). The dual benefits of aposematism: Predator avoidance and enhanced resource collection. *Evolution*, *64*(6), 1622–1633. https://doi.org/10.1111/j.1558-5646.2009.00931.x

Stuart-Fox, D., Aulsebrook, A., Rankin, K. J., Dong, C. M., & McLean, C. A. (2021). Convergence and divergence in lizard colour polymorphisms. *Biological Reviews*, *96*(1), 289–309. https://doi.org/10.1111/brv.12656

Stuckert, A. M. M., Chouteau, M., McClure, M., LaPolice, T. M., Linderoth, T., Nielsen, R., Summers, K., & MacManes, M. D. (2021). The genomics of mimicry: Gene expression throughout development provides insights into convergent and divergent phenotypes in a Müllerian mimicry system. *Molecular Ecology*, *30*(16), 4039–4061. https://doi.org/10.1111/mec.16024

Stuckert, A. M. M., & Summers, K. (2022). Investigating signal modalities of aposematism in a poison frog. *Journal of Evolutionary Biology*, *36*(7), 1003–1009. https://doi.org/10.1111/jeb.14111

Twomey, E., Johnson, J. D., Castroviejo-Fisher, S., & Van Bocxlaer, I. (2020). A ketocarotenoid-based colour polymorphism in the Sira poison frog *Ranitomeya sirensis* indicates novel gene interactions underlying aposematic signal variation. *Molecular Ecology*, *29*(11), 2004–2015. https://doi.org/10.1111/mec.15466

Twomey, E., Melo-Sampaio, P., Schulte, L. M., Bossuyt, F., Brown, J. L., & Castroviejo-Fisher, S. (2023). Multiple routes to color convergence in a radiation of neotropical poison frogs. *Systematic Biology*, 1–15. https://doi.org/10.1093/sysbio/syad051

Willink, B., Brenes-Mora, E., Bolaños, F., & Pröhl, H. (2013). Not everything is black and white: Color and behavioral variation reveal a continuum between cryptic and aposematic strategies in a polymorphic poison frog. *Evolution*, *67*(10), 2783–2794. https://doi.org/10.1111/evo.12153

Winters, A. E., Lommi, J., Kirvesoja, J., Nokelainen, O., & Mappes, J. (2021). Multimodal aposematic defenses through the predation sequence. *Frontiers in Ecology and Evolution*, *9*. https://doi.org/10.3389/fevo.2021.657740

Wollenberg, K. C., Lötters, S., Mora-Ferrer, C., & Veith, M. (2008). Disentangling composite colour patterns in a poison frog species. *Biological Journal of the Linnean Society*, *93*, 433–444. https://academic.oup.com/biolinnean/article/93/3/433/2701352

CAPÍTULO I

Lyra, M. L.*, **Monteiro, J. P. C.***, Rancilhac, L., Irisarri, I., Künzel, S., Sanchez, E., Condez, T. H., Rojas-Padilla, O., Solé, M., Toledo, L. F., Haddad, C. F. B., & Vences, M. (2021). Initial phylotranscriptomic confirmation of homoplastic evolution of the conspicuous coloration and bufoniform morphology of pumpkin-toadlets in the genus *Brachycephalus*. *Toxins*, *13*(816), 1–16. https://doi.org/10.3390/toxins13110816
*These authors contributed equally to this study

“Confirmação filotranscriptômica inicial da evolução homoplástica da coloração conspícua e morfologia bufoniforme de sapos-abóbora do gênero *Brachycephalus*”

Resumo

O gênero *Brachycephalus* é um grupo de anuros miniaturizados da Mata Atlântica brasileira, compreendendo os conspícuos sapinhos-pingo-de-ouro e os discretos sapos-pulga. Sabe-se que os sapinhos-pingo-de-ouro contêm defesas químicas e, portanto, suas cores vibrantes podem desempenhar uma função aposemática. Estudos anteriores, baseados em um número limitado de marcadores mitocondriais e nucleares, sustentaram a existência de dois clados contendo espécies com fenótipo de sapinho-pingo-de-ouro, mas os nós profundos da árvore filogenética permaneceram amplamente sem resolução ou em conflito entre os conjuntos de dados. Utilizamos novos dados de RNAseq de 17 indivíduos de nove espécies de *Brachycephalus* para inferir suas relações evolutivas a partir de uma perspectiva filogenômica. Análises de quase 5300 genes codificadores de proteínas ortólogas nucleares e genomas mitocondriais completos confirmaram a existência de dois clados separados de sapinho-pingo-de-ouro, sugerindo a evolução convergente (ou múltiplas reversões) da morfologia bufoniforme, coloração conspícua e provavelmente toxicidade. Além disso, três espécies (*B*. *hermogenesi*, *B*. *pitanga* e *B*. *rotenbergae*) exibem translocações mitocondriais de diferentes tRNAs (NCY e CYA) do agrupamento WANCY de tRNAs para uma posição entre os genes ATP6 e COIII, demonstrando uma nova disposição para vertebrados. A filogenia recentemente esclarecida sugere que o gênero *Brachycephalus* tem potencial de se tornar um táxon modelo promissor para entender a evolução da coloração, plano corporal e toxicidade. Dado que as informações sobre toxicidade estão disponíveis apenas para algumas espécies de *Brachycephalus*, sem dados para qualquer espécie de sapo-pulga, também enfatizamos a necessidade de uma investigação mais ampla da toxicidade das espécies, juntamente com estudos mais aprofundados sobre funcionalidade e ecologia de seus fenótipos.

toxins

MDPI

Article

Initial Phylotranscriptomic Confirmation of Homoplastic Evolution of the Conspicuous Coloration and Bufoniform Morphology of Pumpkin-Toadlets in the Genus *Brachycephalus*

Mariana L. Lyra [1,†], Juliane P. C. Monteiro [1,†], Loïs Rancilhac [2], Iker Irisarri [3], Sven Künzel [4], Eugenia Sanchez [2], Thais H. Condez [5], Omar Rojas-Padilla [6], Mirco Solé [7], Luís Felipe Toledo [8], Célio F. B. Haddad [1] and Miguel Vences [2,*]

1 Instituto de Biociências, Departamento de Biodiversidade (Campus Rio Claro), Universidade Estadual Paulista (UNESP), Avenida 24A, N 1515, Bela Vista, Rio Claro 13506-900, SP, Brazil; marillyra@gmail.com (M.L.L.); julianepmonteiro@gmail.com (J.P.C.M.); haddad1000@gmail.com (C.F.B.H.)
2 Zoological Institute, Technische Universität Braunschweig, 38106 Braunschweig, Germany; loisrancilhac@gmail.com (L.R.); eu.sanisa@gmail.com (E.S.)
3 Institute for Microbiology and Genetics, Department of Applied Bioinformatics, University of Goettingen, Goldschmidtstr, 1, 37077 Göttingen, Germany; irisarri.iker@gmail.com
4 Max Planck Institute for Evolutionary Biology, 24306 Plön, Germany; kuenzel@evolbio.mpg.de
5 Unidade Passos, Universidade do Estado de Minas Gerais (UEMG), Avenida Juca Stockler 1130, Passos 37900-106, MG, Brazil; thacondez@gmail.com
6 Laboratório de Sistemática de Vertebrados, Pontifícia Universidade Católica do Rio Grande do Sul, Av. Ipiranga 6681, Porto Alegre 90619-900, RS, Brazil; projasomar@gmail.com
7 Departamento de Ciências Biológicas, Universidade Estadual de Santa Cruz, Ilhéus 45662-900, BA, Brazil; mksole@uesc.br
8 Laboratório de História Natural de Anfíbios Brasileiros (LaHNAB), Departamento de Biologia Animal, Instituto de Biologia, Universidade Estadual de Campinas, Campinas 13083-862, SP, Brazil; toledosapo@gmail.com
* Correspondence: m.vences@tu-braunschweig.de; Tel.: +49-531-391-3237
† These authors contributed equally to this study.

Abstract: The genus *Brachycephalus* is a fascinating group of miniaturized anurans from the Brazilian Atlantic Forest, comprising the conspicuous, brightly colored pumpkin-toadlets and the cryptic flea-toads. Pumpkin-toadlets are known to contain tetrodotoxins and therefore, their bright colors may perform an aposematic function. Previous studies based on a limited number of mitochondrial and nuclear-encoded markers supported the existence of two clades containing species of pumpkin-toadlet phenotype, but deep nodes remained largely unresolved or conflicting between data sets. We use new RNAseq data of 17 individuals from nine *Brachycephalus* species to infer their evolutionary relationships from a phylogenomic perspective. Analyses of almost 5300 nuclear-encoded ortholog protein-coding genes and full mitochondrial genomes confirmed the existence of two separate pumpkin-toadlet clades, suggesting the convergent evolution (or multiple reversals) of the bufoniform morphology, conspicuous coloration, and probably toxicity. In addition, the study of the mitochondrial gene order revealed that three species (*B. hermogenesi*, *B. pitanga*, and *B. rotenbergae*) display translocations of different tRNAs (NCY and CYA) from the WANCY tRNA cluster to a position between the genes ATP6 and COIII, showing a new mitochondrial gene order arrangement for vertebrates. The newly clarified phylogeny suggests that *Brachycephalus* has the potential to become a promising model taxon to understand the evolution of coloration, body plan and toxicity. Given that toxicity information is available for only few species of *Brachycephalus*, without data for any flea-toad species, we also emphasize the need for a wider screening of toxicity across species, together with more in-depth functional and ecological study of their phenotypes.

Keywords: Amphibia; Anura; RNAseq; phylogenomics; mitochondrial genomes; mitochondrial gene order; convergence; aposematism

check for updates

Citation: Lyra, M.L.; Monteiro, J.P.C.; Rancilhac, L.; Irisarri, I.; Künzel, S.; Sanchez, E.; Condez, T.H.; Rojas -Padilla, O.; Solé, M.; Toledo, L.F.; et al. Initial Phylotranscriptomic Confirmation of Homoplastic Evolution of the Conspicuous Coloration and Bufoniform Morphology of Pumpkin-Toadlets in the Genus *Brachycephalus*. *Toxins* **2021**, *13*, 816. https://doi.org/10.3390/toxins13110816

Received: 3 September 2021
Accepted: 15 November 2021
Published: 19 November 2021

Publisher's Note: MDPI stays neutral with regard to jurisdictional claims in published maps and institutional affiliations.

Copyright: © 2021 by the authors. Licensee MDPI, Basel, Switzerland. This article is an open access article distributed under the terms and conditions of the Creative Commons Attribution (CC BY) license (https://creativecommons.org/licenses/by/4.0/).

Key Contribution: A phylogenomic analysis based on over 5000 nuclear-encoded markers suggests that the bright-colored and toxic pumpkin-toad phenotype may have evolved convergently twice.

1. Introduction

The evolution of aposematism, i.e the co-occurrence of conspicuous coloration and defensive mechanisms, is fascinating and poorly understood, despite intensive research over many decades (e.g., [1–5]). Whether an apparently bright and conspicuous colour pattern is aposematic (i.e., it has primarily a warning function) rather than serving intraspecific communication or even camouflage [1,6,7] and how warning colour integrates with the evolution of other phenotypic characters [8] are intriguing questions that can only be answered by subjecting a variety of animal systems to experimental (e.g., [9–11], phylogenetic (e.g., [12]), and genomic research (e.g., [13]).

Amphibians have long been a prime group for research on the evolution of aposematism and contain a large number of species that exhibit putative warning signals [14]. They are also the only class of terrestrial vertebrates known to contain tetrodotoxin analogues (TTX; [15]). One example is the Brazilian genus *Brachycephalus* which currently comprises 38 described species [16], all endemic to the Atlantic Forest biome between 15° and 26° latitude from sea level up to 2000 m [17] (Figure 1). Species in this genus are essentially diurnal, leaf-litter inhabitants, miniaturized, and characterized by direct development [18,19]. *Brachycephalus* species are divided into two groups according to their body plans, popularly known as pumpkin-toadlets (34 species) and flea-toads (4 species) [20]. All pumpkin-toadlets are characterized by a "bufoniform" appearance, with a robust body and pectoral girdle, head as wide as long and short snout; the flea-toads instead have a "leptodactyliform" appearance with slender body and pectoral girdle, head longer than wide and long snout (Supplementary Figure S1). The relatively more elongated skull of the flea-toads is also reflected in a skeletal multivariate morphospace [20]. The coloration of pumpkin-toadlets is usually bright, orange/yellow but sometimes greenish/brownish dorsally, and always with some orange components at least on the hands and feet and/or on the ventral surface. Several pumpkin-toadlets are also known to contain toxins: TTX has been reported in *B. ephippium*, *B. nodoterga*, *B. pernix*, *B. pitanga*, and *B. rotenbergae* (as *B. ephippium*) [15,21,22] and bradykinin-potentiating peptides (BPP) have been reported in *B. rotenbergae* ([23]—as *B. ephippium*). On the contrary, flea-toads have an inconspicuous brown coloration [19,20] and their putative toxicity has so far not been assessed. These characteristics make *Brachycephalus* an excellent model for studying the evolution of anti-predator defense mechanisms associated with toxins.

Surprisingly, early molecular phylogenetic evidence (Figure 2A) suggested that these two morphological groups are not reciprocally monophyletic within *Brachycephalus* [18]. Based on DNA sequences of few mitochondrial and two nuclear-encoded genes (tyrosinase and recombination activating gene 1), two major clades of pumpkin-toadlets were recovered: the *B. ephippium* group (with 15 species), characterized by a gradient of increased mineralization in the skull [20,24–27], and the *B. pernix* group (with 19 species), which is not hyperossified [18–20]. The *B. ephippium* group is distributed across the Serra do Mar and Serra da Mantiqueira mountain ranges whereas the *B. pernix* group is distributed across the Serra do Mar, respectively at the north and south of the Guapiara Lineament [19] (Figure 1). However, the relationships of the flea-toad species within *Brachycephalus* (*B. didactylus*, *B. hermogenesi*, *B. pulex*, and *B. sulfuratus*) remain incompletely resolved (Figure 2). Mitochondrial analyses recovered *B. didactylus* sister to the *B. ephippium* group with high support, as well as *B. sulfuratus* sister to the *B. pernix* group [19,20]. *Brachycephalus hermogenesi* was recovered either nested within the *B. ephippium* group [18] or sister to a clade encompassing all other *Brachycephalus* with low support [19]. The northernmost distributed species *B. pulex* (Figure 1) seems to split from a deep node in the *Brachycephalus* tree [20], how-

ever, the relationship between this species and other *Brachycephalus* spp. are not well supported [19,20].

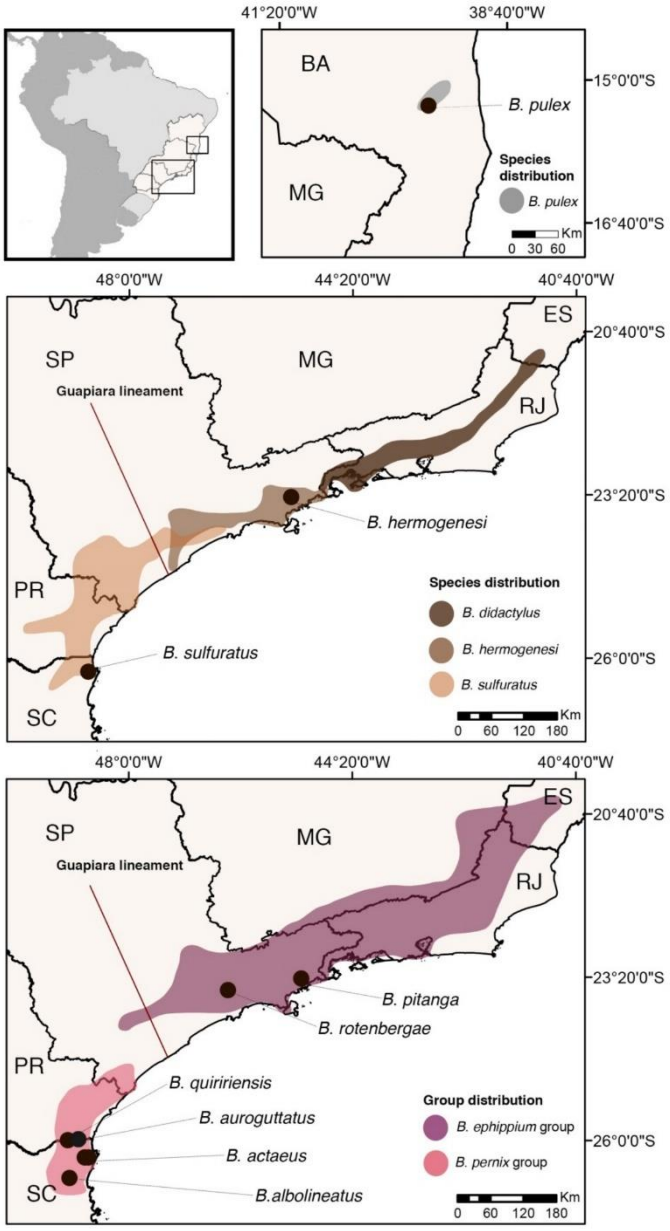


Figure 1. Approximate distribution map for genus *Brachycephalus* based on literature records, with sampling localities for each species included in the phylogenomic analysis. Acronyms for Brazilian states: BA, Bahia; ES, Espírito Santo; MG, Minas Gerais; PR, Paraná; RJ, Rio de Janeiro; SC, Santa Catarina; and SP, São Paulo.

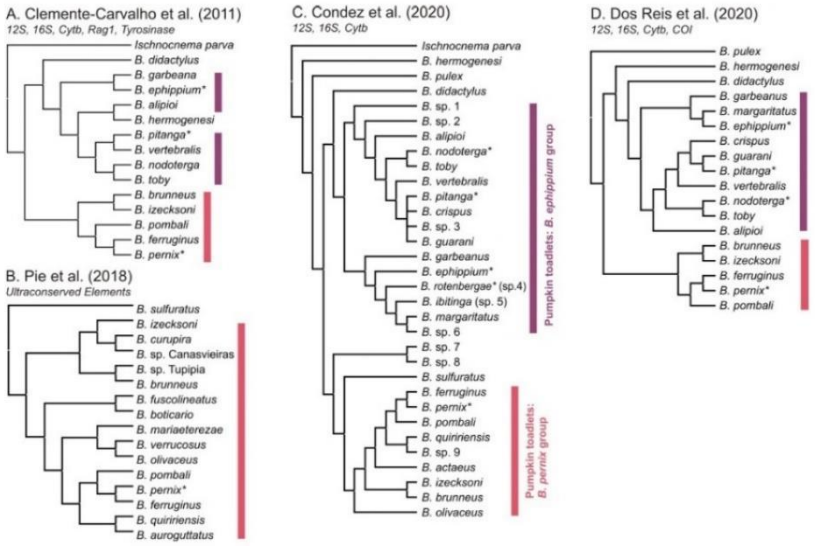


Figure 2. Summary of selected results from previous phylogenetic analyses of the genus *Brachycephalus*: (**A**) Bayesian inference (BI) analysis of a concatenated matrix 4563 bp of three mitochondrial and two nuclear gene fragments [18]; (**B**) BI analysis of 155,683 bp of 303 concatenated ultraconserved (UCE) loci [28]; (**C**) BI analysis of 2372 bp of three concatenated mitochondrial gene fragments [19] (**D**) species tree estimation from 4826 bp of four mitochondrial gene fragments [20]. Purple bars refer to the *B. ephippium* group and pink bars refers to the *B. pernix* group. Asterisks (*) mark species known to contain toxins (TTX). The two groups of pumpkin-toadlets are marked with vertical bars; other species are flea-toads (or outgroup: *Ischnocnema*). Note that *B. rotenbergae* has only recently been recognized as a distinct species and some sequences as well as toxin data assigned to *B. ephippium* in earlier studies may refer to this species.

Although current knowledge suggests homoplasy of the aposematic coloration and body plan in pumpkin-toadlets, the conflicting and often poorly supported phylogenetic placements of various flea-toad species do not allow understanding whether the multiple instances of the pumpkin-toadlet phenotype represents homoplasy or shared ancestry. Here, we aim to assess the relationships within *Brachycephalus* with new phylogenomic data derived from RNAseq from representatives of each major clade of pumpkin-toadlets and three species of flea-toads, thus representing most of the main clades within the genus. We analyzed complete mitochondrial genomes reconstructed from the RNAseq data as well as a comprehensive phylotranscriptomic data set of over 5000 nuclear-encoded protein-coding genes, which resulted in largely congruent and supported hypotheses for the evolutionary history of *Brachycephalus*.

2. Results

2.1. Phylogenetic Relationships

The final phylotranscriptomic dataset consisted of 5296 alignments of ortholog nuclear-encoded protein-coding genes, totaling 7,612,827 aligned nucleotide positions. Partitioned ML analysis of the concatenated data set resulted in a fully resolved tree (Figure 3A) with full support on all internal branches, except for two intraspecific nodes connecting individuals of *B. rotenbergae*. The ASTRAL tree recovered the same topology with fully supported inter-specific relationships as well (Supplementary Figure S2). The ML analysis of the concatenated alignment of 13,938 mitochondrial nucleotide positions (the two rRNA and the 13 protein-coding genes) yielded a tree overall concordant to that obtained from the nuclear-encoded data (Figure 3B; Supplementary Figure S3), the disagreements affecting deep nodes that were poorly resolved by the mitogenomic data and the position of one species within the *B. pernix* group (*B. albolineatus*, see below).

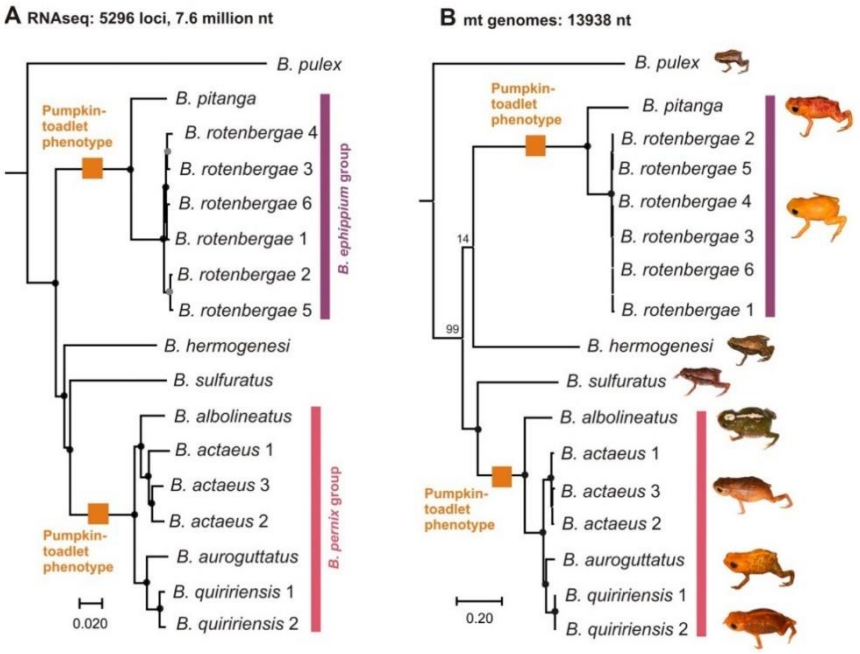


Figure 3. Phylogenomic trees of *Brachycephalus* spp. (**A**) Maximum Likelihood (ML) tree calculated from a concatenated alignment of 7,612,827 nucleotide positions (nt) of 5296 nuclear-encoded protein-coding markers derived from transcriptomes. Black circles at nodes indicate full support from both the analysis of the concatenated dataset (with IQTREE: 100% for 1000 aLRT pseudoreplicates) and from a species tree analysis (with ASTRAL: 1.0 local posterior probability); grey nodes received 100% support in the IQTREE analysis but a posterior probability <1.0 in the ASTRAL analysis. (**B**) Maximum likelihood tree calculated from a concatenated alignment of 13,938 nucleotide positions of the two rRNA genes and the 13 protein coding genes from full mitochondrial genomes. Black circles at nodes indicate 100% bootstrap support, other bootstrap values are written out (except for the most shallow intraspecific nodes). Orange squares mark clades composed of species characterized by the pumpkin-toadlet phenotype (bufoniform morphology, conspicuous orange coloration at least on some parts of the body, and probable toxicity), as opposed to the flea-toad phenotype (leptodactyliform morphology, cryptic coloration and possibly reduced toxicity) of *B. pulex, B. hermogenesi* and *B. sulfuratus.* Both trees were rooted with *Ischnocnema henselii* as outgroup (removed from the figure for better graphical representation of the trees). Scale bars represent expected substitutions per site.

The two data sets are concordant regarding the phylogenetic relationships of the flea-toads *B. pulex* and *B. sulfuratus*. *Brachycephalus pulex* is placed sister to all other included *Brachycephalus* with full support (100% aLRT in the nuclear tree, 99% bootstrap support in the mitochondrial tree; Figure 3). *Brachycephalus sulfuratus* is placed with maximum support in all analyses as sister to one clade of pumpkin-toadlets (the *B. pernix* group). The analyses also recovered the included species of the *B. ephippium* group, and of the *B. pernix* group, as monophyletic, respectively. The phylogenetic position of the flea-toad *B. hermogenesi* was contradictory. Whereas the phylotranscriptomic analyses recovered it sister to the clade containing the *B. pernix* group and *B. sulfuratus* with maximum support, the mitogenomic analysis placed it as sister to the *B. ephippium* group but without support (bootstrap proportion = 14%). The position of *B. albolineatus* within the *B. pernix* group was also different between the datasets: phylotranscriptomic analyses recovered the species as sister to *B. actaeus*, whereas the mitogenomic analysis placed it sister to the *B. pernix* group. These alternative topologies received maximum support by the analyses of the respective data sets. All species covered by multiple samples were monophyletic with high support and displayed short intra-specific branches.

2.2. Reconstruction of Phenotype Evolution

Reconstruction of ancestral character states via Bayesian stochastic character mapping yielded ambiguous results where most deep nodes in the tree had similar probabilities for both phenotypes (Figure 4), with a tendency of higher probabilities for bright color and bufoniform body plan. Similar results were found when the outgroup (*Ischnocnema*) was either included or excluded. An explorative parsimony analysis (Fitch optimization in TNT; [29]) reconstructed a convergent evolution of the pumpkin-toadlet phenotype, i.e., according to this approach, both the bufoniform body plan and bright coloration originated independently in the *B. ephippium* and the *B. pernix* group (Supplementary Figure S4).

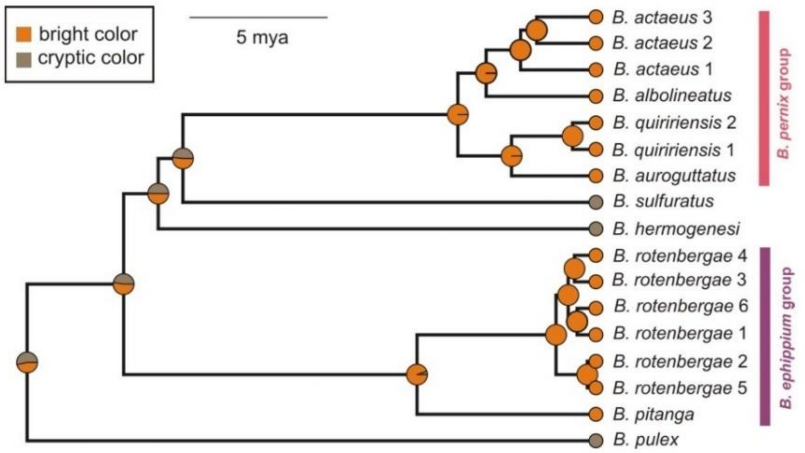


Figure 4. *Brachycephalus* phenotype reconstructed under a Bayesian (stochastic character mapping; SIMMAP) using phytools. Identical reconstructions were obtained for color (shown), and for bufoniform vs. leptodactyliform morphology. The character state "bright color" defines species that have at least some part of the body surface colored bright orange (dorsum, hands and feet, or ventral surface). Scale bar represents 5 million years it is based on calibration of the *Ischnocnema*/*Brachycephalus* split at 35 million years ago (see methods).

2.3. Mitogenome Gene Order

Near-complete mitogenomes were recovered for all specimens, including the two ribosomal genes (12S and 16S rRNA), the 13 protein-coding genes, and most tRNAs (Figure 5). We also recovered partial control region (CR) sequences for *B. pitanga* and *I. henselii*. Most genes are transcribed from the H-strand, except for ND6 and eight tRNA genes, as known for other anurans [30,31]. We found only a few regions with low coverage in all mitogenomes, mostly representing partial tRNA regions and the 3′ or 5′ regions of coding-sequences. This pattern is expected when by-catching mitogenomes from RNAseq data.

The gene arrangement in *B. pulex*, *B. sulfuratus* and species of the *B. pernix* group follows the most common order known for Neobatrachia [31,32] (Figure 5A). However, two novel tRNA gene rearrangements were found for *B. hermogenesi* and for *B. pitanga* + *B. rotenbergae*. In these three species genes from the WANCY tRNA cluster are rearranged to the region between ATP6 and COIII. In *B. hermogenesi* the tRNAs N, C, and Y are translocated, probably in a single translocation event maintaining the same order found in the WANCY cluster (Figure 5B). In *B. pitanga* and *B. rotenbergae*, instead, the tRNAs A, C, and Y were found in between ATP6 and COIII, and furthermore the tRNA-A was found after tRNAs C and Y (Figure 5C). These new arrangements did not affect the position of the origin of replication for the light-strand synthesis (O_L) (Figure 5). Strikingly, the other species of *Brachycephalus* also have a non-coding region between ATP6 and COIII, which is missing in the outgroup (*Ischnocnema*). Given the high coverage and quality of

the fragment spanning between ATP6 and COIII in most assemblies, these arrangements are unlikely to be artefactual. In addition, the de novo assembly using the program mitoZ also recovered these arrangements, and PCR tests confirmed different length fragments for species of rearranged gene order vs. standard gene order (Supplementary Figure S5).

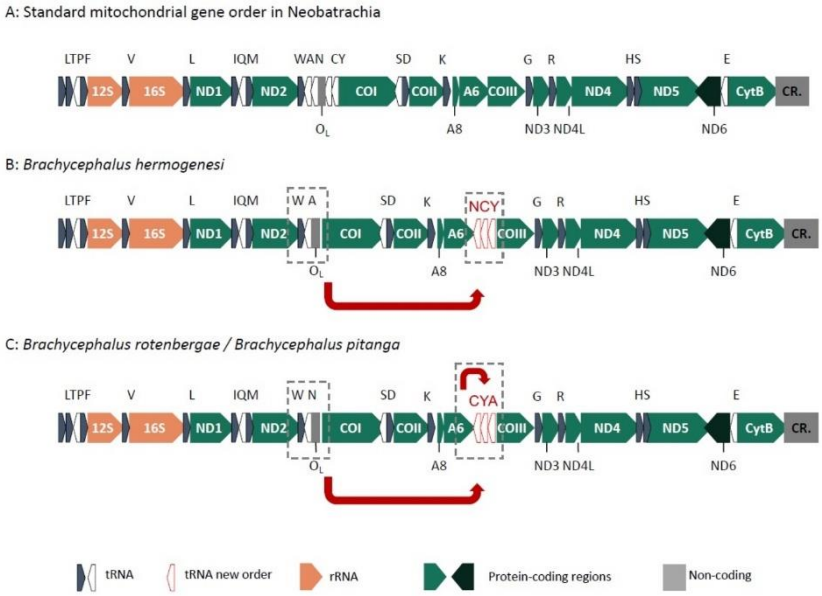


Figure 5. Schematic representation of mitochondrial DNA gene arrangement in *Brachycephalus*. Arrows represent rearrangements in relation to standard gene order of Neobatrachia. The black squares highlight the rearrangement region. Gene alias follows HUGO gene nomenclature committee (https://www.genenames.org/; accessed on 1 September 2021). (**A**) Standard mitochondrial gene order as observed in most Neobatrachia; (**B**) gene order observed in *B. hermogenesi*; (**C**) gene order observed in *B. rotenbergae* and *B. pitanga*.

3. Discussion

3.1. Evolution and Biogeography of Brachycephalus

The phylotranscriptomic and mitogenomic analyses conducted herein support that flea-toads do not represent a monophyletic group exclusive of pumpkin-toadlets. The analyses recovered *B. pulex* as the sister species to all other *Brachycephalus* with high support, as previously suggested [20]. The position of *B. sulfuratus*, sister to the *B. pernix* group, also agrees with previous studies based on mitochondrial DNA markers [19,20]. The phylogenetic position of *B. hermogenesi* was not unambigously solved by the analyses herein; the phylotranscriptomic dataset suggests a novel phylogenetic relationship of this species not recovered by previous studies, being the sister clade of *B. sulfuratus* + *B. pernix* group, whereas its position remained poorly supported in the mitogenomic tree. A single species of flea-toad, *B. didactylus*, is missing from our phylogenomic analyses. However, in all previous works, this taxon was consistently recovered with high support as sister to the *B. ephippium* group [18–20] and this position was also recovered in an analysis including these data along with our mitogenomic sequences (Supplementary Figure S6). Therefore, we expect this position will also be confirmed once phylogenomic data for this species become available.

Our results corroborate previous analyses in recovering two fully supported clades of conspicuous pumpkin-toadlets: (i) the *B. ephippium* group (represented by *B. pitanga* and *B. rotenbergae*), and (ii) the *B. pernix* group (represented by *B. actaeus*, *B. albolineatus*, *B. auroguttatus*, and *B. quiririensis*) [18–20]. As far as known, in *Brachycephalus* the pumpkin-

toadlet phenotype includes two components that in all known species are linked (bufoniform morphology and conspicuous coloration), i.e., all bufoniform species of the genus are also more or less brightly colored (sometimes including green and brownish morphs). Stochastic character mapping could not reliably reconstruct the ancestral phenotype of *Brachycephalus* and the polarization of character states therefore remains ambiguous (Figure 4). The pumpkin-toadlet phenotype can be hypothesized to be derived given its absence in *Ischnocnema*, the sister clade of *Brachycephalus*, and along with other studies [20] we consider the hypothesis of convergent origin of this derived phenotype more likely, rather than postulating multiple reversals. We anticipate that this hypothesis will receive stronger support if the probable sister-group relationship of the *B. ephippium* clade and the flea-toadlet *B. didactylus* [19,20] (Supplementary Figure S6 herein) is confirmed by future phylogenomic data sets and included in the ancestral character state reconstruction, but at present it is clear that the details of the phenotype homoplasy in *Brachycephalus* cannot be resolved with full reliability.

Furthermore, the two pumpkin-toadlet clades show different patterns of ossification. In the *B. ephippium* group, species have remarkably ossified skulls and vertebral columns, sometimes with a bony dorsal shield, and bone sculpturing consisting of ridges and crests inducing a reticulated or pitted pattern in the skull, spinal processes of sacral, and presacral vertebrae [20,25]. In contrast, in the *B. pernix* group, such hyper-ossification is not observed [19,20,27]. This might indicate that the bufoniform appearance of these toadlets is ontogenetically based on different developmental processes, which would be in agreement with an independent evolutionary origin.

From a biogeographical perspective, a previous study [19] hypothesized that the ancestral distribution of *Brachycephalus* was in the northern part of its current range, specifically in high-elevation regions in the northern Serra do Mar mountain range. From the results obtained herein, we can refine this hypothesis relying on the assumptions that (i) our phylotranscriptomic tree correctly represents the evolutionary history of the main *Brachycephalus* clades, and (ii) the phylogenetic position of the flea-toad species *B. didactylus* has been correctly recovered by previous studies (see also Supplementary Figure S6). The flea-toad *B. pulex* was recovered sister to all other *Brachycephalus* spp. and occupies the northernmost distribution range (Figure 1). Hence, it is possible that the initial split in the genus occurred between a northern and central/southern ancestral Atlantic Forest species, both likely possessing a flea-toad morphology. In this hypothesis, the subsequent split may have separated two main further clades characterized by an ancestral flea-toad phenotype. One of these occupied much of the central part of the Atlantic Forest, with a widespread species of flea-toad morphology (*B. didactylus*) and one clade, the *B. ephippium* group, evolving the pumpkin-toadlet phenotype (Figure 1). The second clade would have dispersed southwards where successive stages of this colonization are represented by the flea-toad lineages, *B. hermogenesi* and *B. sulfuratus*, and the *B. pernix* group that evolved the pumpkin-toadlet phenotype (Figure 1).

3.2. Mitogenome Evolution and Cyto-Nuclear Discordance

Gene rearrangements comparable to those observed in *Brachycephalus* have been reported in all lissamphibian orders [30,33–35]. Especially the WANCY genomic region has been previously considered a hotspot for gene order rearrangements [33,34]. For example, the caecilians *Luetkenotyphlus brasiliensis* and some *Siphonops* spp. have different arrangements for tRNAs in this region (NCYWA and ACWNY, respectively) [34]. However, the partial rearrangement of some of these tRNA genes to the position between the ATP6 and COIII genes, as observed in several *Brachycephalus*, is new for vertebrates.

The mitochondrial gene order could be interpreted as supporting a close relationship of *B. hermogenesi* and the *B. ephippium* group, given that in both, genes from the WANCY tRNA cluster were translocated to the region between ATP6 and COIII, an unprecedented position for such translocations among frogs. However, since different tRNAs were affected by this translocation in these taxa, and furthermore in a different order, it is unlikely that

the observed pattern reflects a single, ancestral translocation event. It is more likely that a complex history of multiple translocations and maybe translocation reversals affected the mitochonodrial genomes of *Brachycephalus* species, as supported by the presence of non-coding DNA at this position in all species studied, including the earliest diverging lineage, *B. pulex*. It also cannot be fully ruled out that the shared position of the translocated tRNA clusters in *B. hermogenesi* and the *B. ephippium* group might be due to an early mitochondrial introgression event among ancestral *Brachycephalus* lineages.

The low support found for the deep nodes in the mitogenome tree suggests that mitochondrial data alone–even complete mitochondrial genomes–might be insufficient to reliably resolve several of the deepest nodes in the *Brachycephalus* tree. However, in one case, we detected a clear disagreement between phylotranscriptomic and mitogenomic trees: the mitogenomic tree placed *B. albolineatus* sister to all other included species of the group (in general agreement with the mitochondrial tree of [36]), whereas the phylotranscriptomic tree suggested a sister-group relationship to *B. actaeus*. This cytonuclear discordance in the placement of *B. albolineatus* might reflect inter-lineage gene flow. Our phylotranscriptomic tree includes only a small subset of species of the *B. pernix* group but according to the available mitochondrial gene trees (e.g., [36]) all species in the group are closely related, with maximum uncorrected pairwise distances in the 16S rRNA gene of <5.7%, and <1.4% between many closely related species [36] (Supplementary Figure S6). *Brachycephalus albolineatus* is closely related to *B. boticario*, *B. fuscolineatus*, and *B. mirissimus* based on mitochondrial data ([37]; present study), and a mitochondrial introgression from one of those species could explain the observed discordance. Alternatively, the species could have conserved a mitochondrial genome reflecting its evolutionary origins and its original nuclear genome diluted by frequent gene flow from other lineages close to *B. actaeus*. In amphibians, a similar situation of a divergent "ghost" mitochondrial genome not reflecting the evolutionary affinities of the nuclear genome was found for example in the salamander *Salamandra salamandra longirostris* from Spain [38,39]. Salamandrids have also served as a model to demonstrate pervasive hybridization among ancestral amphibian lineages [40], a phenomenon that might also affect the phylogeny of the genus *Brachycephalus*.

3.3. Challenges and Perspectives for Future Taxonomic and Evolutionary Studies

In our study, the intraspecific genetic variation found for the species with more than one sample analysed was very low. Particularly, for *Brachycephalus actaeus*, we included samples from different collecting points with remarkable colour variation (green, brownish, and orange, Supplementary Figure S1). Both datasets recovered *B. actaeus* as monophyletic with very short branches, providing further evidence for a polytypic species with substantial intra-specific colour variation. One of the phenotypes (orange) is more similar to that of other orange-colored species of the *B. pernix* group such as *B. mirissimus*. This example illustrates a new challenge to the taxonomy of this genus and may be caused by different populations of a species being subject to distinct selective pressures, translated into different frequencies of a dazzling variety of colour phenotypes. There are a few examples of similar systems in anurans, including poison-frogs of the families Dendrobatidae [12,13] and Mantellidae [41,42].

We flag as priorities for future investigation the inclusion of additional species such as *B. didactylus* in the phylotranscriptomic analysis, as well as including more specimens per species to better understand the limits of genetic and geographical variation within polytypic *Brachycephalus* species. It is also worth considering that several of the branches at the base of the phylogenomic tree are very short, including those that are most informative regarding the evolution of the pumpkin-toadlet phenotype, and these relationships may easily be influenced by introgression and thus be less stable than they appear in our tree. Once the crucial missing taxon (*B. didactylus*) has been included in the phylogenomic data set and its relationships reliably reconstructed, it will be crucial to perform introgression tests to better understand the origins of cyto-nuclear discordance and to provide a fully reliable test of the hypothesis of homoplastic evolution of this phenotype. For this purpose,

a more in-depth characterization of the phenotypical groups is also needed. This should include objective assessments of color brightness, ideally with reflectance measurements against the background of the species' habitats, as well as quantification of the body shape differences between pumpkin-toadlets and flea-toads.

While *Brachycephalus* have the potential to become a promising model taxon to understand the evolution of coloration, body plan and toxicity, comprehensive analyses are currently hampered by the poor taxonomic coverage of toxin analyses. Only few species of *Brachycephalus* have been screened for TTX and other toxic compounds, and most importantly, not a single flea-toad species has so far been included in these screens. It is therefore important to conduct a more extensive toxin screening, both in pumpkin-toadlets and flea-toads, to understand if bright colour in this genus is linked to toxicity and/or presence of TTX. In the same context, a broad experimental assessment of their supposed unpalatability to predators and the functions of their bony plates and associated fluorescent skeleton [11,43] are desirable to complement what we know about the complex evolutionary history of *Brachycephalus*.

4. Materials and Methods

4.1. Genetic Sampling

Our sampling includes 18 individuals from nine species representing the main clades within *Brachycephalus* (*B. actaeus*, *B. albolineatus*, *B. auroguttatus*, *B. hermogenesi*, *B. pitanga*, *B. pulex*, *B. quiririensis*, *B. rotenbergae*, and *B. sulfuratus*; Table S1; Supplementary Figure S1) and one outgroup taxon (*Ischnocnema henselii*, a representative for the sister genus *Ischnocnema*; [44]; Supplementary Figure S1). Individuals were collected in the field, euthanized by applying 5% lidocaine to the skin, and the specimens were stored in RNAlater at −80 °C until RNA extraction. Specimens were collected under collection permits issued by ICMBio (Instituto Chico Mendes de Conservação da Biodiversidade; SISBio #13708-2, #17242-5, #49587-7, and #59889-1) and we registered the access to genetic information on the National System for the Management of Genetic Heritage and Associated Traditional Knowledge (SISGen #A58BC2D).

RNA was extracted from about 20–100 mg of tissue (combined or separate skin, muscle, or liver), and the extractions were performed using a standard TRIzol protocol as specified in the Supplementary Methods. Libraries for sequencing were prepared with the Illumina TruSeq Stranded mRNA Library Prep protocol (San Diego, CA, USA). The double-barcoded libraries were sequenced on an Illumina NextSeq instrument at the Max-Planck Institute for Evolutionary Biology in Plön, Germany, in multiple 150 bp or 75 bp paired-end runs (along with other samples of amphibians and reptiles not used for this study) each of which combined 10–14 samples per High-Output NextSeq kit. For species with transcriptomes of multiple individuals (*B. actaeus*, *B. quiririensis*, and *B. rotenbergae*) we chose to analyse each sample separately to assess the performance of our phylotranscriptomic approach in recovering species-level lineages. Reads were quality-trimmed and filtered using Trimmomatic v. 0.32 [45] with default settings, and transcriptomes were de novo assembled using Trinity v. 2.1.0 [46], following published protocols [47].

4.2. Phylotranscriptomic Analyses

To extract orthologous genes from the transcriptomes, we relied on the jawed-vertebrate alignment from [48] which included representative taxa of chondrichthyan and actinopterygian fishes, lungfish, coelacanth, amphibians, reptiles, birds, and mammals. This original data set consisted of a total of 100 taxa and was obtained by inferring putative orthologs from 21 reference proteomes representing most major clades of jawed vertebrates, and enriching them with genome and transcriptome data from 79 additional taxa using the software "42" (D. Baurain, https://metacpan.org/release/Bio-MUST-Apps-FortyTwo; accessed on 27 February 2021). The software "42" adds sequence data to the preexisting multiple sequence alignments (MSAs) after controlling for orthology using strict three-way reciprocal best BLAST hit tests, relying on a set of reference taxa available in the MSAs (*query_orgs*) and as complete proteomes (*ref_orgs*). The software performs a first BLAST search between *query_orgs* and *ref_orgs* and

produces a database of best hits (*query_best_hits*). Then, a second BLAST search uses *query_orgs* to search the new transcriptomes to be added (*org*). Eventually, the identified homologs are BLAST-searched against *ref_orgs* and homologs are considered orthologs if the best hit with each of the reference proteomes is among the sequences in the *query_best_hit* list built earlier. The orthologs identified via this process are then added to the original MSAs, followed by multiple sequence alignment and redundancy filtering.

For the present study, we used the original 100-taxa dataset of [48] and enriched it with the newly sequenced *Brachycephalus* and *Ischnocnema* transcriptomes, using a new, separate round searches and alignments with the software "42". After the protein-level alignment, we searched for sequences from the newly added data (*Brachycephalus* and *Ischnocnema*) that could represent putative contamination from prokaryotes and invertebrates added during the enrichment step. Such contaminant sequences might be added due to their conserved protein motifs or because they represent highly conserved genes throughout the tree of life. Contaminants were identified as significant BLAST hits against a custom protein database, and removed from the alignment.

Subsequently, for each locus the original nucleotide sequences were retrieved from the transcriptomes using leel (D. Baurain, https://metacpan.org/release/Bio-MUST-Apps-FortyTwo; accessed on 27 February 2021). Because data sets derived from low coverage transcriptomes or genomes may contain erroneous sequences caused by misassembly, frameshifts due to sequencing error, or recombination, and paralogs may also remain, a thorough decontamination procedure is necessary for which we employed tree-based orthology inference methods (e.g., [49]), as follows: (1) at the transcript level, highly fragmented sequences were removed (as very short transcripts are likely to produce phylogenetic artefacts simply because of too little information) and single-gene trees were inferred using RAxML v.8 [50] under a GTR + Γ substitution model. In-paralogs were identified based on long internal branches and removed, which represents a usual approach in phylogenomics. Sequences with very long terminal branches (in practice longer than the 99% quantile of the terminal branch length distribution) were interpreted as containing sequence errors or frameshifts and also removed. (2) Next, sequences were re-aligned with MAFFT [51], transcripts were merged with ScaFos v1.25 [52] and gene trees, as well as a concatenation tree, were newly inferred. (3) Individual taxa were removed from single-gene alignments when the exclusion significantly reduced the topological distance between the gene and concatenation trees (Robinson-Foulds distance). In this step, we set very stringent thresholds and manually checked every gene tree from which sequences were to be excluded and proceeded with the exclusion only when gene tree/concatenation tree differences could not be plausibly explained by biological processes such as incomplete lineage sorting or introgression. (4) Lastly, one additional cleaning step identical to step 2 was performed. From the obtained alignments, only those with five or more *Brachycephalus* samples were kept, and positions with >75% missing data were removed. Exploratory trees calculated before these decontamination steps agreed in all relevant nodes with our final tree, suggesting that these very conservative procedure has not biased our phylogenetic results.

A maximum likelihood (ML) tree was inferred from the concatenated alignment using IQ-TREE v1.6.8 [53,54], with best-fitting substitution models and gene partitions selected with BIC in ModelFinder [55], as implemented in IQ-TREE. Branch support was assessed with 1000 pseudoreplicates of SH-like approximate likelihood ratio test (aLRT). Furthermore, to account for possible effects of incomplete lineage sorting on phylogenetic inference, we also inferred a tree from the full data set using ASTRAL-II [56], a summary-tree method statistically consistent with the multispecies coalescent. Gene trees used as input for ASTRAL were inferred using RAxML under a GTR + Γ model. Branch support of the ASTRAL tree was assessed using local posterior probabilities.

4.3. Mitochondrial Genome Analyses

The trimmed RNAseq reads were also used to recover mitochondrial DNA sequences. Paired-end FASTQ files were interleaved, and duplicates removed using Tally v. 14-020 [57]. We assembled mitochondrial genomes by iterative mapping using MITObim v. 1.9.1 [58], which internally uses MIRA v.4.0.2 [59]. The assembly was done in three steps: we first used the complete mitochondrial sequence of *Ischnocnema henselii* (GenBank accession number: MH492733) as initial seed and the mismatch parameter was set to 30 for all samples. Iterations were run until no additional reads could be incorporated into the assemblies. We evaluated the assemblies for completeness and quality by importing the mapping output from MITObim into Geneious R11 (https://www.geneious.com; accessed 1 February 2021). Since it was not possible to retrieve all coding genes for some *Brachycephalus* samples, we selected the most complete *Brachycephalus* mitogenome from the first round and used it as seed to reassemble all *Brachycephalus* samples, setting the mismatch parameter to 10. Finally, we used mitogenomes of each species as retrieved in the second round as seed for a third round of assembly to improve coverage and fill gaps. We did not use the published mitogenome of *Brachycephalus brunneus* as seed (GenBank accession KY355081) because the gene order of the available sequence does not match the gene order described in the original publication [60].

We also used mitoZ [61] to de novo assemble the mitogenome of some species and visually inspected them to confirm new gene arrangements (see results). We furthermore inspected read alignments visually to exclude assembly artefacts, and carried out some further tests to verify gene orders by designing primers spanning the tRNA WANCY region and performing PCRs tests to assess the length of the amplified fragment (Supplementary Methods).

Mitogenome annotations were performed in mitoZ [61] and the annotated contigs were loaded into Geneious R11 [62]. The two rRNAs (12S rRNA and 16S rRNA) and the 13 protein-coding genes were extracted, and the protein coding genes were checked to confirm that no indels or stop codons were present. Sequences of each gene were aligned with MAFFT [51] and aligned sequences were concatenated using SequenceMatrix v1.7.8 [63] for phylogenetic inference.

Data was partitioned by gene and by codon position when appropriate and the best partition scheme was selected using PartitionFinder 2 [64] (Table S2). A mitochondrial ML tree was inferred using RAxML v. 8.2.11 [50], with 100 ML searches and 1000 non-parametric bootstrap replicates, in the CIPRES Science Gateway (http://www.phylo.org; accessed 1 February 2021). The GTR + Γ substitution model was used for all partitions. Additionally we inferred mitochondrial trees using both ML and Bayesian Inference for all *Brachycephalus* species available from GenBank, to further explore hypotheses of phylogenetic relationships among flea-toads and pumpkin toadlets with maximum species coverage (Supplementary Methods; Supplementary Figure S4).

4.4. Reconstruction of Phenotype Evolution

Ancestral character states for body shape and colour were reconstructed using two approaches: a Bayesian Markov chain Monte Carlo approach to sample character histories from their posterior probability distribution (stochastic character mapping) [65]. For this we first transformed the phylotranscriptomic tree into an ultrametric tree using the program pyr8s within the iTaxoTools package [66], fixing the root node (*Brachycephalus/Ischnocnema* split) at an age of 35 million years ago based on a comprehensive anuran timetree [67]. We then used the function "make.simmap" from the R package phytools [68], performing 1000 simulations. Furthermore, we explored a parsimony-based [69] optimization as implemented in TNT v.1.5 [29], also based on the (untransformed) phylotranscriptomic tree.

For reconstruction of color phenotypes, we defined species with bright color as those that have at least some part of the body surface colored bright orange: i.e., even some pumpkin-toadlets with dorsal green or brownish color have orange on hands and feet, and/or part of the ventral surface, while orange color is not observed in any of the flea-

toads. Body shape phenotypes were classified relying on previous classifications (e.g., [20]) of species as bufoniform (robust body and pectoral girdle, head as wide as long and short snout) vs. leptodactyliform (slender body and pectoral girdle, head longer than wide, and long snout).

Supplementary Materials: The following are available online at https://www.mdpi.com/article/10.3390/toxins13110816/s1: Supplementary Methods (RNA extraction protocol, PCR tests including new primers design for WANCY region and mitochondrial DNA inference); Figure S1, Species sampled for this study in life. Figure S2, Species tree obtained using ASTRAL. Figure S3, Maximum likelihood tree calculated from mitogenomes. Figure S4, Maximum Likelihood mitochondrial tree for all available *Brachycephalus* species. Figure S5, Eletrophoresis gel showing different lengths of amplified fragments including the tRNA WANCY cluster. Figure S6, Maximum Likelihood phylogenetic inference for Brachycephalus species including mito-genomes obtained here and sequence data from GenBank. Table S1, List of samples used in the present analysis. Table S2. Best partition scheme selected for the mitogenome phylogenetic analysis. Table S3, Genbank accession numbers for species included in the mitochondrial ML and BI trees shown in Figure S4.

Author Contributions: Conceptualization, M.L.L., J.P.C.M., C.F.B.H. and M.V.; methodology, M.L.L. and S.K.; formal analysis, M.L.L., L.R., I.I.; investigation, M.L.L., L.R. and E.S.; resources, J.P.C.M., E.S., O.R.-P., M.S. and L.F.T. Writing—Original draft preparation, M.L.L., J.P.C.M. and M.V.; Writing—Review and Editing, L.R., I.I., E.S., T.H.C., O.R.-P., M.S., L.F.T. and C.F.B.H.; funding acquisition, C.F.B.H. and M.V. All authors have read and agreed to the published version of the manuscript.

Funding: Work in Brazil was supported by a grant from Coordenação de Aperfeiçoamento de Pessoal de Nível Superior (CAPES; 88881.062205/2014-01) to MLL, CFBH, and MV. MLL was supported by the National Council for Scientific and Technological Development (CNPq; #163546/2020-7). JPCM was supported by São Paulo Research Foundation (FAPESP #2018/09691-0). LR was supported by the Deutsche Forschungsgemeinschaft (grant VE247/16-1–HO 3492/6-1) in the framework of the "TaxonOmics" priority program. THC thanks FAPESP (#2015/00461-1, #2016/871-9, #2017/26281-7) and CNPq (#302308/2019-9, #301381/2020-8, #302386/2020-3, #300810/2021-0, #301404/2021-6) for financial support. ORP acknowledges CAPES (#88887.343060/2019-00) for doctoral fellowship. LFT thanks grants and fellowships from FAPESP (#2016/25358-3; #2019/18335-5) and CNPq (#300896/2016-6; #302834/2020-6). MS acknowledges grants from Bahia Research Foundation (FAPESB, #APP0062/2016) and CNPq, for a research fellowship (#304999/2015-6) and funding through a PROTAX-project (#440615/2015-1). CFBH thanks FAPESP grant (#2013/50741-7, #2014/50342-8) and CNPq (#302518/2013-4), for a research fellowship. ES was supported by a grant of the Deutscher Akademischer Austauschdienst.

Institutional Review Board Statement: Experimental procedures were performed according to the regulations specified by the Conselho Nacional de Controle de Experimentação Animal and Ministério da Ciência, Tecnologia e Inovação, Brazil and were approved by the Ethics Committee on Animal Use (CEUA) of Universidade Estadual Paulista, campus Rio Claro (CEUA-IB # 02/2019) on 13 March 2019. Specimens were collected under collecting permits issued by the Brazilian authorities (ICMBio, SISBio #13708-2, #17242-5, #49587-7, and #59889-1).

Informed Consent Statement: Not applicable.

Data Availability Statement: The raw RNAseq reads are available at the National Center for Biotechnology Information (NCBI) Sequence Read Archive (SRA) (BioProject ID number PRJNA742912). The mitochondrial sequences were submitted to GenBank (accession numbers MZ770735 -MZ770752; Table S1). All assemblies, alignments and tree files were uploaded to Figshare under the DOI 10.6084/m9.figshare.14884362.

Acknowledgments: The phylotranscriptomic alignment process benefited from the constant support and assistance of Hervé Philippe to whom we are enormously grateful.

Conflicts of Interest: The authors declare no conflict of interest. The funders had no role in the design of the study; in the collection, analyses, or interpretation of data; in the writing of the manuscript, or in the decision to publish the results.

References

1. Guilford, T.; Dawkins, M. Are warning colors handicaps? *Evolution* **1993**, *47*, 400–416. [CrossRef] [PubMed]
2. Ruxton, G.D.; Sherratt, T.N.; Speed, M.P. *Avoiding Attack: The Evolutionary Ecology of Crypsis, Warning Signals and Mimicry*; Oxford University Press: Oxford, UK, 2004.
3. Mappes, J.; Marples, N.; Endler, J.A. The complex business of survival by aposematism. *Trends Ecol. Evol.* **2005**, *20*, 598–603. [CrossRef] [PubMed]
4. Toledo, L.F.; Haddad, C.F.B. Colors and some morphological traits as defensive mechanisms in anurans. *Int. J. Zool.* **2009**, 910892. [CrossRef]
5. Rojas, B.; Valkonen, J.; Nokelainen, O. Aposematism. *Curr. Biol.* **2015**, *25*, R350–R351. [CrossRef]
6. Summers, K.; Speed, M.P.; Blount, J.D.; Stuckert, A.M.M. Are aposematic signals honest? A review. *J. Evol. Biol.* **2015**, *28*, 1583–1599. [CrossRef] [PubMed]
7. Rojas, B.; Burdfield-Steel, E.; De Pasqual, C.; Gordon, S.; Hernández, L.; Mappes, J.; Nokelainen, O.; Rönkä, K.; Lindstedt, C. Multimodal aposematic signals and their emerging role in mate attraction. *Front. Ecol. Evol.* **2018**, *6*, 1–24. [CrossRef]
8. Santos, J.C.; Cannatella, D.C. Phenotypic integration emerges from aposematism and scale in poison frogs. *Proc. Natl. Acad. Sci. USA* **2011**, *108*, 6175–6180. [CrossRef]
9. Saporito, R.A.; Zuercher, R.; Roberts, M.; Kenneth, G.; Donnelly, M. A Poison Frog *Oophaga pumilio*. *Society* **2007**, *2007*, 1006–1011.
10. Bordignon, D.W.; Caorsi, V.Z.; Colombo, P.; Abadie, M.; Brack, I.V.; Dasoler, B.T.; Borges-Martins, M. Are the unken reflex and the aposematic colouration of red-bellied toads efficient against bird predation? *PLoS ONE* **2018**, *13*, e0193551. [CrossRef]
11. Rebouças, R.; Carollo, A.B.; Freitas, M.O.; Lambertini, C.; Dos Santos, R.M.N.; Toledo, L.F. Is the conspicuous dorsal coloration of the atlantic forest pumpkin toadlets aposematic? *Salamandra* **2019**, *55*, 39–47.
12. Hagemann, S.; Pröhl, H. Mitochondrial paraphyly in a polymorphic poison frog species (Dendrobatidae; *D. pumilio*). *Mol. Phylogenet. Evol.* **2007**, *45*, 740–747. [CrossRef]
13. Rodríguez, A.; Mundy, N.I.; Ibáñez, R.; Pröhl, H. Being red, blue and green: The genetic basis of coloration differences in the strawberry poison frog (*Oophaga pumilio*). *BMC Genom.* **2020**, *21*, 1–16. [CrossRef]
14. Rudh, A.; Qvarnström, A. Adaptive colouration in amphibians. *Semin. Cell Dev. Biol.* **2013**, *24*, 553–561. [CrossRef] [PubMed]
15. Hanifin, C.T. The chemical and evolutionary ecology of tetrodotoxin (TTX) toxicity in terrestrial vertebrates. *Mar. Drugs* **2010**, *8*, 577–593. [CrossRef] [PubMed]
16. AmphibiaWeb. University of California: Berkeley, CA, USA. Available online: https://amphibiaweb.org (accessed on 1 September 2021).
17. Bornschein, M.R.; Pie, M.R.; Teixeira, L. Conservation status of *Brachycephalus* toadlets (Anura: Brachycephalidae) from the Brazilian Atlantic rainforest. *Diversity* **2019**, *11*, 150. [CrossRef]
18. Clemente-Carvalho, R.B.G.; Klaczko, J.; Ivan Perez, S.; Alves, A.C.R.; Haddad, C.F.B.; Dos Reis, S.F. Molecular phylogenetic relationships and phenotypic diversity in miniaturized toadlets, genus *Brachycephalus* (Amphibia: Anura: Brachycephalidae). *Mol. Phylogenet. Evol.* **2011**, *61*, 79–89. [CrossRef]
19. Condez, T.H.; Haddad, C.F.B.; Zamudio, K.R. Historical biogeography and multi-trait evolution in miniature toadlets of the genus *Brachycephalus* (Anura: Brachycephalidae). *Biol. J. Linn. Soc.* **2020**, *129*, 664–686. [CrossRef]
20. dos Reis, S.F.; Clemente-Carvalho, R.B.G.; dos Santos, C.M.S.F.F.; Lopes, R.T.; Von Zuben, F.J.; Laborda, P.R.; Perez, S.I. Skull diversity and evolution in miniaturized amphibians, genus *Brachycephalus* (Anura: Brachycephalidae). *Anat. Rec.* **2020**, *304*, 1–15. [CrossRef]
21. Pires, O.R.; Sebben, A.; Schwartz, E.F.; Morales, R.A.V.; Bloch, C.; Schwartz, C.A. Further report of the occurrence of tetrodotoxin and new analogues in the Anuran family Brachycephalidae. *Toxicon* **2005**, *45*, 73–79. [CrossRef]
22. Chimetto Tonon, L.A.; Rua, C.; Crnkovic, C.M.; Bernardi, D.I.; Pires Junior, O.R.; Haddad, C.F.B.; Pedrosa, C.S.G.; Souza, L.R.Q.; Rehen, S.K.; de Azevedo, G.P.R.; et al. Microbiome associated with the tetrodotoxin-bearing anuran *Brachycephalus pitanga*. *Toxicon* **2021**, *203*, 139–146. [CrossRef]
23. Arcanjo, D.D.R.; Vasconcelos, A.G.; Comerma-Steffensen, S.G.; Jesus, J.R.; Silva, L.P.; Pires, O.R.; Costa-Neto, C.M.; Oliveira, E.B.; Migliolo, L.; Franco, O.L.; et al. A novel vasoactive proline-rich oligopeptide from the skin secretion of the frog *Brachycephalus ephippium*. *PLoS ONE* **2015**, *10*, e0145071. [CrossRef]
24. Hanken, J. Adaptation of bone growth to miniaturization of body size. *Bone* **1993**, *7*, 79–104.
25. Clemente-Carvalho, R.B.G.; Antoniazzi, M.M.; Jared, C.; Haddad, C.F.B.; Alves, A.C.R.; Rocha, H.S.; Pereira, G.R.; Oliveira, D.F.; Lopes, R.T.; dos Reis, S.F. Hyperossification in miniaturized toadlets of the genus *Brachycephalus* (Amphibia: Anura: Brachycephalidae): Microscopic structure and macroscopic patterns of variation. *J. Morphol.* **2009**, *270*, 1285–1295. [CrossRef]
26. Condez, T.H.; Monteiro, J.P.C.; Malagoli, L.R.; Trevine, V.C.; Schunck, F.; Garcia, P.C.A.; Haddad, C.F.B. Notes on the hyperossified pumpkin toadlets of the genus *Brachycephalus* (Anura: Brachycephalidae) with the Description of a New Species. *Herpetologica* **2021**, *77*, 176–194. [CrossRef]
27. Folly, M.; de Luna-Dias, C.; Miguel, I.R.; Ferreira, J.C.; Machado, A.; Tadeu Lopes, R.; Pombal, J.P. Tiny steps towards greater knowledge: An osteological review with novel data on the Atlantic Forest toadlets of the *Brachycephalus ephippium* species group. *Acta Zool.* **2021**, 1–35. [CrossRef]
28. Pie, M.R.; Faircloth, B.C.; Ribeiro, L.F.; Bornschein, M.R.; Mccormack, J.E. Phylogenomics of montane frogs of the Brazilian Atlantic Forest is consistent with isolation in sky islands followed by climatic stability. *Biol. J. Linn. Soc.* **2018**, 72–82. [CrossRef]

29. Goloboff, P.A.; Catalano, S.A. TNT version 1.5, including a full implementation of phylogenetic morphometrics. *Cladistics* **2016**, *32*, 221–238. [CrossRef] [PubMed]
30. Irisarri, I.; Mauro, D.S.; Abascal, F.; Ohler, A.; Vences, M.; Zardoya, R. The origin of modern frogs (Neobatrachia) was accompanied by acceleration in mitochondrial and nuclear substitution rates. *BMC Genom.* **2012**, *13*, 1–19. [CrossRef] [PubMed]
31. Zhang, P.; Liang, D.; Mao, R.L.; Hillis, D.M.; Wake, D.B.; Cannatella, D.C. Efficient sequencing of anuran mtDNAs and a mitogenomic exploration of the phylogeny and evolution of frogs. *Mol. Biol. Evol.* **2013**, *30*, 1899–1915. [CrossRef] [PubMed]
32. Kurabayashi, A.; Sumida, M. Afrobatrachian mitochondrial genomes: Genome reorganization, gene rearrangement mechanisms, and evolutionary trends of duplicated and rearranged genes. *BMC Genom.* **2013**, *14*. [CrossRef]
33. Mueller, R.L.; Boore, J.L. Molecular mechanisms of extensive mitochondrial gene rearrangement in plethodontid salamanders. *Mol. Biol. Evol.* **2005**, *22*, 2104–2112. [CrossRef] [PubMed]
34. San Mauro, D.; Gower, D.J.; Zardoya, R.; Wilkinson, M. A hotspot of gene order rearrangement by tandem duplication and random loss in the vertebrate mitochondrial genome. *Mol. Biol. Evol.* **2006**, *23*, 227–234. [CrossRef] [PubMed]
35. Xia, Y.; Zheng, Y.; Miura, I.; Wong, P.B.Y.; Murphy, R.W.; Zeng, X. The evolution of mitochondrial genomes in modern frogs (Neobatrachia): Nonadaptive evolution of mitochondrial genome reorganization. *BMC Genom.* **2014**, *15*, 1–15. [CrossRef] [PubMed]
36. Monteiro, J.P.C.; Condez, T.H.; Garcia, P.C.A.; Comitti, E.J.; Amaral, I.B.; Haddad, C.F.B. A new species of *Brachycephalus* (Anura, Brachycephalidae) from the coast of Santa Catarina State, Southern Atlantic Forest, Brazil. *Zootaxa* **2018**, *4407*, 483–505. [CrossRef]
37. Pie, M.R.; Ribeiro, L.F.; Confetti, A.E.; Nadaline, M.J.; Bornschein, M.R. A new species of *Brachycephalus* (Anura: Brachycephalidae) from southern Brazil. *PeerJ* **2018**, *2018*, 1–27. [CrossRef]
38. Vences, M.; Sanchez, E.; Hauswaldt, J.S.; Eikelmann, D.; Rodríguez, A.; Carranza, S.; Donaire, D.; Gehara, M.; Helfer, V.; Lötters, S.; et al. Nuclear and mitochondrial multilocus phylogeny and survey of alkaloid content in true salamanders of the genus *Salamandra* (Salamandridae). *Mol. Phylogenet. Evol.* **2014**, *73*, 208–216. [CrossRef] [PubMed]
39. Burgon, J.D.; Vences, M.; Steinfartz, S.; Bogaerts, S.; Bonato, L.; Donaire-Barroso, D.; Martínez-Solano, I.; Velo-Antón, G.; Vieites, D.R.; Mable, B.K.; et al. Phylogenomic inference of species and subspecies diversity in the Palearctic salamander genus Salamandra. *Mol. Phylogenet. Evol.* **2021**, *157*. [CrossRef]
40. Rancilhac, L.; Irisarri, I.; Angelini, C.; Arntzen, J.W.; Babik, W.; Bossuyt, F.; Künzel, S.; Lüddecke, T.; Pasmans, F.; Sanchez, E.; et al. Phylotranscriptomic evidence for pervasive ancient hybridization among Old World salamanders. *Mol. Phylogenet. Evol.* **2021**, *155*. [CrossRef]
41. Klonoski, K.; Bi, K.; Rosenblum, E.B. Phenotypic and genetic diversity in aposematic Malagasy poison frogs (genus *Mantella*). *Ecol. Evol.* **2019**, *9*, 2725–2742. [CrossRef]
42. Crottini, A.; Orozco-Terwengel, P.; Rabemananjara, F.C.E.; Susanne Hauswaldt, J.; Vences, M. Mitochondrial introgression, color pattern variation, and severe demographic bottlenecks in three species of malagasy poison frogs, genus *Mantella*. *Genes* **2019**, *10*, 317. [CrossRef]
43. Goutte, S.; Mason, M.J.; Christensen-Dalsgaard, J.; Montealegre-Z, F.; Chivers, B.D.; Sarria-S, F.A.; Antoniazzi, M.M.; Jared, C.; Almeida Sato, L.; Felipe Toledo, L. Evidence of auditory insensitivity to vocalization frequencies in two frogs. *Sci. Rep.* **2017**, *7*, 1–9. [CrossRef]
44. Padial, J.M.; Grant, T.; Frost, D.R. Molecular systematics of terraranas (Anura: Brachycephaloidea) with an assessment of the effects of alignment and optimality criteria. *Zootaxa* **2014**, *3825*, 1–132. [CrossRef]
45. Bolger, A.M.; Lohse, M.; Usadel, B. Trimmomatic: A flexible trimmer for Illumina sequence data. *Bioinformatics* **2014**, *30*, 2114–2120. [CrossRef] [PubMed]
46. Grabherr, M.G.; Haas, B.J.; Yassour, M.; Levin, J.Z.; Thompson, D.A.; Amit, I.; Adiconis, X.; Fan, L.; Raychowdhury, R.; Zeng, Q. Trinity: Reconstructing a full-length transcriptome without a genome from RNA-Seq data. *Nat. Biotechnol.* **2013**, *29*, 644–652. [CrossRef] [PubMed]
47. Haas, B.J.; Papanicolaou, A.; Yassour, M.; Grabherr, M.; Blood, P.D.; Bowden, J.; Couger, M.B.; Eccles, D.; Li, B.; Lieber, M.; et al. De novo transcript sequence reconstruction from RNA-seq using the Trinity platform for reference generation and analysis. *Nat. Protoc.* **2013**, *8*, 1494–1512. [CrossRef] [PubMed]
48. Irisarri, I.; Baurain, D.; Brinkmann, H.; Delsuc, F.; Sire, J.Y.; Kupfer, A.; Petersen, J.; Jarek, M.; Meyer, A.; Vences, M.; et al. Phylotranscriptomic consolidation of the jawed vertebrate timetree. *Nat. Ecol. Evol.* **2017**, *1*, 1370–1378. [CrossRef] [PubMed]
49. Yang, Y.; Smith, S.A. Orthology inference in nonmodel organisms using transcriptomes and low-coverage genomes: Improving accuracy and matrix occupancy for phylogenomics. *Mol. Biol. Evol.* **2014**, *31*, 3081–3092. [CrossRef]
50. Stamatakis, A. RAxML version 8: A tool for phylogenetic analysis and post-analysis of large phylogenies. *Bioinformatics* **2014**, *30*, 1312–1313. [CrossRef] [PubMed]
51. Katoh, K.; Standley, D.M. MAFFT multiple sequence alignment software version 7: Improvements in performance and usability. *Mol. Biol. Evol.* **2013**, *30*, 772–780. [CrossRef]
52. Roure, B.; Rodriguez-Ezpeleta, N.; Philippe, H. SCaFoS: A tool for selection, concatenation and fusion of sequences for phylogenomics. *BMC Evol. Biol.* **2007**, *7*, 1–12. [CrossRef]
53. Nguyen, L.T.; Schmidt, H.A.; Von Haeseler, A.; Minh, B.Q. IQ-TREE: A fast and effective stochastic algorithm for estimating maximum-likelihood phylogenies. *Mol. Biol. Evol.* **2015**, *32*, 268–274. [CrossRef] [PubMed]

54. Chernomor, O.; Von Haeseler, A.; Minh, B.Q. Terrace aware data structure for phylogenomic inference from supermatrices. *Syst. Biol.* **2016**, *65*, 997–1008. [CrossRef]
55. Kalyaanamoorthy, S.; Minh, B.Q.; Wong, T.K.F.; Von Haeseler, A.; Jermiin, L.S. ModelFinder: Fast model selection for accurate phylogenetic estimates. *Nat. Methods* **2017**, *14*, 587–589. [CrossRef] [PubMed]
56. Mirarab, S.; Warnow, T. ASTRAL-II: Coalescent-based species tree estimation with many hundreds of taxa and thousands of genes. *Bioinformatics* **2015**, *31*, i44–i52. [CrossRef] [PubMed]
57. Davis, M.P.A.; Van Dongen, S.; Abreu-Goodger, C.; Bartonicek, N.; Enright, A.J. Kraken: A set of tools for quality control and analysis of high-throughput sequence data. *Methods* **2013**, *63*, 41–49. [CrossRef]
58. Hahn, C.; Bachmann, L.; Chevreux, B. Reconstructing mitochondrial genomes directly from genomic next-generation sequencing reads—A baiting and iterative mapping approach. *Nucleic Acids Res.* **2013**, *41*, e129. [CrossRef]
59. Chevreux, B.; Wetter, T.; Suhai, S. Genome sequence assembly using trace signals and additional sequence information. In Proceedings of the German Conference on Bioinformatics (GCB99), Hannover, Germany, 4–6 October 1999.
60. Pie, M.R.; Ströher, P.R.; Bornschein, M.R.; Ribeiro, L.F.; Faircloth, B.C.; McCormack, J.E. The mitochondrial genome of *Brachycephalus brunneus* (Anura: Brachycephalidae), with comments on the phylogenetic position of Brachycephalidae. *Biochem. Syst. Ecol.* **2017**, *71*, 26–31. [CrossRef]
61. Meng, G.; Li, Y.; Yang, C.; Liu, S. MitoZ: A toolkit for animal mitochondrial genome assembly, annotation and visualization. *Nucleic Acids Res.* **2019**, *47*, e63. [CrossRef]
62. Kearse, M.; Moir, R.; Wilson, A.; Stones-Havas, S.; Cheung, M.; Sturrock, S.; Buxton, S.; Cooper, A.; Markowitz, S.; Duran, C.; et al. Geneious Basic: An integrated and extendable desktop software platform for the organization and analysis of sequence data. *Bioinformatics* **2012**, *28*, 1647–1649. [CrossRef]
63. Vaidya, G.; Lohman, D.J.; Meier, R. SequenceMatrix: Concatenation software for the fast assembly of multigene datasets with character set and codon information. *Cladistics* **2011**, *27*, 171–180. [CrossRef]
64. Lanfear, R.; Frandsen, P.B.; Wright, A.M.; Senfeld, T.; Calcott, B. Partitionfinder 2: New methods for selecting partitioned models of evolution for molecular and morphological phylogenetic analyses. *Mol. Biol. Evol.* **2017**, *34*, 772–773. [CrossRef] [PubMed]
65. Huelsenbeck, J.P.; Nielsen, R.; Bollback, J.P. Stochastic mapping of morphological characters. *Syst. Biol.* **2003**, *52*, 131–158. [CrossRef] [PubMed]
66. Vences, M.; Miralles, A.; Brouillet, S.; Ducasse, J.; Fedosov, A.; Kharchev, V.; Kostadinov, I.; Kumari, S.; Patmanidis, S.; Scherz, M.D.; et al. iTaxoTools 0.1: Kickstarting a specimen-based software toolkit for taxonomists. *Megataxa* **2021**, *6*, 77–92. [CrossRef]
67. Feng, Y.J.; Blackburn, D.C.; Liang, D.; Hillis, D.M.; Wake, D.B.; Cannatella, D.C.; Zhang, P. Phylogenomics reveals rapid, simultaneous diversification of three major clades of Gondwanan frogs at the Cretaceous–Paleogene boundary. *Proc. Natl. Acad. Sci. USA* **2017**, *114*, E5864–E5870. [CrossRef]
68. Revell, L.J. phytools: An R package for phylogenetic comparative biology (and other things). *Methods Ecol. Evol.* **2012**, *3*, 217–223. [CrossRef]
69. Fitch, W.M. Toward defining the course of evolution: Minimum change for a specific tree topology. *Syst. Zool.* **1971**, *20*, 406–416. [CrossRef]

toxins

MDPI

Supplementary Materials: Initial Phylotranscriptomic Confirmation of Homoplastic Evolution of the Conspicuous Coloration and Bufoniform Morphology of Pumpkin-Toadlets in the Genus *Brachycephalus*

Mariana L. Lyra, Juliane P. C. Monteiro, Loïs Rancilhac, Iker Irisarri, Sven Künzel, Eugenia Sanchez, Thais H. Condez, Omar Rojas-Padilla, Mirco Solé, Luís Felipe Toledo, Célio F. B. Haddad and Miguel Vences

Supplementary Methods

RNA extraction protocol:

Tissues (20–100 mg) from each sample were homogenized in 2 mL tubes with steel beads in 1 mL TRIzol using the tissue lyser Precellys (speed 6000, 2× 55 sec in between 10 sec break). The samples were centrifuged for 10 min at 12,000 g at 4 °C. The solution was transferred to a new tube and incubated at room temperature (RT) for 5 min, after which 200 µl chloroform was added, samples were vortexed for 15 sec, incubated for 3 min at RT and centrifuged for 15 min at 12,000 g at 4 °C. The upper phase was transferred to a new tube and 500 µL isopropanol was added. The solution was incubated for 10 min at RT and centrifuged for 15 min at 12,000 g at 4 °C. The supernatant was removed, 1 ml 75% EtOH was added to the pellet (using DEPC water) and the sample was vortexed until the pellet was resuspended. The samples were centrifuged for 5 min at 7500 g at 4 °C and the supernatant was removed. The pellet was dried and dissolved in DEPC water. The RNA was precipitated by adding 200 µL 5M LiCl solution and incubated for 1.5 h at −20 °C. After incubation, the solution was centrifuged for 20 min at 14,000 g at 4 °C. The supernatant was removed, the pellet washed with 500 µL 75% EtOH and then centrifuged for 10 min at 14,000 g at 4 °C. The pellet was again dried and dissolved in DEPC water.

Mitochondrial tRNA WANCY cluster amplification:

For verifying the gene order arrangement, independently of the *in silico* mitogenome DNA assembly algorithms, we performed amplification tests to assess the length variation of the WANCY region from different species. We first extracted total DNA from new individuals of the analyzed species using a standard ammonium acetate precipitation method [S1] (adapted by [S2]). Then, we designed two new primers flanking the WANCY region based on the sequences obtained from mitogenomes, one at the 3′ region of the ND2 gene (ND2_F2L_Brachy: 5′-ACCYTRGCCCCAAAY-TCAAC-3′) and one at the 5′ region of the COI gene (CO1_RH_Brachy: 5′-ARATTATYACGAAGGCGTG-3′). Finally, we PCR amplified the specimens using the following protocol: The amplification reactions were carried out in a 20-µL reaction, using the Ampliqon Taq DNA Polymerase Master Mix, 0.5 uL of each primer (10 µM) and 1 uL of extracted DNA. The thermal cycling conditions were: 3 min at 95 °C, 40 cycles of 20 s at 95 °C, 20 s at 50 °C, and 1min 20 s at 68 °C, and a final extension of 3 min at 68 °C.

The fragments were separated by electrophoresis in 1.5 % agarose gel, stained with GelRed (Bioyium inc.). The size of the fragments was estimated by comparison with the molecular size standard DNA Ladder GeneRuler 1 Kb (Thermo Scientific).

Mitochondrial phylogenetic inference for the genus Brachycephalus

To infer the mitochondrial phylogenetic relationship between species of the genus *Brachycephalus*, we used two optimality criteria: Bayesian inference (BI) and maximum likelihood (ML). For both analyses we gathered mitochondrial sequences (fragments of the 12S rRNA gene, 16S rRNA gene and Cytochrome B) from GenBank for one or two individuals per species available (Table S4) and extracted only these genes from the mitogenomes available We only used the mitochondrial sequences to avoid many missing data on data matrix. Final matrix contained 47 individuals and 3850 base-pairs.

Genes were aligned using MAFFT v7.130b [S3] and concatenated using SequenceMatrix [S4]. We computed BI analysis in MrBayes 3.2.6 [S5] using two independent runs of 10 × 106 generations, starting with random trees and eight Markov chains (one cold), sampled every 1000 generations. We performed the run using GTR+Γ model. We used the standard deviation of split frequencies (<0.01) and Estimated Sample Size (ESS > 200) to assess run convergence. We discarded 25% of generations and trees as burnin and obtained he 50% majority rule consensus tree. We computed ML analysis in RAxML v.8.2.10 [50], using GTR+Γ model, searching the most likely tree 1000 times and conducting 1000 non-parametric bootstrap replicates. We used *Ischnocnema henselii* as the root for all analyses, and we drew the trees using FigTree 1.4.2 [S6]. We performed all phylogenetic analyses using the CIPRES Science gateway portal [S7].

Supplementary Materials References

S1. Maniatis, T.; Fritsch, E.F.; Sambrook, J. *Molecular Cloning: A Laboratory Manual*. Cold Spring Harbor Laboratory Press, New York, 1982.

S2. Lyra, M.L.; Haddad, C.F.B.; de Azeredo-Spin, M.L. Toward defining the course of evolution: minimum change for a specific tree topology. *Mol. Ecol.* **2017**, *17*, 966–980, doi: 10.1111/1755-0998.12648.

S3. Katoh, K.; Standley, D.M. MAFFT multiple sequence alignment software version 7: improvements in performance and usability. *Mol. Biol. Evol.* **2013**, *30*, 772–780, doi:10.1093/molbev/mst010.

S4. Vaidya, G.; Lohman, D.J.; Meier, R. SequenceMatrix: concatenation software for the fast assembly of multigene datasets with character set and codon information. *Cladistics* **2011**, *27*, 171–180.

S5. Ronquist F.; Teslenko, M.; Van Der Mark, P.; Ayres, D.L.; Darling, A.; Hohna, S.; Larget, B.; Liu, L.; Suchard, M.A; Huelsenbeck, J.P. Mrbayes 3.2: efficient Bayesian phylogenetic inference and model choice across a large model space. *Syst. Biol.* **2012**, 61, 539–542, doi: 10.1093/sysbio/sys029.

S6. Rambaut, A.; Suchard, M.A.; Xie, D.; Drummond, A.J. Tracer v1.6. **2014**. University of Edinburgh, UK.

S7. Miller, M.A.; Pfeiffer, W.; Schwartz, T. Creating the CIPRES Science Gateway for inference of large phylogenetic trees. *Proc. Gatew. Comput. Environ. Workshop*, 2010, 1–8, doi: 10.1109/GCE.2010.5676129.



Figure S1. Species sampled for this study as representatives of the main clades within *Brachycephalus* (A–K) and species used as outgroup taxon, *Ischnocnema henselii* (L). The flea-toads with leptodactyliform body plan: (A) *B. hermogenesi*; (B) *B. pulex*; and (C) *B. sulfuratus*. The pumpkin-toadlets with bufoniform body plan of the *B. ephippium* group (D–E) and of the *B. pernix* group (F–K): (D) *B. pitanga*; (E) *B. rotenbergae*; (F–H) *B. actaeus*, morphotypes green, brownish, and orange, respectively; (I) *B. albolineatus*; (J) *B. auroguttatus*; and (K) *B. quiririensis*. Credits for the photos: Condez, TH (A–C, E, F, H, J, and K); Monteiro, JPC (D); and Vences, M (G, I, and L).

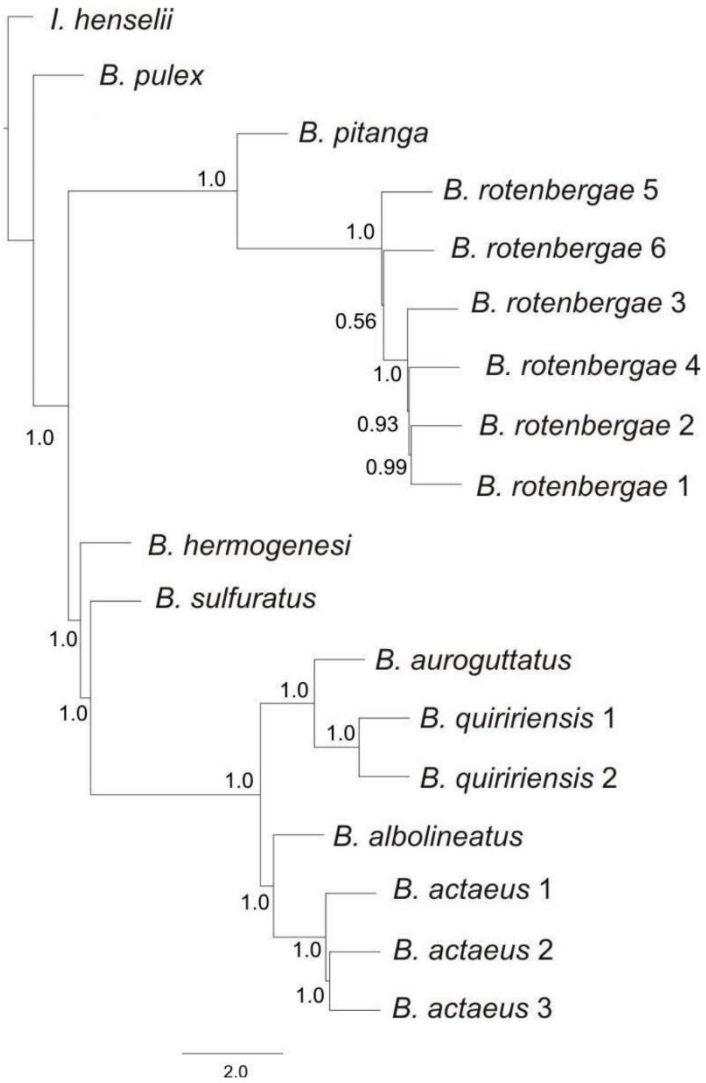


Figure S2. Species tree obtained using ASTRAL from 5296 gene trees of nuclear-encoded protein-coding markers derived from transcriptomes. Numbers at nodes show local posterior probabilities.



Figure S3. Maximum Likelihood tree calculated from a concatenated alignment of 13,938 nucleotide positions of the two rRNA genes and the 13 protein coding genes from full mitochondrial genomes. The tree represents a detailed version of Fig. 3A in the main paper, and is here shown to give full information on outgroup and node support values, as non-parametric bootstrap support shown at each node.

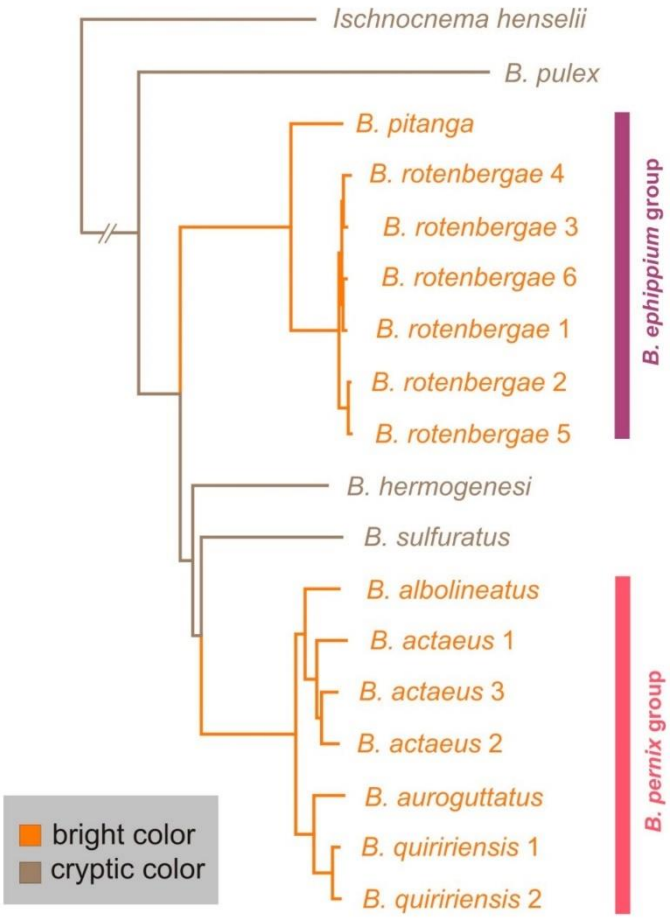


Figure S4. *Brachycephalus* phenotype reconstructed under a parsimony approach using TNT (Fitch optimization). Identical reconstructions were obtained for color (shown), and for bufoniform vs. leptodactyliform morphology. The character state "bright color" defines species that have at least some part of the body surface colored bright orange (dorsum, hands and feet, or ventral surface).

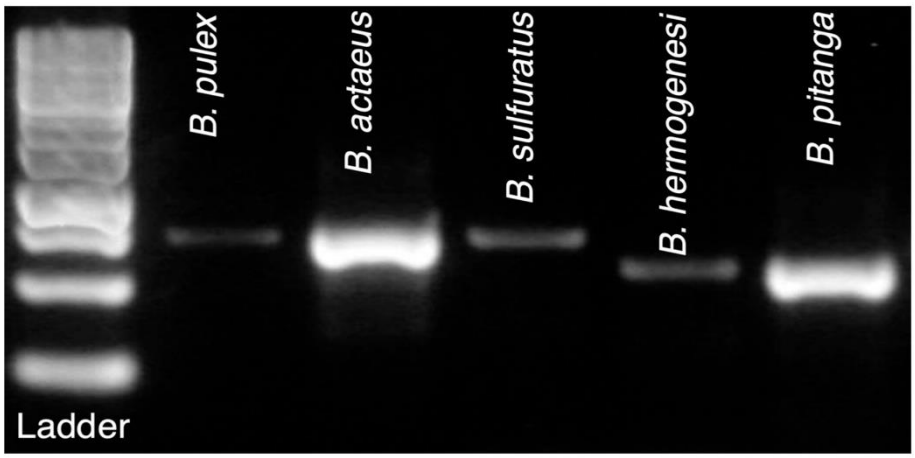


Figure S5. Electrophoresis 1.5% agarose gel showing different length fragment for the tRNA WANCY cluster region of different *Brachycephalus* species. Both *B. hermogenesi* and *B. pitanga* [resented smaller fragments as expected based on the tRNAs translocations.

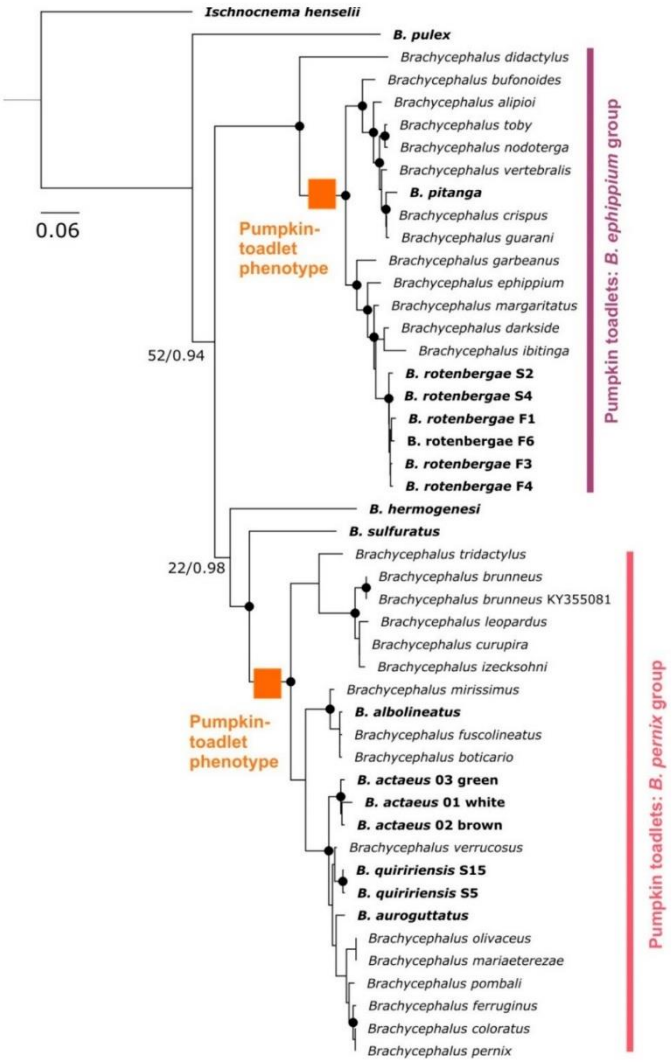


Figure S6. Maximum Likelihood phylogenetic inference for *Brachycephalus* species including mitogenomes obtained here and sequence data from GenBank (see Table S3 for additional accession numbers). Maximum likelihood non-parametric bootstrap support (BS) and posterior probabilities (PP) are shown near the branches for deep nodes (to the left and to the right of the bar, respectively). Black dots indicate fully supported clades (BS=100%, PP=1.0) and support values are not shown for nodes with low support (BS <0.9; PP<0.95) within each pumpkin-toadlet clade are not shown. Taxa in bold are those with complete mitogenomes obtained in the present study. Colored squares mark the two clades of pumpkin toadlet phenotype but do not symbolize evolutionary transitions.**Table S1.** List of samples used in the present analysis, their geographic provenance, sample/voucher number, body plan characteristic, mitogenome accession number and amont of reads analysed. Note that for most specimens, the full sample was used for DNA/RNA extraction and no separate voucher specimen was preserved. mtDNA reads: total number of reads recovered with MITObim; Total reads: Total of interleaved and non-duplicated RNAseq reads obtained for each specie.

Table S1. List of samples used in the present analysis, their geographic provenance, sample/voucher number, body plan characteristic, mitogenome accession number and amont of reads analysed. Note that for most specimens, the full sample was used for DNA/RNA extraction and no separate voucher specimen was preserved. mtDNA reads: total number of reads recovered with MITObim; Total reads: Total of interleaved and non-duplicated RNAseq reads obtained for each specie.

Species	Locality	Sample ID	Latitude	Longitude	Name in trees	Body plan	mtDNA acc. No.	mtDNA reads	Total reads
Ischnocnema henselii	Morro Boa Vista, Jaraguá do Sul, SC	Feb2017-RNA-A-FeedExp-C	-26.51611°	-49.05389°	*I. henselii*	--	MZ770752	426708	25247956
Brachycephalus pulex	PN Serra das Lontras, Arataca, BA	MVTIS 3204	-15.16198	-39.34381	*B. pulex*	leptodactyliform	MZ770742	266248	17702335
Brachycephalus hermogenesi	PESM Santa Virginia, São Luiz do Paraitinga, SP	MVTIS 3210	-23.33867°	-45.14815°	*B. hermogenesi*	leptodactyliform	MZ770740	618797	38589735
Brachycephalus sulfuratus	Casarão Backmeyer, São Francisco do Sul, SC	Feb2017-RNA44	-26.17528°	-48.71222°	*B. sulfuratus*	leptodactyliform	MZ770751	322432	12120096

Copyright: © 2021 by the authors. Licensee MDPI, Basel, Switzerland. This article is an open access article distributed under the terms and conditions of the Creative Commons Attribution (CC BY) license (https://creativecommons.org/licenses/by/4.0/).

Brachycephalus actaeus	Morro do Cantagalo, São Francisco do Sul, SC	MVTIS 3206 white strip	-26.18928°	-48.73229°	*B. actaeus* 1	bufoniform	MZ770735	447693	46194049
Brachycephalus actaeus	Estrada do Saí, São Francisco do Sul, SC	Feb2017-RNA56-green	-26.20167°	-48.69361°	*B. actaeus* 2	bufoniform	MZ770737	341395	17444017
Brachycephalus actaeus	Casarão Backmeyer, São Francisco do Sul, SC	Feb2017-RNA58-orange/brown	-26.17528°	-48.71222	*B. actaeus* 3	bufoniform	MZ770736	315185	14296301
Brachycephalus albolineatus	Morro Boa Vista, Jaraguá do Sul, SC	Feb2017-RNA02	-26.51611°	-49.05389°	*B. albolineatus*	bufoniform	MZ770738	306481	13310687
Brachycephalus auroguttatus	Pedra da Tartaruga, Garuva, SC	MVTIS 3207	-26.00583°	-48.92361°	*B. auroguttatus*	bufoniform	MZ770739	395248	31667155
Brachycephalus quiririensis	Campos do Quiriri, Garuva, SC	Feb2017-RNA-D FeedExp	-26.02556°	-48.97333°	*B. quiririensis* 1	bufoniform	MZ770743	377825	30154214
Brachycephalus quiririensis	Campos do Quiriri, Garuva, SC	Feb2017-RNA-C FeedExp	-26.02556°	-48.97333°	*B. quiririensis* 2	bufoniform	MZ770744	221775	18034035
Brachycephalus pitanga	PESM Santa Virginia, São Luiz do Paraitinga, SP	MVTIS 3205	-23.33°	-45.14°	*B. pitanga*	bufoniform	MZ770741	1132042	38736692
Brachycephalus rotenbergae	Mogi das Cruzes, SP, Brazil	MVTIS 3213	-23.49°	-46.19°	*B. rotenbergae* 1	bufoniform	MZ770745	1244504	24982826
Brachycephalus rotenbergae	Mogi das Cruzes, SP, Brazil	Brachy2 Ftcontrol	-23.49°	-46.19°	*B. rotenbergae* 2	bufoniform	MZ770749	711077	15084723
Brachycephalus rotenbergae	Mogi das Cruzes, SP, Brazil	MVTIS 3214	-23.49°	-46.19°	*B. rotenbergae* 3	bufoniform	MZ770746	1141170	21059190
Brachycephalus rotenbergae	Mogi das Cruzes, SP, Brazil	MVTIS 3215	-23.49°	-46.19°	*B. rotenbergae* 4	bufoniform	MZ770747	818811	33299329

Brachycephalus rotenbergae	Mogi das Cruzes, SP, Brazil	Brachy3 FT-infected	-23.49°	-46.19°	*B. rotenbergae* 5	bufoniform	MZ770750	904389	13876164
Brachycephalus rotenbergae	Mogi das Cruzes, SP, Brazil	MVTIS 3216	-23.49°	-46.19°	*B. rotenbergae* 6	bufoniform	MZ770748	1111026	21930389

Table S2. Best partition scheme selected with PartitionFinder2 for mitogenome tree analyses.

Subset	Best Model	# sites	Partition
1	GTR+G	977	12S
2	GTR+G	1664	16S
3	GTR+I+G	1127	COIII_codon_pos1, ND4_codon_pos1, ND1_codon_pos1, ND4L_codon_pos1
4	GTR+G	1627	COIII_codon_pos2, ND5_codon_pos2, ND4_codon_pos2, ND1_codon_pos2
5	GTR+I+G	864	ND1_codon_pos3, ND4_codon_pos3, ND4L_codon_pos3
6	GTR+G	575	ATP6_codon_pos1, ND2_codon_pos1
7	GTR+G	1171	CytB_codon_pos2, ND4L_codon_pos2, ND2_codon_pos2, ATP6_codon_pos2, ND3_codon_pos2
8	GTR+I+G	399	ND2_codon_pos3, ATP8_codon_pos3
9	GTR+G	513	COI_codon_pos1
10	GTR+I+G	513	COI_codon_pos2
11	GTR+I+G	512	COI_codon_pos3
12	GTR+I+G	781	COII_codon_pos1, CytB_codon_pos1, ND3_codon_pos1, ATP8_codon_pos2
13	GTR+G	229	COII_codon_pos2
14	GTR+I+G	829	COII_codon_pos3, ND5_codon_pos3
15	GTR+I+G	55	ATP8_codon_pos1
16	GTR+I+G	345	ATP6_codon_pos3, ND3_codon_pos3
17	GTR+I+G	643	COIII_codon_pos3, CytB_codon_pos3
18	GTR+G	601	ND5_codon_pos1
19	GTR+G	171	ND6_codon_pos1
20	GTR+G	171	ND6_codon_pos2
21	GTR+I+G	171	ND6_codon_pos3

Table S3. GenBank accession number for sequences included in the *Brachycephalus* spp. tree analyses. * mitogenome available: for this specimen we also included all other coding genes in the Maximum likelihood phylogenetic inference analyses.

Terminal name	Body plan	Voucher	12S rRNA	16S rRNA	CytB
Brachycephalus didactylus	leptodactyliform	MNRJ68818	MK697418.1	MK697363.1	MK697465.1
Brachycephalus alipioi	bufoniform	CFBH11759	MK697414.1	MK697360.1	MK697462.1
Brachycephalus boticario	bufoniform	Bboticario1		KX025370.1	
Brachycephalus brunneus	bufoniform		HQ435677.1	HQ435691.1	HQ435704.1
*Brachycephalus brunneus**	bufoniform	mitogenome	KY355081	KY355081	KY355081
Brachycephalus bufonoides	bufoniform	ZUFRJ15424		MH259790	
Brachycephalus coloratus	bufoniform	ind1		MT928335.1	
Brachycephalus crispus	bufoniform	CFBH27859	MK697415.1	MK697361.1	MK697463.1
Brachycephalus curupira	bufoniform	BSalto3		KX025380.1	
Brachycephalus darkside	bufoniform	PPGT600		MT734440.1	
Brachycephalus ephippium	bufoniform	CFBH12355	MK697421.1	MK697367.1	MK697467.1
Brachycephalus ferruginus	bufoniform		HQ435681.1	HQ435695.1	HQ435708.1
Brachycephalus fuscolineatus	bufoniform	Bfuscolineatus5		KX025340.1	
Brachycephalus garbeanus	bufoniform	CFBH12688	MK697424.1	MK697370.1	MK697470.1
Brachycephalus guarani	bufoniform	CFBH12997	MK697425.1	MK697371.1	MK697471.1
Brachycephalus ibitinga	bufoniform	CFBH44449		MT734431.1	
Brachycephalus izecksohni	bufoniform		HQ435683.1	HQ435696.1	HQ435710.1
Brachycephalus leopardus	bufoniform	Bleopardus1		KX025239.1	
Brachycephalus margaritatus	bufoniform	CFBH2420	MK697427.1	MK697377.1	MK697475.1
Brachycephalus mariaterezae	bufoniform	Bmariaterezae1		KX025316.1	
Brachycephalus mirissimus	bufoniform			MH136570.1	
Brachycephalus nodoterga	bufoniform	CFBH34912	MK697429.1	MK697379.1	MK697477.1
Brachycephalus olivaceus	bufoniform	CFBH40440	MK697432	MG889435.1	
Brachycephalus pernix	bufoniform		HQ435685.1	HQ435698.1	HQ435712.1
Brachycephalus pombali	bufoniform		HQ435687.1	HQ435700.1	HQ435714.1
Brachycephalus toby	bufoniform	CFBH44397	MK697436.1	MK697387.1	MK697484.1
Brachycephalus tridactylus	bufoniform	TRID-1		MG889431.1	
Brachycephalus verrucosus	bufoniform	Bverrucosus9		KX025234.1	
Brachycephalus vertebralis	bufoniform	CFBH1389	MK697442.1	MK697393.1	MK697490.1

CAPÍTULO II

Monteiro, J. P. C., Pröhl, H., Lyra, M. L., Brunetti, A. E., Nardin, E. C., Condez, T. H., Haddad, C. F. B., & Rodríguez, A. Expression patterns of melanin-related genes are linked to crypsis and aposematism in a pumpkin toadlet. Submitted to *Molecular Ecology*.

"Padrões de expressão gênica relacionados à melanina estão ligados à crípse e ao aposematismo em um sapinho-pingo-de-ouro"

Resumo

Sinais de cor desempenham papéis fundamentais em diferentes sistemas de comunicação e a evolução desses caracteres tem sido associada à ecologia comportamental, aos processos de produção tegumentar e aos mecanismos perceptivos das espécies envolvidas. Um exemplo notável é a coloração aposemática, ou seja, sinais de advertência, que em anfíbios tem sido predominantemente estudada em sapos-venenosos. Aqui, apresentamos as primeiras informações sobre a base molecular e histológica do polimorfismo de cor dentro de uma espécie miniaturizada de sapinho-pingo-de-ouro (Brachycephalidae), representando potencialmente o menor limiar de tamanho para aposematismo em tetrápodes. *Brachycephalus actaeus* exibe coloração dorsal que varia do verde críptico ao laranja aposemático e nossas descobertas sugerem que os morfos de cor diferem em sua visibilidade para potenciais predadores. O perfil de expressão dos genes relacionados à coloração foi predominantemente associado à síntese de melanina (incluindo *dct*, *edn1*, *mlana*, *oca2*, *pmel*, *slc24a5*, *tyrp1* e *wnt9a*). Além disso, a distribuição e abundância de cromatóforos são variáveis nos diferentes morfos de cor. A regulação positiva de genes de melanina em peles cinza, verde e marrom estava associada a uma maior abundância de melanóforos do que em peles laranja, onde predominam xantóforos. Ao examinar os mecanismos moleculares subjacentes à variação de cor na pele dentro da espécie, nossos resultados fornecem uma base significativa para comparar e compreender o significado adaptativo de sinais de cor em animais.

Expression patterns of melanin-related genes are linked to crypsis and conspicuousness in a pumpkin toadlet

Juliane P. C. Monteiro[1,2,3,4], Heike Pröhl[4], Mariana L. Lyra[5], Andrés E. Brunetti[6,7], Eli C. de Nardin[2], Thais H. Condez[8], Célio F. B. Haddad[2,3], Ariel Rodríguez[4]

[1]Post-graduate Program in Biodiversity, Institute of Biosciences, São Paulo State University (UNESP), Rio Claro, São Paulo, Brazil

[2]Department of Biodiversity and Aquaculture Center (CAUNESP), Institute of Biosciences, São Paulo State University (UNESP), Rio Claro, São Paulo, Brazil

[3]Center for Research on Biodiversity Dynamics and Climate Change, Institute of Biosciences, São Paulo State University (UNESP), Rio Claro, São Paulo, Brazil

[4]Institute of Zoology, University of Veterinary Medicine of Hannover, Hannover, Lower Saxony, Germany

[5]New York University Abu Dhabi, Saadiyat Island, Abu Dhabi, United Arab Emirates

[6]Institute of Subtropical Biology (IBS, UNaM-CONICET), Posadas, Misiones, Argentina

[7]Department of Insect Symbiosis, Max Planck Institute of Chemical Ecology, Jena, Germany

[8]Department of Earth Sciences, Carleton University, Ottawa, Ontario, Canada

Correspondence

Juliane P. C. Monteiro, Department of Biodiversity and Aquaculture Center, Institute of Biosciences, São Paulo State University (UNESP), Rio Claro, São Paulo, 13506-900, Brazil.

Email: julianepmonteiro@gmail.com

Ariel Rodríguez, Institute of Zoology, University of Veterinary Medicine of Hannover, Hannover, Lower Saxony, 30559, Germany.

Email: ariel.rodriguez@tiho-hannover.de

Funding information

This work was supported by grants from the São Paulo Research Foundation to JPCM (FAPESP #2018/09691-0 and #2021/08744-9) and CFBH (FAPESP#2021/10639-5). The work of CFBH and MLL was also funded by The National Council for Scientific and Technological Development (CNPq #306623/2018; CNPq-PDS #163546/2020-7).

The work of AEB was funded by Agencia Nacional de Promoción Científica y Tecnológica (PICT #2020/2939) and Consejo Nacional de Investigaciones Científicas y Técnicas (CONICET #PIP/2021-2023). Sequencing costs were covered by a Deutsche Forschungsgemeinschaft (DFG) research grant to AR (RO5508/2-1), a Deutsche Gesellschaft für Herpetologie und Terrarienkunde (DGHT) grant to HP and JPCM (WP-01/2022), and FAPESP (#2021/08744-9).

Abstract

Color signals play pivotal roles in different communication systems, and the evolution of these characters has been associated with behavioral ecology, integumentary production processes, and perceptual mechanisms of the species involved. Here, we present the first insight into the molecular and histological basis of skin color polymorphism within a miniaturized species of pumpkin toadlet, potentially representing the lowest size threshold for color polytypism in tetrapods. *Brachycephalus actaeus* exhibits a coloration ranging from cryptic green to conspicuous orange skin, and our findings suggest that color morphs differ in their capability to be detected by potential predators. We also found that the distribution and abundance of chromatophores are variable in the different color morphs. The expression pattern of coloration-related genes was predominantly associated with melanin synthesis (including *dct*, *edn1*, *mlana*, *oca2*, *pmel*, *slc24a5*, *tyrp1*, and *wnt9a*). Up-regulation of melanin genes in gray, green, and brown skin was associated with higher melanophore abundance than in orange skin, where xanthophores predominate. Our findings provide a significant foundation for comparing and understanding the diverse pathways that contribute to the evolution of pigment production in the skin of amphibians.

KEYWORDS

Anura; *Brachycephalus*, color polymorphism, gene expression, skin chromatophores, visual modeling

1 | INTRODUCTION

Coloration in animals is involved in different evolutionary functions related to physical protection (e.g., thermoregulation and UV protection), inter and intraspecific signaling (e.g., sexual and social selection), and/or as a strategy to avoid predation (e.g., camouflage, mimicry, or aposematism) (Hutton et al., 2015; Rojas, 2017; Ruxton et al.,

2018). Color is a physical phenomenon and emerges from the intricate interplay between the reflection of light from the skin, scales, feathers, or hairs of the bearer, as well as the sensory receptors and the cognitive architecture of the observer (Maia et al., 2019; Osorio & Vorobyev, 2008; Renoult et al., 2017). Understanding the diversity of color phenotypes provides valuable insights into the adaptive significance of coloration and the complex mechanisms driving biodiversity in the natural world (Briolat et al., 2019; Caro, 2017; Emberts & Wiens, 2022). However, while ecological functions of coloration in animals have been studied for over a century (Caro, 2017; Müller, 1879), the molecular and structural bases of color determination are less known (Hashimoto et al., 2021; Shawkey & D'Alba, 2017).

Amphibians are one of the most diverse classes of vertebrates, with an extraordinary diversity of colors at inter- and intraspecific levels (Rojas, 2017), though this diversity has been addressed only recently and for a few species' groups (Rojas, 2017). Within anurans, studies of color variation were centered on poison frogs (Anura: Dendrobatidae), which exhibit classical color variability within species, from color polymorphism (within populations) to polytypism (between populations) (e.g., Brusa et al., 2013; Rojas et al., 2019; Twomey et al., 2020). Studies employing genomic approaches showed that color variation in poison frogs is controlled by multiple genes (Stuckert et al., 2019; Rodríguez et al., 2020). In addition, they demonstrated that various pathways like carotenoid processing (Rodríguez et al., 2020; Twomey et al., 2020), melanin synthesis (Posso-Terranova & Andrés, 2017; Stuckert et al., 2019), pteridine synthesis (Rodríguez et al., 2020), as well as the genes involved in structural coloration and pigment cell development (Stuckert et al., 2019), have a significant contribution to skin color variation. Nevertheless, similar phenotypes in closely related species may exhibit divergent mechanisms of color production (Twomey et al., 2023).

Concerning the structural bases of color variation, amphibians attain this variability by combining complex structural and pigmentary cell components. Bagnara et al. (1968) identified three cell components as the main ones responsible for amphibian coloration and defined it as the "dermal chromatophore unit." In this arrangement, the layer closest to the epidermis consists of xanthophores containing carotenoid and pteridine pigments reflecting from yellow to red hues. The middle layer comprises iridophores containing reflective purine (e.g., guanine) crystal platelets that contribute to structural colors. The deepest layer consists of melanophores, which have melanosomes with melanin pigments absorbing light across a broad spectrum,

producing dark colors (Andrade & Carneiro, 2021; McNamara et al., 2021; Shawkey & D'Alba, 2017). However, this cellular structural arrangement is not observed in several species, like those with vibrant green colors lacking melanophores (Taboada et al., 2020). Color differences among body regions within the same individual can also be explained by the presence of only xanthophores and/or iridophores (Frost & Robinson, 1984; Kinderman & Hero, 2006) or pigment variation within xanthophores and platelets morphology in iridophores (e.g., Twomey et al., 2020). Although the link between genetic and morphological data might seem obvious, studies correlating these two sources of evidence are rare (Posso-Terranova & Andrés, 2017).

Recent advances in genomics have enabled several investigations of evolutionary mechanisms associated with genotype-phenotype interaction in non-model species (Andrade et al., 2022; Goutte et al., 2022; San-Jose & Roulin, 2017). The direct-developed species of the genus *Brachycephalus* (Anura: Brachycephalidae) are miniaturized amphibians with ground-dwelling and daily activity, endemic to the Brazilian Atlantic Forest (dos Reis et al., 2020). Species in this genus have a wide range of skin color variation, from bright yellow/orange (the pumpkin toadlets, N = 36) to dark brown species (the flea toads, N = 5) (Condez et al., 2020; Frost, 2024; Lyra et al., 2021). The evolution of bright coloration in pumpkin toadlets seems to be related to body plan (bufoniform) and the presence of tetrodotoxin, a potent neurotoxin (Chimetto-Tonon et al., 2021; Hanifin, 2010; Pires et al., 2005). Because of this color-toxin association, pumpkin toadlets are assumed to have aposematic antipredator strategies, though experimental evidence testing this inference is rare (Rebouças et al., 2019).

The pumpkin toadlet *Brachycephalus actaeus* has a restricted and relatively small distribution range of approximately 80 km^2, inhabiting pristine forests in the northeastern Brazilian state of Santa Catarina (Monteiro et al., 2018). The populations of this species present intriguing color polytypism (Lyra et al., 2021; Monteiro et al., 2018), with at least four distinct color morphs: brown, gray, green, and orange (Monteiro, J.P.C. pers. obs.). It is the unique species in the genus known to have such intraspecific color variation. By using a population dataset from this species, we first tested if a potential bird predator can perceive the distinct color morphs of *B. actaeus*. Second, we characterized the skin histology from the different color morphs. Finally, we used comparative transcriptomic analyses from the skin to identify candidate coloration-related genes in the different color morphs. Our results represent the first step to

understanding color polytypism in *Brachycephalus*. They significantly contribute to testing hypotheses regarding color divergence, its ecological significance, and the underlying molecular mechanisms in amphibians.

2 | MATERIAL AND METHODS

2.1 | Field sampling and procedures

We conducted fieldwork from 01 to 08 October 2021 at six geographic localities across the known distribution range of *B. actaeus* in the northeastern state of Santa Catarina, Brazil. We sampled at least five individuals per locality, totaling 39 collected specimens covering all color morphs (Table S1). The localities are in the two municipalities: Itapoá (Alto Braço do Norte [BNb; brown morph]; and Baixo Braço do Norte [BNg; green morph]); São Francisco do Sul at the Distrito do Saí (Casarão [CAS; gray morph]; Morro do Cantagalo [CAG; orange morph]; and Vila da Glória [GLO; green morph]); and at São Francisco do Sul Island (Serra da Palha [SPA; green morph]). At all sampling localities, the air humidity was around 90–100%, and the temperature range was 18–22°C.

The collected specimens were euthanized by cutaneous anesthetic overdose (5% lidocaine). Immediately afterward, we skinned the specimens, resected them, and divided the skin into sagittal halves. One-half of the skin was stored in RNAlater for RNAseq analyses at -80°C until the RNA extraction and the other half was used in histological analyses (see below). All samples were collected in compliance with the Ethic Committee of the São Paulo State University, Rio Claro, São Paulo, Brazil (UNESP; protocols #02/19), under the research permit issued by the Sistema de Autorização e Informação em Biodiversidade from Instituto Chico Mendes de Conservação da Biodiversidade - Ministério do Meio Ambiente, Brazil (SISBIO #63104-4). We also registered access to genetic information on the National System for the Management of Genetic Heritage and Associated Traditional Knowledge (SISGen #A91405E). Voucher specimens were deposited in the Célio F. B. Haddad (CFBH) Amphibian Collection, housed at the Departamento de Biodiversidade, Instituto de Biociências, UNESP, Rio Claro, São Paulo, Brazil.

2.2 | Color morph classification and bird visual modeling

To classify *B. actaeus* individuals according to color morph, we first tested whether they could be perceived by potential predators as four distinct colors in the same way as we

do. While specific predators of *B*. *actaeus* and also from other *Brachycephalus* species remain unknown, there is a rare record of a tinamou bird (Palaeognathae: Tinamidae, *Tinamus solitarius*) preying on *B*. *ephippium* (Carvalho, 1940), and an experimental test of *Brachycephalus*' aposematic role under chicken predation (Rebouças et al., 2019). Considering that and given that birds are considered significant predators of Neotropical poison frogs (Casas-Cardona et al., 2018; Dreher et al., 2015; Willink et al., 2014), we choose the visual system of the peafowl (Neognathae: Phasianidae, *Pavo cristatus)*, a ground feeder bird, as a model for testing the perception of a potential predator. Galliforms (peafowl and chicken) and tinamou birds lack ultraviolet sensitivity (Write & Bowmaker, 2001) and were assumed to represent the best available model for our dataset.

Briefly, we captured RAW format images of the 39 toadlets and the natural backgrounds using neutral reflectance grayscale within the human visible spectrum, (400–700 nm). The camera's sensitivity in the red, blue, and green (RGB) channels was determined and calibrated to generate a cone catch model for the visual system of the peafowl under daylight D65 illuminant. Next, multispectral images (mspec) were created from toadlets and backgrounds. Finally, we obtained the photon catches from short-wave-sensitive (SWS; blue), medium-wave-sensitive (MWS; green), long-wave sensitive (LWS; red), and double cones (DC) receptors in the bird's retina. We used micaToolbox v.2.2.2 (Troscianko & Stevens, 2015) in ImageJ v1.52k (Schneider et al., 2012) for all steps of image calibration.

For color morph classification, we utilized the peafowl photon catch sensitivities from both dorsal and lateral images of *B*. *actaeus* individuals (eight variables; see Supplementary Material). These data were employed to investigate overall variation and categorize individuals into discrete color morph categories. Three non-correlated variables (Pearson's $r > 0.7$), SWS and MWS from lateral and LWS from dorsal images were used as input for Gaussian mixture modeling using mclust version 6.0.0 (Fraley et al., 2012) in R 4.1.2 (R Core Team, 2021). Multiple models were run with k = 1–10 clusters in the data and 999 bootstrap replicates, combining the data's orientation, volume, and shape (Fraley et al., 2012). The best-fit model was determined using the Bayesian Information Criterion (BIC). Finally, we performed the receptor noise-limited bird visual model (Vorobyev & Osorio, 1998) to quantify and compare perceptual differences among *B*. *actaeus* morphs.

Supplementary Material provides detailed information on macro photography procedures, camera calibration, image processing, and visual modeling.

2.3 | Structural and ultrastructural analyses of the skin

The dorsal and ventral skin of *B*. *actaeus* from 12 individuals (two individuals per locality) were processed and examined (Table S1). Detailed methods of skin preparation are given in supplementary materials. To analyze the skin structure, preparations of semithin (for Light Microscopy, LM) and ultrathin (for Transmission Electron Microscopy, TEM) were performed at the Multiuser Laboratory of Electronic Microscopy of the University of São Paulo (Faculdade de Medicina de Ribeirão Preto, Ribeirão Preto, São Paulo, Brazil). The semithin preparations were examined under an Olympus BX51 light microscope coupled to a DP71 digital camera using a magnification strength of 60x and 100x to capture images with a resolution of 432 dpi. The ultrathin sections were observed with a JEOL JEM 100CXII transmission electron microscope at 80 kV acceleration voltage. Contrast and brightness were adjusted using the equipment software.

We used LM images to describe the skin layers (i.e., epidermis, dermal *stratum spongiosum* and *compactum*, and calcified layer) following Brunetti et al. (2016) and Toledo & Jared (1992). We measured the thickness of layers using the image analysis in Fiji version 2.9.0 (Schindelin et al., 2012). To obtain the average skin thickness, we took three calibrated measurements per layer (anterior, medial, and posterior sections) for each sample, measuring two replicates per sample.

We used semithin LM and TEM images to characterize chromatophores. We followed Bagnara et al. (1968) and Frost & Robinson (1984) to identify intracellular pterinosome and carotenoid vesicles and melanosomes from xanthophores and melanophores, respectively. We quantified the chromatophores of semithin samples using the Trainable Weka Segmentation plugin version 3.0 (Weka; Arganda-Carreras et al., 2017) in Fiji version 2.9.0 (Schindelin et al., 2012). First, we manually picked the chromatophore layer to measure the total area. Next, we trained the algorithm using Weka, selecting similar pixels corresponding to the attributes background, melanosome, and xanthophore, including a minimum of 20 ROI sets for each class. Finally, we create a mask to measure the coverage of the melanosomes and xanthophores based on image segmentation results. We considered the area covered by melanosomes or xanthophores divided by the total area of the chromatophore layer in each color morph (Figure S1).

2.4 | RNA sequencing, reference transcriptome assembly, and annotation

RNA extraction from the skin (sagittal half) and library preparation were performed by Genewiz® (Leipzig, Germany) with PolyA selection using Illumina® NovaSeq™ sequencing system for 26 individuals of *B. actaeus* (four to five individuals per locality; Table S1). Samples were then prepared using the Illumina© stranded Tru-Seq© library protocol and pair-end sequenced with 150 bp reads in an Illumina© NovaSeq platform.. The methodology employed for constructing the reference transcriptome followed these steps: (i) conducting quality check and pre-processing of raw reads, (ii) performing *de-novo* transcriptome assembler, (iii) generating non-redundant transcript data and evaluating transcriptome assembly, and (iv) annotation of a reference transcriptome.

We performed a quality control of sequencing stats per sample using FastQC version 0.12.1 (Andrews, 2010). We then used Trimmomatic version 0.32 (Bolger et al., 2014) to remove adapters and low-quality fragments before pooling the samples per locality. Reads were then concatenated by locality, normalized to a target depth of 50x using bbnorm version 38.08 (Bushnell, 2014), and rRNA decontaminated with SortMeRNA version 2.0, using contaminant database version 4.3 (Kopylova et al., 2012). To minimize variant-derived assembly artifacts, we opted for a stratified consensus approach in which we performed a *de-novo* transcriptome assembly from the pool of sequencing reads per locality before constructing a consensus transcriptome assembly for the species. Then, we used three different *de-novo* transcriptome assembly algorithms using their default setting unless specified to assemble the read collections per locality: Trinity version 2.14.0 (--SS_lib_type RF and --min_kmer_cov 2 options) (Haas et al., 2013); rnaSPADES version 3.9 (--ss rf) (Bushmanova et al., 2019); and SOAPdenovo-Trans version 1.03 (executed four times, with k-mers = 19, 37, 55, and 73, max read length = 150, average insert size = 400, and nasm_flag = 3) (Xie et al., 2014). The resulting 36 assemblies (6x Trinity, 6x rnaSPADES, and 24x SOAPdenovo-Trans) were combined into a comprehensive reference transcriptome using EvidentialGene version 4 (Gilbert, 2019), which filters the collection of transcripts by selecting the most extended coding sequence and related isoforms while removing redundant sequences. We evaluated transcriptome completeness by their BUSCO scores against the 3,354 vertebrate benchmarking genes in the vertebrate odb_database version 10 (Simão et al., 2015).

The resulting reference transcriptome was annotated using EnTap pipeline version 0.10.9 (Hart et al., 2020). The pipeline was configured with Transdecoder (https://github.com/TransDecoder) for open reading frame (ORF) detection, RefSeq Vertebrates (https://www.ncbi.nlm.nih.gov/refseq/; accessed on June 2022), UniProt (The_UniProt_Consortium, 2019; accessed on June 2022) protein databases for similarity searches with Diamond version 0.9.22 (Buchfink et al., 2014), and EggNOG version 5 database (Huerta-Cepas et al., 2019; accessed on March 2022) for orthology searches. Blast hits on bacteria, fungi, nematodes, and viruses were flagged as contaminants and excluded. The final annotation of protein names used the results of reciprocal best blast hits (E-value: 1e-5) against *Xenopus tropicalis* proteome complemented with UniProt protein database hits obtained from EnTap.

2.5 | Population structure

We used Lace software version 3.17 (Davidson et al., 2017) to concatenate the transcripts in the reference transcriptome into a set of super-transcripts, each containing all exon sequences of a given gene concatenated without redundancy. A gene-to-transcript map was obtained with Corset version 1.09 (Davidson and Oshlack, 2014) and was used as input to Lace to guide the concatenation of transcripts. The resulting super transcriptome was used as a reference against which all RNA-Seq reads were mapped using STAR version 1.1.13 (Dobin et al., 2012). Variants were called using GATK software version 1.8 (McKenna et al., 2010), following the best-practice workflow for RNA-Seq SNP calling (Van der Auwera & O'Connor, 2020). This pipeline includes aligning, sorting, and marking duplicate read mappings, split reads into exon segments, and clip sequences overhanging the intronic regions (SplitNCigarReads). Variants were called with phred-scaled confidence threshold > 20 and later filtered to retain those with fisher strand values (FS) > 30.0 and quality by depth values (QD) < 2.0. The resulting VCF file was further filtered using vcftools (Danecek et al., 2011) to include only bi-allelic SNPs, with a minor allele frequency > 0.04 (more than two allele copies in 26 diploid individuals) and < 50% missing data across individuals.

The SNP dataset was pruned to remove variants in linkage disequilibrium, as estimated by the correlation of genotypes using the “--indep-pairwise 50 5 0.2” options in PLINK version 1.9 (Purcell et al., 2007). We then used the resulting genotypes to ascertain population structure by running 20 repetitions of ADMIXTURE version 1.3 (Alexander et al., 2009) for K = 1 to 10. A principal component analysis (PCA)

inspection was performed using PLINK version 1.9 (Purcell et al., 2007), and the results were visualized using the R package tidyverse version 2.0.0 (Wickham et al., 2019).

2.6 | Differential gene expression analyses

Transcript abundance in the skin samples was estimated by pseudo-aligning the quality-trimmed reads to the EvidentialGene reference transcriptome with Kallisto software version 2.8.12 (Bray et al., 2016) using 100 bootstraps for uncertainty estimation.

Differential expression analyses were then conducted with the 3DRNASeq package version 2.0.1 (Guo et al., 2021). We imported Kallisto transcript abundance estimates, normalizing them by transcript per million (TPM), and scaled them to library size and feature length. We summarized these at the transcript and gene levels using the gene-to-transcripts mapping output from EvidentialGene. We retained transcripts occurring in ≥ 4 samples and showing ≥ 1 CPM. Then, we inspected the data, plotting a PCA of gene expression by sample. After filtering, expression estimates were normalized using the trimmed mean of M values (TMM) between-sample normalization. We performed statistical tests for differential expression genes (DEGs) between pairwise color morph contrast groups, one versus (vs.) all contrasts between color, and (orange + brown) vs. (green + gray). Statistical tests were conducted using the limma-voom analysis) (Ritchie et al., 2015). A Benjamini-Hochberg procedure for error rate correction was applied before evaluating statistical significance with an alpha = 0.05 and a log2 fold change of 1.

We focused on coloration-related genes since we were interested in color morph variation. To identify them, we compiled a list of genes linked in the melanin synthesis pathway, carotenoid metabolism, pteridine synthesis, iridophore guanine synthesis (Braasch et al., 2007; Higdon et al., 2013; McLean et al., 2017), and other pigmentation-associated genes with diverse functions (Baxter et al., 2019) (Table S2). This list is undoubtedly not exhaustive, as the molecular mechanisms of color production in amphibians, particularly in these toadlets, are poorly known. For gene nomenclature, we followed Xenbase version 6.0.0 (Fisher et al., 2023).

We compared our list of DEGs with those detected in differential gene expression analyses between color phenotypes in three other hyloidean anurans *Dendrobates auratus* (Stuckert et al., 2019), *Oophaga pumilio* (Rodríguez et al., 2020), and *R. sirensis* (Twomey et al., 2020).

2.7 | Transcriptome-wide association analysis

Classical gene expression tests are limited to comparisons of samples grouped into two or a few categorical conditions. Although coloration phenotypes can be discretized into categorical variables, as we did with the 3DRNASeq analysis above, the variation in color among individuals is continuous by nature. Therefore, the analyses of the relationship between gene expression and coloration should gain power when a continuous variable represents color. We used the chromatic discriminability in units of just noticeable differences of the toadlets from bird perceptual space to access visual perceptual distances (from the *jnd2xyz* function output in pavo2 version 2.7.1, see Supplementary Material; Maia et al., 2019; Pike, 2012). The y-coordinate of perceptual space scores was strongly correlated with the x-coordinate values, and only the uncorrelated x-axis and luminance scores were included in this analysis. We implemented a linear regression model that correlates changes in the TPM normalized expression values aggregated at the gene level (as obtained with Kallisto and 3DRNASeq, see above) with x-axis and luminance scores to test for gene expression association using Olivia package version 0.1.0 (Sofer et al., 2021). We filtered out low-expressed genes by removing those with more than 25% of samples with zero counts, maximum expression > 5, and maximum expression < 10. Zero values were replaced with half the minimum non-zero values in the sample, and the expression values were log2-transformed ("log_replace_half_min" transformation). Subsequently, we fit the linear regression model to the transformed expression values, incorporating population structure as a covariate in the model (represented by the averaged admixture proportions obtained for K = 2 in the admixture runs). To evaluate the statistical significance of our results, we ran 100 residual permutations, considering them as associated in expression with the perceptual space coordinates of those genes with false detection rate (FDR) with P-values < 0.05.

2.8 | Gene co-expression network analyses

Correlations in the expression profile of multiple genes across samples can be represented by gene-gene interaction networks. We used the normalized expression values from 3DRNASeq (already excluding lowly expressed genes) as input for a weighted gene co-expression network analysis using the WGCNA package (Langfelder & Horvath, 2008) in R. We selected appropriate soft-thresholding power for network construction (12 in our case) by inspecting the mean connectivity/scale independence vs

soft-threshold power plots. A signed network adjacency was then calculated from the expression data using a Pearson correlation and the selected soft-threshold power and translated into topological overlap measure (TOM) dissimilarities. Genes were then clustered into a dendrogram based on their TOM dissimilarity, and gene modules were defined by applying a dynamic tree cut with a minimum module size of 30 genes (minClusterSize = 30) and a medium sensitivity to branch splitting (deepSplit = 2). We then computed the eigengene values per module (i.e., the scores on the first principal component of expression) and correlated these with the two continuous uncorrelated frog color variables (x-coordinate and luminance in bird perceptual space, see section above) using a Pearson correlation (alpha = 0.05). An overall description of the genes included in those color-associated modules was obtained via an overrepresentation analysis of Gene Ontology terms in PANTHER version 18.0 (Thomas et al., 2022) using the *Homo sapiens* database at the biological process level and with FDR correction for multiple testing.

3 | RESULTS

3.1 | Color classification and bird visual modeling

According to the modeled peafowl perception of the spectral reflectance values, the mclust algorithm classified the individuals of *B. actaeus* into four clusters (BIC = 573.7876; Table S2). The classification error of the best-fitting Gaussian multivariate model (mixture of ellipsoidal, varying volume, shape, and orientation coded as VVV in Figure S2) was 0.04. The composition of these clusters matched the categorization into color morphs by a human observer (JPCM; Table S3) with a 0.15 error. We hereafter refer to these morphotypes as brown, gray, green, and orange morphs.

The toadlet-to-background contrasts for peafowl showed in the dorsal view that orange (CAG) and gray (CAS) color morphs were the most distinctive in both color contrast (ΔS) and brightness contrast (ΔL) values, while the green and brown morphs clustered together. In lateral view, however, the orange and brown morphs were distinct from the green and gray morphs, with this differentiation being more evident in ΔS values (Figure 1; Figure S3). In summary, the orange morph is the most conspicuous phenotype in dorsal and lateral coloration. The brown morph is conspicuous only when viewed laterally, where present orange color. The green and gray morphs are the least contrasting against the background, both in dorsal and lateral views.

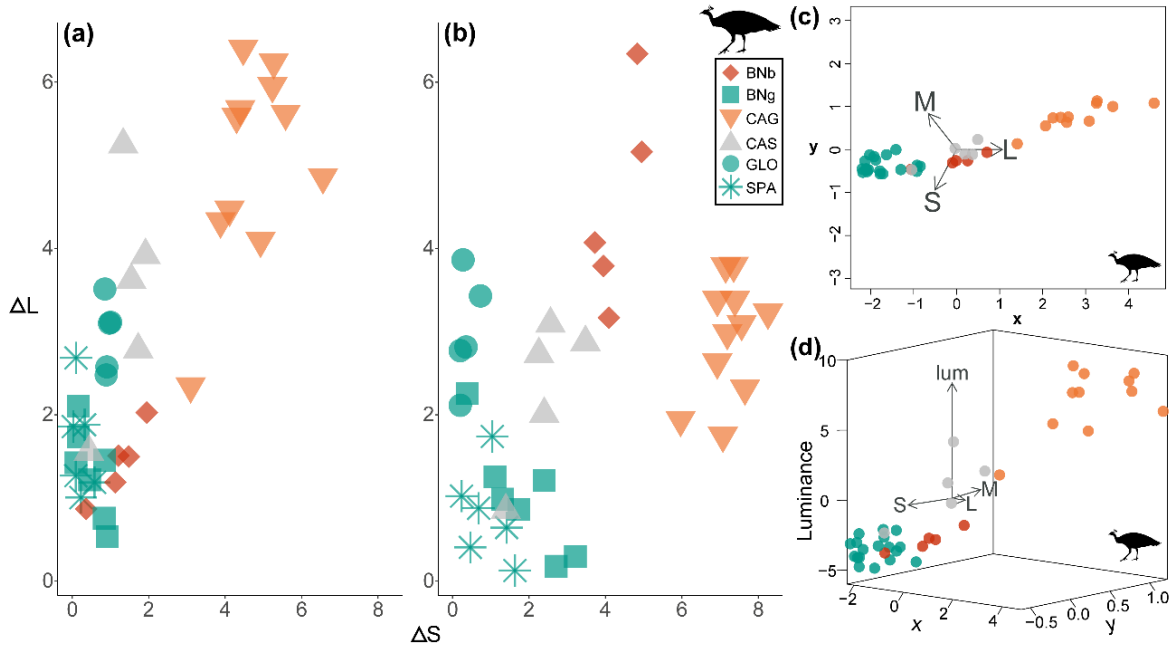


FIGURE 1 Plots show the position of individuals in the perceptual space of predatory bird (peafowl). Color (ΔS) and brightness (ΔL) visual contrasts of *Brachycephalus actaeus* individuals from the six study sites in dorsal (a) and lateral (b) views. The averages of inter-individual scores from color and brightness contrasts were projected into x and y coordinates representing the average perceptual space (c) and their positions into x, y, and luminance coordinates in a tetrahedral model of bird vision (d). Loadings of the original quantum catch variables are represented with dark gray arrows. Individuals are colored by their color morphs. Contrasts were calculated for each toadlet against the original background, assuming natural light conditions. Abbreviations: BNb, Alto Braço do Norte; BNg, Baixo Braço do Norte; CAG, Cantagalo; CAS, Casarão; GLO, Vila da Glória; and SPA, Serra da Palha. Colors represent morphs identified (brown [BNb], gray [CAS], green [BNg, GLO, SPA], and orange [CAG]).

3.2 | Skin characterization

Overall, two distinct dermal regions (i.e., *stratum spongiosum* and *stratum compactum*) were easily recognized in the skin of *B. actaeus*, which are separated by a thickened calcified Eberth-Kastschenko (EK) (Figures 2, S4, and S5; Table 1 and S4). Only two types of chromatophores (melanophores and xanthophores) were identified in the *stratum spongiosum* of dorsal and ventral skin, with no iridophores recognized in any sample. The distribution and abundance of melanophores and xanthophores vary among morphs and between dorsal and ventral skin (Figures 2 and S5; Table 1 and S4).

In the dorsal skin of orange toadlets, melanophores were either absent or very scarce, while xanthophores were abundant and contained both carotenoid vesicles and pterinosomes (Figure 2A–B; Table 1). In the brown and gray toadlets, the melanophores and xanthophores occurred similarly, with melanophores located either below or mingled with xanthophores (Figure 2C–F). Meanwhile, in the green toadlets, the

melanophores were more abundant, whereas xanthophores were much rarer (Figure 2G–H). Unlike the orange morph, xanthophores of grey, brown, and green morphs only have pterinosomes but no carotenoid vesicles (Figure 2B, 2D, 2F, and 2H).

In the ventral skin of green morphs, the melanophores occurred in clusters, and the xanthophores were more abundant than in the dorsal region. This pattern can be linked to the orange skin with dark blotches observed externally (Figure S5J–L; Table 1). In contrast, the very scarce presence of melanophores in the gray morph or their absence in the ventral skin of brown and orange morphs supports the occurrence of homogeneous orange bellies observed externally (Figure S5A–I). Carotenoid vesicles and pterinosomes were observed in both orange and brown morphs (Figure S5C and S5I).

3.3 | Reference transcriptome assembly and annotation

Assemblies with rnaSPADES and SOAPdenovo-trans produced the most complete transcript collections (Table S5, Figure S6). The entire collection of 8.9 million redundant transcripts was then reduced with EvidentialGene. The final consensus reference transcriptome (EvidentialGene's OK-group of transcripts) contained 764,760 transcripts with a N50 of 2098 bp and a BUSCO score with 94.4% completeness, 1.5% fragmentation, and 4.1% of missing genes (Table S5). Annotations with EnTap revealed that 405,769 transcripts had open reading frames (ORFs), and 251,354 had a hit against UniProt or RefSeq protein sequence databases. Only 6,651 out of 764,760 transcripts were flagged as contaminants in this annotation pipeline and excluded for subsequent analyses. Gene family and ontology searches against the EggNOG database assigned 252,134 transcripts to gene families. Together with similarity searches against *Xenopus tropicalis* proteome and Uniprot protein databases, it allowed the functional annotation of 263,618 transcripts.

3.4 | Genetic structure

We recovered a total of 78,819 SNPs in the superTranscriptome of *B. actaeus*. Of these, 23,579 bi-allelic SNPs were used for population structure analysis (Figure 3). The PCA analysis based on SNPs showed three clusters composed of two mainland groups: (1) BNb and BNg; (2) CAS, CAG, and GLO; and (3) the island population SPA (Figure 3C). The SPA samples were distinct from others in the first and second components, explaining 21.13% of the variance. The Admixture analysis exhibited the best-fit K

TABLE 1. Summary of skin layers measurements (in µm) and chromatophores coverage (%)* of *Brachycephalus actaeus* morphs from dorsal and ventral regions. Values were presented following minimum–maximum.

	Dorsal				Ventral			
Trait	Orange	Gray	Brown	Green	Orange	Gray	Brown	Green
Epidermis (µm)	9.68 ± 1.27 (3.54–14.00)	7.55 ± 1.49 (2.66–14.09)	10.29 ± 2.45 (5.88–16.43)	11.44 ± 3.99 (3.89–24.89)	7.43 ± 1.83 (3.96–12.46)	8.38 ± 0.71 (5.66–10.04)	9.21 ± 2.16 (3.35–16.72)	10.31 ± 2.38 (5.62–25.21)
stratum spongiosum (µm)	13.56 ± 7.5 (5.41–35.98)	15.12 ± 8.45 (3.66–47.71)	25.63 ± 23.38 (5.67–81.03)	17.42 ± 9.51 (3.20–47.88)	11.85 ± 6.3 (3.20–32.05)	10.02 ± 9.88 (2.70–45.78)	10.19 ± 9.53 (2.24–68.18)	18.81 ± 12.17 (4.59–60.00)
EK (µm)	6.26 ± 2.91 (1.77–13.58)	3.74 ± 2.4 (0.65–13.77)	6.24 ± 3.76 (2.76–13.01)	7.76 ± 3.79 (1.63–19.61)	12.9 ± 6.89 (0.79–27.12)	16.69 ± 7.21 (4.94–33.68)	11.97 ± 9.64 (2.86–39.43)	13.09 ± 6.89 (3.26–42.23)
stratum compactum (µm)	38.28 ± 4.11 (24.41–51.64)	26.93 ± 3.86 (16.07–47.58)	31.62 ± 7.83 (20.89–43.08)	48.03 ± 6.97 (18.39–80.38)	42.35 ± 9.45 (23.73–56.57)	28.74 ± 4.58 (22.99–44.23)	34.84 ± 6.47 (24.57–47.88)	42.26 ± 7.31 (18.54–77.90)
Melanophores coverage (%)	0.26 ± 0.26 (0–1.06)	1.52 ± 0.14 (1.38–1.66)	1.74 ± 1.47 (0.27–3.21)	7.97 ± 3.61 (3.59–12.43)	0	0	0	5.06 ± 2.61 (2.62–8.68)
Xanthophores coverage (%)	10.45 ± 8.06 (9.58–18.51)	8.78 ± 5.63 (3.16–14.41)	3.75 ± 2.99 (0.77–6.74)	2.23 ± 1.61 (0.20–4.14)	15.11 ± 3.41 (11.70–18.53)	7.43 ± 1.01 (6.42–8.44)	12.37 ± 8.61 (3.75–20.98)	2.61 ± 3.26 (0.13–7.22)

*The area covered by melanosomes or xanthophores was divided by the total area of the chromatophore layer in each color morph (see Material and Methods).

value for two populations: one containing island samples (SPA) and another with all other samples (BNb, BNg, CAS, CAG, and GLO; Figure 3C; Figure S7). The K value for three recovered the same population structure as PCA analyses (Figure 3B–C). In both analyses, the populations were not structured by color morphs.

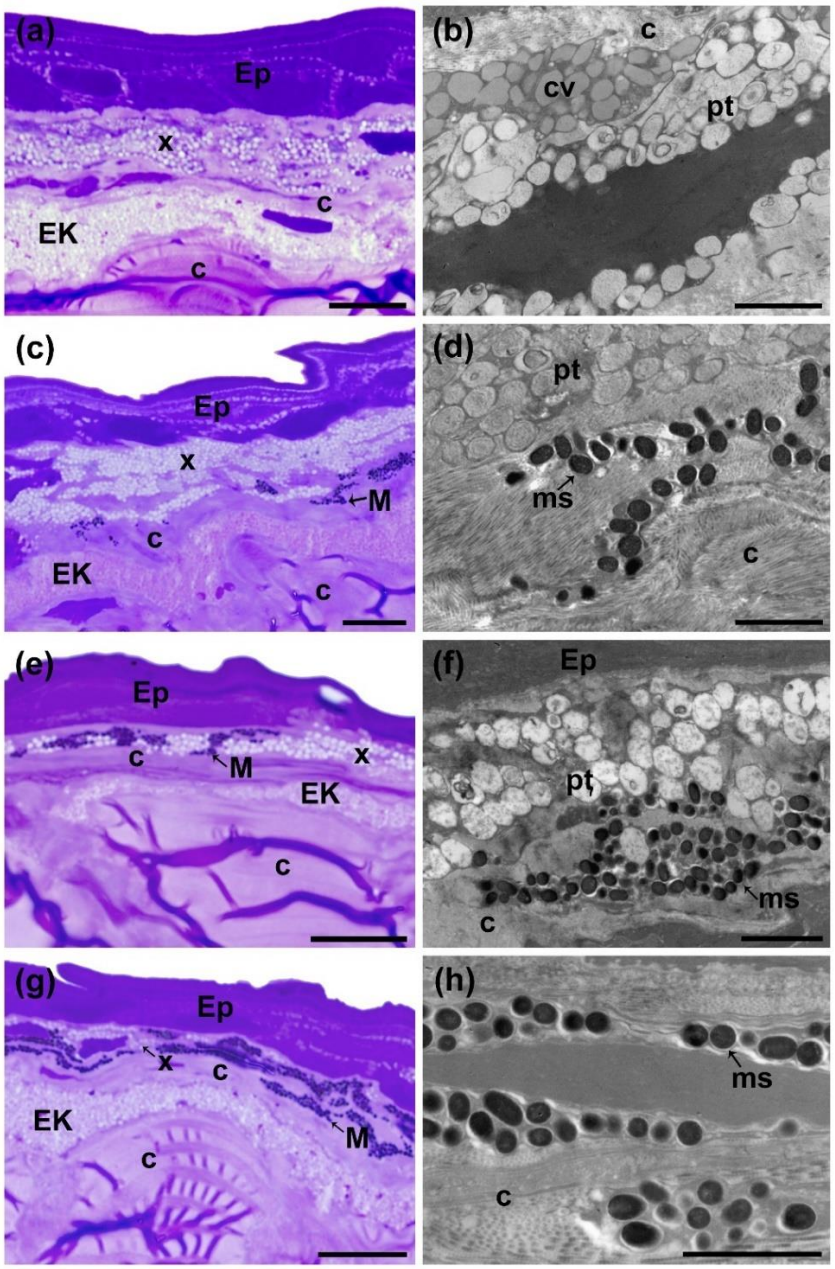


FIGURE 2 Dorsal skin structure of *Brachycephalus actaeus* in transversal section highlighting chromatophores organization and distribution. Light microscope photomicrographs stained with toluidine blue (left) obtained with Olympus BX51 light microscope coupled to a DP71 digital camera; and Electron microphotographs (right) obtained with JEOL JEM 100CXII transmission electron microscope at 80 kV acceleration voltage. (a, b) Orange morphotype (JPCM1025); (c, d) gray morphotype (JPCM1062); (e, f) brown morphotype (JPCM1046); and (g, h) green morphotype (JPCM1033). Abbreviations: c, collagen fibers; cv, carotenoid vesicle; EK, Eberth-Kastschenko; Ep, epidermis; M, melanophore; ms, melanosome; pt, pterinosome; x, xanthophore. Scale bar: a, c, e, g = 10 µm; b, d, f, h = 2 µm.

3.4 | Genetic structure

We recovered a total of 78,819 SNPs in the superTranscriptome of *B. actaeus*. Of these, 23,579 bi-allelic SNPs were used for population structure analysis (Figure 3). The PCA analysis based on SNPs showed three clusters composed of two mainland groups: (1) BNb and BNg; (2) CAS, CAG, and GLO; and (3) the island population SPA (Figure 3C). The SPA samples were distinct from others in the first and second components, explaining 21.13% of the variance. The Admixture analysis exhibited the best-fit K value for two populations: one containing island samples (SPA) and another with all other samples (BNb, BNg, CAS, CAG, and GLO; Figure 3C; Figure S7). The K value for three recovered the same population structure as PCA analyses (Figure 3B–C). In both analyses, the populations were not structured by color morphs.

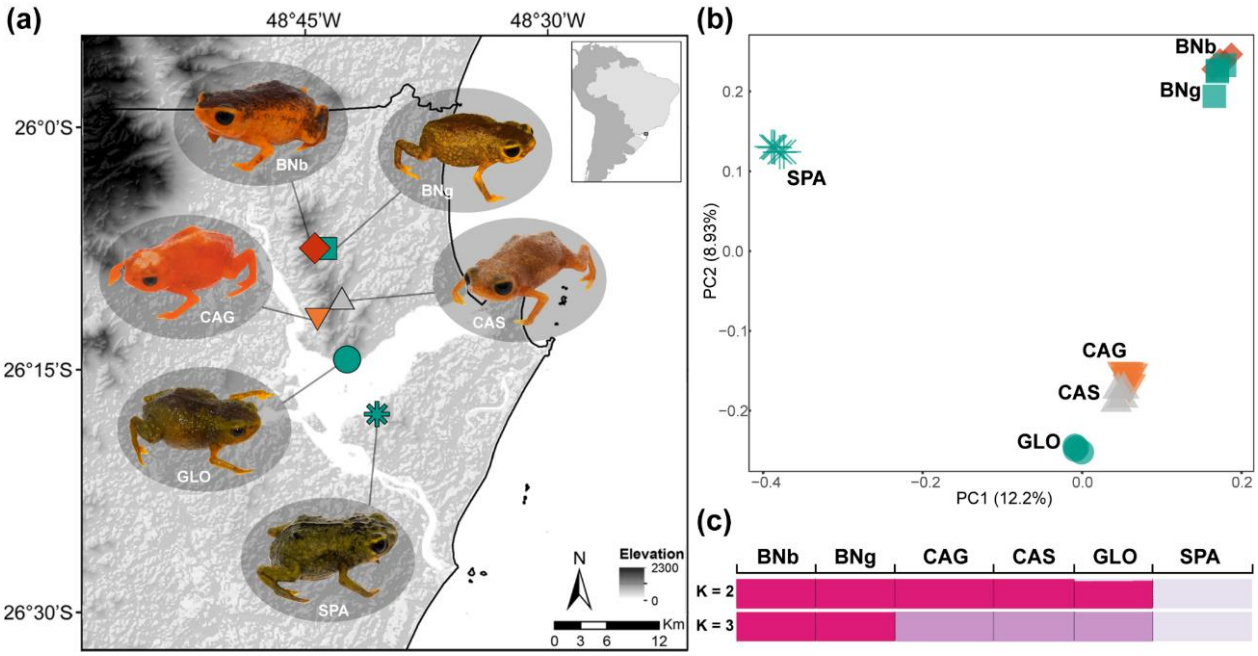


FIGURE 3 General genetic structure through geographic distribution of *Brachycephalus actaeus* color morphs northeastern state of Santa Catarina, Brazil. (a) Topographic map indicating the geographic location of the color morphs and their corresponding symbols: diamond = BNb, Alto Braço do Norte, brown morph; square = BNg, Baixo Braço do Norte, green morph; inverted triangle = CAG, Cantagalo, orange morph; triangle = CAS, Casarão, gray morph; circle = GLO, Vila da Glória, green morph; and asterisk = SPA, Serra da Palha, green morph. (b) Scores of 23,579 bi-allelic SNPs from 26 individuals in the first two principal components. (c) Population structure estimated with Admixture software for models with 2–3 ancestral populations (K). Ancestry proportions are represented by pink gradient bars (best-fit model K = 2). The colors of symbols represent the color morph classification.

3.5 | Differential expression analyses

Expression values from 79,567 transcripts from 12,943 genes with functional annotation and expressed above the cutoff values were used for differential expression testing among the color phenotypes. The PCA plot of log2 transformed TPM normalized gene expression estimates showed a noteworthy level of clustering of samples by locality, with samples from SPA followed CAS showing the most significant divergence from the rest (Figure S8). Also, the PCA of gene expression did not present a color morph structure. 3DRNASeq pairwise and one-vs-all contrasts between color phenotypes identified 454 differentially expressed genes (DEGs). Among these, we identified 26 color-associated DEGs. Eight of these were genes from the melanin synthesis pathway (*pmel*, *edn1*, *wnt9a, dct*, *slc24a5*, *tyrp1*, *oca2*, *egfr*), two from the melanosome transport and biogenesis (*mlana*, *mreg*), two DEGs are linked to the carotenoid metabolism (*aldh1a2*, *rpe65*), and one DEG of the purine synthesis pathway (*gart*). In addition, we found 13 other DEGs previously linked to chromatophore differentiation in vertebrates (Figure 4; Table 2).

The DEGs in the melanin synthesis pathway showed four different expression profiles: three genes (*oca2*, *slc24a5*, *tyrp1*) were down-regulated in orange toadlets and up-regulated in green and, to a lesser extent, brown and gray toadlets; the other four (*dct*, *edn1*, *mlana*, *pmel*) were down-regulated in orange and brown toadlets and up-regulated in gray and green toadlets; only one gene (*wnt9a*) was exclusively down-regulated in orange toadlets; and only one gene (*mreg*) was exclusively up-regulated in orange and, to a lesser extent, in green toadlets (Table 2).

The two DEGs associated with the carotenoid metabolism showed up-regulation in gray toadlets. For *rpe65*, this up-regulation was pronounced, and all the three other color morphs were down-regulated, but for *aldh1a2*, some up-regulation was detected in green toadlets as well. The purine synthesis enzyme *gart* gene, associated with iridophore-based pigmentation, was up-regulated in brown and gray color phenotypes and down-regulated in orange and green ones.

Among all the DEGs between color morphs of *B. actaeus* identified in this study, 115 out of 454 (25% of the DEGs) also appeared in one or more published lists of DEGs among color morphs of *Dendrobates auratus*, *Oophaga pumilio*, and *Ranitomeya sirensis*. Interestingly, only 12 genes in this group, supported by cumulative evidence, have been previously linked to pigmentation in vertebrates, while the other 103 genes have no known association with pigmentation (Table S6).

TABLE 2. Differentially expressed genes across *Brachycephalus actaeus* skin color morphs with previous links to color variation.

Gene symbol	Gene name	Pathway	Contrast group	Regulation state	q value	log2FC
dct	*L-dopachrome tautomerase precursor*	melanin synthesis	orange-gray	down-regulated	0.021	-3.769
edn1	*endothelin-1*	melanin synthesis	orange-gray	down-regulated	0.010	-1.758
pmel	*melanocyte protein PMEL isoform X1*	melanin synthesis	orange-gray	down-regulated	0.009	-2.674
dct	*L-dopachrome tautomerase precursor*	melanin synthesis	orange-green	down-regulated	0.006	-4.290
oca2	*P protein isoform X1*	melanin synthesis	orange-green	down-regulated	0.049	-7.942
pmel	*melanocyte protein PMEL isoform X1*	melanin synthesis	orange-green	down-regulated	0.003	-2.736
dct	*L-dopachrome tautomerase precursor*	melanin synthesis	orange-(green+brown+gray)	down-regulated	0.017	-3.584
edn1	*endothelin-1*	melanin synthesis	orange-(green+brown+gray)	down-regulated	0.038	-1.187
pmel	*melanocyte protein PMEL isoform X1*	melanin synthesis	orange-(green+brown+gray)	down-regulated	0.015	-2.096
wnt9a	*protein Wnt-9a isoform X1*	melanin synthesis	orange-(green+brown+gray)	down-regulated	0.040	-1.239
edn1	*endothelin-1*	melanin synthesis	gray-(orange+green+brown)	up-regulated	0.029	1.158
pmel	*melanocyte protein PMEL isoform X1*	melanin synthesis	green-brown	up-regulated	0.048	1.858
dct	*L-dopachrome tautomerase precursor*	melanin synthesis	green-(orange+brown+gray)	up-regulated	0.009	2.136
pmel	*melanocyte protein PMEL isoform X1*	melanin synthesis	green-(orange+brown+gray)	up-regulated	0.018	1.552
slc24a5	*sodium/potassium/calcium exchanger 5 isoform X1*	melanin synthesis	green-(orange+brown+gray)	up-regulated	0.024	2.748
tyrp1	*5,6-dihydroxyindole-2-carboxylic acid oxidase precursor*	melanin synthesis	green-(orange+brown+gray)	up-regulated	0.041	3.807
oca2	*P protein isoform X1*	melanin synthesis	green-(orange+brown+gray)	up-regulated	0.013	4.325
wnt3a	*protein Wnt-3a*	pigmentation variation	orange-brown	down-regulated	0.038	-1.306
cdh2	*cadherin-2 precursor*	pigmentation variation	orange-gray	down-regulated	0.033	-2.495
cdh11	*cadherin-11 precursor*	pigmentation variation	orange-gray	down-regulated	0.018	-1.939
egfr	*epidermal growth factor receptor*	pigmentation variation	orange-gray	up-regulated	0.021	1.061
fanci	*Fanconi anemia group I protein*	pigmentation variation	orange-gray	down-regulated	0.031	-1.622
mcm2	*DNA replication licensing factor mcm2*	pigmentation variation	orange-gray	down-regulated	0.024	-2.193
mlana	*melanoma antigen recognized by T-cells 1 isoform X1*	pigmentation variation	orange-gray	down-regulated	0.045	-1.716
rb1	*retinoblastoma-associated protein*	pigmentation variation	orange-gray	down-regulated	0.028	-1.985
wif1	*wnt inhibitory factor 1 precursor*	pigmentation variation	orange-gray	down-regulated	0.024	-1.534
wnt3a	*protein Wnt-3a*	pigmentation variation	orange-gray	down-regulated	0.028	-1.221
zeb2	*zinc finger E-box-binding homeobox 2 isoform X1*	pigmentation variation	orange-gray	down-regulated	0.003	-2.054
mlana	*melanoma antigen recognized by T-cells 1 isoform X1*	pigmentation variation	orange-green	down-regulated	0.001	-2.570

Gene symbol	Gene name	Pathway	Contrast group	Regulation state	q value	log2FC
mreg	*melanoregulin isoform X1*	pigmentation variation	orange-green	up-regulated	0.044	1.471
rab38	*ras-related protein Rab-38*	pigmentation variation	orange-green	down-regulated	0.038	-1.990
zeb2	*zinc finger E-box-binding homeobox 2 isoform X1*	pigmentation variation	orange-green	down-regulated	0.024	-1.352
inpp5b	*type II inositol 1,4,5-trisphosphate 5-phosphatase isoform X1*	pigmentation variation	orange-(green+brown+gray)	down-regulated	0.046	-1.268
mlana	*melanoma antigen recognized by T-cells 1 isoform X1*	pigmentation variation	orange-(green+brown+gray)	down-regulated	0.013	-1.859
mreg	*melanoregulin isoform X1*	pigmentation variation	orange-(green+brown+gray)	up-regulated	0.012	2.065
rb1	*retinoblastoma-associated protein*	pigmentation variation	orange-(green+brown+gray)	down-regulated	0.038	-1.598
wnt3a	*protein Wnt-3a*	pigmentation variation	orange-(green+brown+gray)	down-regulated	0.012	-1.152
zeb2	*zinc finger E-box-binding homeobox 2 isoform X1*	pigmentation variation	orange-(green+brown+gray)	down-regulated	0.016	-1.371
brca2	*breast cancer type 2 susceptibility protein isoform X4*	pigmentation variation	green-gray	down-regulated	0.045	-1.225
cbs	*cystathionine beta-synthase isoform X2*	pigmentation variation	green-gray	up-regulated	0.016	1.284
sdc4	*syndecan 4 precursor*	pigmentation variation	green-gray	up-regulated	0.050	1.271
mlana	*melanoma antigen recognized by T-cells 1 isoform X1*	pigmentation variation	green-(orange+brown+gray)	up-regulated	0.004	1.568
cdh2	*cadherin-2 precursor*	pigmentation variation	gray-(orange+green+brown)	up-regulated	0.024	1.857
cdh11	*cadherin-11 precursor*	pigmentation variation	gray-(orange+green+brown)	up-regulated	0.026	1.461
wif1	*wnt inhibitory factor 1 precursor*	pigmentation variation	gray-(orange+green+brown)	up-regulated	0.031	1.232
zeb2	*zinc finger E-box-binding homeobox 2 isoform X1*	pigmentation variation	gray-(orange+green+brown)	up-regulated	0.009	1.367
aldh1a2	*retinal dehydrogenase 2*	carotenoid metabolism	orange-gray	down-regulated	0.034	-1.672
rpe65	*retinoid isomerohydrolase*	carotenoid metabolism	gray-(orange+green+brown)	up-regulated	0.030	1.438
gart	*trifunctional purine biosynthetic protein adenosine-3*	guanine synthesis in iridophores	green-brown	down-regulated	0.042	-1.124

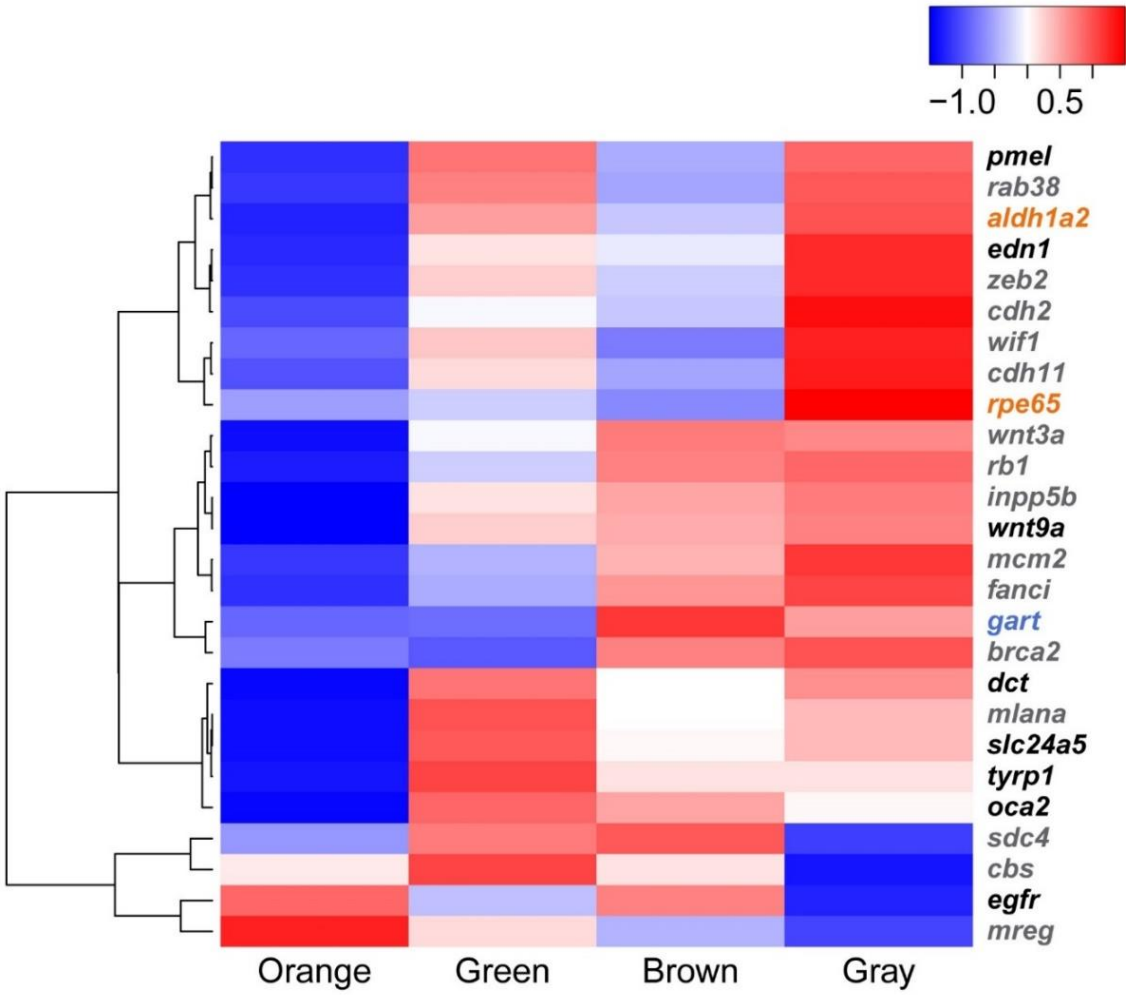


FIGURE 4 Expression patterns of color-associated genes in four color morphs of *Brachycephalus actaeus*. The heatmap plot represents the averaged expression values of all genes across all samples in each morph. 26 differentially expressed genes are highlighted following functional groups: melanin synthesis (in black), carotenoid metabolism (in orange), iridophores in guanine synthesis (in blue), and other pigmentation-associated genes (in gray).

3.6 | Gene expression association with continuous coloration traits

Expression filtering across the expression matrix of 25,142 genes, based on functional annotation (263,618 transcripts), in 26 individuals of *B. actaeus* removed 9,858 low-expressed genes, and the remaining 15,284 genes were included in *Olivia* expression association analyses. For the x-axis values, 18 candidate genes were identified, of which five are pigmentation-associated. Four genes participate in the melanin synthesis pathway (*dct*, *oca2*, *slc24a5*, *tyrp1*), and one in the melanosome biogenesis (*mlana*). All these melanosome-associated genes decrease their expression as the x-axis scores

increase (Table 3, Figure S9). Analyses with luminance values as predictors did not identify any expression-associated genes.

TABLE 3. Results of the transcriptome-wide association analysis with *Olivia* software relating gene expression change and the scores of individual *Brachycephalus actaeus* in the x-coordinate of avian perceptual space. Genes related to pigmentation variation are highlighted in bold.

Gene	AdjLogFC	SE	T-stat.	df	P-value	BH FDR	E. P-value	BH P-value
tyrp1	-1.254	0.128	-9.796	23	0.000	0.000	0.000	0.001
slc24a5	-0.968	0.141	-6.865	23	0.000	0.003	0.000	0.001
dct	-0.885	0.154	-5.747	23	0.000	0.019	0.000	0.013
c7h10orf95	-0.724	0.146	-4.972	23	0.000	0.045	0.000	0.045
oca2	-0.714	0.092	-7.747	23	0.000	0.001	0.000	0.001
yipf7	-0.495	0.096	-5.153	23	0.000	0.037	0.000	0.035
bmp2	-0.492	0.100	-4.902	23	0.000	0.051	0.000	0.049
mlana	-0.471	0.086	-5.483	23	0.000	0.023	0.000	0.019
ppp1r3c.2	-0.449	0.088	-5.134	23	0.000	0.037	0.000	0.035
sik1	-0.416	0.082	-5.102	23	0.000	0.037	0.000	0.038
klhdc7b	-0.390	0.060	-6.528	23	0.000	0.004	0.000	0.001
jun_2	-0.250	0.045	-5.579	23	0.000	0.023	0.000	0.019
lca5	-0.183	0.037	-4.975	23	0.000	0.045	0.000	0.045
znf574	0.119	0.023	5.150	23	0.000	0.037	0.000	0.035
derl3	0.205	0.037	5.464	23	0.000	0.023	0.000	0.019
jmjd7	0.279	0.053	5.260	23	0.000	0.034	0.000	0.029
LOC116412396	1.286	0.220	5.854	23	0.000	0.018	0.000	0.013
cdhr3_3	1.286	0.234	5.490	23	0.000	0.023	0.000	0.019

Abbreviations: AdjLogFC, adjusted Log-Fold Change per unit increase of x-coordinate scores (increase = more orange-red coloration); SE, standard error; T-stat., T-statistic of regression model; df, degrees of freedom; BH FDR, Benjamini-Hochberg false detection ratio; E. P-value, empirical P-value; BH P-value, Benjamini-Hochberg corrected P-value.

3.7 | Gene co-expression network analyses

The WGCNA identified 32 gene modules, five significantly correlated with the coloration variables (4 with color and 1 with luminance). Albeit statistically significant, all these correlations were relatively weak ($-0.43 < r < 0.51$) (Figure S10), and we interpreted them with caution. Magenta and royal blue modules showed the strongest correlations with the color variable, while the tan module showed the strongest correlation with the luminance variable. Among the 967 genes in the magenta module, the five most overrepresented biological functions were very generic: nitrogen compound metabolic process (GO:0006807), metabolic process (GO:0008152), primary metabolic process (GO:0044238), organic substance metabolic process (GO:0071704) and cellular nitrogen compound metabolic process (GO:0034641). In the royal blue

module, only the transposition (GO:0032196) was overrepresented, while in the tan module, no statistically significant overrepresentation was detected. The other two modules statistically correlated with coloration variables, light cyan and midnight blue, were also overrepresented with generic biological processes like primary metabolic process (GO:0044238), metabolic process (GO:0008152), nitrogen compound metabolic process (GO:0006807), cellular metabolic process (GO:0044237), and organic substance metabolic process (GO:0071704).

As expected, the average DEGs content of the five color-correlated modules (2.5% of DEGs in the modules) nearly doubled that of the uncorrelated modules (1.3 %). The representation of color-related genes (from our *a priori* list, see methods) in the modules was, however, not different between the five color-correlated modules (3.6 %) and uncorrelated modules (3.4 %).

4 | DISCUSSION

In amphibians, the genetic mechanism underlying color variation has barely been studied, particularly in non-model species (Rodríguez et al., 2020; Stuckert et al., 2023; Twomey et al., 2020). Our study on *Brachycephalus actaeus* provides the first insight into the molecular basis of color polymorphism in a small Neotropical toadlet of the family Brachycephalidae, likely representing the lowest size limit of color polytypism in tetrapods.

4.1 | Ecological and evolutionary implications of polytypism in *B. actaeus*

Intraspecific color variation (polymorphism and polytypism) in anurans has been associated with diurnal activity, conspicuous colorations, and toxicity (Wollenberg et al., 2008). In particular, polytypism in poison frogs has been suggested as a strategy for balancing detection costs by different predators (Pröhl & Ostrowski, 2011; Willink et al., 2013). This scenario is usually interpreted within the aposematic and cryptic antipredator strategies, in which a species utilizes conspicuous coloration to advertise toxic compounds or colors that mimic the environment to reduce the possibility of being detected by a potential predator, respectively (Caro & Ruxton, 2019; Rojas et al., 2015; Ruxton et al., 2019). Given the presence of tetrodotoxin in some species of pumpkin toadlets (Chimetto-Tonon et al., 2021; Pires et al., 2005) and the diurnality of the genus, the bright orange morphs of *B. actaeus* can be reasonably interpreted in terms of aposematic signal. However, there is no data on the presence of tetrodotoxin in *B.*

actaeus, precluding a selective predation pressure based on color variation and a crypsis/aposematic strategy.

In addition, although birds are considered one of the main predators of frogs (e.g., Dreher et al., 2015; Casa-Cardona et al., 2017; Maan & Cumming, 2012), there is only one report of predation in *Brachycephalus* by a tinamou (Carvalho, 1940). This lack of information also prevents an understanding of how the color variation from *B. actaeus* is perceived by other potential predators and, with it, whether the predator community is indeed exerting selective pressure on this trait. Natural history observations and predation experiments need to be conducted to clarify the role of predation in shaping color variation in *B. actaeus*. This should include consideration of other visually oriented predators such as crabs, spiders, mammals, lizards, and other frogs.

An alternative scenario to explain color variation in *B. actaeus* is intraspecific social interactions. The presence of distinct opsins in the retina of *Brachycephalus* and other diurnal frogs, enables the perception of wavelength sensitivity, resulting in color discrimination (Yovanovich et al., 2017; Wan et al., 2023). For instance, dorsal coloration was revealed to be important for male competition and female mating preference in *Oophaga pumilio* (Crothers et al., 2011; Maan & Cumming, 2008), and it was shown that color variation could also be related to sexual selection (Palacios-Rodriguez et al., 2022). However, the inter and intraspecific color communication and signaling in *Brachycephalus* remains unstudied (see Pombal Jr. et al., 1994). A third alternative scenario to explain this polytypism can be random genetic drift, given the likely isolation of some populations of *B. actaeus* (Chouteau & Angers, 2012; Mallet & Joron, 1999; Reynolds & Fitzpatrick, 2007).

4.2 | Population analyses and phylogenetic relationships

Our results indicate that color variation in *B. actaeus* populations is not linked to genetic structure but to geographic barriers and distances between populations. Similar patterns of genetic structure have been found for other polytypic frogs (Rojas et al., 2020; Roland et al., 2017). The population from São Francisco do Sul Island (SPA) is the most genetically distinct, likely due to geographic isolation by the Babitonga Bay. Despite this isolation, genetic distances between clusters remain relatively low on mitochondrial markers (Monteiro et al., 2018), suggesting recent isolation. The mainland cluster is further divided into two genetic groups that follow the geographic proximities (see

Figure 3), each containing different colored populations. The genetic differences observed in these two groups may be influenced by distance, low vagility, and species-specific microhabitat preferences (Pie et al., 2013), although further studies are needed to address this question. In addition, the sampling gap among these localities may overshadow a clinal pattern of genetic variation.

As discussed in the previous section, the lack of information on toxin profile and natural history hampers solid bases for understanding the origin and maintenance of distinct colored populations in *B*. *actaeus*. Previous works on polytypic frogs suggested that natural and/or sexual selection is not required to increase and maintain color variation (Lehman et al., 2024; Yeager et al., 2023). In fact, in species with small population sizes, which might be the case of the studied species, phenotype fixation may occur randomly through genetic drift (Chouteau & Angers, 2012). Further research on ecology and population genetics is needed to shed light on the roles of selection and drift in maintaining color polytypism in *B. actaeus*. These findings also underscore the importance of re-evaluating the inclusion of only coloration as a diagnostic character in new species descriptions of *Brachycephalus* (Pie et al., 2018; Ribeiro et al., 2017), particularly in cases with low genetic distances or lack of genetic data. Therefore, we emphasize the necessity of incorporating populational genetic variation into the taxonomic context.

4.3 | Insights of skin structural and ultrastructural

Histological examinations allowed us to trace the observed skin color variation of *B*. *actaeus* to the distribution of chromatophores. Specifically, the scarce number or complete absence of melanophores in the orange morphs, along with their more aggregated distribution in the brown, followed by the gray and green morphs, supports a pivotal role of melanin in the color variation observed in this species. We also documented differences in the location of melanophores above and among xanthophores in the green and brown morphs and basal to the xanthophores in the gray morph. Xanthophores were more abundant in the orange skin and contained carotenoids and pteridines (pterinosomes) (Figure 3). These findings align with recent studies on the European fire salamander (*Salamandra salamandra bernardezi*), where melanophores are more abundant in black than brown skin and are rare in yellow skin (Burgon et al., 2020).

In a model proposed by Bagnara & Matsumoto (2006), they used a differential light absorbance and reflecting phenomena generated by the three chromatophore layers to explain the amphibian skin color perceived by a human observer. In this model, green coloration is derived from the interaction of these three layers. In contrast, although not explicitly mentioned, an orange/reddish coloration might be derived from the reflection of these wavelengths in other tissue or cell components and the absence of melanophores. Notably, we did not identify iridophores in the skin of any *B. actaeus* morphs. Thus, our results support this model for the orange coloration perceived in *B. actaeus*, though the component responsible for orange/reddish reflection is still unresolved, while it suggests that the green color is derived from a different phenomenon. Since green coloration is one of the most studied colors in amphibians, our findings, along with recent publications on the role of biliverdin and biliverdin binding proteins in tree frogs (Taboada et al., 2020), reveal that we still ignored many aspects of amphibians' coloration.

4.4 | Gene expression differences between color morphs

In general, previous studies in vertebrates have associated darker colors (brown or green) with a greater expression of melanin genes (Henning et al., 2013; McNamara et al., 2021). By contrast, orange color has been frequently correlated with carotenoids and pteridines genes (Andrade & Carneiro, 2021; Hubbard et al., 2010). Surprisingly, most genes identified in our study were directly or indirectly related to the melanin pathway (19 out of 26). These included significant members of the tyrosinase family (*dct*, *pmel*, *tyrp1*) and melanosome biogenesis or transporter genes (*oca2*, *slc24a5*, *mlana*, *mreg*) (Braasch et al., 2007). We conclude that color variation in *B. actaeus* mainly derives from the differential regulation of melanin production. These results were also concordant with the morphological configuration of the skin revealed in our histological analyses. Finally, given the limited number of color-related genes in our results, we briefly examine each gene’s contribution, indexed by subsections below.

The overlap between our list of DEGs and those in other hyloidean species points to candidate genes for color variation specific to anurans. Of particular interest is a subset of 12 genes (*adamtsl4*, *aldh9a1*, *ccdc80*, *col6a3*, *egfr*, *fat4*, *mrc2*, *pdgfra*, *pnp*, *pnrc2*, *slc29a1*, and *tyrp1*) which have been found differentially expressed between color morphs in three separate studies including ours. Except for *egfr* and *tyrp1*, genes in this list have not previously been associated with pigmentation in other vertebrates

and should be the focus of future studies on amphibians. The collagen alpha-3(VI) chain gene (*col6a3*) is an exciting candidate as the role of the dermic collagen arrays in the pigmentation of anurans has been experimentally verified (Bagnara et al., 2007), but the underlying genetic mechanism is yet to be uncovered.

4.4.1 | Melanin synthesis and pigment associated genes

In vertebrates, melanin is well established to be the primary pigment of darker skin, fur, and feathers (Braasch et al., 2007; Hofreiter & Schöneberg, 2010; Mills & Patterson, 2009; Bajpai et al., 2023). Accordingly, we found a suite of differentially expressed melanin-related genes that contribute to skin pigmentation in the brown, gray, green, and orange color morphs of *B. actaeus*.

Overall, DEGs that were identified to be involved in melanin synthesis were down-regulated or undetectable in orange skin (see below), and this observation matches the lack of or little melanophores in skin structural and ultrastructural analyses. The only higher expressed gene in orange versus all morphs was *mreg*, which plays a role in melanosome transport and is involved in pigmentation (Stuckert et al., 2019). *mreg* was found differentially expressed across color morphs of *D. auratus* but without any noticeable color association (Stuckert et al., 2019). In fishes, *mreg* was positively related to dark colors (Henning et al., 2013). Also, the orange and brown morphs showed the gene *egfr* up-regulated, while in the gray and green morphs, it is down-regulated. Its contribution to orange pigmentation is unknown.

We found a profile of up-regulation of DEGs relating to melanin synthesis contributing to gray and green coloration. Interestingly, the DEGs profile found in the green morph is related to melanosome formation (*dct*, *oca2*, *mlana*, *pmel*, *slc24a5*, and *tyrp1*), whereas in the gray morph DEGs profile likely plays a role in melanin regulation/concentration (*cdh11*, *cdh2*, *edn1*, *wif1*, and *zeb2*). This pattern is supported by the skin structural and ultrastructural analyses.

The expression patterns of the melanosome formation genes *dct*, *tyrp1*, and *pmel* found in the green morph agree with that observed in non-amphibian vertebrates with dark coloration (Higdon et al., 2013; Hoekstra, 2006; McNamara et al., 2021). *dct* (also known as *tyrp2*) and *tyrp1* stimulate the production of eumelanin (McNamara et al., 2021; Vachtenheim & Borovanský, 2010). *pmel* (also known as *silv* or *pmel17*) is involved in melanosome formation, promoting a fibrillar matrix in the melanosome cell to optimize the sequestration and condensation of melanin pigment (McNamara et al.,

2021). Further, the green morph shows the genes *oca2* and *slc24a5* up-regulated, which encode proteins that maintain the ionic stability of the processes during melanosome maturation (Braasch et al., 2007; Lamason et al., 2002).

Furthermore, we identified in the green morph the genes *mlana* (also known as *mart-1* and *melan*) and *rab38* higher expressed. *mlana* is a crucial element controlling the expression of *pmel*, which displays a critical role in melanosome formation (Hoashi et al., 2005). This matches perfectly with the expression profile observed in our study and supports the role of *mlana* for melanin control in the green skin of *B. actaeus*. Correspondingly, *mlana* and *pmel* were down-regulated in yellow skin compared to black skin in European fire salamander (Burgon et al., 2020). *rab38* encodes a protein rab38, playing a significant role in sorting the melanosomal protein tyrp1. Mutational forms cause brown pigmentation in mice (Loftus et al., 2002).

The green versus gray morph shows an unexpected up-regulated gene. The *cbs* gene is linked to pheomelanin synthesis, a key factor for red skin formation (Fang et al., 2022; Zhu et al., 2016). Pheomelanin is an alternative product of the melanin synthesis pathway (e.g., Megía-Palma et al., 2018; Wolnicka-Glubisz et al., 2012). In lizards, pheomelanin was detected in brownish, gray, and black skin coloration (Megía-Palma et al., 2018). Supplementary studies are needed to evaluate the presence of pheomelanin in *Brachycephalus* and the function of associated genes.

Remarkably, most pre-melanosome genes were highly expressed in the gray morph (*brca2*, *cdh2*, *cdh11*, *edn1*, *wif1*, *wnt3a*, *wnt9a*, and *zeb2*). In the initial stages of cell development, *edn1* mediates a specific signaling pathway that modulates melanin synthesis, regulating the production or distribution of melanin in the skin (Braasch & Schartl, 2014). *zeb2*, *cdh2*, and *cdh11* play a role in cell adhesion, regulation, and migration, all influencing melanocyte differentiation (Higdon et al., 2013; Maître & Heisenberg, 2013). Many of these DEGs, *brca2*, *wif1*, *wnt9a*, *egfr*, and *wnt3a*, are from several key signaling pathways influencing or involved in transcription factors preceding melanogenesis (Bagnara & Matsumoto, 2006). Precisely, they directly affect the transcriptional activity of the role MIFT block called the master regulator of melanocyte development, which has a pivotal control in melanogenesis and regulates the expression of the main melanogenic enzymes (Bagnara & Matsumoto, 2006; McLean et al., 2017; McNamara et al., 2021). In *O. pumilio*, the *wnt9a* gene was up-regulated in red and green morphs in contrast to blue (Rodríguez et al., 2020). Finally, we also found the gene *rb1* up-regulated in the gray morph; *rb1* is fundamental for the

cell cycle progression of melanocytes and is a tumor suppressor gene (Carreira et al., 2005). Although this gene was recovered in research on other amphibians, its association with color variation is still unclear (Stuckert et al., 2019).

The DEGs' profiles described here differ from studies in the poison frogs *D. auratus* and *O. histrionica*, which have assigned *mc1r* a role in color variation (Posso-Terranova & Andrés, 2017; Stuckert et al., 2019). In *O. pumilio*, *mc1r*, *kit*, *and tyrp1* are higher expressed in dorsal (green) coloration, whereas *asip* and *tyr* are higher expressed in ventral (yellow) (Stuckert et al., 2023). Another study in *O. pumilio* shows *oca2* up-regulated in blue compared to green and red morphs (Rodríguez et al., 2020). Our results allow us to propose the functional involvement of these melanin-candidate genes in the color morphs of *B. actaeus*. To provide a more precise understanding, we depicted the functions of these genes in melanin synthesis (Figure 5).

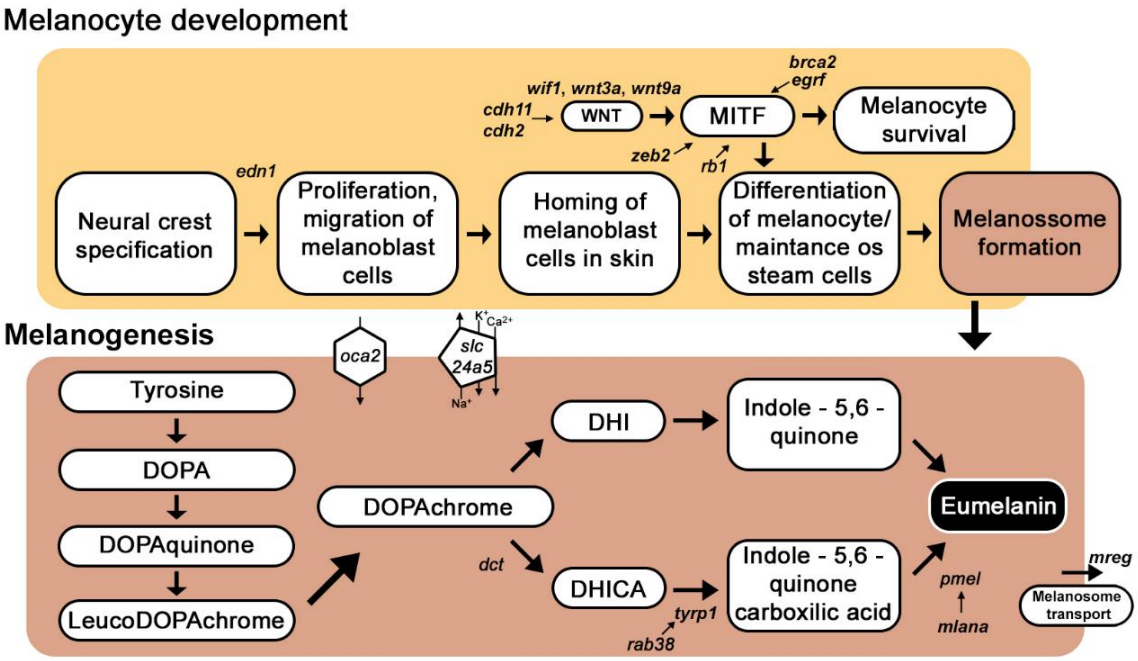


FIGURE 5. Summary of regulatory effects detected on the melanin pathway in *Brachycephalus actaeus*. Steps of the melanocyte development and melanogenesis pathways (adapted from Braasch et al., 2007 and Cieslak et al., 2011) were annotated with the differentially expressed genes identified in our study (in italics) and their putative roles. WNT and MITF are transcription regulators. Gene names: *brca2*, *BRCA2 DNA repair associated*; *cdh11*, *cadherin 11*; *cdh2*, *cadherin 2*; *dct*, *dopachrome tautomerase*; *edn1*, *endothelin 1*; *egfr*, *epidermal growth factor receptor*; *mlana*, *melan-A*; *mreg*, *melanoregulin*; *oca2*, *oculocutaneous albinism II*; *pmel*, *premelanosome protein*; *rab38*, *ras-related protein Rab-38*; *rb1*, *retinoblastoma-associated protein*; *slc24a5*, *solute carrier family 24 member 5*; *tyrp1*, *tyrosinase-related protein 1*; *wif1*, *WNT inhibitory factor 1*; *wnt3a*, *Wnt family member 3A*; *wnt9a*, *wingless-type MMTV integration site family member 9A*; *zeb2*, *zinc finger E-box binding homeobox 2*.

4.4.2 | Genes involved in carotenoid metabolism and purine synthesis

The gray morph of *B. actaeus* shows two up-regulated genes (*aldh1a2*, *rpe65*) involved in carotenoid metabolism. Despite not being directly associated with chromatophores, both genes can influence the regulation of melanocyte stem cells, as well as melanocyte differentiation and proliferation (Amann et al., 2012; VanBuren & Everts, 2022). *aldh1a2* was found higher expressed in green (dorsal) than yellow (ventral) skin coloration during the early development of *O. pumilio* (Stuckert et al., 2023). Gene members from the *aldehyde dehydrogenase 1* family (*aldh1a1* and *aldh1a3*) are associated with blue/green color in frogs (Rodríguez et al., 2020) and red/yellow or blue skin color of lizard species (McLean et al., 2017, 2019; Nicolaï et al., 2021). The gene *rpe65* primarily plays a crucial role in the visual cycle and is essential for rod and cone photoreceptors (VanBuren & Everts, 2022).

The single gene involved in purine synthesis, *gart*, was higher expressed in brown than in green morphs of *B. actaeus*. In *O. pumilio*, *gart* and other genes, which code for enzymes influencing guanine production, showed higher expression in blue frogs (Rodríguez et al., 2020), whereas, in *D. auratus*, the *gart* gene was expressed at low levels in the "green microspot" population (Stuckert et al., 2019). In zebrafish, *gart* mutants present pigmentation defects and microphthalmia, displaying invisible xanthophores and iridophores, while melanophore pigmentation is reduced (Ng et al., 2009). The genes *aldh1a2*, *rpe65*, and *gart* were lower expressed in the orange morph of *B. actaeus*, likely assisting the regulation and playing a functional link with the melanin synthesis genes. The contradiction between the gene expression in guanine synthesis and the lack of iridophores suggests that these genes may also be implicated in other pathways or that the purines accumulate in other chromatophores.

In contrast with melanin, the genetic mechanisms underlying carotenoids and, especially, pteridine pigments are poorly characterized (Andrade & Carneiro, 2021). These candidate genes are essential for producing yellow, orange, or red pigmentation in several amphibians (Bagnara & Hadley, 1969; Rodríguez et al., 2020; Twomey et al., 2020). For example, a carotenoid ketolase gene more highly expressed in the liver than the skin, *cyp3a80*, was recently reported as a color candidate for red morph in *Ranitomeya sirensis* (Twomey et al., 2020). Similarly, in other ectotherms like fishes and reptiles, yellow and orange colorations are associated with the expression of genes of these two pigment classes (Andrade & Carneiro, 2021; McLean et al., 2019; Sefc et al., 2014). The predominance of xanthophores in the skin of orange *B. actaeus* morphs

and the absence of differentially expressed genes linked to carotenoids and pteridines synthesis were unexpected. One possible explanation for this discrepancy is that carotenoid-related genes might be rather expressed in the liver, as shown in *Ranitomeya sirensis* (Twomey et al., 2020). Alternatively, most of these genes might have been expressed during development (Stuckert et al., 2023), with some basal expression levels in the adults that we could not detect.

4.4.3 | Other genes associated with pigmentation

Additional color-related genes were identified in our data set, but the involvement in color differentiation needs to be clarified. Among these DEGs, the gray vs. orange morph has two genes up-regulated (*fanci*, *mcm2*); the orange vs. all morphs has one gene down-regulated (*inpp5b*); and the green vs. gray morph has one gene up-regulated (*sdc4*). They all have putative structural functions that might be in DNA repair or replication and encoding several functions influencing the cell cycle (Ooms et al., 2009; Baxter et al., 2019). *fanci* was linked with hyperpigmentation or spots in human skin, *mcm2* influences hair graying with age in mice, and *sdc4* might be related to melanin abnormalities (Baxter et al., 2019).

4.4.4 | Transcriptome-wide association analysis between gene expression and predator perceptual space

Our results strongly support the contribution of melanin-related genes *oca2*, *dct*, *mlana*, *slc24a5*, and *tyrp1* to color variation in *B. actaeus* individuals. All these genes show decreased expression associated with higher values in the x-coordinate axis of predator perception (red-orange hues) (Table 3). An additional set of 13 genes was also found to be associated with color variation in our results but have not been related to color variation in the literature. Of these, *bmp2*, *c7h10orf95*, *lca5*, *ppp1r3c.2*, *sik1*, *klhdc7b*, *yipf7*, and a paralog of *jun* decrease their expression as the skin color changes to more orange, while the other five genes (*derl3*, *jmjd7*, *LOC116412396*, *znf574*, and a *cdhr3* paralog) increase in expression. These genes constitute interesting candidates for future studies, necessary to understand the molecular mechanisms responsible for color variation in frogs. Remarkably, there exists a compelling to investigate genes heretofore unrecognized (Figure S9), primarily due to the prevailing constraints associated with non-model species.

4.5 | General perspectives

By employing an integrative approach, our study has raised intriguing questions on color variation in a non-model organism, *B. actaeus*. Our bird visual modeling consistently indicates that visually oriented observers perceive color variation among *B. actaeus* morphs differently. Also, our findings revealing the absence of iridophores in the skin of *B. actaeus* morphs may appear to contradict previous findings used to explain how green color arises from the interaction of three chromatophores: xanthophores, iridophores, and melanophores (Bagnara & Matsumoto, 2006). Further, our transcriptomic analysis of skin identified DEGs primarily linked to melanin synthesis, underscoring their role in color polytypism.

Notably, many of the same genes identified actively participate in the typical pigmentation pathways observed in vertebrates. This correlation between divergent genetic profiles (gene expression) and convergent analogous color phenotypes or patterns supports the idea of genetic constraints existing across species. However, it also underscores the inherent flexibility of adaptive mechanisms in color production. For example, among the species of the genus *Ranitomeya*, similar color phenotypes can be explained by parallel and nonparallel convergence related to carotenoid and pterin pigments (Twomey et al., 2023). Similarly, studies in other vertebrates have shown that intrapopulation divergence produces similar phenotypes despite variations in color-related genes and/or functional mechanisms within those genes (Henning et al., 2010; Hubbard et al., 2010; Manceau et al., 2010; Sköld et al., 2016).

We emphasize the need for further research in the *Brachycephalus* system to gain insights into the mechanisms underlying color polytypism, given its distinct biology compared to dendrobatids. Future studies should: 1) identify predators potentially sensitive to UV through visual models and *in situ* experiments; 2) assess the chemical defense; 3) compare toxicity levels among morphs; 4) investigate color's potential role in predator avoidance and sexual selection; 5) elucidate the observed green color derived of skin structures containing xanthophores and melanophores; 6) characterize skin pigments through biochemical identification to clarify expression patterns of the *cbs* gene and assess potential masking effects of melanin on other pigments; and 7) analyze differential expression in organs involved in pigment uptake and metabolism.

5 | CONCLUSIONS

In this study, we addressed the phenotypic variation and the genetic basis for the color polytypism in *Brachycephalus actaeus*. Through bird visual modeling, we classified color morphs and explored their potential functions. We identified pigment cells in toadlet skin corresponding to color and structure. We recognized various candidate color-related genes differentially expressed among this species' brown, gray, green, and orange morphs. Most of these genes are strongly associated with melanin production, highlighting their importance in color variation, aligning with variation in melanophores abundance among morphs. These findings provide the first molecular explanation for amphibian color variation beyond poison frogs and salamanders, integrating molecular data with structural information. Our study underscores the importance of investigating polymorphic species across other groups to gain a comprehensive understanding of the diverse pathways that contribute to the evolution of pigment production in amphibian skin. Future studies should integrate behavior, ecology, and phylogenetic relationships to elucidate the evolutionary process driving adaptive coloration and its potential impact on reproductive isolation. Given this, polytypic species offer valuable insights into fundamental biological processes, including, but not limited to, local adaptation, the persistence of genetic diversity, and speciation. Conservation efforts are crucial to preserving the evolutionary history of each species' color morph.

AUTHORS CONTRIBUTIONS

Conceptualization: J.P.C.M., H.P., M.L.L, A.E.B., C.F.B.H., A.R. Conducting the field work: J.P.C.M., M.L.L, A.E.B, E.C.N. Performing research: J.P.C.M., H.P., M.L.L, A.E.B., C.F.B.H., A.R. Conducting bioinformatic analyses: J.P.C.M., A.R. Analyzing data: J.P.C.M., H.P., M.L.L., A.E.B., A.R. Drafting of the manuscript: J.P.C.M., H.P., M.L.L., A.E.B., A.R. Review and editing of the manuscript: J.P.C.M., H.P., M.L.L, A.E.B., C.F.B.H., T.H.C., E.C.N, A.R. All authors read, reviewed, and approved the final manuscript.

ACKNOWLEDGMENTS

We thank Patricia Maltempi and Marcelo Silva in Brazil and Felix Felmy and Alina Zacher in Hannover for the helpful access to photomicroscopes. We are grateful to Ariadne Sabbag for her invaluable help with TEM images. We also thank A. Sabbag, Carla Lopes, Evan Twomey, Marcus Thadeu Santos Mariana Vasconcellos, P. Maltempi, and Taran Grant for their comments on the previous version of the manuscript.

Computations were performed at the Zentrale Informations- und Datenverarbeitungsservice der Stiftung TiHo Hannover (TiHo-IDS) and were kindly facilitated by Silvester Jordan and Frank Burkhart. J.P.C.M. thanks the Institute of Zoology of TiHo Hannover for its support. This work was supported by grants from the São Paulo Research Foundation to JPCM (FAPESP #2018/09691-0 and #2021/08744-9) and CFBH (FAPESP#2021/10639-5). The work of CFBH and MLL was also funded by The National Council for Scientific and Technological Development (CNPq #306623/2018; CNPq-PDS #163546/2020-7). The work of AEB was funded by Agencia Nacional de Promoción Científica y Tecnológica grant number PICT 2020 #2939 and Consejo Nacional de Investigaciones Científicas y Técnicas (CONICET) grant #PIP 2021-2023. Sequencing costs were covered by a Deutsche Forschungsgemeinschaft (DFG) research grant to AR (RO5508/2-1), a Deutsche Gesellschaft für Herpetologie und Terrarienkunde (DGHT) grant to HP and JPCM (WP-01/2022), and FAPESP (#2021/08744-9).

CONFLICT OF INTEREST STATEMENT

The authors declare no conflicts of interest.

OPEN RESEARCH BADGES

This article has earned an Open Data Badge for making the digitally shareable data publicly available to reproduce the reported results. The data is available at (update).

DATA AVAILABILITY STATEMENT

All raw data, transcriptome assembly, and annotations are (update).
Code for assemblies, annotation, and all subsequent analyses are all available on GitHub (https://github.com/ArielRodrig/update) and in Monteiro and Rodríguez (update).
The data have been deposited with links to BioProject in the NCBI BioProject database (accession number PRJNAxxxxxx; https://www.ncbi.nlm.nih.gov/bioproject/update)

BENEFIT-SHARING STATEMENT

This research project is a collaborative effort between Brazilian, German, Argentinian, and Cuban scientists, building upon the initiative of the Brazilian scientific community. The outcomes of this study will be disseminated to the relevant authorities tasked with implementing conservation measures for the species under consideration.

ORCID

Juliane P.C. Monteiro https://orcid.org/0000-0002-1172-4560
Heike Pröhl https://orcid.org/0000-0003-4918-5838
Mariana L. Lyra https://orcid.org/0000-0002-7863-4965
Andrés E. Brunetti https://orcid.org/0000-0001-7974-6099
Eli C. de Nardin https://orcid.org/0009-0009-7602-4504

Thais H. Condez https://orcid.org/0000-0003-0736-4651
Célio F. B. Haddad https://orcid.org/0000-0003-1057-5660
Ariel Rodríguez https://orcid.org/0000-0003-1936-793X

REFERENCES

Alexander, D. H., Novembre, J., & Lange, K. (2009). Fast model-based estimation of ancestry in unrelated individuals. *Genome Research*, *19*(9), 1655–1664. https://doi.org/10.1101/gr.094052.109

Amann, P. M., Luo, C., Owen, R. W., Hofmann, C., Freudenberger, M., Schadendorf, D., Eichmüller, S. B., & Bazhin, A. V. (2012). Vitamin A metabolism in benign and malignant melanocytic skin cells: Importance of lecithin/retinol acyltransferase and RPE65. *Journal of Cellular Physiology*, *227*(2), 718–728. https://doi.org/10.1002/jcp.22779

Andrade, P., Lyra, M. L., Zina, J., Bastos, D. F. O., Brunetti, A. E., Baêta, D., Afonso, S., Brunes, T. O., Taucce, P. P. G., Carneiro, M., Haddad, C. F. B., & Sequeira, F. (2022). Draft genome and multi-tissue transcriptome assemblies of the Neotropical leaf-frog *Phyllomedusa bahiana*. *G3: Genes, Genomes, Genetics*, *12*(12), 1–9. https://doi.org/10.1093/g3journal/jkac270

Andrade, P., & Carneiro, M. (2021). Pterin-based pigmentation in animals. *Biology Letters*, *17*(20210221), 1–12. https://doi.org/10.1098/rsbl.2021.0221

Andrews, S. (2010). FastQC: A Quality Control Tool for High Throughput Sequence Data. Available online at: http://www.bioinformatics.babraham.ac.uk/projects/fastqc/ (accessed on 4 April 2022)

Bagnara, J. T., Fernandez, P. J., & Fujii, R. (2007). On the blue coloration of vertebrates. *Pigment Cell Research*, *20*(1), 14–26. https://doi.org/10.1111/j.1600-0749.2006.00360.x

Bagnara, J. T. & Matsumoto, J. Comparative anatomy and physiology of pigment cells. In Nonmammalian Tissues Nordlund, J. J., Boissy, R. E., Hearing, V. J., King, R. A., Oetting, W. S., & Ortonne, J.-P. (Eds.). (2006). *The Pigmentary System: Physiology and Pathophysiology* (2nd ed.). Blackwell Publishing Ltd. https://doi.org/10.1002/9780470987100

Bagnara, J. T., & Hadley, M. E. (1969). The control of bright colored pigment cells of fishes and amphibians. *American Zoologist*, *9*, 465–478. https://academic.oup.com/icb/article/9/2/465/200549

Bagnara, J. T., Taylor, J. D., & Hadley, M. E. (1968). The dermal chromatophore unit. *The Journal of Cell Biology*, *38*, 67–79.

Baxter, L. L., Watkins-Chow, D. E., Pavan, W. J., & Loftus, S. K. (2019). A curated gene list for expanding the horizons of pigmentation biology. *Pigment Cell and Melanoma Research*, *32*(3), 348–358. https://doi.org/10.1111/pcmr.12743

Bolger, A. M., Lohse, M., & Usadel, B. (2014). Trimmomatic: A flexible trimmer for Illumina sequence data. *Bioinformatics*, *30*(15), 2114–2120. https://doi.org/10.1093/bioinformatics/btu170

Braasch, I., & Schartl, M. (2014). Evolution of endothelin receptors in vertebrates. In *General and Comparative Endocrinology*, *209*, 21–34. https://doi.org/10.1016/j.ygcen.2014.06.028

Braasch, I., Schartl, M., & Volff, J. N. (2007). Evolution of pigment synthesis pathways by gene and genome duplication in fish. *BMC Evolutionary Biology*, *7*, 1–18. https://doi.org/10.1186/1471-2148-7-74

Bray, N. L., Pimentel, H., Melsted, P., & Pachter, L. (2016). Near-optimal probabilistic RNA-seq quantification. *Nature Biotechnology*, *34*(5), 525–527. https://doi.org/10.1038/nbt.3519

Briolat, E. S., Burdfield-Steel, E. R., Paul, S. C., Rönkä, K. H., Seymoure, B. M., Stankowich, T., & Stuckert, A. M. M. (2019). Diversity in warning coloration: selective paradox or the norm? *Biological Reviews*, *94*(2), 388–414. https://doi.org/10.1111/brv.12460

Brunetti, A. E., Hermida, G. N., Iurman, M. G., & Faivovich, J. (2016). Odorous secretions in anurans: Morphological and functional assessment of serous glands as a source of volatile compounds in the skin of the treefrog *Hypsiboas pulchellus* (Amphibia: Anura: Hylidae). *Journal of Anatomy*, *228*(3), 430–442. https://doi.org/10.1111/joa.12413

Brusa, O., Bellati, A., Meuche, I., Mundy, N. I., & Pröhl, H. (2013). Divergent evolution in the polymorphic granular poison-dart frog, *Oophaga granulifera*: Genetics, coloration, advertisement calls and morphology. *Journal of Biogeography*, *40*(2), 394–408. https://doi.org/10.1111/j.1365-2699.2012.02786.x

Buchfink, B., Xie, C., & Huson, D. H. (2014). Fast and sensitive protein alignment using DIAMOND. *Nature Methods*, *12*(1), 59–60. https://doi.org/10.1038/nmeth.3176

Bushnell, B. BBtools. Available online at: https://sourceforge.net/projects/bbmap/ (accessed on 4 April 2020).

Burgon, J. D., Vieites, D. R., Jacobs, A., Weidt, S. K., Gunter, H. M., Steinfartz, S., Burgess, K., Mable, B. K., & Elmer, K. R. (2020). Functional colour genes and signals of selection in colour-polymorphic salamanders. *Molecular Ecology*, *29*(7), 1284–1299. https://doi.org/10.1111/mec.15411

Bushmanova, E., Antipov, D., Lapidus, A., & Prjibelski, A. D. (2019). RnaSPAdes: A de novo transcriptome assembler and its application to RNA-Seq data. *GigaScience*, *8*(9). https://doi.org/10.1093/gigascience/giz100

Caro, T. (2017). Wallace on coloration: Contemporary perspective and unresolved insights. *Trends in Ecology and Evolution*, *32*(1), 23–30. https://doi.org/10.1016/j.tree.2016.10.003

Caro, T., & Ruxton, G. (2019). Aposematism: Unpacking the defences. *Trends in Ecology and Evolution*, *34*(7), 595–604. https://doi.org/10.1016/j.tree.2019.02.015

Carreira, S., Goodall, J., Aksan, I., La Rocca, S. A., Galibert, M.-D., Denat, L., Larue, L., & Goding, C. R. (2005). Mitf cooperates with Rb1 and activates $p21^{Cip1}$ expression to regulate cycle cell progression. *Nature*, *433*(17), 764–769.

Carvalho, A. L. (1940). Observações sobre casos de batracofagia entre as aves. *Memórias do Instituto Oswaldo Cruz*, *35*(3), 575–576.

Casas-Cardona, S., Márquez, R., & Vargas-Salinas, F. (2018). Different colour morphs of the poison frog *Andinobates bombetes* (Dendrobatidae) are similarly effective visual predator deterrents. *Ethology*, *124*(4), 245–255. https://doi.org/10.1111/eth.12729

Chimetto Tonon, L. A., Rua, C., Crnkovic, C. M., Bernardi, D. I., Pires Junior, O. R., Haddad, C. F. B., Pedrosa, C. S. G., Souza, L. R. Q., Rehen, S. K., de Azevedo, G. P. R., Thompson, C. C., Thompson, F. L., & Berlinck, R. G. S. (2021). Microbiome associated with the tetrodotoxin-bearing anuran *Brachycephalus pitanga*. *Toxicon*, *203*, 139–146. https://doi.org/10.1016/j.toxicon.2021.10.002

Chouteau, M., and B. Angers. 2012. Wright's shifting balance theory and the diversification of aposematic signals. *PLoS ONE*, *7*(3), 1–8. https://doi.org/10.1371/journal.pone.0034028

Condez, T. H., Haddad, C. F. B., & Zamudio, K. R. (2020). Historical biogeography and multi-trait evolution in miniature toadlets of the genus *Brachycephalus* (Anura: Brachycephalidae). *Biological Journal of the Linnean Society*, *129*(3), 664–686. https://doi.org/10.1093/biolinnean/blz200

Crothers, L., Gering, E., & Cummings, M. (2011). Aposematic signal variation predicts male-male interactions in a polymorphic poison frog. *Evolution*, *65*(2), 599–605.

Danecek, P., Auton, A., Abecasis, G., Albers, C. A., Banks, E., DePristo, M. A., Handsaker, R. E., Lunter, G., Marth, G. T., Sherry, S. T., McVean, G., & Durbin, R. (2011). The variant call format and VCFtools. *Bioinformatics*, *27*(15), 2156–2158. https://doi.org/10.1093/bioinformatics/btr330

Davidson, N. M., Hawkins, A. D. K., & Oshlack, A. (2017). SuperTranscripts: A data driven reference for analysis and visualisation of transcriptomes. *Genome Biology*, *18*(1). https://doi.org/10.1186/s13059-017-1284-1

Davidson, N. M., & Oshlack, A. (2014). Corset: Enabling differential gene expression analysis for de novo assembled transcriptomes. *Genome Biology*, *15*(410), 1–14. https://doi.org/10.1186/s13059-014-0410-6

Dobin, A., Davis, C. A., Schlesinger, F., Drenkow, J., Zaleski, C., Jha, S., Batut, P., Chaisson, M., & Gingeras, T. R. (2013). STAR: Ultrafast universal RNA-seq aligner. *Bioinformatics*, *29*(1), 15–21. https://doi.org/10.1093/bioinformatics/bts635

dos Reis, S. F., Clemente-Carvalho, R. B. G., dos Santos, C. M. S. F. F., Lopes, R. T., Von Zuben, F. J., Laborda, P. R., & Perez, S. I. (2020). Skull diversity and evolution in miniaturized amphibians, genus *Brachycephalus* (Anura: Brachycephalidae). Anatomical Record, 304(6), 1–15. https://doi.org/10.1002/ar.24554

Dreher, C. E., Cummings, M. E., & Pröhl, H. (2015). An analysis of predator selection to affect aposematic coloration in a poison frog species. *PLoS ONE*, *10*(6). https://doi.org/10.1371/journal.pone.0130571

Emberts, Z., & Wiens, J. J. (2022). Why are animals conspicuously colored? Evolution of sexual versus warning signals in land vertebrates. Evolution, 76(12), 2879–2892. https://doi.org/10.1111/evo.14636

Fang, W., Huang, J., Li, S., & Lu, J. (2022). Identification of pigment genes (melanin, carotenoid and pteridine) associated with skin color variant in red tilapia using transcriptome analysis. *Aquaculture*, *547*. https://doi.org/10.1016/j.aquaculture.2021.737429

Fisher, M., James-Zorn, C., Ponferrada, V., Bell, A. J., Sundararaj, N., Segerdell, E., Chaturvedi, P., Bayyari, N., Chu, S., Pells, T., Lotay, V., Agalakov, S., Wang, D. Z., Arshinoff, B. I., Foley, S., Karimi, K., Vize, P. D., & Zorn, A. M. (2023). Xenbase: Key features and resources of the *Xenopus* model organism knowledgebase. *Genetics*, *224*(1). https://doi.org/10.1093/genetics/iyad018

Fraley, C., Raftery, A. E., & Murphy, T. B. (2012). *mclust Version 4 for R: Normal Mixture Modeling for Model-Based Clustering, Classification, and Density Estimation*. http://cran.r-project.org/web/packages/mclust/index.html.

Frost, S. K., & Robinson, S. J. (1984). Pigment cell differentiation in the fire-bellied toad, *Bombina orientalis*. I. structural, chemical, and physical aspects of the adult pigment pattern. *Journal of Morphology*, *179*, 229–242.

Gilbert, D. G. (2019). Longest protein, longest transcript or most expression, for accurate gene reconstruction of transcriptomes? *BioRxiv*, 1–27. https://doi.org/10.1101/829184

Goutte, S., Hariyani, I., Utzinger, K. D., Bourgeois, Y., & Boissinot, S. (2022). Genomic analyses reveal association of ASIP with a recurrently evolving adaptive color

pattern in frogs. *Molecular Biology and Evolution*, *39*(11). https://doi.org/10.1093/molbev/msac235

Guo, W., Tzioutziou, N. A., Stephen, G., Milne, I., Calixto, C. P. G., Waugh, R., Brown, J. W. S., & Zhang, R. (2021). 3D RNA-seq: A powerful and flexible tool for rapid and accurate differential expression and alternative splicing analysis of RNA-seq data for biologists. *RNA Biology*, *18*(11), 1574–1587. https://doi.org/10.1080/15476286.2020.1858253

Haas, B. J., Papanicolaou, A., Yassour, M., Grabherr, M., Blood, P. D., Bowden, J., Couger, M. B., Eccles, D., Li, B., Lieber, M., Macmanes, M. D., Ott, M., Orvis, J., Pochet, N., Strozzi, F., Weeks, N., Westerman, R., William, T., Dewey, C. N., … Regev, A. (2013). De novo transcript sequence reconstruction from RNA-seq using the Trinity platform for reference generation and analysis. *Nature Protocols*, *8*(8), 1494–1512. https://doi.org/10.1038/nprot.2013.084

Hashimoto, H., Godo, M., Futahashi, R., Kelsh, R., & Akiyama, T. (2021). Pigments, pigment cells and pigment patterns. In H. Hashimoto, M. Goda, R. Futahashi, R. Kelsh, & T. Akiyama (Eds.), *Pigments, Pigment Cells and Pigment Patterns* (1st ed.). Springer International Publishing. https://doi.org/10.1007/978-981-16-1490-3

Hanifin, C. T. (2010). The chemical and evolutionary ecology of tetrodotoxin (TTX) toxicity in terrestrial vertebrates. *Marine Drugs*, *8*(3), 577–593. https://doi.org/10.3390/md8030577

Hart, A. J., Ginzburg, S., Xu, M., Fisher, C. R., Rahmatpour, N., Mitton, J. B., Paul, R., & Wegrzyn, J. L. (2020). EnTAP: Bringing faster and smarter functional annotation to non-model eukaryotic transcriptomes. *Molecular Ecology Resources*, *20*(2), 591–604. https://doi.org/10.1111/1755-0998.13106

Henning, F., Jones, J. C., Franchini, P., & Meyer, A. (2013). Transcriptomics of morphological color change in polychromatic Midas cichlids. *BMC Genomics*, *14*(1). https://doi.org/10.1186/1471-2164-14-171

Henning, F., Renz, A. J., Fukamachi, S., & Meyer, A. (2010). Genetic, comparative genomic, and expression analyses of the Mc1r locus in the polychromatic Midas cichlid fish (Teleostei, Cichlidae *Amphilophus* sp.) species group. *Journal of Molecular Evolution*, *70*(5), 405–412. https://doi.org/10.1007/s00239-010-9340-4

Higdon, C. W., Mitra, R. D., & Johnson, S. L. (2013). Gene expression analysis of zebrafish melanocytes, iridophores, and retinal pigmented epithelium reveals indicators of biological function and developmental origin. *PLoS ONE*, *8*(7). https://doi.org/10.1371/journal.pone.0067801

Hoashi, T., Watabe, H., Muller, J., Yamaguchi, Y., Vieira, W. D., & Hearing, V. J. (2005). MART-1 is required for the function of the melanosomal matrix protein PMEL17/GP100 and the maturation of melanosomes. *Journal of Biological Chemistry*, *280*(14), 14006–14016. https://doi.org/10.1074/jbc.M413692200

Hoekstra, H. E. (2006). Genetics, development and evolution of adaptive pigmentation in vertebrates. *Heredity*, *97*(3): 222–234. https://doi.org/10.1038/sj.hdy.6800861

Hofreiter, M., & Schöneberg, T. (2010). The genetic and evolutionary basis of colour variation in vertebrates. *Cellular and Molecular Life Sciences*, *67*(15), 2591–2603. https://doi.org/10.1007/s00018-010-0333-7

Hubbard, J. K., Uy, J. A. C., Hauber, M. E., Hoekstra, H. E., & Safran, R. J. (2010). Vertebrate pigmentation: From underlying genes to adaptive function. *Trends in Genetics*, *26*(5), 231–239. https://doi.org/10.1016/j.tig.2010.02.002

Huerta-Cepas, J., Szklarczyk, D., Heller, D., Hernández-Plaza, A., Forslund, S. K., Cook, H., Mende, D. R., Letunic, I., Rattei, T., Jensen, L. J., Von Mering, C., & Bork, P. (2019). EggNOG 5.0: A hierarchical, functionally and phylogenetically

annotated orthology resource based on 5090 organisms and 2502 viruses. *Nucleic Acids Research*, *47*(D1), D309–D314. https://doi.org/10.1093/nar/gky1085

Hutton, P., Seymoure, B. M., McGraw, K. J., Ligon, R. A., & Simpson, R. K. (2015). Dynamic color communication. *Current Opinion in Behavioral Sciences*, *6*, 41–49. https://doi.org/10.1016/j.cobeha.2015.08.007

Kindermann, C., & Hero, J. M. (2016). Pigment cell distribution in a rapid colour changing amphibian (*Litoria wilcoxii*). *Zoomorphology*, *135*(2), 197–203. https://doi.org/10.1007/s00435-016-0303-1

Kopylova, E., Noé, L., & Touzet, H. (2012). SortMeRNA: Fast and accurate filtering of ribosomal RNAs in metatranscriptomic data. *Bioinformatics*, *28*(24), 3211–3217. https://doi.org/10.1093/bioinformatics/bts611

Kosch, T. A., Crawford, A. J., Mueller, R. L., Wollenberg Valero, K. C., Rodríguez, A., O'connell, L. A., Young, N. D., & Skerratt, L. F. (*in press*). Comparative analysis of amphibian genomes: an emerging resource for basic and applied research. https://doi.org/10.1101/2023.02.27.530355

Langfelder, P., & Horvath, S. (2008). WGCNA: An R package for weighted correlation network analysis. *BMC Bioinformatics*, *9*, 1–13. https://doi.org/10.1186/1471-2105-9-559

Lehman, M. R., González-Santoro, M., & Richards-Zawacki, C. L. (2024). Little evidence for color- or size-based mating preferences by male strawberry poison frogs (*Oophaga pumilio*). *Behavioral Ecology and Sociobiology*, *78*(2), 11. https://doi.org/10.1007/s00265-024-03436-9

Lamason, R. L., Mohideen, M.-A. P., Mest, J. R., Wong, A. C., Norton, -Heather L, Aros, M. C., Jurynec, M. J., Mao, X., Humphreville, V. R., Humbert, J. E., Sinha, S., Moore, J. L., Jagadeeswaran, P., Zhao, W., Ning, G., Makalowska, I., McKeigue, P. M., Kittles, R., Parra, E. J., … Cheng, K. C. (2002). SLC24A5, a putative cation exchanger, affects pigmentation in zebrafish and humans. *Science*, *310*, 1782–1786.

Loftus, S. K., Larson, D. M., Baxter, L. L., Antonellis, A., Chen, Y., Wu, X., Jiang, Y., Bittner, M., Hammer III, J. A., & Pavan, W. J. (2002). Mutation of melanosome protein RAB38 in chocolate mice. *The Proceedings of the National Academy of Sciences*, *99*(7), 4471–4476.

Lyra, M. L., Monteiro, J. P. C., Rancilhac, L., Irisarri, I., Künzel, S., Sanchez, E., Condez, T. H., Rojas-Padilla, O., Solé, M., Toledo, L. F., Haddad, C. F. B., & Vences, M. (2021). Initial phylotranscriptomic confirmation of homoplastic evolution of the conspicuous coloration and bufoniform morphology of pumpkin-toadlets in the genus *Brachycephalus*. *Toxins*, *13*(11). https://doi.org/10.3390/toxins13110816

Maan, M. E., & Cummings, M. E. (2008). Female preferences for aposematic signal components in a polymorphic poison frog. *Evolution*, *62*(9), 2334–2345.

Maan, M. E., & Cummings, M. E. (2012). Poison frog colors are honest signals of toxicity, particularly for bird predators. *The American Naturalist*, *179*(1), 1–14. https://doi.org/10.5061/dryad.t979dp85

Maia, R., Gruson, H., Endler, J. A., & White, T. E. (2019). pavo 2: New tools for the spectral and spatial analysis of colour in r. *Methods in Ecology and Evolution*, *10*(7), 1097–1107. https://doi.org/10.1111/2041-210X.13174

Maître, J. L., & Heisenberg, C. P. (2013). Three functions of cadherins in cell adhesion. *Current Biology*, *23*(14), 626–633. https://doi.org/10.1016/j.cub.2013.06.019

Mallet, J., and M. Joron. 1999. Evolution of diversity in warning color and mimicry: Polymorphisms, shifting balance, and speciation. *Annual Review of Ecology and Systematics*, *30*, 201–233. http://abacus.gene.ucl.ac.uk/jim/;and

Manceau, M., Domingues, V. S., Linnen, C. R., Rosenblum, E. B., & Hoekstra, H. E. (2010). Convergence in pigmentation at multiple levels: Mutations, genes and function. *Philosophical Transactions of the Royal Society B: Biological Sciences*, *365*(1552), 2439–2450. https://doi.org/10.1098/rstb.2010.0104

McKenna, A., Hanna, M., Banks, E., Sivachenko, A., Cibulskis, K., Kernytsky, A., Garimella, K., Altshuler, D., Gabriel, S., Daly, M., & DePristo, M. A. (2010). The genome analysis toolkit: A MapReduce framework for analyzing next-generation DNA sequencing data. Genome Research, 20(9), 1297–1303. https://doi.org/10.1101/gr.107524.110

McLean, C. A., Lutz, A., Rankin, K. J., Elliott, A., Moussalli, A., & Stuart-Fox, D. (2019). Red carotenoids and associated gene expression explain colour variation in frillneck lizards. *Proceedings of the Royal Society B: Biological Sciences*, *286*, 1–9. https://doi.org/10.1098/rspb.2019.1172

McLean, C. A., Lutz, A., Rankin, K. J., Stuart-Fox, D., & Moussalli, A. (2017). Revealing the biochemical and genetic basis of color variation in a polymorphic lizard. *Molecular Biology and Evolution*, *34*(8), 1924–1935. https://doi.org/10.1093/molbev/msx136

McNamara, M. E., Rossi, V., Slater, T. S., Rogers, C. S., Ducrest, A. L., Dubey, S., & Roulin, A. (2021). Decoding the evolution of melanin in vertebrates. *Trends in Ecology and Evolution*, *36*(5), 430–443. https://doi.org/10.1016/j.tree.2020.12.012

Megía-Palma, R., Jorge, A., & Reguera, S. (2018). Raman spectroscopy reveals the presence of both eumelanin and pheomelanin in the skin of lacertids. *Journal of Herpetology*, *52*(1), 67–73. https://doi.org/10.1670/16-140

Miller, M. A., Pfeiffer, W., & Schwartz, T. (2010). Creating the CIPRES Science Gateway for inference of large phylogenetic trees. *2010 Gateway Computing Environments Workshop, GCE 2010*. https://doi.org/10.1109/GCE.2010.5676129

Mills, M. G., & Patterson, L. B. (2009). Not just black and white: Pigment pattern development and evolution in vertebrates. *Seminars in Cell and Developmental Biology*, 20(1), 72–81. https://doi.org/10.1016/j.semcdb.2008.11.012

[dataset] Monteiro, J. P. C., & Rodríguez, A. (update). ArielRodrig/Brachycephalus_actaeus_genome: Expression patterns of melanin-related genes are linked to crypsis and aposematism in a pumpkin toadlet (Version v1.0). Zenodo. https://doi.org/10.5281/zenodoupdate

Monteiro, J. P. C., Condez, T. H., Garcia, P. C. A., Comitti, E. J., Amaral, I. B., & Haddad, C. F. B. (2018). A new species of *Brachycephalus* (Anura, Brachycephalidae) from the coast of Santa Catarina State, Southern Atlantic Forest, Brazil. *Zootaxa*, *4407*(4), 483–505. https://doi.org/10.11646/zootaxa.4407.4.2

Müller, F. (1879). *Ituna* and *Thyridia*; a remarkable case of mimicry in butterflies. *Proceedings of the Royal Entomological Society London*, *May*, xx–xxix.

Ng, A., Uribe, R. A., Yieh, L., Nuckels, R., & Gross, J. M. (2009). Zebrafish mutations in *gart* and *paics* identify crucial roles for de novo purine synthesis in vertebrate pigmentation and ocular development. *Development*, *136*(15), 2601–2611. https://doi.org/10.1242/dev.038315

Nicolaï, M. P. J., D'Alba, L., Goldenberg, J., Gansemans, Y., Van Nieuwerburgh, F., Clusella-Trullas, S., & Shawkey, M. D. (2021). Untangling the structural and molecular mechanisms underlying colour and rapid colour change in a lizard,

Agama atra. *Molecular Ecology*, *30*(10), 2262–2284. https://doi.org/10.1111/mec.15901

Nilsson-Sköld, H. N., Aspengren, S., Cheney, K. L., & Wallin, M. (2016). Fish Chromatophores-from molecular motors to animal behavior. *International Review of Cell and Molecular Biology*, *321*, 171–219. https://doi.org/10.1016/bs.ircmb.2015.09.005

Noonan, B. P., & Comeault, A. A. (2009). The role of predator selection on polymorphic aposematic poison frogs. *Biology Letters*, *5*(1), 51–54. https://doi.org/10.1098/rsbl.2008.0586

Ooms, L. M., Horan, K. A., Rahman, P., Seaton, G., Gurung, R., Kethesparan, D. S., & Mitchell, C. A. (2009). The role of the inositol polyphosphate 5-phosphatases in cellular function and human disease. *Biochemical Journal* 419 (1), 29–49. https://doi.org/10.1042/BJ20081673

Osorio, D., & Vorobyev, M. (2008). A review of the evolution of animal colour vision and visual communication signals. *Vision Research*, *48*(20), 2042–2051. https://doi.org/10.1016/j.visres.2008.06.018

Palacios-Rodríguez, P., González-Santoro, M., Amézquita, A., & Brunetti, A. E. (2022). Sexual dichromatism in a cryptic poison frog is correlated with female tadpole transport. *Evolutionary Ecology*, *36*(1), 153–162. https://doi.org/10.1007/s10682-021-10147-4

Pie, M. R., Meyer, A. L. S., Firkowski, C. R., Ribeiro, L. F., & Bornschein, M. R. (2013). Understanding the mechanisms underlying the distribution of microendemic montane frogs (*Brachycephalus* spp., Terrarana: Brachycephalidae) in the Brazilian Atlantic Rainforest. *Ecological Modelling*, *250*, 165–176. https://doi.org/10.1016/j.ecolmodel.2012.10.019

Pie, M. R., Ribeiro, L. F., Confetti, A. E., Nadaline, M. J., & Bornschein, M. R. (2018). A new species of *Brachycephalus* (Anura: Brachycephalidae) from Southern Brazil. *PeerJ*, *6*(e5683), 1–27. https://doi.org/10.7717/peerj.5683

Pires, O. R., Sebben, A., Schwartz, E. F., Morales, R. A. V., Bloch, C., & Schwartz, C. A. (2005). Further report of the occurrence of tetrodotoxin and new analogues in the anuran family Brachycephalidae. *Toxicon*, *45*(1), 73–79. https://doi.org/10.1016/j.toxicon.2004.09.016

Pombal Jr., J. P., Sazima, I., & Haddad, C. F. B. (1994). Breeding behavior of the pumpkin toadlet, *Brachycephalus ephippium* (Brachycephalidae). *Journal of Herpetology*, *28*(4),516–519.

Posso-Terranova, A., & Andrés, J. (2017). Diversification and convergence of aposematic phenotypes: truncated receptors and cellular arrangements mediate rapid evolution of coloration in harlequin poison frogs. *Evolution*, *71*(11), 2677–2692. https://doi.org/10.1111/evo.13335

Pröhl, H., & Ostrowski, T. (2011). Behavioural elements reflect phenotypic colour divergence in a poison frog. *Evolutionary Ecology*, *25*(5), 993–1015. https://doi.org/10.1007/s10682-010-9455-5

Purcell, S., Neale, B., Todd-Brown, K., Thomas, L., Ferreira, M. A. R., Bender, D., Maller, J., Sklar, P., De Bakker, P. I. W., Daly, M. J., & Sham, P. C. (2007). PLINK: A tool set for whole-genome association and population-based linkage analyses. *American Journal of Human Genetics*, *81*(3), 559–575. https://doi.org/10.1086/519795

R Core Team. (2021). R: A language and environment for statistical computing. R Foundation for Statistical Computing, Vienna, Austria. https://www.R-project.org/

Rebouças, R., Carollo, A. B., Freitas, M. de O., Lambertini, C., Dos Santos, R. M. N., & Toledo, L. F. (2019). Is the conspicuous dorsal coloration of the Atlantic Forest pumpkin toadlets aposematic? *Salamandra*, *55*(1), 39–47.

Renoult, J. P., Kelber, A., & Schaefer, H. M. (2017). Colour spaces in ecology and evolutionary biology. *Biological Reviews*, *92*(1), 292–315. https://doi.org/10.1111/brv.12230

Reynolds, R. G., & Fitzpatrick, B. M. (2007). Assortative mating in poison-dart frogs based on an ecologically important trait. *Evolution*, *61*(9), 2253–2259. https://doi.org/10.1111/j.1558-5646.2007.00174.x

Ribeiro, L. F., Blackburn, D. C., Stanley, E. L., Pie, M. R., & Bornschein, M. R. (2017). Two new species of the *Brachycephalus pernix* group (Anura: Brachycephalidae) from the state of Paraná, southern Brazil. *PeerJ*, *5*(e3603), 1–28. https://doi.org/10.7717/peerj.3603

Ritchie, M. E., Phipson, B., Wu, D., Hu, Y., Law, C. W., Shi, W., & Smyth, G. K. (2015). Limma powers differential expression analyses for RNA-sequencing and microarray studies. *Nucleic Acids Research*, *43*(7), e47. https://doi.org/10.1093/nar/gkv007

Rodríguez, A., Mundy, N. I., Ibáñez, R., & Pröhl, H. (2020). Being red, blue and green: The genetic basis of coloration differences in the strawberry poison frog (*Oophaga pumilio*). *BMC Genomics*, *21*(1), 1–16. https://doi.org/10.1186/s12864-020-6719-5

Rojas, B. (2017). Behavioural, ecological, and evolutionary aspects of diversity in frog colour patterns. *Biological Reviews*, *92*(2), 1059–1080. https://doi.org/10.1111/brv.12269

Rojas, B., Burdfield-Steel, E., De Pasqual, C., Gordon, S., Hernández, L., Mappes, J., Nokelainen, O., Rönkä, K., & Lindstedt, C. (2018). Multimodal aposematic signals and their emerging role in mate attraction. *Frontiers in Ecology and Evolution*, *6*, 1–24. https://doi.org/10.3389/fevo.2018.00093

Rojas, B., Valkonen, J., & Nokelainen, O. (2015). Aposematism. *Current Biology*, *25*(9), R350–R351. https://doi.org/10.1016/j.cub.2015.02.015

Roland, A. B., Santos, J. C., Carriker, B. C., Caty, S. N., Tapia, E. E., Coloma, L. A., & O'Connell, L. A. (2017). Radiation of the polymorphic little devil poison frog (*Oophaga sylvatica*) in Ecuador. Ecology and Evolution, 7(22), 9750–9762. https://doi.org/10.1002/ece3.3503

Ruxton, G. D., Allen, W. L., Sherratt, T. N. & Speed, M. P. (2018). *Avoiding Attack: The Evolutionary Ecology of Crypsis, Warning Signals and Mimicry*. 2nd ed., Oxford University Press.

San-Jose, L. M., & Roulin, A. (2017). Genomics of coloration in natural animal populations. *Philosophical Transactions of the Royal Society B: Biological Sciences*, *372*, 1–13. https://doi.org/10.1098/rstb.2016.0337

Schindelin, J., Arganda-Carreras, I., Frise, E., Kaynig, V., Longair, M., Pietzsch, T., Preibisch, S., Rueden, C., Saalfeld, S., Schmid, B., Tinevez, J. Y., White, D. J., Hartenstein, V., Eliceiri, K., Tomancak, P., & Cardona, A. (2012). Fiji: An open-source platform for biological-image analysis. *Nature Methods*, *9*(7), 676–682. https://doi.org/10.1038/nmeth.2019

Schneider, C. A., Rasband, W. S., & Eliceiri, K. W. (2012). NIH Image to ImageJ: 25 years of Image Analysis HHS Public Access. *Nature Methods*, *9*(7), 671–675.

Sefc, K. M., Brown, A. C., & Clotfelter, E. D. (2014). Carotenoid-based coloration in cichlid fishes. *Comparative Biochemistry and Physiology - A Molecular and Integrative Physiology*, *173*, 42–51. https://doi.org/10.1016/j.cbpa.2014.03.006

Shawkey, M. D., & D'Alba, L. (2017). Interactions between colour-producing mechanisms and their effects on the integumentary colour palette. *Philosophical Transactions of the Royal Society B: Biological Sciences*, *372*, 1–9. https://doi.org/10.1098/rstb.2016.0536

Simão, F. A., Waterhouse, R. M., Ioannidis, P., Kriventseva, E. V., & Zdobnov, E. M. (2015). BUSCO: Assessing genome assembly and annotation completeness with single-copy orthologs. *Bioinformatics*, *31*(19), 3210–3212. https://doi.org/10.1093/bioinformatics/btv351

Sofer, T., Kurniansyah, N., Aguet, F., Ardlie, K., Durda, P., Nickerson, D. A., Smith, J. D., Liu, Y., Gharib, S. A., Redline, S., Rich, S. S., Rotter, J. I., & Taylor, K. D. (2021). Benchmarking association analyses of continuous exposures with RNA-seq in observational studies. *Briefings in Bioinformatics*, *22*(6), 1–10. https://doi.org/10.1093/bib/bbab194

Stuart-Fox, D., Aulsebrook, A., Rankin, K. J., Dong, C. M., & McLean, C. A. (2021). Convergence and divergence in lizard colour polymorphisms. *Biological Reviews*, *96*(1), 289–309. https://doi.org/10.1111/brv.12656

Stuckert, A. M. M., Moore, E., Coyle, K. P., Davison, I., MacManes, M. D., Roberts, R., & Summers, K. (2019). Variation in pigmentation gene expression is associated with distinct aposematic color morphs in the poison frog *Dendrobates auratus*. *BMC Evolutionary Biology*, *19*(85), 1–15. https://doi.org/10.1186/s12862-019-1410-7

Stuckert, A. M. M., Freeborn, L., Howell, K. A., Yang, Y., Nielsen, R., Richards-Zawacki, C., & MacManes, M. D. (2023). Transcriptomic analyses during development reveal mechanisms of integument structuring and color production. *Evolutionary Ecology*, 1–22. https://doi.org/10.1007/s10682-023-10256-2

Taboada, C., Brunetti, A. E., Lyra, M. L., Fitak, R. R., Soverna, A. F., Ron, S. R., Lagorio, M. G., Haddad, C. F. B., Lopes, N. P., Johnsen, S., Faivovich, J., Chemes, L. B., & Bari, S. E. (2020). Multiple origins of green coloration in frogs mediated by a novel biliverdin-binding serpin. *Proceedings of the National Academy of Sciences of the United States of America*, *117*(31), 18574–18581. https://doi.org/10.1073/pnas.2006771117

Thomas, P. D., Ebert, D., Muruganujan, A., Mushayahama, T., Albou, L. P., & Mi, H. (2022). PANTHER: Making genome-scale phylogenetics accessible to all. *Protein Science*, *31*(1), 8–22. https://doi.org/10.1002/pro.4218

Toledo, R. C., & Jared, C. (1993). The calcified dermal layer in anurans. *Comparative Biochemistry and Physiology*, *104*(3), 443–448.

Troscianko, J., & Stevens, M. (2015). Image calibration and analysis toolbox - a free software suite for objectively measuring reflectance, colour and pattern. *Methods in Ecology and Evolution*, *6*(11), 1320–1331. https://doi.org/10.1111/2041-210X.12439

Twomey, E., Johnson, J. D., Castroviejo-Fisher, S., & Van Bocxlaer, I. (2020). A ketocarotenoid-based colour polymorphism in the Sira poison frog *Ranitomeya sirensis* indicates novel gene interactions underlying aposematic signal variation. *Molecular Ecology*, *29*(11), 2004–2015. https://doi.org/10.1111/mec.15466

Twomey, E., Kain, M., Claeys, M., Summers, K., Castroviejo-Fisher, S., & Van Bocxlaer, I. (2020). Mechanisms for color convergence in a mimetic radiation of poison frogs. *American Naturalist*, *195*(5), E132–E149. https://doi.org/10.1086/708157

Twomey, E., Melo-Sampaio, P., Schulte, L. M., Bossuyt, F., Brown, J. L., & Castroviejo-Fisher, S. (2023). Multiple routes to color convergence in a radiation of

Neotropical poison frogs. *Systematic Biology*, *72*(6), 1247–1261. https://doi.org/10.1093/sysbio/syad051

Vachtenheim, J., & Borovanský, J. (2010). "Transcription physiology" of pigment formation in melanocytes: Central role of MITF. *Experimental Dermatology*, *19*(7), 617–627. https://doi.org/10.1111/j.1600-0625.2009.01053.x

VanBuren, C. A., & Everts, H. B. (2022). Vitamin A in skin and hair: An update. *Nutrients*, *14*(2952), 1–12. https://doi.org/10.3390/nu14142952

Vorobyev, M., & Osorio, D. (1998). Receptor noise as a determinant of colour thresholds. *Proceedings of the Royal Society B: Biological Sciences*, *265*, 351–358.

Wan, Y. C., Méndez, M. J. N., O'Connell, L. A., Uricchio, L. H., Roland, A. B., Maan, M. E., Ron, S. R., Betancourth-Cundar, M., Pie, M. R., Howell, K. A., Richards-Zawacki, C. L., Cummings, M. E., Cannatella, D. C., Santos, J. C., & Tarvin, R. D. (2023). Selection on visual opsin genes in diurnal Neotropical frogs and loss of the SWS2 opsin in poison frogs. *Molecular Biology and Evolution*, *40*(10), 1–19. https://doi.org/10.1093/molbev/msad206

Wickham, H., Averick, M., Bryan, J., Chang, W., McGowan, L., François, R., Grolemund, G., Hayes, A., Henry, L., Hester, J., Kuhn, M., Pedersen, T., Miller, E., Bache, S., Müller, K., Ooms, J., Robinson, D., Seidel, D., Spinu, V., … Yutani, H. (2019). Welcome to the Tidyverse. *Journal of Open Source Software*, *4*(43), 1686. https://doi.org/10.21105/joss.01686

Willink, B., Brenes-Mora, E., Bolaños, F., & Pröhl, H. (2013). Not everything is black and white: Color and behavioral variation reveal a continuum between cryptic and aposematic strategies in a polymorphic poison frog. *Evolution*, *67*(10), 2783–2794. https://doi.org/10.1111/evo.12153

Willink, B., García-Rodríguez, A., Bolaños, F., & Pröhl, H. (2014). The interplay between multiple predators and prey colour divergence. Biological Journal of the Linnean Society, 113, 580–589. https://academic.oup.com/biolinnean/article/113/2/580/2415924

Wollenberg, K. C., Lötters, S., Mora-Ferrer, C., & Veith, M. (2008). Disentangling composite colour patterns in a poison frog species. *Biological Journal of the Linnean Society*, *93*, 433–444. https://academic.oup.com/biolinnean/article/93/3/433/2701352

Wolnicka-Glubisz, A., Pecio, A., Podkowa, D., Kolodziejczyk, L. M., & Plonka, P. M. (2012). Pheomelanin in the skin of *Hymenochirus boettgeri* (Amphibia: Anura: Pipidae). *Experimental Dermatology*, 21(7), 537–540. https://doi.org/10.1111/j.1600-0625.2012.01511.x

Wright, M. W., & Bowmaker, J. K. (2001). Retinal photoreceptors of paleognathous birds: the ostrich (*Struthio camelus*) and rhea (*Rhea americana*). *Vision Research*, *41*, 1–12. www.elsevier.com/locate/visres

Xie, Y., Wu, G., Tang, J., Luo, R., Patterson, J., Liu, S., Huang, W., He, G., Gu, S., Li, S., Zhou, X., Lam, T. W., Li, Y., Xu, X., Wong, G. K. S., & Wang, J. (2014). SOAPdenovo-Trans: De novo transcriptome assembly with short RNA-Seq reads. *Bioinformatics*, *30*(12), 1660–1666. https://doi.org/10.1093/bioinformatics/btu077

Yang, Y., Blomenkamp, S., Dugas, M. B., Richards-Zawacki, C. L., & Pröhl, H. (2019). Mate choice versus mate preference: inferences about color-assortative mating differ between field and lab assays of poison frog behavior. *American Naturalist*, *193*(4), 598–607. https://doi.org/10.5061/dryad.fs24q30

Yeager, J., Derryberry, G. E., Blum, M. J., & Richards-Zawacki, C. L. (2023). Selection and admixture in a polytypic aposematic frog. *American Naturalist*, *201*(2), 215–228. https://doi.org/10.1086/722559

Yovanovich, C. A. M., Koskela, S. M., Nevala, N., Kondrashev, S. L., Kelber, A., & Donner, K. (2017). The dual rod system of amphibians supports colour discrimination at the absolute visual threshold. *Philosophical Transactions of the Royal Society B: Biological Sciences*, *372*(1717), 1–10. https://doi.org/10.1098/rstb.2016.0066

Zhu, W., Wang, L., Dong, Z., Chen, X., Song, F., Liu, N., Yang, H., & Fu, J. (2016). Comparative transcriptome analysis identifies candidate genes related to skin color differentiation in red tilapia. *Scientific Reports*, *6*, 1–11. https://doi.org/10.1038/srep31347

SUPPORTING INFORMATION

Additional supporting information can be found online in the Supporting Information section at the end of this article. (see p.100)

SUPPORTING INFORMATION

Expression patterns of melanin-related genes are linked to crypsis and conspicuousness in a pumpkin toadlet

Juliane P. C. Monteiro, Heike Pröhl, Mariana L. Lyra, Andrés E. Brunetti, Eli C. de Nardin, Thais H. Condez, Célio F. B. Haddad, Ariel Rodríguez

Correspondence: julianepmonteiro@gmail.com; ariel.Rodriguez@tiho-hannover.de

1 Supplementary Methods

1.1 Color morph classification and bird visual modeling

Macrophotography: camera calibration and image processing

We took images of the natural substrate with a Canon EOS Rebel T7 DSLR Camera coupled to an EF-S 15-55mm lens (without zoom), using the flash mode, shutter speed 1/125, aperture size f/22, and ISO 400, at a distance of ~50 cm. We included a scale quadrant (400 cm^2) to delimit where the focal frog was collected. We took dorsal and lateral photographs of the frogs at a distance of ~25 cm with the same camera coupled to an EF 100mm f/2.8L Macro IS USM lens using the flash mode, shutter speed 1/125, aperture size f/22, and ISO 400. We positioned the camera on a tripod using the same settings of angle, distance, and light. We included in each image a 17.10% and 72.96% neutral reflectance grey scale (for measuring the reflectance, see below), and all images were taken with high resolution in RAW format. All photographs were taken under cloudy daylight illuminance, and we restricted our subsequent reflectance analyses to the human visible spectrum (400-700 nm).

The processing of digital images requires reliable estimates of the camera's spectral sensitivity (Stevens et al., 2009; Troscianko & Stevens, 2015). To obtain this information, we first measured the reflectance spectra Rf (λ) from 30 color and grey patches (N_c=18, N_g=12) on the ColorGauge Micro Target matte (Image Science Associates: ColorGauge ISa). We used a bifurcated optical fiber (Ocean Optics R-200-7-UV/VIS, fiber core size: 200 μm) connected to a spectrometer (Ocean Optics HR2000+) and a deuterium–tungsten DT-Mini-2GS lamp (Ocean

Optics) light source. The spectroscopy software OceanView v.2.0 was applied to measure and average five spectral scans with an integration time of 200 ms and a boxcar width of five. The sensor was positioned perpendicular to the surface of each color patch at a distance of 2 mm. For calibration, we measured the WS-1-SS as white standard (diffuse reflectance standard, Ocean Optics) and switched off the light of DT-Mini-2GS for measuring the dark standard. We repeated the calibration after every six measurements to account for the lamp drift. All color measurements were taken in a dark room to avoid ambient light entering the spectrometer. In addition, we also took reflectance measurements of the grey scale with the spectrophotometer (at the same configurations and conditions listed above). We calculated the reflectance for each 1nm interval in the range of the visual spectrum from 400 nm to 700 nm with the pavo2 package v.2.7.1 (Maia et al., 2019) in R v.4.1.2 (R Core Team 2021). Additionally, we calculated the average reflectance across all 300-nm-intervals by summarizing all reflectance values (in %) and dividing the sum by 300. By doing this, our subsequent analyses were thus restricted to the visible spectrum (VIS; 400-700 nm).

Next, we took pictures of the ColorGauge ISa in natural daylight with the same camera and lenses as used before. This was necessary to estimate the sensitivity of the camera in the red, blue, and green (RGB) channel by measuring all color patches in the picture of the ColorGauge ISa with the help of the micaToolbox v.2.2.2 (Troscianko & Stevens, 2015) in ImageJ v1.52k (Schneider et al., 2012). Standardization was achieved with a measured average reflectance of the eight gray patches in the center on ColorGauge ISa. Finally, with the RGB sensitivity data, we generated a cone catch model for the visual system of the peafowl (*Pavo cristatus*, Phasianidae), with the specific camera and the D65 illuminant (daylight). After, we obtained the photon catches in short-wave-sensitive (SWS; blue), medium-wave-sensitive (MWS; green), long-wave sensitive (LWS; red), and double cone (DC) receptors in the retina of the bird.

For measuring the background reflectance (Rf; n = 39), we selected from each image ten circular regions of interest (ROI´s, 400 pixels; n = 390) delimitated by the quadrant mentioned above. For each frog (n = 39), the Rf was also averaged throughout circular ROI´s (100 pixels) over seven dorsal (two of the head and five of the dorsum; n = 273), and five lateral measurements (n = 195). In all images, overexposed regions were avoided when placing the ROIs. We analyzed males and females together because *B*. *actaeus* does not show sexual dimorphism in coloration (Monteiro et al., 2018), and because our study did not focus on differences between sexes.

Peafowl photoreceptors and visual modeling

In general, birds have four types of photoreceptors (tetrachromatic vision): ultraviolet-sensitive (UVS), short-wave-sensitive (SWS; blue), medium-wave-sensitive (MWS; green) and long-wave sensitive (LWS; red) (Vorobyev et al., 1998) responsible for perceiving color differences. The receptors of the peafowl have spectral peak sensitivities (λ_{max}) at 421 nm for VS, 457 nm for SWS, 505 nm for MWS, and 566 nm for LWS, with a ratio of 1.0 : 1.9 : 2.2 : 2.1 (VS : SWS : MWS : LWS), respectively (Hart, 2001, 2002). Peafowl also possesses double cones (DC, λ_{max}: 567 nm; Hart, 2002), mainly involved in achromatic vision (Hart & Vorobyev, 2005), i.e. for perceiving differences in brightness.

Precisely, we used the mspec images from the dorsal and lateral body of the toadlets generated with the cone catch model using micaToolbox (Troscianko & Stevens, 2015) to calculate quantum catches in the receptors (Q^F) of peafowl. Equally, quantum catches were calculated for the substrates (Q^B). To visualize these perceptual differences in Cartesian coordinates, we computed brightness contrast (ΔL) and color contrast (ΔS) between toadlets and their backgrounds, measuring the Euclidean distances for each locality through the *coldist* function in pavo2 version 2.7.1 (Maia et al., 2019; Pike, 2012) in R. The ΔS was calculated based on the sensitivities of the cone types considering a Weber fraction ω = 0.1 (noise-to-signal ratio) of the bird LWS, and the ΔL was calculated based on the sensitivity of the DC with ω = 0.05 as achromatic Weber fraction, both are typical values employed in bird visual model (Vorobyev et al., 1998; Endler & Mielke, 2005; Pröhl & Ostrowski, 2011). These distances were expressed in "just noticeable differences" (JNDs), where higher ΔL and ΔS denote the conspicuousness of the frogs to bird observers against their natural substrates (Hart & Vorobyev, 2005). Lastly, ΔL and ΔS values were noise-corrected using the *jnd2xyz* function in pavo2 (Maia et al., 2019; Pike, 2012).

1.2 Structural and ultrastructural skin preparation

Small pieces of ~ 0.3 x 0.3 mm were cut from the dorsal and ventral skin regions of *B. actaeus*. These skin samples were fixed for 24 h in a Karnovsky solution (glutaraldehyde 5%, formaldehyde 4%, and 0.1M phosphate buffer, pH 7.2) and rinsed in phosphate buffer (pH 7.2) with two changes after three and six days. The skin samples were kept refrigerated at ~10°C during the entire process. The skin samples were washed in 0.1 mol L-1 phosphate buffer to remove fixative, postfixed in 1% OsO4 for 1 h in the same buffer, then dehydrated in ethanol

followed by a propylene oxide series, and embedded in Araldite resin. Then, semithin sections (1 μm thickness) were stained with 1% Toluidine Blue in 1% Na2CO3. To observe skin ultrastructure, the ultrathin sections (0.50 μm thickness) were stained with 1% uranyl acetate for 25 min at 377°C and lead citrate for 5 min at room temperature.

References

Hart, N. S. (2001). Variations in cone photoreceptor abundance and the visual ecology of birds. *Journal of Comparative Physiology - A Sensory, Neural, and Behavioral Physiology*, *187*(9), 685–697. https://doi.org/10.1007/s00359-001-0240-3

Hart, N. S. (2002). Vision in the peafowl (Aves: *Pavo cristatus*). *The Journal of Experimental Biology*, *205*, 3925–3935.

Hart, N. S., & Vorobyev, M. (2005). Modelling oil droplet absorption spectra and spectral sensitivities of bird cone photoreceptors. *Journal of Comparative Physiology A: Neuroethology, Sensory, Neural, and Behavioral Physiology*, *191*(4), 381–392. https://doi.org/10.1007/s00359-004-0595-3

Maia, R., Gruson, H., Endler, J. A., & White, T. E. (2019). pavo 2: New tools for the spectral and spatial analysis of colour in r. *Methods in Ecology and Evolution*, *10*(7), 1097–1107. https://doi.org/10.1111/2041-210X.13174

Monteiro, J. P. C., Condez, T. H., Garcia, P. C. D. A., Comitti, E. J., Amaral, I. B., & Haddad, C. F. B. (2018). A new species of *Brachycephalus* (Anura, Brachycephalidae) from the coast of Santa Catarina State, Southern Atlantic Forest, Brazil. *Zootaxa*, *4407*(4), 483–505. https://doi.org/10.11646/zootaxa.4407.4.2

Pike, T. W. (2012). Preserving perceptual distances in chromaticity diagrams. *Behavioral Ecology*, *23*(4), 723–728. https://doi.org/10.1093/beheco/ars018

Schneider, C. A., Rasband, W. S., & Eliceiri, K. W. (2012). NIH Image to ImageJ: 25 years of Image Analysis HHS Public Access. *Nature Methods*, *9*(7), 671–675.

Stevens, M., Stoddard, M. C., & Higham, J. P. (2009). Studying primate color: Towards visual system-dependent methods. *International Journal of Primatology*, *30*(6), 893–917. https://doi.org/10.1007/s10764-009-9356-z

Troscianko, J., & Stevens, M. (2015). Image calibration and analysis toolbox - a free software suite for objectively measuring reflectance, colour and pattern. *Methods in Ecology and Evolution*, *6*(11), 1320–1331. https://doi.org/10.1111/2041-210X.12439

2 Supplementary Tables & Figures

Table S1 - List of samples of *Brachycephalus actaeus* used in the present study

Details of samples for mRNA sequencing (RNA), histology (skin voucher) and visual modeling (photo). Acronyms: Juliane Petry de Carli Monteiro field collection number (JPCM). Abbreviations: F = female; M = male; SFS = São Francisco do Sul. Samples with failed RNA extractions are indicated with X.

Sample	Species	Color	Sex	RNA	Skin voucher (dorsal/ventral)	Photo	Locality	Municipality	Latitude (S)	Longitude (W)	Elevation (meters)
JPCM1021	*B. actaeus*	orange	F	OK		OK	Morro do Cantagalo (CAG)	SFS	-26.19363°	-48.73745°	125
JPCM1022	*B. actaeus*	orange	M	OK		OK	Morro do Cantagalo (CAG)	SFS	-26.19363°	-48.73745°	125
JPCM1023	*B. actaeus*	orange	M	OK		OK	Morro do Cantagalo (CAG)	SFS	-26.19363°	-48.73745°	125
JPCM1024	*B. actaeus*	orange	M	OK	9793/9794	OK	Morro do Cantagalo (CAG)	SFS	-26.19363°	-48.73745°	125
JPCM1025	*B. actaeus*	orange	F	**X**	9795/9796	OK	Morro do Cantagalo (CAG)	SFS	-26.19363°	-48.73745°	125
JPCM1026	*B. actaeus*	orange	M			OK	Morro do Cantagalo (CAG)	SFS	-26.19363°	-48.73745°	125
JPCM1027	*B. actaeus*	orange	M			OK	Morro do Cantagalo (CAG)	SFS	-26.19363°	-48.73745°	125
JPCM1028	*B. actaeus*	orange	M			OK	Morro do Cantagalo (CAG)	SFS	-26.19363°	-48.73745°	125
JPCM1029	*B. actaeus*	orange	M			OK	Morro do Cantagalo (CAG)	SFS	-26.19363°	-48.73745°	125
JPCM1030	*B. actaeus*	orange	M	OK		OK	Morro do Cantagalo (CAG)	SFS	-26.19363°	-48.73745°	125
JPCM1031	*B. actaeus*	orange	M			OK	Morro do Cantagalo (CAG)	SFS	-26.19363°	-48.73745°	125
JPCM1032	*B. actaeus*	green	M	OK		OK	Vila da Glória (GLO)	SFS	-26.23945°	-48.70655°	45
JPCM1033	*B. actaeus*	green	F	OK	9797/9798	OK	Vila da Glória (GLO)	SFS	-26.23945°	-48.70655°	45
JPCM1034	*B. actaeus*	green	M	OK	9813/9814	OK	Vila da Glória (GLO)	SFS	-26.23945°	-48.70655°	45
JPCM1035	*B. actaeus*	green	M	OK		OK	Vila da Glória (GLO)	SFS	-26.23945°	-48.70655°	45
JPCM1036	*B. actaeus*	green	F	**X**		OK	Vila da Glória (GLO)	SFS	-26.23945°	-48.70655°	45
JPCM1037	*B. actaeus*	green	M	OK		OK	Vila da Glória (GLO)	SFS	-26.23945°	-48.70655°	45
JPCM1038	*B. actaeus*	green	M	OK	9815/9816	OK	Serra da Palha, Ilha de SFS (SPA)	SFS	-26.29509°	-48.67547°	25
JPCM1039	*B. actaeus*	green	M	OK	9799/9800	OK	Serra da Palha, Ilha de SFS (SPA)	SFS	-26.29509°	-48.67547°	25
JPCM1040	*B. actaeus*	green	M	OK		OK	Serra da Palha, Ilha de SFS (SPA)	SFS	-26.29509°	-48.67547°	25
JPCM1041	*B. actaeus*	green	M	OK		OK	Serra da Palha, Ilha de SFS (SPA)	SFS	-26.29509°	-48.67547°	25
JPCM1042	*B. actaeus*	green	M			OK	Serra da Palha, Ilha de SFS (SPA)	SFS	-26.29509°	-48.67547°	25
JPCM1043	*B. actaeus*	brown	M	OK	9801/9802	OK	Alto Braço do Norte (BNb)	Itapoá	-26.12238°	-48.73989°	455
JPCM1044	*B. actaeus*	brown	M	**X**		OK	Alto Braço do Norte (BNb)	Itapoá	-26.12238°	-48.73989°	455
JPCM1045	*B. actaeus*	brown	M	OK		OK	Alto Braço do Norte (BNb)	Itapoá	-26.12238°	-48.73989°	455
JPCM1046	*B. actaeus*	brown	M	OK	9803/9804	OK	Alto Braço do Norte (BNb)	Itapoá	-26.12238°	-48.73989°	455
JPCM1047	*B. actaeus*	brown	M	OK		OK	Alto Braço do Norte (BNb)	Itapoá	-26.12238°	-48.73989°	455
JPCM1048	*B. actaeus*	green	F	OK	9805/9806	OK	Baixo Braço do Norte (BNg)	Itapoá	-26.12482°	-48.73002°	235
JPCM1049	*B. actaeus*	green	M			OK	Baixo Braço do Norte (BNg)	Itapoá	-26.12482°	-48.73002°	235
JPCM1050	*B. actaeus*	green	F	OK		OK	Baixo Braço do Norte (BNg)	Itapoá	-26.12482°	-48.73002°	235
JPCM1051	*B. actaeus*	green	F	OK	9817/9818	OK	Baixo Braço do Norte (BNg)	Itapoá	-26.12482°	-48.73002°	235
JPCM1052	*B. actaeus*	green	F	OK		OK	Baixo Braço do Norte (BNg)	Itapoá	-26.12482°	-48.73002°	235
JPCM1053	*B. actaeus*	green	F			OK	Baixo Braço do Norte (BNg)	Itapoá	-26.12482°	-48.73002°	235
JPCM1054	*B. actaeus*	green	M			OK	Baixo Braço do Norte (BNg)	Itapoá	-26.12482°	-48.73002°	235
JPCM1058	*B. actaeus*	gray	M			OK	Casarão Backmayer (CAS)	SFS	-26.17532°	-48.71249°	130

Sample	Species	Color	Sex	RNA	Skin voucher (dorsal/ventral)	Photo	Locality	Municipality	Latitude (S)	Longitude (W)	Elevation (meters)
JPCM1059	*B. actaeus*	gray	M	OK	9809/9810	OK	Casarão Backmayer (CAS)	SFS	-26.17532°	-48.71249°	130
JPCM1060	*B. actaeus*	gray	F	OK		OK	Casarão Backmayer (CAS)	SFS	-26.17532°	-48.71249°	130
JPCM1061	*B. actaeus*	gray	F	OK		OK	Casarão Backmayer (CAS)	SFS	-26.17532°	-48.71249°	130
JPCM1062	*B. actaeus*	gray	F	OK	9811/9812	OK	Casarão Backmayer (CAS)	SFS	-26.17532°	-48.71249°	130

Table S2 - Compiled list of color-related genes (see .xlsx separated file)
List of genes linked in the melanin synthesis pathway, carotenoid metabolism, pteridine synthesis, iridophore guanine synthesis, and other pigmentation-associated genes with diverse functions (based on Braasch et al., 2007; Baxter et al., 2019; Higdon et al., 2013; McLean et al., 2017).
Observation: It was included in a separate table due to an extensive number of lines.

Table S3 - Color classification of *Brachycephalus actaeus*

Color classification using peafowl non-correlated variables selected by the best-fit model VVV. The model was based on the Bayesian Information Criterion performed with mclust method (Fraley et al., 2012). See Material and Methods for details. Abbreviations: BNb, Alto Braço do Norte; BNg, Baixo Braço do Norte; CAG, Cantagalo; CAS, Casarão; GLO, Vila da Glória; LWS, long-wave sensitive; SPA, Serra da Palha; and SWS, short-wave-sensitive. Acronym: JPCM, Juliane Petry de Carli Monteiro.

Voucher	Locality	Morph	SWS dorsal	SWS side	LWS side	MClust group
JPCM1021	CAG	orange	0.380	0.120	0.149	1
JPCM1022	CAG	orange	0.427	0.129	0.156	1
JPCM1023	CAG	orange	0.335	0.118	0.145	1
JPCM1024	CAG	orange	0.259	0.121	0.141	2
JPCM1025	CAG	orange	0.409	0.120	0.145	1
JPCM1026	CAG	orange	0.414	0.112	0.133	1
JPCM1027	CAG	orange	0.328	0.110	0.130	1
JPCM1028	CAG	orange	0.416	0.125	0.162	1
JPCM1029	CAG	orange	0.417	0.115	0.142	1
JPCM1030	CAG	orange	0.345	0.122	0.154	1
JPCM1031	CAG	orange	0.388	0.129	0.162	1
JPCM1032	GLO	green	0.145	0.126	0.134	3
JPCM1033	GLO	green	0.137	0.130	0.135	3
JPCM1034	GLO	green	0.152	0.130	0.140	3
JPCM1035	GLO	green	0.144	0.137	0.149	3
JPCM1036	GLO	green	0.138	0.118	0.125	3
JPCM1037	SPA	green	0.154	0.119	0.131	3
JPCM1038	SPA	green	0.127	0.121	0.126	3
JPCM1039	SPA	green	0.141	0.111	0.122	3
JPCM1040	SPA	green	0.132	0.107	0.117	3
JPCM1041	SPA	green	0.137	0.097	0.111	3
JPCM1042	SPA	green	0.144	0.103	0.117	3
JPCM1043	BNb	brown	0.155	0.137	0.161	2
JPCM1044	BNb	brown	0.183	0.138	0.172	2
JPCM1045	BNb	brown	0.173	0.124	0.144	2
JPCM1046	BNb	brown	0.200	0.132	0.155	2
JPCM1047	BNb	brown	0.180	0.155	0.195	2
JPCM1048	BNg	green	0.157	0.118	0.129	3
JPCM1049	BNg	green	0.169	0.130	0.136	3
JPCM1050	BNg	green	0.173	0.130	0.141	2
JPCM1051	BNg	green	0.147	0.127	0.135	3
JPCM1052	BNg	green	0.156	0.125	0.136	3
JPCM1053	BNg	green	0.138	0.129	0.136	3
JPCM1054	BNg	green	0.143	0.121	0.124	3
JPCM1058	CAS	gray	0.228	0.128	0.141	4
JPCM1059	CAS	gray	0.239	0.136	0.158	4
JPCM1060	CAS	gray	0.213	0.126	0.149	4
JPCM1061	CAS	gray	0.262	0.136	0.153	4
JPCM1062	CAS	gray	0.169	0.121	0.130	2

Table S4 - Skin layers measurements (in µm) of *Brachycephalus actaeus* morphs from dorsal and ventral regions
Values were presented following mean ± standard deviation (minimum–maximum). Abbreviation: BNb, Alto Braço do Norte; BNg, Baixo Braço do Norte; CAG, Cantagalo; CAS, Casarão; GLO, Vila da Glória; EK, calcified Eberth-Kastschenko; and SPA, Serra da Palha. Acronym: JPCM, Juliane Petry de Carli Monteiro.

Voucher	Slide	Locality	Morph	RNA	Layer	Dorsal region	Ventral region
JPCM1024	9793	CAG	orange	OK	Epidermis	9.20 ± 1.89 (3.54–14.00)	5.77 ± 0.99 (3.96–8.64)
					Stratum spongiosum	14.34 ± 5.46 (9.03–26.47)	10.58 ± 8.77 (3.20–32.05)
					EK	7.23 ± 3.22 (1.77–13.57)	13.17 ± 8.65 (0.79–22.99)
					Stratum compactum	43.18 ± 4.35 (33.27–51.64)	36.16 ± 8.53 (23.73–44.46)
JPCM1025	9795	CAG	orange	fail	Epidermis	10.16 ± 0.64 (8.43–12.13)	9.08 ± 2.67 (6.08–12.46)
					Stratum spongiosum	12.78 ± 9.54 (5.41–35.98)	13.11 ± 3.83 (5.05–17.24)
					EK	5.29 ± 2.60 (2.26–10.80)	12.62 ± 5.13 (5.25–27.12)
					Stratum compactum	33.37 ± 3.87 (24.41–38.08)	48.54 ± 10.37 (29.71–56.57)
JPCM1033	9797	GLO	green	OK	Epidermis	6.20 ± 1.01 (3.89–8.62)	15.03 ± 5.31 (10.35–25.21)
					Stratum spongiosum	7.80 ± 4.63 (3.20–21.76)	14.22 ± 10.77 (5.50–43.41)
					EK	2.78 ± 1.27 (1.63–5.98)	13.91 ± 10.30 (4.50–37.93)
					Stratum compactum	23.78 ± 1.87 (18.39–32.59)	42.71 ± 6.93 (32.84–51.32)
JPCM1034	9813	GLO	green	OK	Epidermis	9.33 ± 2.88 (7.22–14.18)	10.48 ± 1.06 (8.12–11.86)
					Stratum spongiosum	17.55 ± 12.35 (7.12–34.6)	18.51 ± 8.06 (7.82–26.95)
					EK	11.72 ± 5.85 (5.28–19.11)	17.08 ± 11.2 (3.26–42.23)
					Stratum compactum	65.75 ± 8.2 (54.01–75.22)	50.8 ± 13.00 (36.18–77.9)
JPCM1038	9815	SPA	green	OK	Epidermis	12.89 ± 4.77 (7.27–18.81)	9.50 ± 1.19 (7.18–12.95)
					Stratum spongiosum	25.48 ± 13.21 (8.91–45.43)	18.66 ± 10.29 (7.75–33.44)
					EK	9.80 ± 5.15 (4.54–15.69)	15.06 ± 8.66 (7.33–34.48)
					Stratum compactum	57.93 ± 11.13 (42.33–80.38)	25.07 ± 5.15 (18.54–34.87)
JPCM1039	9799	SPA	green	OK	Epidermis	14.69 ± 7.23 (5.95–24.89)	9.38 ± 1.31 (6.94–12.85)
					Stratum spongiosum	17.57 ± 9.44 (9.11–32.14)	13.31 ± 11.53 (4.59–45.86)

Voucher	Slide	Locality	Morph	RNA	Layer	Dorsal region	Ventral region
					EK	6.58 ± 2.55 (1.95–10.88)	9.12 ± 4.09 (3.64–20.11)
					Stratum compactum	38.79 ± 6.66 (26.72–54.35)	37.39 ± 5.77 (22.03–52.76)
JPCM1043	9801	BNb	brown	OK	Epidermis	13.05 ± 3.52 (9.4–16.43)	11.73 ± 2.05 (8.95–16.72)
					Stratum spongiosum	35.73 ± 39.26 (11.47–81.03)	16.89 ± 17.83 (3.83–68.18)
					EK	7.2 ± 5.21 (2.92–13.01)	14.47 ± 11.85 (5.69–39.43)
					Stratum compactum	35.59 ± 12.73 (20.89–43.08)	36.94 ± 4.61 (26.69–47.22)
JPCM1046	9803	BNb	brown	OK	Epidermis	7.52 ± 13.38 (5.88–9.5)	6.68 ± 2.26 (3.35–11.50)
					Stratum spongiosum	15.53 ± 7.49 (5.67–36.78)	3.49 ± 1.22 (2.24–5.73)
					EK	5.28 ± 2.31 (2.76–8.22)	9.46 ± 7.43 (2.86–22.73)
					Stratum compactum	27.64 ± 2.93 (22.91–30.57)	32.74 ± 8.32 (24.57–47.88)
JPCM1048	9805	BNg	green	OK	Epidermis	11.51 ± 3.36 (6.14–15.46)	8.74 ± 2.08 (6.48–13.10)
					Stratum spongiosum	19.52 ± 6.64 (6.43–31.49)	32.8 ± 20.11 (15.45–60.00)
					EK	10.59 ± 5.36 (3.72–19.61)	9.45 ± 1.45 (6.68–12.73)
					Stratum compactum	50.69 ± 2.16 (28.15–73.84)	50.59 ± 3.74 (41.6–54.58)
JPCM1051	9817	BNg	green	OK	Epidermis	14.03 ± 4.71 (7.02–19.85)	8.74 ± 3.31 (5.62–14.30)
					Stratum spongiosum	16.6 ± 10.79 (4.47–47.88)	15.37 ± 12.26 (6.08–48.04)
					EK	5.06 ± 2.57 (1.74–8.25)	13.94 ± 5.63 (6.85–20.31)
					Stratum compactum	51.26 ± 11.77 (41.43–66.99)	47.01 ± 9.34 (35.68–53.32)
JPCM1059	9809	CAS	gray	OK	Epidermis	3.92 ± 0.70 (2.66–4.96)	8.2 ± 1.00 (5.66–10.04)
					Stratum spongiosum	8.13 ± 6.43 (3.66–16.01)	8.86 ± 6.78 (2.7–22.32)
					EK	2.02 ± 0.91 (0.65–2.84)	9.88 ± 5.59 (4.94–22.17)
					Stratum compactum	18.32 ± 1.11 (16.07–20.11)	25.06 ± 2.75 (22.99–31.15)
JPCM1062	9811	CAS	gray	OK	Epidermis	11.17 ± 2.28 (7.23–14.09)	8.55 ± 0.42 (7.88–8.95)
					Stratum spongiosum	22.11 ± 10.46 (11.77–47.71)	11.18 ± 12.97 (3.30–45.78)
					EK	5.45 ± 3.89 (1.59–13.77)	23.49 ± 8.82 (11.64–33.68)

Voucher	Slide	Locality	Morph	RNA	Layer	Dorsal region	Ventral region
					Stratum compactum	35.54 ± 6.60 (27.7–47.58)	32.41 ± 6.41 (25.91–44.23)

Table S5 - Descriptive statistics of the transcriptome assemblies
The first three columns describe the assemblies used as input for the final ensemble assembly with EvidentialGene pipeline (last column). The three input transcriptomes in this table represent the de-duplicated collection of all transcriptomes produced by each assembler (24x SOAPdenovo-trans, 6x rnaSPADES, and 6x Trinity sets to one file for the concatenated transcript collection).

	SOAPdenovo-trans	rnaSPADES	Trinity	EvidentialGene (final Ensemble)
Number of transcripts	4,942,020	1,364,522	2,642,442	764,760
Mean transcript length	641	794	521	1,153
Longest transcript	43,552	43,456	31,228	43,465
Transcript N50	1,385	1,760	721	2,098
BUSCO score	94.3%	94.2%	92.7%	94.4%

Table S6 – Differentially expressed genes cross-comparison among anurans

Comparison of DEGs from skin color morphs between anuran species available in the literature: *Brachycephalus actaeus* (this study), *Dendrobates auratus* (Stuckert et al., 2019), *Oophaga pumilio* (Rodríguez et al., 2020), and *Ranitomeya sirensis* (Twomey et al., 2020). Abbreviation: Cum. = cumulative evidence.

Symbol	Gene name	*B. actaeus*	*R. sirensis*	*D. auratus*	*O. pumilio*	Color-related	Function	Cum.
adam11	*ADAM metallopeptidase domain 11*	X		X		NO		2
adamts1	*ADAM metallopeptidase with thrombospondin type 1 motif 1*	X			X	NO		2
adamtsl4	*ADAMTS like 4*	X		X	X	NO		3
adh1	*alcohol dehydrogenase 1*	X			X	NO		2
adm	*adrenomedullin*	X			X	NO		2
aldh9a1	*aldehyde dehydrogenase 9 family member A1*	X		X	X	NO		3
atf3	*activating transcription factor 3*	X			X	NO		2
atg4d	*autophagy related 4D, cysteine peptidase*	X			X	NO		2
b3galt5	*Beta-1,3-galactosyltransferase 5*	X			X	NO		2
bmp6	*bone morphogenetic protein 6*	X			X	NO		2
brca2	*BRCA2, DNA repair associated*	X	X			YES	pigmentation variation	2
c1d	*C1D nuclear receptor corepressor*	X			X	NO		2
carhsp1	*calcium regulated heat stable protein 1*	X		X		NO		2
cbs	*cystathionine-beta-synthase*	X			X	YES	pigmentation variation	2
ccdc80	*coiled-coil domain containing 80*	X		X	X	NO		3
cdh11	*cadherin 11*	X		X		YES	pigmentation variation	2
cfap53	*cilia and flagella associated protein 53*	X			X	NO		2
chtf18	*chromosome transmission fidelity factor 18*	X			X	NO		2
cnn1	*calponin 1, basic, smooth muscle*	X		X		NO		2
col14a1	*collagen, type XIV, alpha 1*	X		X		NO		2
col18a1	*collagen type XVIII alpha 1*	X		X		NO		2
col6a3	*collagen type VI alpha 3 chain*	X		X	X	NO		3
cpxm2	*carboxypeptidase X (M14 family), member 2*	X		X		NO		2
cyp2k4	*cytochrome P450 2K4 gene 1*	X			X	NO		2
dcn	*decorin*	X		X		NO		2
ddit3	*DNA damage inducible transcript 3*	X			X	NO		2
dlc1	*DLC1 Rho GTPase activating protein*	X			X	NO		2
ednrb2	*endothelin receptor B subtype 2*	X		X		NO		2
egfr	*epidermal growth factor receptor*	X		X	X	YES	pigmentation variation	3

Symbol	Gene name	*B. actaeus*	*R. sirensis*	*D. auratus*	*O. pumilio*	Color-related	Function	Cum.
ethe1	*ethylmalonic encephalopathy 1*	X			X	NO		2
fat4	*FAT atypical cadherin 4*	X		X	X	NO		3
fkbp15	*FKBP prolyl isomerase family member 15*	X		X		NO		2
fos	*Fos proto-oncogene, AP-1 transcription factor subunit*	X			X	NO		2
gart	*phosphoribosylglycinamide formyltransferase, phosphoribosylglycinamide synthetase, phosphoribosylaminoimidazole synthetase*	X		X		YES	guanine synthesis in iridophores	2
ggct	*gamma-glutamylcyclotransferase*	X			X	NO		2
gpm6b	*glycoprotein M6B*	X			X	NO		2
gramd1a	*GRAM domain containing 1A*	X		X		NO		2
herpud1	*homocysteine inducible ER protein with ubiquitin like domain 1*	X			X	NO		2
hgd	*homogentisate 1,2-dioxygenase*	X			X	NO		2
ipo4	*importin 4*	X			X	NO		2
kank2	*KN motif and ankyrin repeat domains 2*	X		X		NO		2
kctd12	*potassium channel tetramerization domain containing 12*	X			X	NO		2
klf4	*KLF transcription factor 4*	X			X	NO		2
klhdc7b	*kelch domain containing 7B*	X			X	NO		2
lcmt1	*leucine carboxyl methyltransferase 1*	X			X	NO		2
lin1	*LINE-1 reverse transcriptase homolog*	X			X	NO		2
lorf2	*LINE-1 retrotransposable element ORF2 protein*	X			X	NO		2
loxl2	*lysyl oxidase like 2*	X		X		NO		2
lum	*lumican*	X		X		NO		2
ly75	*lymphocyte antigen 75*	X			X	NO		2
mamdc2	*MAM domain containing 2*	X		X		NO		2
manf	*mesencephalic astrocyte-derived neurotrophic factor*	X			X	NO		2
map1lc3a	*microtubule associated protein 1 light chain 3 alpha*	X		X		YES	pigmentation variation	2
mlana	*melan-A*	X			X	YES	pigmentation variation	2
mmp16	*matrix metallopeptidase 16*	X			X	NO		2
mmp28	*matrix metalloproteinase 28*	X			X	NO		2
mrc2	*mannose receptor C type 2*	X		X	X	NO		3
msx2	*msh homeobox 2*	X		X		NO		2
mthfs	*5,10-methenyltetrahydrofolate synthetase (5-formyltetrahydrofolate cyclo-ligase)*	X			X	NO		2
ndnf	*neuron-derived neurotrophic factor*	X			X	NO		2
nedd1	*NEDD1 gamma-tubulin ring complex targeting factor*	X			X	NO		2

Symbol	Gene name	*B. actaeus*	*R. sirensis*	*D. auratus*	*O. pumilio*	Color-related	Function	Cum.
nnmt	*nicotinamide N-methyltransferase*	X			X	NO		2
nr1i3	*nuclear receptor subfamily 1 group I member 3*	X		X		NO		2
nr4a1	*nuclear receptor subfamily 4 group A member 1*	X			X	NO		2
nxpe4	*neurexophilin and PC-esterase domain family member 4*	X			X	NO		2
oca2	*oculocutaneous albinism II*	X			X	YES	melanin synthesis	2
olfml2a	*olfactomedin like 2A*	X		X		NO		2
osmr	*oncostatin M receptor*	X		X		NO		2
p4ha2	*prolyl 4-hydroxylase, alpha polypeptide 2*	X			X	NO		2
pdgfra	*platelet derived growth factor receptor alpha*	X		X	X	NO		3
plp1	*proteolipid protein 1*	X		X		NO		2
pmel	*premelanosome protein*	X	X			YES	melanin synthesis	2
pnp	*purine nucleoside phosphorylase*	X	X		X	NO		3
pnrc2	*proline rich nuclear receptor coactivator 2*	X		X	X	NO		3
pol	*pol polyprotein*	X			X	NO		2
ppfia3	*protein tyrosine phosphatase, receptor type, f polypeptide (PTPRF), interacting protein (liprin), alpha 3*	X			X	NO		2
ptprd	*protein tyrosine phosphatase receptor type D*	X			X	NO		2
rgn	*regucalcin*	X			X	NO		2
rif1	*replication timing regulatory factor 1*	X		X		NO		2
rtn4rl1	*reticulon 4 receptor-like 1*	X			X	NO		2
s100pbp	*S100P binding protein*	X		X		NO		2
scara5	*scavenger receptor class A member 5*	X		X		NO		2
sdc1	*syndecan 1*	X			X	NO		2
sdc3	*syndecan 3*	X		X		NO		2
sdc4	*syndecan 4*	X		X		YES	pigmentation variation	2
sec14l5	*SEC14-like lipid binding 5*	X		X		NO		2
serpinf1	*serpin peptidase inhibitor, clade F (alpha-2 antiplasmin, pigment epithelium derived factor), member 1*	X			X	NO		2
sfmbt2	*Scm like with four mbt domains 2*	X			X	NO		2
slc29a1	*solute carrier family 29 member 1 (Augustine blood group)*	X	X		X	NO		3
slc34a2	*solute carrier family 34 member 2*	X			X	NO		2
slc4a1	*solute carrier family 4 member 1 (Diego blood group)*	X	X			NO		2
slc6a14	*solute carrier family 6 member 14, gene 1*	X			X	NO		2
slit1	*slit guidance ligand 1*	X		X		NO		2

Symbol	Gene name	*B. actaeus*	*R. sirensis*	*D. auratus*	*O. pumilio*	Color-related	Function	Cum.
slit2	*slit guidance ligand 2*	X		X		NO		2
smad9	*SMAD family member 9*	X			X	NO		2
sorbs1	*sorbin and SH3 domain containing 1*	X			X	NO		2
srprb	*SRP receptor subunit beta*	X			X	NO		2
st3gal3	*ST3 beta-galactoside alpha-2,3-sialyltransferase 3*	X			X	NO		2
taok1	*TAO kinase 1*	X		X		NO		2
tdrd3	*tudor domain containing 3*	X			X	NO		2
tfb2m	*transcription factor B2, mitochondrial*	X			X	NO		2
tmem120b	*transmembrane protein 120B*	X			X	NO		2
tnip2	*TNFAIP3 interacting protein 2*	X			X	NO		2
ttc1	*tetratricopeptide repeat domain 1*	X			X	NO		2
ttc9	*tetratricopeptide repeat domain 9*	X			X	NO		2
ty3b-i	*transposon Ty3-I Gag-Pol polyprotein*	X			X	NO		2
tyrp1	*tyrosinase-related protein 1*	X		X	X	YES	melanin synthesis	3
vcan	*versican*	X		X		NO		2
vwf	*von Willebrand factor*	X		X		NO		2
wnt9a	*wingless-type MMTV integration site family member 9A*	X			X	YES	melanin synthesis	2
wsb1	*WD repeat and SOCS box containing 1*	X			X	NO		2
*xlcof22**	*oocyte zinc finger protein XlCOF22*	X			X	NO		2
zbed6	*zinc finger, BED-type containing 6*	X		X		NO		2
zfp36	*ZFP36 ring finger protein*	X			X	NO		2
znf638	*zinc finger protein 638*	X		X		NO		2

*as *zo22* in Rodríguez et al. (2020).

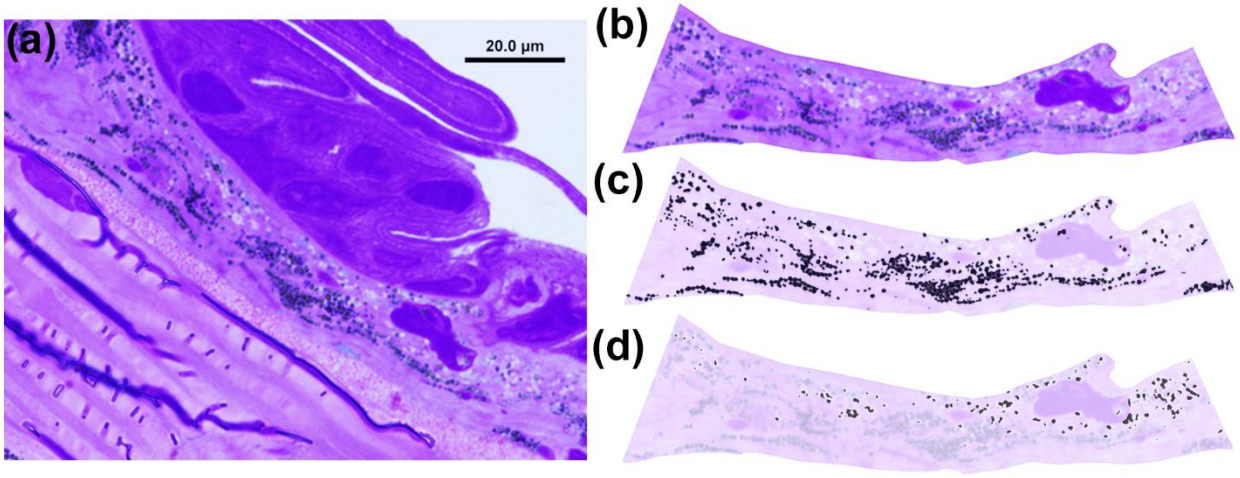


Figure S1 –Quantification of chromatophores in *Brachycephalus actaeus* skin
Procedure for quantifying coverage of melanophores and xanthophores in the skin of *B*. *actaeus*. (a) Representative image of the skin of *B*. *actaeus* used for analysis. (b) Manual selection of the chromatophore layer to measure the total area. Creation of a mask for measuring the coverage of (c) melanosomes and (d) xanthophores, obtained through image segmentation using Trainable Weka Segmentation plugin version 3.0.

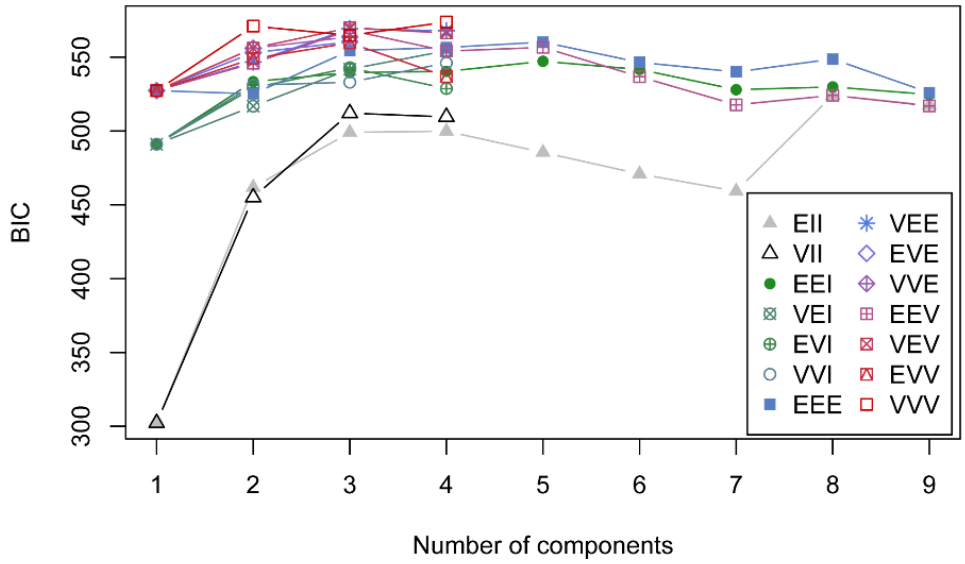


Figure S2 - Color classification model for *Brachycephalus actaeus* morphs
The best-fit model by Bayesian Inference Criterium (BIC) using the mclust method to classify the color morphs of *Brachycephalus actaeus* was ellipsoidal, varying volume, shape, and orientation (VVV = 573.7876 score). The three non-correlated variables (short-wave-sensitive in dorsal and lateral views and long-wave sensitive in lateral view) were based on photon catch sensitivities of peafowl obtained from frog images in micaToolbox. The legend shows multivariate model names from package mclust (Fraley et al., 2022).

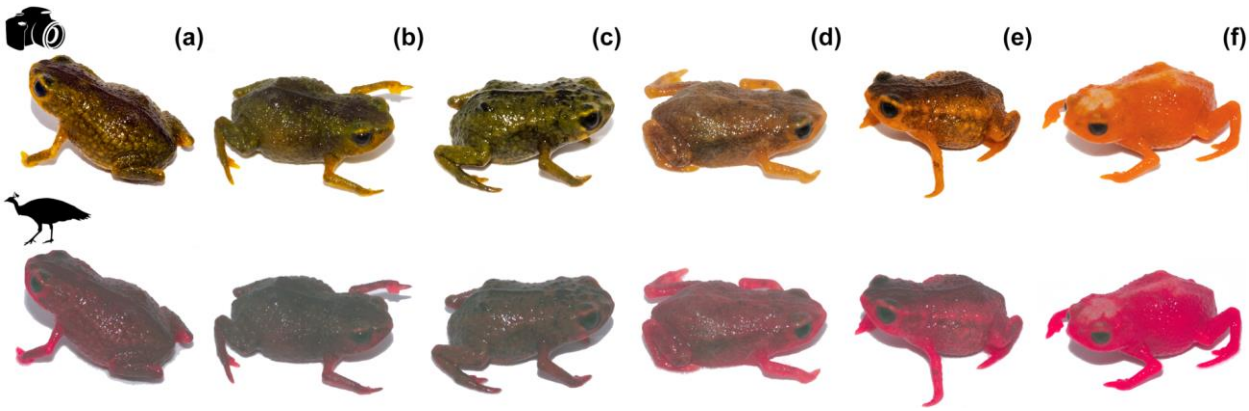


Figure S3 - Original calibrated photographs and simulated bird visual perception of *Brachycephalus actaeus* morphs

Original calibrated photographs and simulated bird visual perception of *Brachycephalus actaeus* morphs. Icons at the left of each row indicate original camera captures and peafowl simulated vision, respectively. (a–c) green morphs (JPCM 1048, 1033, 1039); (d) gray morph (JPCM1059); (e) brown morph (JPCM1046); and (f) orange morph (JPCM1025). See voucher details in Table S1.

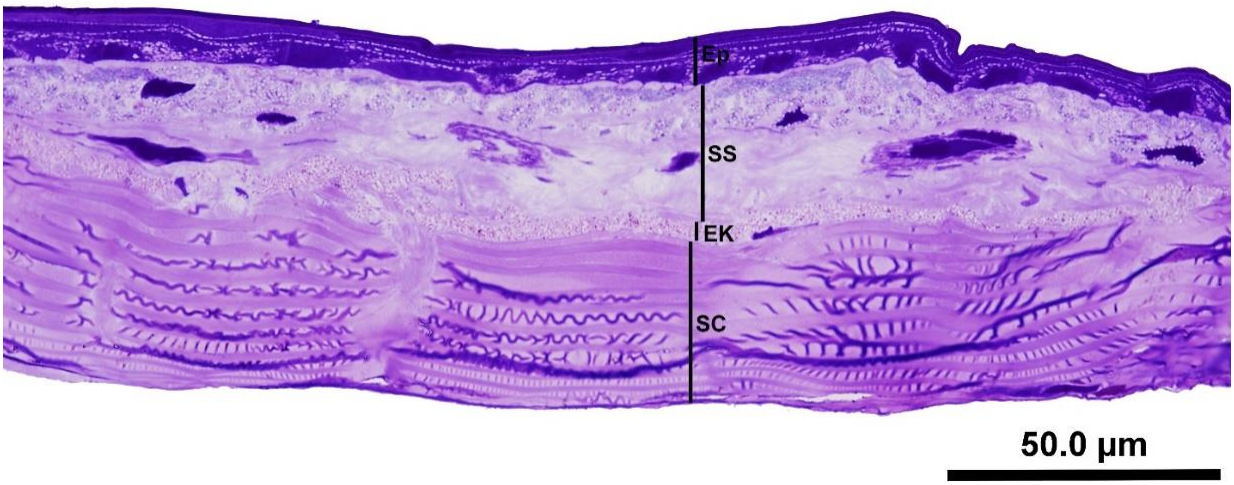


Figure S4 - Scheme of skin structure of *Brachycephalus actaeus*
Skin structure of *Brachycephalus actaeus* (orange morphotype, JPCM1025) in dorsal view in light microscope photomicrographs of vertical section stained with toluidine blue. Layer's abbreviation: Ep = epidermis; EK = calcified Eberth-Kastschenko; SC = *stratum compactum*; and SS = *stratum spongiosum*.

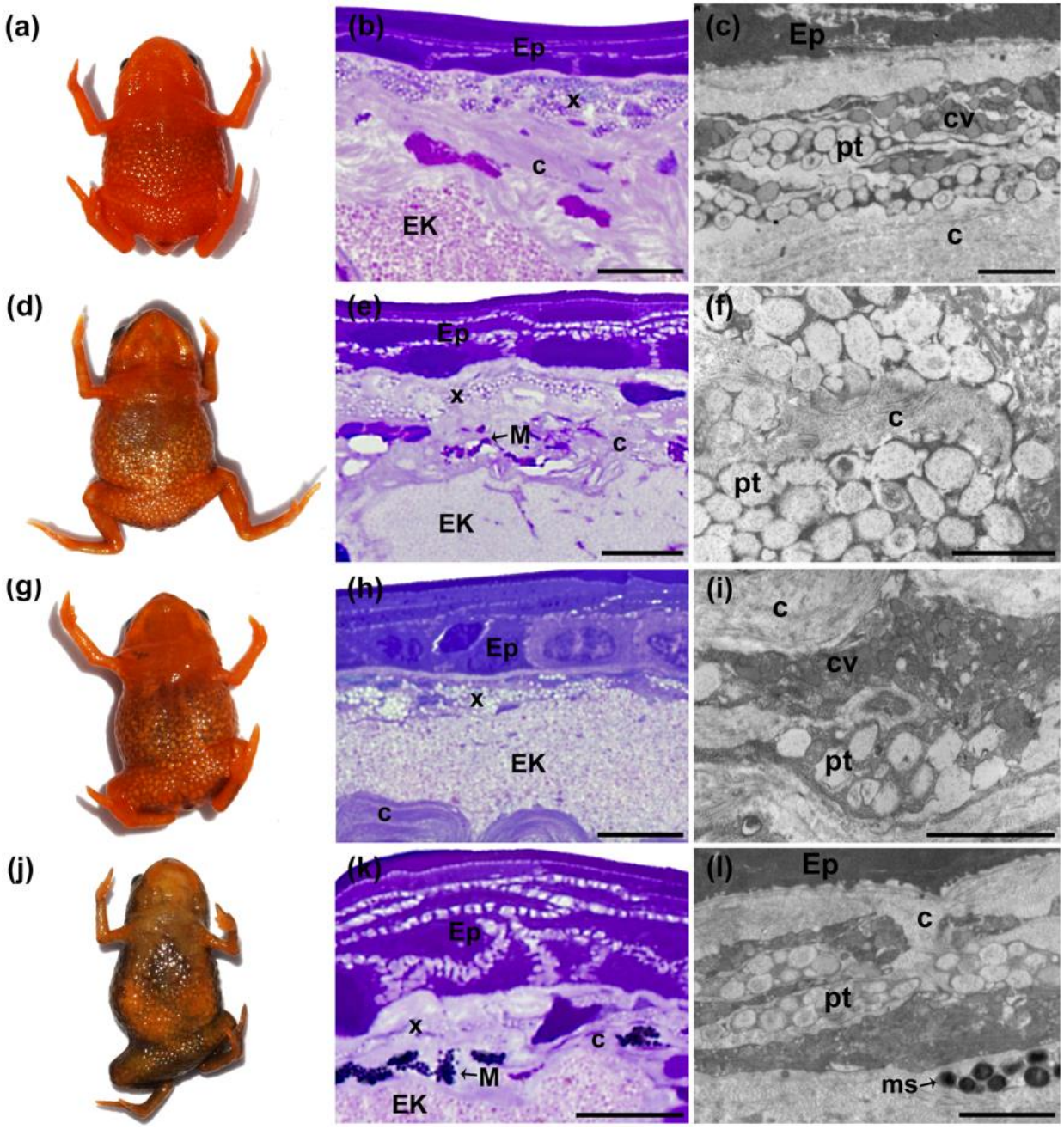


Figure S5 - Ventral skin in life and skin structure of *Brachycephalus actaeus*

Ventral skin in life (left) and ventral skin structure of *Brachycephalus actaeus* in transversal section highlighting chromatophores organization and distribution. Light microscope photomicrographs stained with toluidine blue (center) obtained with an Olympus BX51 light microscope coupled to a DP71 digital camera, and Electron microphotographs (right) obtained with JEOL JEM 100CXII transmission electron microscope at 80 kV acceleration voltage. (a, b, c) Orange morph (JPCM1025); (d, e, f) gray morph (JPCM1062); (g, h, i) brown morph (JPCM1046); and (j, k, l) green morph (JPCM1033). Abbreviations: c, collagen fibers; cv, carotenoid vesicle; EK, Eberth-Kastschenko; Ep, epidermis; M, melanophore; ms, melanosome; pt, pterinosome; x, xanthophore. Scale bar: b, e, h, k = 10 μm; c, f, i, l = 2 μm.

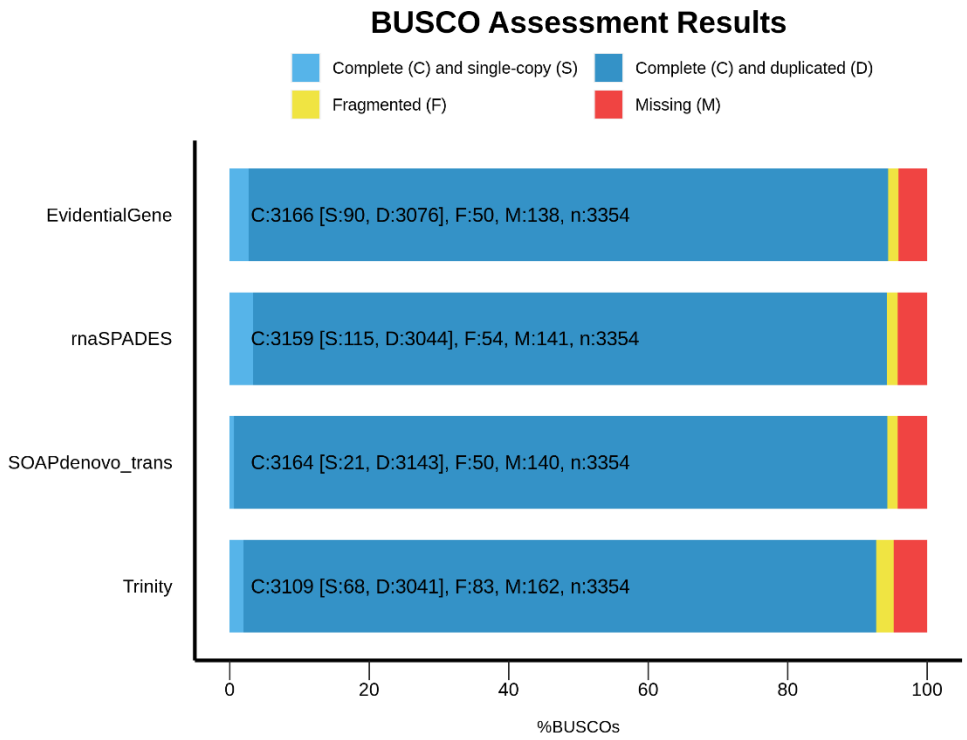


Figure S6 – BUSCO statistics results

BUSCO completeness statistics of the three transcript collections resulting from each assembler (rnaSPADES, SOAPdenovo-trans, and Trinity) and the final ensemble transcriptome obtained by EvidentialGene pipeline. Completeness was estimated against 3354 benchmarking genes in the vertebrata orthologous database collection v10.

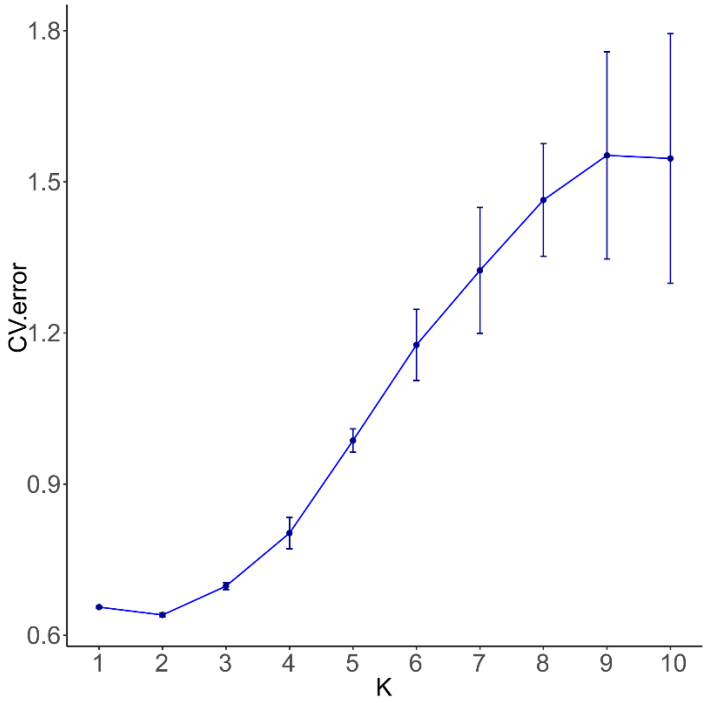


Figure S7 - ADMIXTURE estimation of *Brachycephalus actaeus*
ADMIXTURE estimation of *Brachycephalus actaeus* based on 23,579 biallelic SNPs. Cross-validation (CV) error is minimal when the ancestry groups are two (K = 2) by running 20 repetitions for K = 1 to 10.

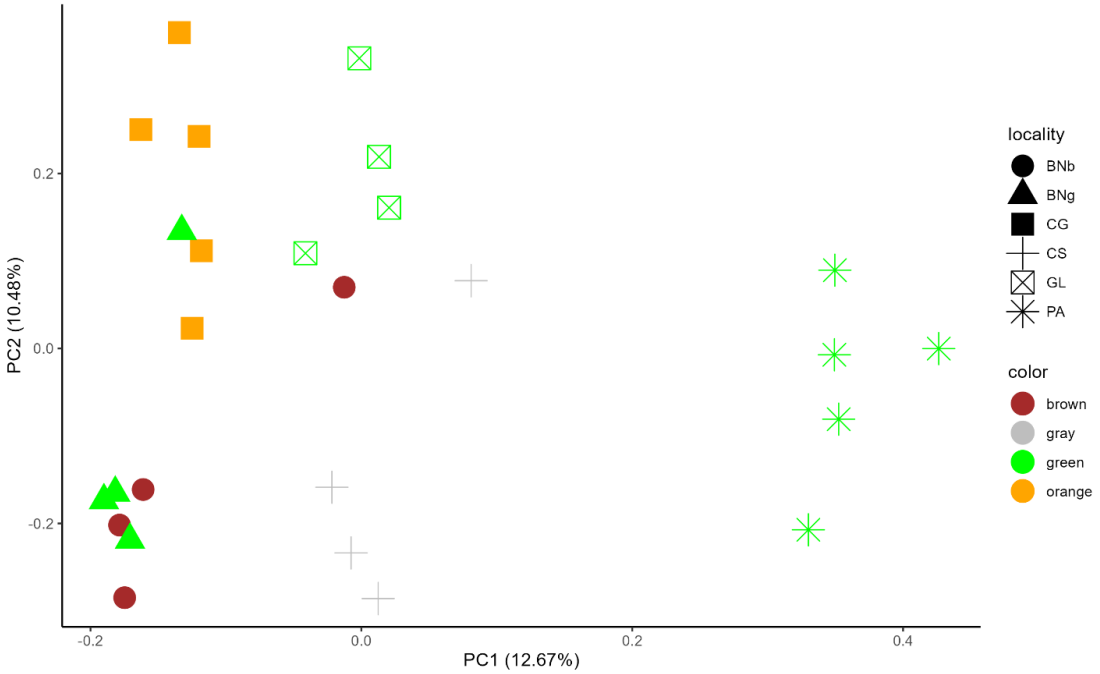


Figure S8 - PCA of gene expression estimates of *Brachycephalus actaeus* by sample
Principal component analyses of gene expression estimates of *Brachycephalus actaeus* by sample TPM normalized read counts per sample were log2 transformed and the first two PCs are plotted by color morph and locality. See main text for the locality abbreviations.

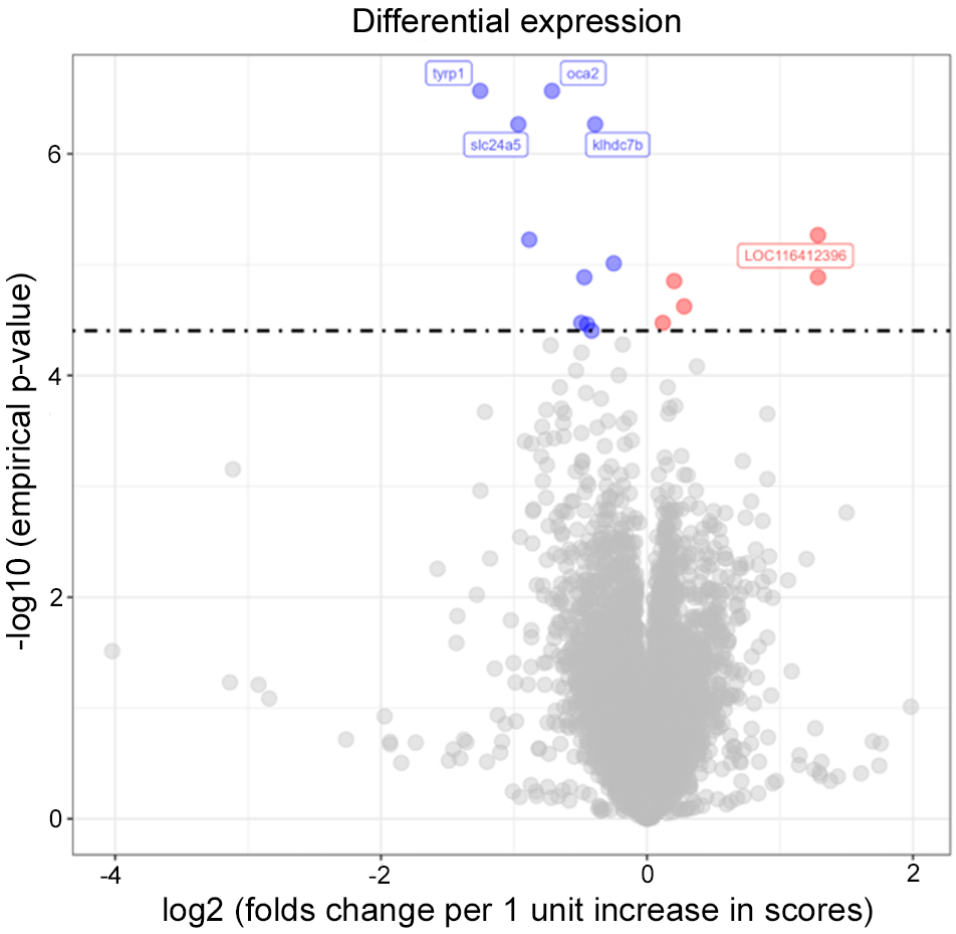


Figure S9 - Volcano plot reflects the transcriptome-wide association's statistical
Volcano plot reflects the transcriptome-wide association's statistical results between gene expression estimates and the coloration (x-coordinate scores in bird perceptual space) from 15,284 genes of *Brachycephalus actaeus* morphs. Statistically significant associations are highlighted with colored dots (blue: down-regulated, red: up-regulated genes).

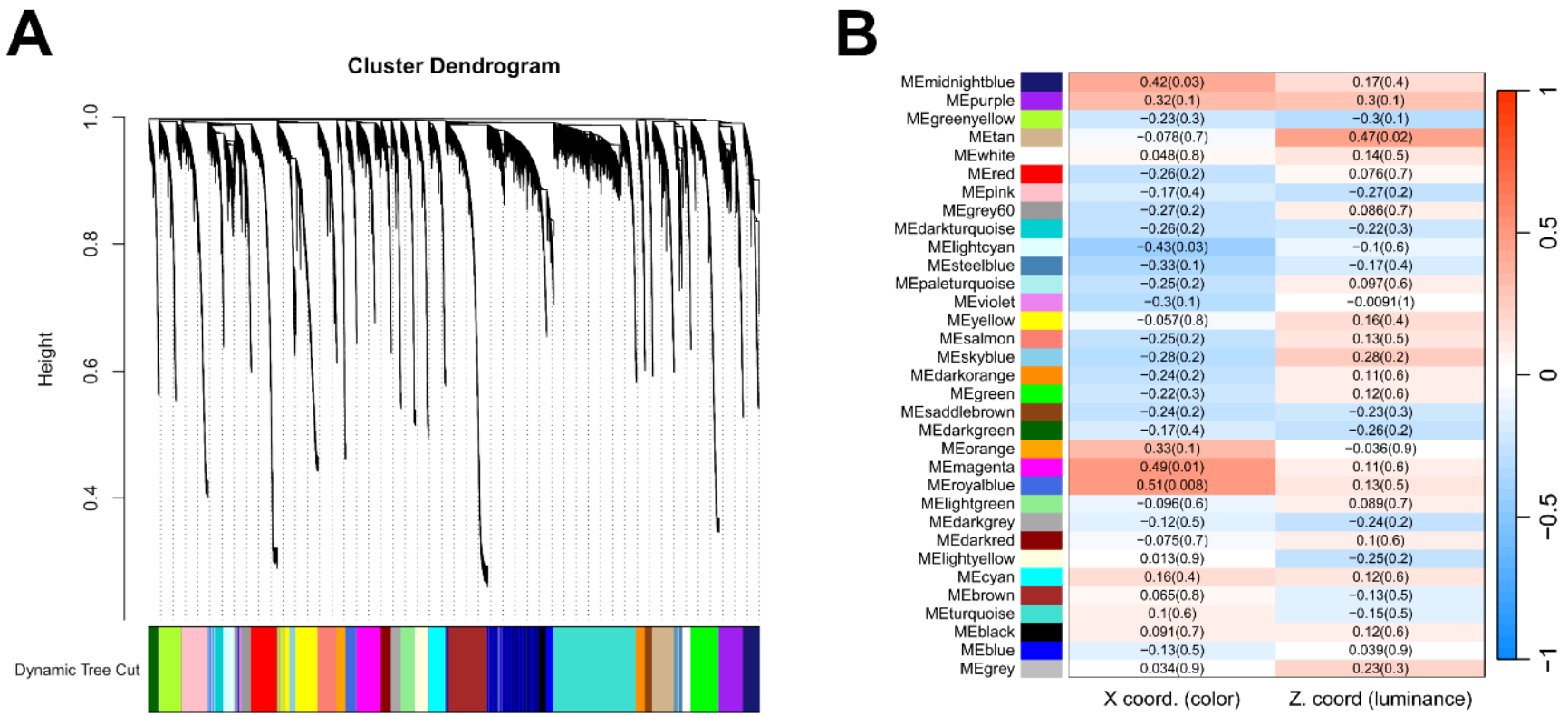


Figure S10 - Gene co-expression network analyses WGCNA
WGCNA results. A) The dendrogram of the gene topological overlap measures dissimilarity with the resulting clusters defined by a dynamic tree-cut threshold. B) Correlation between the module eigen expression values and the two *Brachycephalus actaeus* coloration variables representing color and luminance in avian perceptual space. For each cell, the Pearson correlation and associated p-values are provided with darker cell colors indicating stronger positive (red) or negative (blue) correlations.

CAPÍTULO III

Monteiro, J. P. C., Lyra, M. L., Condez, T. H., Carvalho, T. R., Zamudio, K. R., & Célio F. B. Haddad. Aposematism and miniaturization: The evolutionary miscellany in *Brachycephalus* taxonomy.

Artigo em preparação.

"Aposematismo e miniaturização: A miscelânea evolutiva na taxonomia de *Brachycephalus*"

Resumo

Estratégias de coloração intraespecífica, e.g. polimorfismo e politipismo, evoluíram em muitas espécies não relacionadas filogeneticamente, como um meio de adaptação para garantir a aptidão em determinado ambiente. A diversificação fenotípica pode aumentar a divergência genética e potencializar características envolvidas no isolamento reprodutivo. Em anfíbios, espécies aposemáticas, quimicamente defendidas e diurnas apresentam polimorfismo e politipismo de maneira recorrente, manifestando múltiplas estratégias de cor que variam entre sinais de alerta e padrões discretos para camuflagem. Os miniaturizados e endêmicos sapinhos-pingo-de-ouro do gênero *Brachycephalus* habitam a serrapilheira das montanhas da Mata Atlântica brasileira e são aposemáticos, tóxicos e diurnos. O recente politipismo demonstrado na espécie *B. actaeus*, proporciona uma oportunidade para investigar este inédito sistema modelo relacionando dados de genótipo e fenótipo. Para estudar a diversidade populacional, amostramos diversas localidades ao longo da distribuição da espécie para fornecer uma perspectiva da divergência genética, morfológica e acústica dos morfos de cores conhecidos—verde, marrom, cinza e laranja. Nossos dados suportaram a estruturação geográfica de quatro populações, as quais não são relacionadas com a coloração: norte (morfos marrom e verde), centro (morfos cinza e laranja), sul (morfo verde) e ilha (morfo verde). Entre as populações continentais, norte, centro e sul, identificamos a presença de fluxo gênico, principalmente entre centro (morfo cinza) e sul, indicando uma zona de transição. Os dados morfológicos revelaram uma profunda variação intraespecífica, não correlacionada com coloração, localidade ou população. Por outro lado, dados acústicos sugerem uma diversificação no canto de anúncio da população do centro, que pode estar relacionada ao aposematismo como um sinal multimodal. Nossos resultados trazem contribuição significativa em *Brachycephalus*,

destacando a miniaturização e o aposematismo como fenômenos potenciais para a elevada variação intraespecífica e enfatizando os desafios na determinação de divergências interespecíficas. Futuros estudos são necessários para reavaliar as espécies descritas e contribuir para o entendimento da evolução da coloração e do uso dos sinais de cor neste grupo de sapos aposemáticos.

To be submitted to BMC Evolutionary Biology (?)

Aposematism and miniaturization: The evolutionary miscellany in *Brachycephalus* taxonomy

Juliane P. C. Monteiro[1,2,3*], Mariana L. Lyra[4], Thais H. Condez[5], Thiago R. Carvalho[6], Kelly R. Zamudio[7], and Célio F. B. Haddad[2,3]

[1]Programa de Pós-graduação em Zoologia, Instituto de Biociências, Universidade Estadual Paulista (UNESP), Rio Claro, São Paulo, Brazil

[2]Universidade Estadual Paulista (UNESP), Instituto de Biociências, Departamento de Biodiversidade e Centro de Aquicultura (CAUNESP), Rio Claro, São Paulo, Brazil

[3]Center for Research on Biodiversity Dynamics and Climate Change, Institute of Biosciences, São Paulo State University (UNESP), Rio Claro, São Paulo, Brazil

[4]New York University Abu Dhabi, Abu Dhabi, Saadiyat Island, United Arab Emirates

[5]Carleton University, Department of Earth Sciences, Ottawa, Ontario, Canada

[6]Departamento de Zoologia, Instituto de Ciências Biológicas, Universidade Federal de Minas Gerais, Belo Horizonte, Minas Gerais, Brazil

[7]Department of Integrative Biology, College of Natural Sciences, University of Texas, Austin, Texas, United States

[*]correspondence: julianepmonteiro@gmail.com

Abstract

Intraspecific coloration strategies, e.g., polymorphism and polytypism, have evolved in many phylogenetically unrelated species as an adaptation mechanism to ensure fitness in a specific environment. Phenotypic diversification can increase genetic divergence and enhance features involved in reproductive isolation. In amphibians, aposematic, chemically defended, and diurnal species recurrently exhibit polymorphism and polytypism, displaying multiple color strategies ranging from warning signals to discrete patterns for camouflage. The miniaturized and endemic pumpkin toadlets of the *Brachycephalus* genus inhabit the leaf litter of the Brazilian Atlantic Forest mountains and are aposematic, chemically defended, and diurnal. The recent polytypism demonstrated in the species *B. actaeus* provide an opportunity to investigate this novel model system by linking genotype-phenotype data. For studying population diversity, we sampled several localities along the species distribution to provide insight into the genetic, morphological, and acoustic divergence of known color morphs—green, brown, gray, and orange. Our data supported the geographic structuring of four populations unrelated to coloration: Northern (brown and green

morphs), Center (gray and orange morphs), Southern (green morph), and Island (green morph). Among mainland populations (Northern, Center, and Southern), we identified gene flow, particularly between the Center (gray morph) and Southern, indicating a transition zone. Morphological data revealed in-deep intraspecific variation not correlated with coloration, location, or population. Conversely, acoustic data suggest diversification in the advertisement call of the Central population, potentially related to aposematism as a multimodal signal. Our results provide a significant contribution to *Brachycephalus*, emphasizing miniaturization and aposematism as potential phenomena for high intraspecific variation and underscoring challenges in determining interspecific divergences. Future studies are strongly necessary to reassess described species and contribute to understanding the evolution of coloration and the use of color signals in this group of aposematic toadlets.

Keywords: Amphibia, Anura, Atlantic Forest, bioacoustics, coloration, morphology, population genetics, osteology, polymorphism, SNPs

1 INTRODUCTION

The diversity of color in animals plays a crucial role in communication systems, influencing detection and recognition within and between species (Baden & Osorio, 2019; Endler, 1993; Osorio & Vorobyev, 2008). Color polymorphism – characterized by multiple distinct color morphs within a species – has independently evolved across diverse animal groups, including fishes, amphibians, lizards, birds, and mammals (Caro, 2017; Emberts & Wiens, 2022; Ford, 1945). While cryptic coloration provides undetectability when blending with the environment, aposematic coloration signals chemical defences or harm to potential predators, favoring the diversity of signaling strategies within species (Briolat et al., 2019; Rojas et al., 2015). Hence, many of aposematic species are polymorphic or, more restrictively, polytypic, which involves distinct locally selected morphs (Caro & Ruxton, 2019; Mappes et al., 2005).

The effectiveness of visual signals is shaped by environmental features (e.g. ambient light and substrate) and the perceptual systems of receivers (Endler, 1992, 1993). Consequently, the interactions between color attributes and environmental fitness favor individuals better adapted to that location (Endler, 1991; Mclean et al., 2014; Yewers et al., 2019). Species color patterns may assist multiple, often conflicting roles, including communication and camouflage (Hutton et al., 2015; Rojas, 2017; Ruxton et al., 2018), likely as a result from lineage-specific solutions to

evolutionary trade-offs between these functions (Cummings & Endler, 2018; Endler, 1992; Mclean & Stuart-Fox, 2014). Mechanisms driving intraspecific polymorphism or polytypism, such as geographic variation, may be precursors to speciation, contributing to genetic differentiation and reproductive isolation between local morphs (Mclean & Stuart-Fox, 2014). For example, in birds, color polymorphism associated with ecological, geographic, and genetic processes can promote rapid speciation (Hugall & Stuart-Fox, 2012).

Color polymorphism in aposematic anurans has been observed as a convergent evolution among distantly related taxa, driven by similar selection pressures (Hoffman & Blouin, 2000; Rojas, 2017; Rojas et al., 2015). This phenomenon explains the presence of striking color patterns in unrelated clades of diurnal and chemically defended frog lineages, exemplified by the Neotropical poison frogs (Dendrobatidae) and the Malagasy genus *Mantella* (Mantellidae). Poison frogs stands out as extensively studied, exhibiting different levels of color strategies that promote survival and reproductive success, not necessarily implying speciation (Lorioux-Chevalier et al., 2023; Dreher et al., 2015; Twomey et al., 2020). Some polytypic poison frog species represent examples of multiple color strategies, displaying signals that range from cryptic camouflage to conspicuous warning coloration, including intermediate signals (Pröhl & Ostrowski, 2011; Rojas, 2017; Willink et al., 2013). The color differences contribute to different levels of individual fitness, promoting divergence in behavior (Pröhl & Ostrowski, 2011; Rößler et al., 2019; Willink et al., 2013), call characteristics (Brusa et al., 2013; González-Acosta et al., 2023; Vargas-Salinas & Amézquita, 2013), morphology (Rudh, 2013; Winebarger et al., 2018), and chemical compounds (Lawrence et al., 2023; Saporito et al., 2007; Wang, 2011).

Conspicuous color patters, diurnal activity, and chemical defences also may characterize the pumpkin toadlets (Brachycephalidae) from Brazilian Atlantic Forest. These miniaturized members of the *Brachycephalus* genus inhabit the forest leaf-litter, displaying dorsal hues that range from bright orange/yellow to cryptic green/brown colors (Condez et al., 2020; Lyra et al., 2021). While some studies have focused on delimiting species based on color divergences and presumed absence of gene flow (e.g. Pie et al., 2018), no integrative approach has explored morphological and genetic variation in *Brachycephalus* species.

Commonly, body coloration has been considered as an taxonomic informative character among *Brachycephalus* species, resulting from a selection effect by rapid evolution (Pie et al., 2018, 2013). The use of color pattern as diagnostic character leads to exceptionally high levels of

endemism, increasing the number of recognized species (Bornschein et al., 2019; Pie et al., 2018). Although the genus *Brachycephalus* encompasses 41 species (Frost, 2023), research has predominantly focused on species descriptions, resulting in a notable gap in basic information. Occasional studies report behavior (Dorigo et al., 2012; Lima et al., 2013; Pombal Jr. et al., 1994), calling activity (Oliveira & Haddad, 2017; Verdade et al., 2008), parental care (Pombal Jr., 1999), chemical defences (Arcanjo et al., 2015; Chimetto Tonon et al., 2021; Pires et al., 2005), as well as the use of aposematic signals (Rebouças et al., 2019).

Recently, new approaches have highlighted the adaptative role of color evolution in *Brachycephalus*, offering evidence of polytypism in *B. actaeus* (Lyra et al., 2021; see chapter II here [hereafter Monteiro et al., unpublished]). The color morphs in this species, ranging from cryptic green to conspicuous orange, seems not be associated with population structure but might be correlated with geographic distribution (Monteiro et al., unpublished). Thus, *B. actaeus* represents an opportunity to investigate the relationship among genotype-phenotype and its likely role in speciation. Hence, exploring the genetic and phenotypic differences across the species' distribution is crucial to understanding divergence patterns at the population level.

In this study, we aim to evaluate the relationships among color diversity, genetics, and geographical variation in traits that are potentially involved in reproductive isolation within *B. actaeus* populations. Specifically, we assessed the population structure, morphological traits, and advertisement calls to investigate how they relate to color variation. Through initial comparisons, we demonstrated the consequences of phenotypic variation in these polymorphic aposematic lineages, carrying implications for conservation and further evolutionary studies on *Brachycephalus*.

2 MATERIAL AND METHODS

2.1 Species studied

Brachycephalus actaeus, a miniaturized species within the *B. pernix* group, occurs in a small area of approximately 80 km² in the northeastern state of Santa Catarina, Brazil. This diurnal pumpkin toadlet is ground-dwelling species that reproduces in the ground by direct-development. Unlike most pumpkin toadlets, which are found at higher altitudes, *B. actaeus* inhabits areas near the sea level, reaching up to 500 meters in elevation (Monteiro et al., 2018; Lyra et al., 2021). Notably, *B. actaeus* is the first species within the genus shown to exhibit significant color variation,

displaying colors that range from cryptic green to aposematic orange across its distribution. We followed color name classification as presented in Monteiro et al. (unpublished): brown, green, gray, and orange.

2.2 Field sampling

We conducted multiple fieldwork surveys over the past eight years (2013 – 2021) to collect data on *B*. *actaeus* in the Babitonga Bay region, northeastern of the state of Santa Catarina, Brazil (Fig. 1; Appendix I). A total of 98 individuals were collected from 11 localities across three municipalities: two localities at Garuva (Alto Bom Futuro, brown morph [BFb]; and Baixo Bom Futuro, green morph [BFg]), three localities at Itapoá (Alto Braço do Norte, brown morph [BNb]; Baixo Braço do Norte, green morph [BNg]; and Fazenda Palmito Juriti, green morph [PAJ]), and six localities at São Francisco do Sul (Centro de Estudos e Pesquisas Ambientais da Univille, green morph [CEPA]; Morro Cantagalo, orange morph [CAG]; Casarão Backmeyer, gray morph [CAS]; Estrada do Saí, green morph [SAI]; Morro Grande, green morph [MOG]; and Serra da Palha, green morph [SPA]).

The study area encompasses approximately 80 km², corresponding to the currently known species distribution range. Specimens were found during the daytime under leaf litter, usually located by their calls, and were collected by hand. Additionally, we conducted supplementary fieldwork surveys to gather topotype specimens from *B*. *pernix* group species for inclusion in the phylogenetic analyses. The genetic data available for these species on GenBank show certain sections excluded (see Monteiro et al., 2018). The specimens were temporarily placed in plastic bags for transportation to the laboratory. Whenever possible, we photographed the specimens and then euthanized them using 5% lidocaine. Muscle tissue was extracted and stored in absolute ethanol, while the specimen was fixed in 10% formalin and preserved in 70% ethanol for permanent storage. All specimens were deposited in the Célio F. B. Haddad (CFBH) Amphibian Collection at Departamento de Biodiversidade, Instituto de Biociências, Universidade Estadual Paulista, Rio Claro, São Paulo, Brazil. All research procedures were conducted in accordance with the Universidade Estadual Paulista's institutional animal care and use committee protocol n° 6896, under the collection permits SISBIO #23501-6, # 49587-1, and #63104-4.

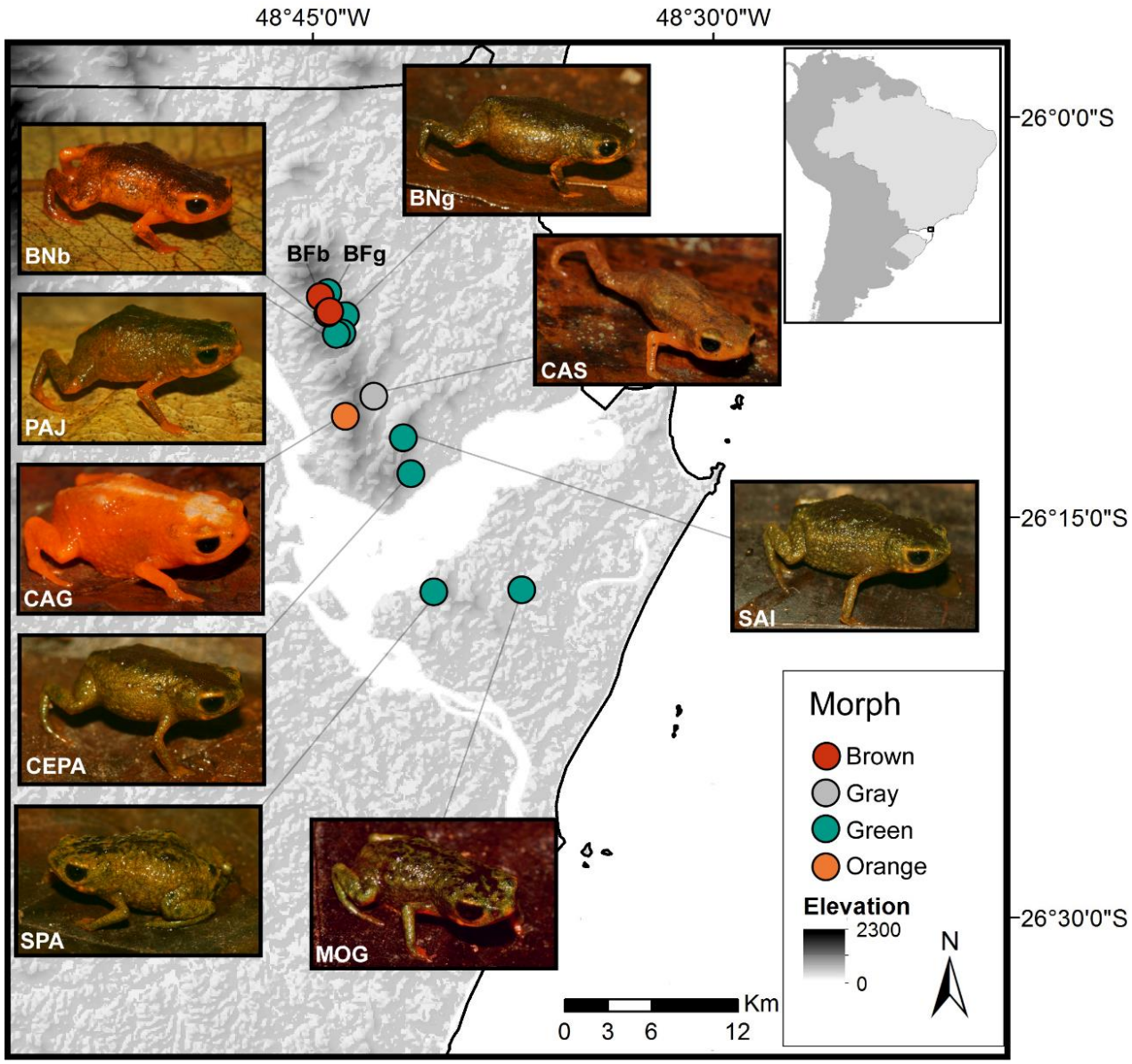


Figure 1. Distribution of *Brachycephalus actaeus* in northeastern of the state of Santa Catarina, Brazil. Color circles indicate the color morph at each locality. Abbreviations: BFb = Bom Futuro brown morph (no photo); BFg = Bom Futuro green morph (no photo); BNb = Braço do Norte brown morph; BNg = Braço do Norte green morph; CEPA = Centro de Estudos e Pesquisas Ambientais da Univille; CAG = Morro Cantagalo; CAS = Casarão Backmeyer; MOG = Morro Grande; SPA= Serra da Palha; PAJ = Fazenda Palmito Juriti; SAI = Estrada do Saí. Credit photos: J.P.C. Monteiro (BNb, CAG, and CAS) and T.H. Condez (BNg, CEPA, MOG, SPA, PAJ, and SAI).

2.3 Genomic data and analyses

2.3.1 DNA extraction and ddRADseq data generation

To evaluate *B. actaeus* genetics, we sampled 70 individuals representing all color morphs across the previously mentioned localities (Appendix I). Total genomic DNA was isolated from liver and muscle tissue samples with QIAamp DNA Micro Kit, which is supplied with a carrier RNA that enhances binding of DNA to the QIAmp MinElute column membrane (Qiagen, Valencia, CA, USA). We quantified the extracted DNA concentration in a Qubit® 2.0 fluorometer (Thermo Fisher Scientific, CA, USA). Samples with lesser DNA content, such as those from small muscle tissues, were concentrated by three consecutive times water elution's and dryings on a SpeedVac (Thermo Fisher Scientific), until the DNA concentration reached at least 20 ng/µl. We then employed a double-digest restriction-site associated DNA sequencing (ddRADseq) protocol (Peterson et al., 2012) to generate DNA libraries comprising thousands of short nuclear fragments across entire genome of *B. actaeus*.

Genomic DNA was double-digested with the restriction enzymes SbfI-HF (5′ CCTGCAGG 5′) and MspI (5′ CCGG 3′), ligated to adapters containing multiplexed individual barcodes. In a reaction volume of 30 µl, we combined 100 ng genomic DNA (10 µl at 10 ng/µl); 15 units of both SbfI-HF and MspI (NEB, Ipswich, MA; 0.75 µl each); 300 units of T4 DNA ligase (NEB, 0.75 µl); 3 µl of 10xCutSmart ligase buffer (NEB); 1.0 µl each of a uniquely barcoded SbfI-P1 adapter (one of 24) and MspI-P2 adapter (Integrated DNA Technologies, Coralville, IA, USA; 0.25 µM each); 3 µl of 10 mM ATP (NEB); and 9.75 µl of ddH2O. The restriction-ligation mixture was incubated at 37 °C for 30 min and 20 °C for 1 h, before pooling 20 µl from each of the 24 barcoded samples. Each pool was PCR-amplified using 20 ng P1/P2 adapted DNA template (10 µl at 2 ng µl), 12.5 µl 2X Phusion PCR Master Mix (2X, NEB), and 1.25 µl each of forward index primer and a uniquely indexed reverse primer (one of 12; 5 µM each, Integrated DNA Technologies). *B. actaeus* samples were distributed with other samples (not included here) across four libraries, with the maximum number of 48 uniquely barcoded/indexed individuals per library. Each library was supplied with two technical replicates to monitor possible errors. Fragments were pooled across index groups, PCR amplified and size-selected to retain fragments between 300 and 1000 bp. Final libraries were visualized on agarose gels to ensure correct fragment size. Each library was single-end sequenced to 100 bp on one lane of the Illumina HI-SEQ 2500 at the Cornell University Genomics Facility, Ithaca, United States.

We verified the quality of Illumina sequences reads and the presence of adapter contamination with FastQC v0.11.9 (Andrews, 2010). Data were demultiplexed using *process_ratags* scripts from Stacks 2.3 pipeline (Catchen et al., 2013), where reads for each index group were divided by barcode, trimmed to a standard length of 94 bp and sequences flagged by the Illumina quality filter were removed. This processing step is necessary to remove ambiguous radtags. After renaming the samples based on their unique index and barcode combinations, we checked the processed radtags and counted the reads by sample using *summarize_Radtags* and *ReadCount* scripts. The ddRADseq library protocol generated an average of 2,6 million reads per individual, ranging from 237,532 to 6,080,752.

2.3.2 ddRADseq alignment

For quality filtering, de novo assembly, and reads alignments we performed ipyrad v0.9.77 pipeline (Eaton & Overcast, 2020). First, we include all samples together following default parameters yielding 41,841 loci, with 78% of missing data. Low-quality samples (those lacking 50% of the loci, N = 13) were excluded from the dataset using Matrix Condenser (de Medeiros & Farrell, 2018). This filtering strategy yielded a total of 49,609 loci for 57 samples of *B*. *actaeus*, with 56% of missing data (see Table S1 for ipyrad summary results).

Afterward, we retained 228,403 biallelic SNPs out of 234,575, with > 5% missing data for SNPs, and minor allele count (MAC) > 2 via vcftools v0.1.16 (Auton & Marcketta, 2015) for use in subsequent analyses. Also, PLINK v1.9 (Purcell et al., 2007) was used to convert the SNPs data into PED and MAP format and binary files (BED, RAW, and BIM), using the flags "--make-bed --recode --chr-set 95 and allow-extra-chr". PLINK files were imported into R v4.1.2 (R Core Team, 2021) and stored in a genlight object using function 'read.PLINK' with adegenet v2.1.10 (Jombart et al., 2018; Jombart, 2008). Except for Principal Component Analysis (PCA), the handling and subsequent analyses of SNP data were performed in R using wrapper functions from SambaR v1.09 package (de Jong et al., 2021).

2.3.3 Population structure and genetic diversity

As a prior, we implemented a stringent missing data cutoff to prevent the overestimation of genetic clusters. Population structure analyses, relying on allele frequency estimation, are particularly susceptible to the impact of rare alleles (Falush et al., 2007). Thus, we employed

SambaR to filter variants based on the following criteria: exclusion of SNPs with high read depth (determined by fitting a normal distribution to the lowest 99.5% of observed depth values and subsequently calculating a Bonferroni-corrected threshold value); and identification and removal of potential paralogs through heterozygosity excess.

Admixture analysis was conducted to explore population structure and the optimal number of populations (K) was determined via cross-validation (Frichot et al., 2014). Analyses was performed using sparse Non-negative Matrix Factorization algorithm (sNMF) using LEA package v3.6.0 (Frichot & François, 2015), which does not assume Hardy–Weinberg equilibrium (HWE) to identify clusters. The best-fit number was estimated with K = 1–10, with 100 replicates for each K. Additionally, we investigated individual clustering within the SNP dataset through PCA in PLINK v1.9. PCA results were visualized using tidyverse version 2.0.0 (Wickham et al., 2019) in R.

We then calculated F_{ST} (Wright, 1943) and absolute diversity D_{xy} (Nei & Li, 1979) as separated metrics to estimate population differentiation based on populations structure identified in admixture analyses (Cruickshank & Hahn, 2014). To perform subsequent analyses we considered the we allowed 60% of missing data per sample and 15% of missing data per SNPs, and kept other parameters as defined before (Table S2). Also, two measures of nucleotide diversity were assessed: proportion of segregating sites (Watterson's theta, θ_W) (Watterson, 1975), and nucleotide diversity (π) (Nei, 1987). After, we performed the neutrality statistics Tajima's D which considers the difference between π and θ_W (Tajima, 1989).

2.3.4 Mitochondrial genetic comparisons and phylogenetic inference

We amplified mitochondrial fragment of the 16S rRNA gene (16S) from *B. actaeus* using ddRAD extractions. Also, we extracted genomic DNA from muscle tissue ethanol-preserved from 18 species of the *B. pernix* group which we has successfully collected (*B. albolineatus*, *B. auroguttatus*, *B. boticario*, *B. brunneus*, *B. curupira*, *B. ferruginus*, *B. fuscolineatus*, *B. izecksohni*, *B. leopardus*, *B. mariaterezae*, *B. mirissimus*, *B. olivaceus*, *B. pernix*, *B. pombali*, *B. quiririensis*, *B. tridactylus*, and *B. verrucosus*), using a standard ammonium acetate extraction protocol adapted from Maniatis et al. (1982) to amplify 16S. This fragment is currently available for several *Brachycephalus* species in the GenBank database. We performed DNA amplification in a 21 µl volume reaction using Fermentas Taq Polymerase master mix and reagents (MBI Fermentas, USA)

with the primers 16Sar-L (3' CGCCTGTTTATCAAAAACAT 5') and 16Sbr-H (5' CCGGTCTGAACTCAGATCACGT 3') (Palumbi et al., 1991). The polymerase chain reactions (PCRs) started with an initial hold at 95 °C (3 min), followed by 35 cycles of denaturation at 95 °C (15 s), annealing at 50 °C (15 s), extension at 60 °C (30 s), and then by a final hold at 60 °C (3 min). PCR products were purified using Exonuclease and Shrimp Alkaline Phosphatase (Affimetrix/USB, Cleveland, OH) and sequenced in both directions by Macrogen Inc. (Seoul, Republic of Korea). Sequences were quality-checked and trimmed in Geneious v.7 (Biomatters Ltd.). Newly generated mitochondrial sequences were uploaded to GenBank (accession numbers to be provided; Table S4).

We executed a multiple sequence alignment in MAFFT v.7 online version, using the G-INS-i strategy in default parameters (Katoh et al., 2019). The haplotype network of 16S was generated for *B*. *actaeus* individuals using the Median Joining Network algorithm (Bandelt et al., 1999) in PopART v.1.7 (Leigh et al., 2015). Furthermore, we estimated intraspecific distance using uncorrected p-values in Mega v.X (Kumar et al., 2018). Moreover, we inferred the mitochondrial phylogenetic relationship among species of the genus *Brachycephalus* to determine *B*. *actaeus*' position using Maximum Likelihood (ML) inference in RAxML v.8 (Stamatakis, 2014), implemented in the online CIPRES Science gateway portal (Miller et al., 2010). Our compilation included 39 out of 40 *Brachycephalus* species from present study and GenBank (Table S4). We added five species of *Ischnocnema* as outgroup, since this genus is the sister taxa of *Brachycephalus*, and used *Haddadus binotatus* to root the tree (Padial et al., 2014). Final matrix comprised 186 individuals and 490 base-pairs (Table S4). We searched for the best tree using the GTRCAT model and 1,000 starting points. After, we performed 1,000 non-parametric bootstrap replicates to access node support. We interpreted bootstrap values above 90 as evidence of high support, values below 75 as poor support, and intermediate bootstrap values as moderate support.

2.4 Phenotypic and acoustic traits

2.4.1 Morphometric measurements and analyses

Morphometric measurements were obtained from 74 adult specimens of *B*. *actaeus* from nine localities (Appendix I). We followed Duellman (2015) for the definitions of snout-vent length (SVL), head length (HL), head width (HW), eye diameter (ED), eye-nostril distance (END), interorbital distance (IOD), nostril diameter (ND), internarial distance (IND), tibia length (TIBL),

and foot length (FL). We followed Heyer et al. (1990) for the definitions of upper arm length (AL), forearm length (FAL), hand length (HAL), and thigh length (THL). We measured specimens in a Zeiss Stemi SV 11 stereomicroscope equipped with an ocular micrometer. SVL was measured using calipers (± 0.1 mm of accuracy).

To fit the morphometric dataset, we removed the potential effect of SVL from dependent variables using a regression model and the residuals were retained in a new dataset to be used in subsequent analyses. After, we standardized the variables using z-scores to reduce dimensionality (Gotelli & Ellison, 2011). Thus, we performed a PCA assessing the significance of each Principal Component (PC) and variables along each axis using permutation-based statistical tests with the PCAtest v0.0.1 package (Camargo, 2022). In addition, we conducted a Kruskal-Wallis test to check potential differences in SVL of males and females across localities (Kruskal & Wallis, 1952).

Next, we ran a discriminant analysis of principal components (DAPC) using the package adegenet v2.1.10 (Jombart and Collins, 2015). The morphometric dataset is referred as the response variables, while predictor variables included color morphs (brown, gray, green, and orange), locality (BNb, BNg, CEPA, CAG, CAS, PAJ, SAI, and SPA), and population (Northern, Center, Southern, and Island). In this context, 'population' corresponds to K = 4 based on the best-fit model of genetic populations (see Results section). Samples from BFb (N = 2) and BFg (N = 2) were excluded because of the low sample size. The calculations were performed separately for female and male due to sexual dimorphism (Monteiro et al., 2018). All analyses were carried out using R v. 4.1.2 (R Core Team, 2021).

2.4.2 Micro-CT scanning and osteology characterization

For osteology comparisons, we analyzed four individuals of *B. actaeus* representing all color morphs (CFBH 39872 [green morph], JPCM351 [orange morph], JPCM410 [brown morph], and TC256 [gray morph]). The specimens were scanned using micro-X-ray computed tomography in a phoenix v|tome|x s 240 (GE Measurement & Control, Wunstorf, Germany). Scans were conducted at a voltage of 50 kV and a current of 150 µA for 30 minutes (1300 ms per image). We allocated the specimens into the plastic tube with floral foam soaked in ethanol to prevent desiccation, so that prevented them from moving while they were being scanned. For 3D skull reconstruction we used 3DSlicer v.4.10.2 (open source http://www.slicer.org/; Fedorov et al., 2012). Scan data are available from MorphoSource.org at the following URL:

https://www.morphosource.org/update. Osteological characterization followed the nomenclature of bone structures as outlined by Trueb (1993) and Campos et al. (2010). The characterization of green morph also included the cleared and double stained specimen (CFBH 39848) mentioned in the original description of the species (Monteiro et al., 2018). This decision was made due to anomalous bones observed in the individual scanned in Micro-CT representing this morph (CFBH 39872), as detailed in the Results section.

2.4.3 Advertisement call recordings and acoustic analyses

Anurans often have species-specific advertisement calls that are thought to act as reproductive barriers between closely related and sympatric species (Boul et al., 2007). Consequently, we conducted a comprehensive analysis of various aspects of the advertisement call to explore potential differences among *B. actaeus* males, based on color morph, population, and locality. Male advertisement calls of 51 individuals were recorded by J.P.C. Monteiro during field trips over the past seven years (2013 – 2019), mainly on periods of heightened *B. actaeus* calling activity – during the morning (0600 – 1000 h) and the afternoon (1500 – 1830 h). Our call recordings overlaps most sites sampled for genomic data and included all morphs for comparison. Advertisement calls were recorded in the field using a Marantz PMD 661 MKII digital recorder (sampling rate: 44.1 kHz; sample size: 16 bits) coupled with a Sennheiser ME66/K6 unidirectional microphone positioned 50 – 100 cm from calling males. We collected voucher males whenever possible and call recordings were deposited in the CFBH acoustic collection (Table S3). Air humidity and temperature were measured *in situ* after each recording to assess the temperature effect on the recorded calls.

Acoustic analysis was carried out using Raven Pro 1.5 (Bioacoustics Research Program, 2014), generating spectrograms with a Hann window type, window size 512 samples, overlap 75% (locked), hop size 128 samples, DFT size 512 samples (locked), grid spacing 86.1 Hz, and color map Cool. Ten acoustic parameters were selected following Köhler et al. (2017): call duration (s), inter-call interval (s), call rate, number of pulses per note, pulse rate, dominant frequency (kHz), lower and upper frequencies (kHz), bandwidth (kHz), and peak time (%). In this species, each emitted note was considered one call, and the average values of each variable per male were used for statistical analyses.

For statistical analyses, we calculated a z-score standardization to make variables dimensionless and comparable (Borcard et al., 2018). We performed a PCA reducing variable space and significance was assessed via permutation-based statistical tests with package PCAtest v0.0.1 (Camargo, 2022). To evaluate the effect of color morph, population structure (pop), and geographic distance (geo) on call structure, we modeled the call parameters with geographic and morph distances matrices, conducting a redundancy analysis (RDA) with the package vegan v2.6.4 (Oksanen et al., 2022). RDA, a canonical form of PCA, uncovers linear combinations of variables in the explanatory matrix that explain the most variance in the response matrix (Legendre et al., 2011).

We excluded four correlated variables *a priori* (Pearson's $r > 0.7$; note repetition rate, pulse repetition rate, minimum and maximum frequencies). The temperature effect on each call trait was statistically removed using linear regression analysis and residuals were used in subsequent analyses (Gerhardt & Huber, 2002; Gotelli & Ellison, 2011). Accounting for a potential body size effect was challenging due to the limited number of vouchers collected in the field (see Monteiro et al., 2018 for detailed discussion on this topic). The geographic coordinates data (latitude and longitude) were transformed in geodetic coordinates (Euclidian distance) using SoDA v1.0-6.1 (Chambers, 2015) to apply distance-based Moran's eigenvector maps (dbMEM) with adespatial v0.3.21 (Dray et al., 2012). dbMEM decomposes spatial structure into several orthogonal eigenvectors, allowing testing the importance of spatial structure on call parameters. The first eigenvectors describe broad-scale patterns, while the last eigenvectors pronounce variation in fine-scale patterns, i.e. eigenvectors describe variation from the entire geographic area to sampling site (Borcard et al., 2018; Borcard & Legendre, 2002). Significance of dbMEMs ($p < 0.05$) was assessed using the moran.randtest function (defined by Moran's I).

We performed forward selection for each set of predicted variables (morph, pop, and geo) to select only the significative variables for a final RDA. The adjusted R^2 value was assessed for the stopping criterion in forward selection test, identifying the significant variables. The overall significance of RDAs, independent variables, and canonical axes were assessed using the anova.cca function in vegan, applying Monte Carlo tests with 1000 permutations (Borcard et al., 2018). Finally, we checked the models for collinearity via variation inflation factor (VIF), assuming a threshold of $VIF > 10$ (Legendre and Legendre, 2012). All analyses were completed with R version 4.1.2 (R Core Team, 2022).

3 RESULTS

3.1 Color variation in *B. actaeus*

B. actaeus displays remarkable color variation, ranging from cryptic green to aposematic orange, including intermediate brown and gray morphs. Each locality predominantly exhibits a single-color category, with individuals displaying only slight variations in color and pattern, except for individuals collected at CAS that seem to be polymorphic. Throughout its geographic distribution, the green morph is the only widespread distributed (Figs. 1 and 2). The morphs can be characterized by: i) brown, dominant on the dorsal region, with variations between brown and orange on the lateral side (Fig. 2A – D), and a completely orange ventral region; ii) green, predominantly found on the dorsal and lateral regions of the body (Fig. 2E – H, U – AB), with orange spots on the ventral region; iii) orange, prevalent across the entire body with a white vertebral stripe on the dorsal region (Fig. 2I – L); and iv) gray, with variable shades of white, brown, and green on the dorsal and lateral regions (Fig. 2M – T), and entirely orange on the ventral region. In addition, we observed irises with golden dots in some individuals of gray morph (Fig. 2Q and N).

3.2 Population analyses

3.2.1 *Populations genetic structure*

We recovered 5,039 biallelic SNPs out of 228,403, with 56% of missing data, using a stringent filtration strategy. The sNMF analysis inferred four populations (K) from 57 individuals of *B. actaeus* (alpha = 100; cross-entropy = 0.426; Fig. 3). These populations exhibit a clear signal of geographic structure, henceforth defined as Northern (BFb, BFg, BNb, BNg, and PAJ), Center (CAG and CAS), Southern (CEPA and SAI), and Island (SPA and MOG) (Fig. 3). Admixture was pronounced between Northern and Center populations, as well as between Center (specifically CAS) and Southern populations. The presence of a shared gene pool was evident in all populations.



Figure 2. Color diversity in *Brachycephalus actaeus*. A – D, Brown morph from Alto Braço do Norte; E – H, green morph from Baixo Braço do Norte; I – L, orange morph from Morro Cantagalo; M – T, gray morph from Casarão Backmeyer; U, green morph from Estrada do Saí; V – X, green morph from Centro de Estudos e Pesquisas Ambientais da Univille; Y – AA, green morph from Serra da Palha, Island; and AB, Fazenda Morro Grande, Island. Credit photos: Juliane Monteiro (B, C, E, G, I, K, M, O, P – R, and Y) and Thais Condez (A, D, F, H, J, L, N, S, T, U – X, and Z – AB).

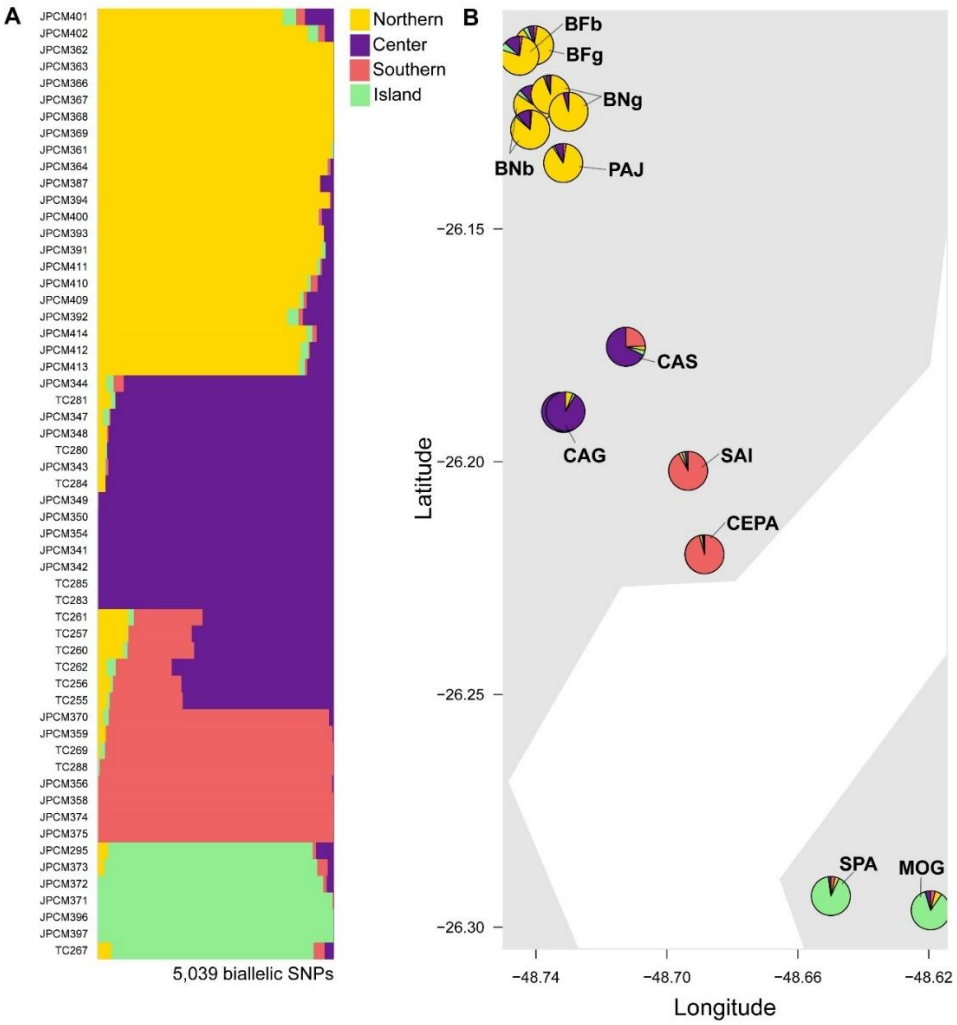


Figure 3. Genetic structure of *Brachycephalus actaeus* in northeastern state of Santa Catarina, Brazil. Population genomic structure estimated from 5,039 biallelic SNPs from ddRAD dataset. A) Ancestry proportions are represented by yellow, purple, pink, and green bars depict the relative proportion of alleles in each individual (best-fit model K = 4). B) Pie charts on map indicate the admixture of ancestry proportions corresponding to each site. Abbreviations by population: Northern (BFb = Bom Futuro brown morph; BFg = Bom Futuro green morph; BNb = Braço do Norte brown morph; BNg = Braço do Norte green morph; and PAJ = Fazenda Palmito Juriti); Center (CAG = Cantagalo and CAS = Casarão); Southern (CEPA = Centro de Estudos e Pesquisas Ambientais da Univille and SAI = Estrada do Saí); and Island (MOG = Morro Grande and SPA = Serra da Palha).

The first two principal components (PCs) of PCA analysis account for 21.95% of the total variance in the genomic dataset. Like in the population structure analyses, the results revealed four grouping segregated, by geographic location (Fig. 4). The Center and Southern groups did not overlap but formed a close situated cluster, in agreement with the previous findings. Neither of these analysis grouped populations based on color morph.

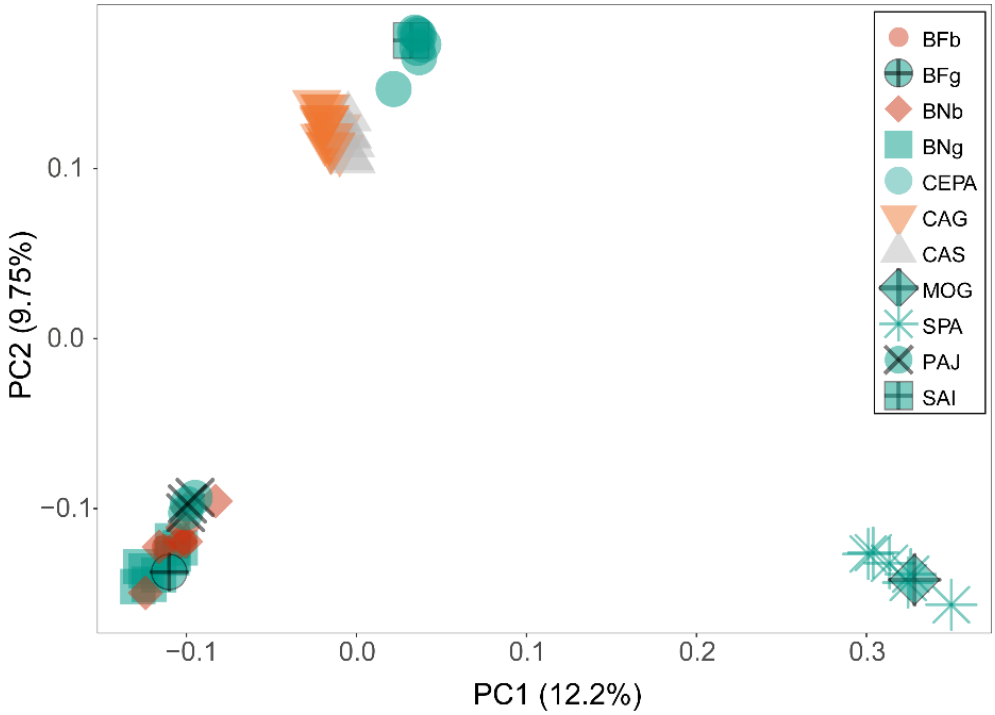


Figure 4. Plot of the two first principal component (PCs) summarizing nuclear dataset from 5,039 biallelic SNPs across *Brachycephalus actaeus* in northeastern state of Santa Catarina, Brazil. Colors indicate color morph (brown, gray, green, and orange). Abbreviations: BFb = Bom Futuro; BFg = Bom Futuro; BNb = Braço do Norte; BNg = Braço do Norte; CAG = Cantagalo CAS = Casarão; CEPA = Centro de Estudos e Pesquisas Ambientais da Univille; MOG = Morro Grande; PAJ = Fazenda Palmito Juriti; SAI = Estrada do Saí; and SPA= Serra da Palha.

3.2.2 Genetic divergence and gene flow

The second filtering strategy retained 39 out of 57 individuals (5 – 16 per population) and 21,545 biallelic SNPs out of 228,403, with 51% of missing data. The lowest F_{ST} value was found between Northern vs. Center (F_{ST} = 0.117), followed by Center vs. Southern (F_{ST} = 0.144), Northern vs. Southern (F_{ST} = 0.196), Northern vs. Island (F_{ST} = 0.367), Center vs. Island (F_{ST} = 0.378), and the highest value was Southern vs. Island (F_{ST} = 0.416). In contrast, D_{xy} results showed similar absolute divergence variation among all pairwise populations. The lowest ancestral variation value was found between Center vs. Southern (D_{xy} = 0.144), followed by Northern vs. Center (D_{xy} = 0.154), Southern vs. Island (D_{xy} = 0.162), Northern vs. Southern (D_{xy} = 0.163), Center vs. Island (D_{xy} = 0.165), and Northern vs. Island (D_{xy} = 0.179). Both F_{ST} and D_{xy} values were significant (P-value < 0.05).

Nucleotide diversity within mainland populations exhibited a similar profile in terms of the number of segregating sites, θ_W and π. The Northern population displayed higher genetic diversity

compared to the others (S = 13379, θ_W = 0.180, and π = 0.137), while the Island showed the lowest genetic diversity (S = 4359, θ_W = 0.082, and π = 0.062). Tajima's neutrality values were negative for all populations, suggesting historical population expansions or positive selection, with excess of polymorphic sites, especially notable in the Southern population (Table 1).

Table 1. Genetic diversity and neutrality statistics for the four populations of *Brachycephalus actaeus* evidencing non-equilibrium histories among lineages. Abbreviations: MAF, minor allele frequency; S, number of segregating sites; θ_W, the proportion of segregating sites (Watterson's theta); π, proportion of nucleotide diversity. P-values are associated with the Tajima's D test for neutrality.

Population	MAF	S	θ_W	π	Tajima's D	P-value
Northern (N = 16)	0.16	13379	0.180	0.137	-0.043	0.00
Center (N = 10)	0.19	10215	0.155	0.124	-0.031	0.00
Southern (N = 8)	0.26	7786	0.120	0.114	-0.007	0.01
Island (N = 5)	0.54	4359	0.082	0.062	-0.020	0.00
Metapop (N = 39)	0.09	21545	0.232	0.022	-0.083	0.00

3.3 Haplotype network and pairwise distance based on mtDNA

The 16S mtDNA haplotype network corroborated genetic similarities among Northern, Center, Southern, and Island populations. We identified 12 haplotypes, with 13 variable sites. The haplotypes differed by a maximum of two mutational steps and shown one haplotype shared with the gray, green and orange morphs. Three out of 12 haplotypes were privative to the green morph, two to the orange morph, two to the brown morph, and one to the gray morph (Fig. 5A). No association was found between color categories and the genetic structure inferred from mtDNA. However, privative haplotypes were linked to specific locations (Fig. 5B) and haplotypes distributions tend to organize by population structure (Fig. 5C).

The uncorrected p-distances for pairwise divergence among individuals from four morphs across ten *B*. *actaeus* localities range from 0.2% to 1.5% for 16S (Table 2). The lowest distance is found among individuals from Island, SPA, and MOG (0.2 %), while the highest distance between individuals is observed between BFb and BNb against CAG (1.5%). The BFb locality exhibits the highest intraspecific variation (1.1%).

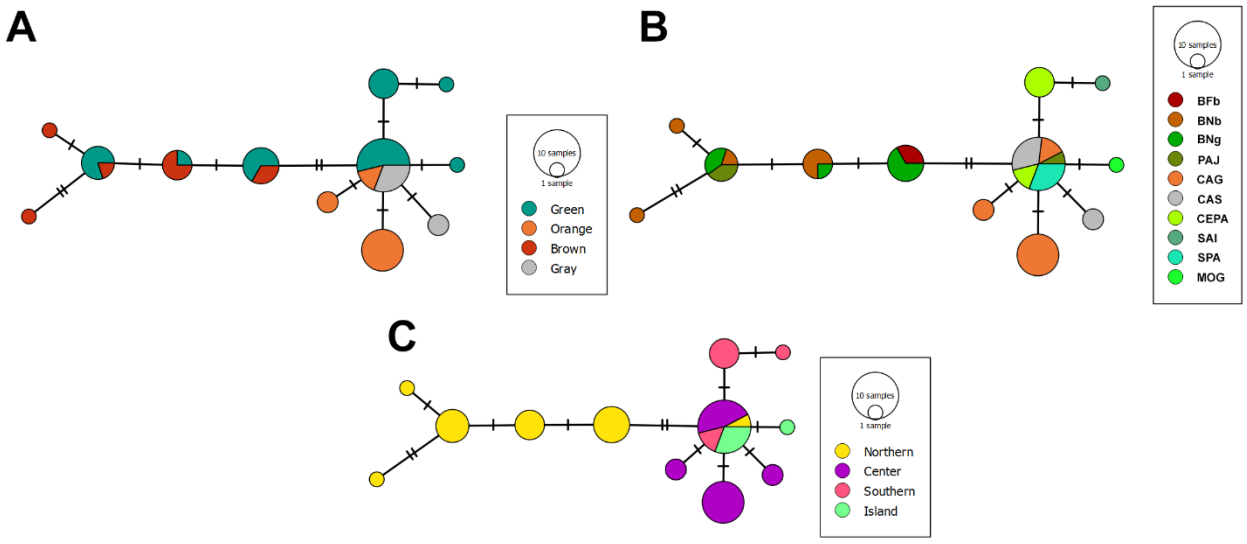


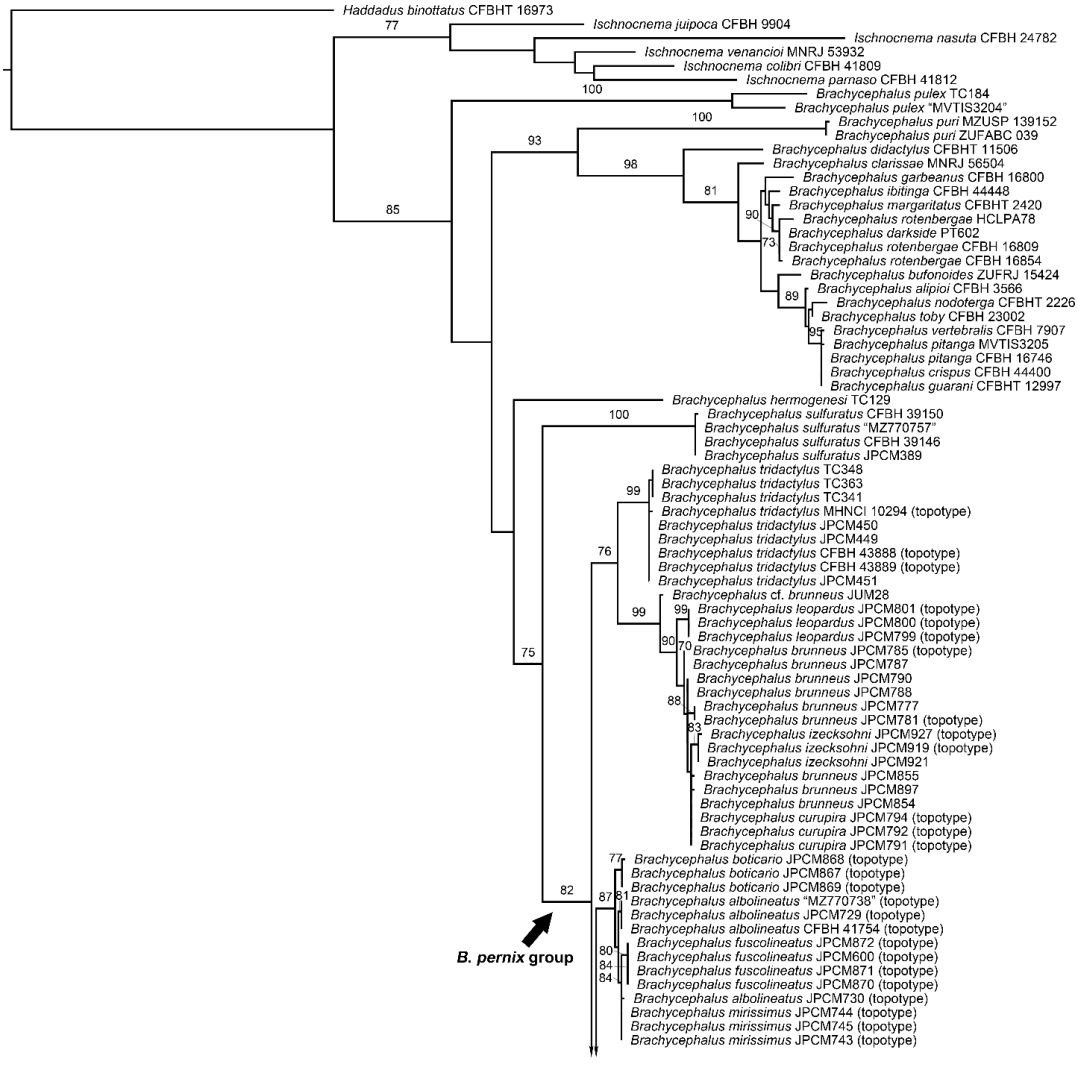
Figure 5. Median-joining haplotype network based on 16S rRNA mitochondrial fragment (473 bp) from 48 individual of *Brachycephalus actaeus*. The haplotypes are represented by circles and haplotype frequency is proportional to circle size. Colors show the proportion of individuals in each category: A) morphs; B) localities; C) genetic population. Abbreviations: BFb = Bom Futuro; BNb = Braço do Norte; BNg = Braço do Norte; CAG = Cantagalo CAS = Casarão; CEPA = Centro de Estudos e Pesquisas Ambientais da Univille; MOG = Morro Grande; PAJ = Fazenda Palmito Juriti; SAI = Estrada do Saí; and SPA= Serra da Palha.

Table 2. Genetic p-distance based on the mitochondrial 16S rRNA fragment (473 bp) across *Brachycephalus actaeus* sampled in the northeastern Santa Catarina, Brazil. Average distances among individuals within each locality are highlighted in bold.

Locality	BFb	BNb	BNg	PAJ	CAG	CAS	CEPA	SAI	SPA	MOG
BFb (n = 2)	**1.1%**									
BNb (n = 6)	1.0%	**0.3%**								
BNg (n = 7)	0.7%	0.6%	**0.5%**							
PAJ (n = 3)	0.9%	0.5%	0.6%	**0.9%**						
CAG (n = 12)	1.5%	1.5%	1.2%	1.1%	**0.3%**					
CAS (n = 6)	1.3%	1.4%	1.1%	0.9%	0.6%	**0.5%**				
CEPA (n = 6)	1.1%	0.9%	0.9%	0.7%	0.6%	0.6%	**0.1%**			
SAI (n = 1)	1.4%	1.1%	1.2%	1.0%	0.9%	0.8%	0.3%	-		
SPA (n = 4)	0.9%	1.3%	0.9%	0.9%	0.4%	0.3%	0.5%	0.7%	**0.0%**	
MOG (n = 1)	1.1%	1.2%	1.0%	1.0%	0.6%	0.5%	0.4%	0.7%	0.2%	-

*BFb = Bom Futuro brown morph; BNb = Braço do Norte brown morph; BNg = Braço do Norte green morph; PAJ = Fazenda Palmito Juriti; CAG = Cantagalo; CAS = Casarão; CEPA = Centro de Estudos e Pesquisas Ambientais da Univille; SAI = Estrada do Saí; SPA = Serra da Palha; and MOG = Morro Grande.

ML analysis based on 16S sequences supports the monophyly of *B. actaeus* including all color morphs, although with moderate to high bootstrap value (Fig. 6). There is no clear structure among lineages inferred by nuclear data (Northern, Center, Southern, and Island) on mitochondrial fragment. The reconstructed phylogeny revealed low support among most species of *B. pernix* group (Fig. 6). We also recovered paraphyly in the *B. brunneus* clade (*B. brunneus* + *B. curupira* + *B. izecksohni* + *B. leopardus*), in the *B. albolineatus* clade (*B. albolineatus* + *B. boticario* + *B. fuscolineatus* + *B. mirissimus*), and in the *B. pernix* clade (*B. auroguttatus* + *B. coloratus* + *B. ferruginus* + *B. mariaterezae* + *B. olivaceus* + *B. pernix* + *B. pombali* + *B. quiririensis* + *B. tabuleiro* + *B. verrucosus*).



Part 1/2.

Figure 6. Maximum Likelihood phylogenetic inference for *Brachycephalus* species based on 490 bp of 16S mtDNA sequences. Maximum likelihood non-parametric bootstrap support values is shown near the branches (values ≥ 70%). GenBank accession numbers, localities abbreviations for *B. actaeus*, and sequences details are available in Table S4.

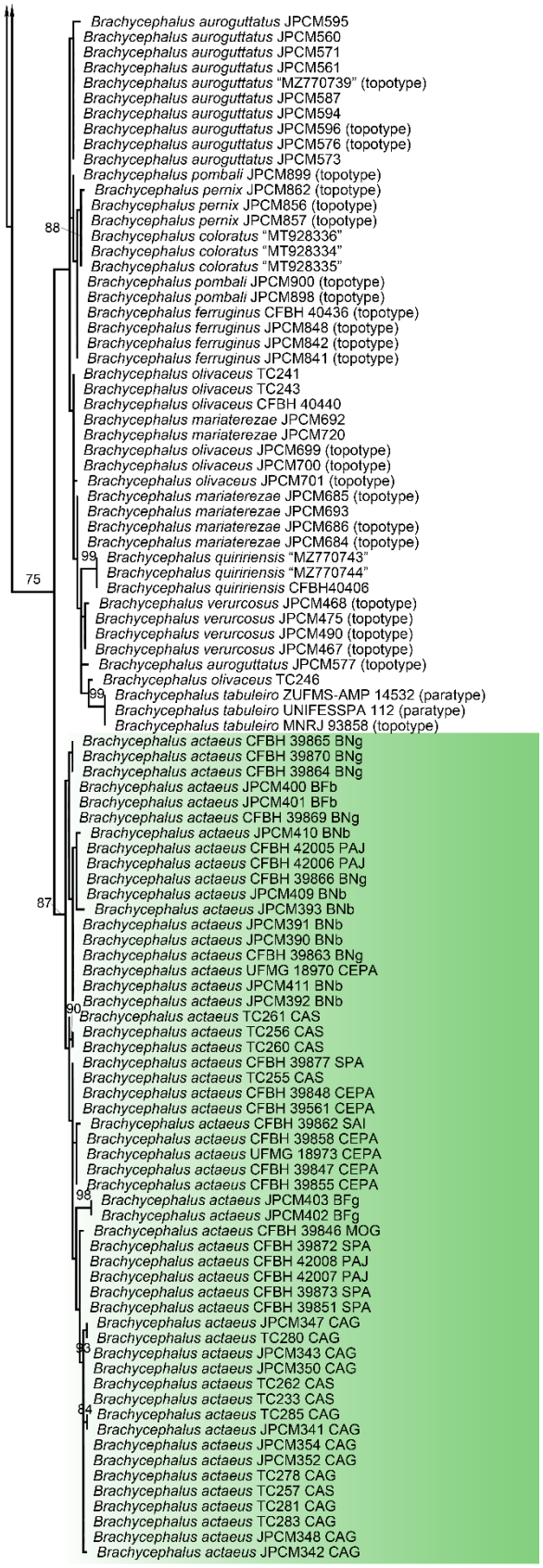


Figure 6. *Part 2/2*.

3.4 Variation in phenotypic and acoustic traits

3.4.1 Morphometry

In total, we measured 31 females and 39 males of adult specimens (Table S5). The first three PCs account for 41.94% of the total morphometric variance in females and 44.61% in males. Permutation-based statistical tests were not significant for females' data, while the first two axes were significant for male's data, explaining 33.4% of the total variance. Variables HW, IOD, IND, and HAL had significant loadings in PC1, and AL, THL, and FL had significant loadings in PC2 (Fig. 7A; Table S6). The Kruskal-Wallis test was not significant for both male (P-value = 0.37) and female (P-value = 0.09) SVL across localities.

Bidimensional discriminant analysis of principal components (DAPC) scatterplots depicted an overlapped distribution of two significant axes for male data, indicating a lack of distinction in morphometric traits among color morphs (Fig. 7B). Only HL and HW had contribution to the linear discriminant (LD) axes. In the first axis, HL had a higher contribution than HW (60% and 40% respectively) and, in the second axis, HW had a higher contribution (68% and 32%, respectively) (Fig. 7B). HL was positively related to LD1, while HW was negatively related to LD2. Our results suggest variation in morphometric traits among individual from the same locality, as the analyses did not reveal any distinct cluster.

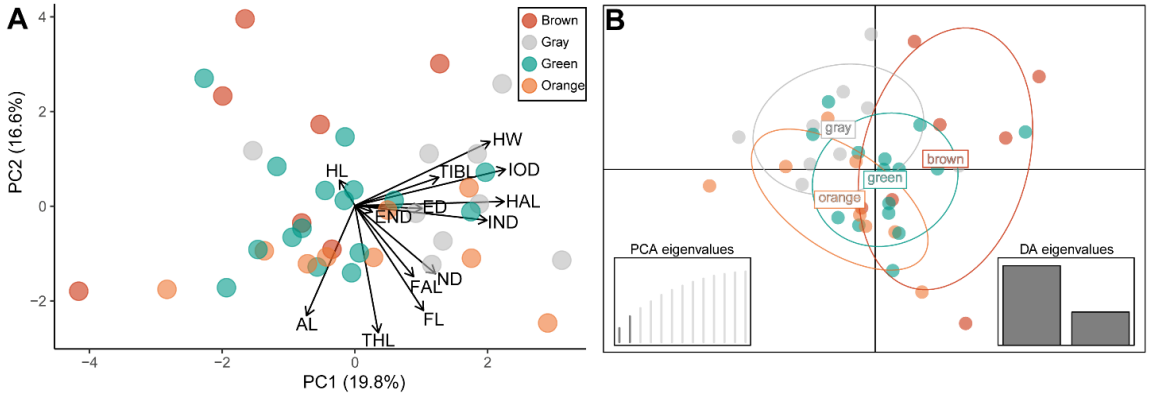


Figure 7. Morphometric analyses based on thirteen traits of *Brachycephalus actaeus* males (N = 39). A) Principal component analysis represents the significative axes PC1 and PC2. B) Discriminant analysis of principal components (DAPC) of significative PCs axes from male data by morph. The axes represent the two linear discriminants (LD). The PCA eigenvalues shows the portion of variance retained when maintaining 13 PCA axes. The DA eigenvalues shows the relative percent variation explained by each of the retained discriminant analysis (DA) eigenvectors. Abbreviation: AL, upper arm length; FAL, forearm length; ED, eye diameter; END, eye-nostril distance; FL, foot length; HAL, hand length; IND, internarial distance; IOD, interorbital distance; HL, head length; HW, head width; ND, nostril diameter; TIBL, tibia length; and THL, thigh length.

3.4.2 Osteology

The osteology examination of the four specimens of *B*. *actaeus* (CFBH 39872, JPCM351, JPCM410, and TC256) revealed significant variations when compared with single specimen used in the original description of the species (CFBH 39848, Monteiro et al., 2018; Fig. 8). We carefully assigned these variations, considering all five specimens mentioned. Arytenoid cartilages were found to be mineralized in all specimens of *B*. *actaeus* (contrary to the earlier cartilaginous characterization in Monteiro et al. 2018; Fig. 8E – H). Also, the procoracoid and epicoracoid were observed to be fused with the clavicle and coracoid, with the clavicle separated from the coracoid by a wide ovoid fenestra (contrary to the statement in Monteiro et al., 2018: "procoracoid and epicoracoid fused with coracoid but separated from the clavicle by an ovoid fenestra, distant from the epicoracoid"). The pectoral girdle showed variable degrees of mineralization in the dorsal and ventral regions (Fig. 8A – D).

We observed anomalies in the vertebral column of CFBH 39872. In this individual, the spinal plates from the vertebrae III to vertebrae VI and from the vertebrae VII to Sacral are fused in dorsal view, and the centra and the transverse processes may also be fused in ventral view, forming a unique element (Fig. 8D; Fig. S1H). Furthermore, spinal plate VIII and sacral are fused in CFBH 39848, JPCM351, and TC256 (Fig. 8A – B). The orientation of transverse processes in *B*. *actaeus* exhibits variability: Presacral III in the anomalous specimen (CFBH 39872) is perpendicular and diagonally twisted; Presacral V is posteriorly oriented (CFBH 39848, JPCM351, and JPCM410) or perpendicular (CFBH 39872 and TC256); Presacral VI is oriented anteriorly (CFBH 39848) or perpendicular to the notochordal axis (CFBH 39872, JPCM351, JPCM410, and TC256); and Presacral VII is oriented anteriorly (JPCM410) or perpendicular to the notochordal axis (CFBH 39848, CFBH 39872, JPCM351, and TC256). Lengths of transverse processes of presacrals differ among all examined specimens: VIII < II < VI ~ VII < V <III < IV (paratype, CFBH 39848); VIII < II ~ VI ~ VII < III ~ V < IV (paratype, CFBH 39872); VIII < II ~ VII < V ~ VI < III < IV (JPCM351); VIII < II ~ VI ~ VII < V < III ~ IV (TC256); and VIII < VI ~ VII < II ~ V < III ~ IV (JPCM410) (Fig. 8A – D). In the manus, distal carpals are partially fused (I–II) or fused (III–IV) with the centrale but distinguishable (JPCM351 and JPCM410). Tips of fingers II are pointed (JPCM351 and JPCM410) or arrow-shaped (CFBH 39848) (Fig. S1). Two specimens presented indistinguishable tip of fingers due to CT resolution (CFBH 39872 and TC256). In the

pes, phalangeal formula varies between 0 – 2 – 3 – 4 – 0 (JPCM351 and CFBH 39872) and 1 – 2 – 3 – 4 – 0 (CFBH 39848, JPCM410, and TC256) (Fig. S1).

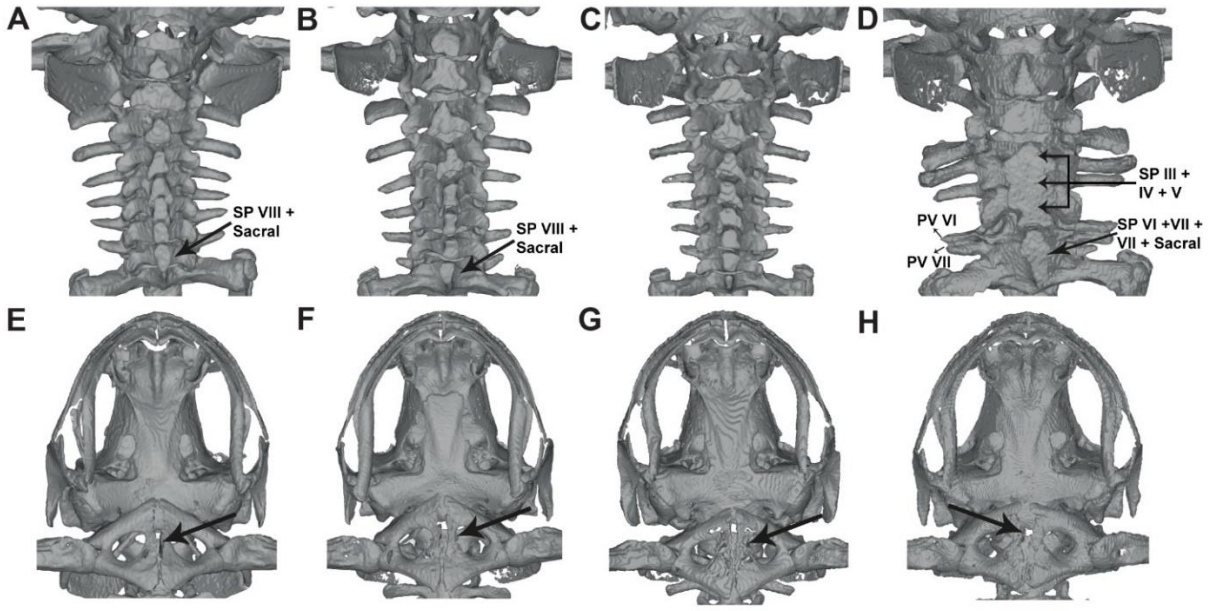


Figure 8. High-resolution computed tomography (Micro-CT) scans of *Brachycephalus actaeus*. A and E: orange morph (JPCM351); B and F: gray morph (TC256); C and G: brown morph (JPCM410); and D and H: green morph (CFBH 39872). Above in dorsal view, arrows indicate vertebrae anomalies. Below in ventral view, arrows indicate mineralized arytenoid cartilages. Abbreviations: PV, Presacral vertebrae; and SP, spinal plate.

3.4.3 Advertisement call

To evaluate the distinctiveness of advertisement calls within *B. actaeus*, we analyzed 816 calls from 51 individuals across nine localities (Table S3; Table S7). The PCA based on the acoustic dataset did not reveal distinct clades among color morphs, localities, or populations (Fig. 9A). The first two PCs axes were significant, explaining 57.3% of the total variation (Table S8). In PC1, there were significative loadings of temporal traits, such call repetition rate and pulse repetition rate, as well as the number of pulses, all exhibiting negative correlations. In contrast, another temporal trait, the inter-call interval, together with the spectral frequency traits (dominant, lower and upper frequencies), presented positive correlations. All these variables had significant loadings in PC1. In PC2, lower, upper, and dominant frequencies were positively correlated and had significant loadings (Table S8).

The analysis of spatial eigenfunction using dbMEM resulted in three positive spatial correlation Moran's eigenvector maps (MEMs) (Fig. S2). Significance was observed in the Monte-Carlo tests for all three MEMs (P-value < 0.05). The forward selection test from RDA models

identified the green morph, Northern and Center populations, and MEM1 as significant predictors of call variation in *B*. *actaeus* (Table 3). MEM1 refers to the variation among call traits across broad-scale patterns. The permutation test selected the Center population and MEM1 as the best variables to explain the model, and this was confirmed by low collinearity (VIF > 10; Legendre and Legendre, 2012). The final RDA was globally significant (P-value = 0.02) and revealed an adjusted coefficient of determination of 4,00%. The first two axes of RDA accounted for 3.69% and 0.31% of total call variation, respectively (Table 3). The Center population was positively correlated with the number of pulses and call duration, and MEM1 negatively correlated with rise time, frequency bandwidth, and inter-call interval (Fig. 9B and Table 3).

Table 3. Results of redundancy analyses testing the relationship between acoustic variables* and morphs, populations, geographic distance and environmental data for *Brachycephalus actaeus*. Inertia = amount of variation in the data set; adjusted R^2 (Adj. R^2) = selected more useful variables; adjusted R^2 cumulative = cumulative determination of variables in Adj. R^2; F = calculated f-scores; d.f. = degrees freedom in the model. The test was considered significant at P-value < 0.05 (in bold).

Variable	**RDA**					**Forward selection**			
	Inertia	Adj. R^2 (%)	F	d.f.	P	Significative variable	Adj. R^2 cum. (%)	F	P
Geographic distance MEM1 + MEM2 + MEM3	0.60	4.20	1.73	0.60	**0.05**	MEM1	3.77	2.96	**0.01**
Morphs brown + gray + green + orange	0.95	10.39	2.93	0.95	**0.01**	Green morph	8.90	5.89	**0.01**
Population Northern + Center + Southern + Island	0.90	9.53	2.76	0.90	**0.00**	Northern	6.75	4.62	**0.00**
						Center	9.24	2.35	**0.04**
Significative variables MEM1 + green morph + Northern + Center	0.94	8.35	2.14	0.94	**0.00**				
Best variables by permutation test** Center and MEM1	0.47	4.00	2.04	0.47	**0.02**				

*The acoustic variables lower and upper frequencies, call repetition rate, and pulse repetition rate were not included because they were significantly correlated with other variables. **Main statistics of the permutation test to simplify the model: MEM1 (AIC = 89.775; F = 2.375; and P-value = 0.050); and Center (AIC = 91.382; F = 3.988; and P-value = 0.005).

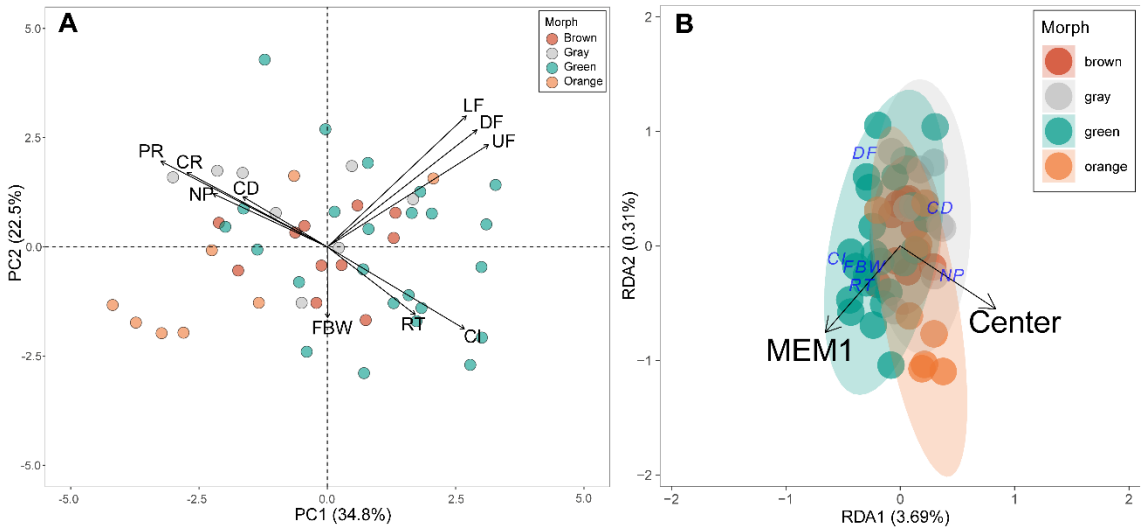


Figure 9. Acoustic analyses comparing *Brachycephalus actaeus* calls. A) Principal component analysis plot of the first two significant axes in whole acoustic data. B) Redundant analyses (RDA) of significant predictive variables, MEM1 (geographic structure) and Center (genetic population), and non-correlated acoustic traits. Only the first axis of global RDA was significant and explain 3.69% of variance. Abbreviations: CD, call duration; CI, inter-call interval; CR, call rate; DF, dominant frequency; FBW, frequency bandwidth; LF, lower frequency; NP, number of pulses; RT, rise time; PR, pulse rate; and UP, upper frequency.

4 DISCUSSION

Our findings revealed clear intrapopulation color variation in *Brachycephalus actaeus*, supported by multiple evidence, including genetics, morphology, osteology, and bioacoustics, in agreement with previous studies by Lyra et al. (2021) and Monteiro et al. (unpublished). Color polytypism within species has long been documented in aposematic frogs, guided by the central prediction that if color variance exists, it should be correlated with signal differences through adaptative roles (Briolat et al., 2019; Caro, 2017; Mayr, 1963). Specifically, in *Brachycephalus* species, cryptic and conspicuous colors have been putatively associated with antipredator strategies (Monteiro et al., unpublished; Rebouças et al., 2019). Our contribution reinforces the predominance of color polymorphism and polytypism in *B. actaeus*, offering insights for future studies on *Brachycephalus* species.

The color morphs in *B. actaeus* exhibit patterns proposed as precursors to the evolution of aposematism (Loeffler-Henry et al., 2023). These patterns are characterized by fully conspicuous (orange morph), dorsal cryptic with small patches of conspicuous coloration on ventral surfaces (green morph), and dorsal cryptic with fully conspicuous ventral surface (brown and gray morphs). In this way, it is essential to trace the history of aposematism in this species to understand whether

these color morphs represent a continuum in the acquisition of aposematism, or if the aposematic coloration observed currently evolves back to cryptic.

The distribution of color morphs in *B*. *actaeus* differs from the four identified populations, corresponding to Northern (BFb, BFg, BNb, BNg, and PAJ), Center (CAG and CAS), Southern (CEPA and SAI), and Island (MOG and SPA). The color of CAS individuals is predominantly gray, varying to brownish and greenish, occasionally with a weakly delimited white vertebral stripe, which is clearly displayed by the orange morph (Fig. 2M – T). Also, CAS individuals showed wide genetic admixture in comparison to relatives. Additionally, the broader distribution observed for the green morph might indicate greater fitness plasticity across different environmental conditions and pressures. The green morph were found exclusively in the Island population (MOG and SPA), which is geographically fragmented due to human occupation and is currently isolated from mainland populations by Babitonga Bay (Monteiro et al., 2018).

The F_{ST} results for pairwise populations support lower gene flow between mainland (Northern, Center, and Southern) and the Island, which is likely an indicative of the physical barrier imposed by Babitonga Bay to gene exchange. Among mainland populations, we detected highest genetic diversity, low genetic differentiation, and probable level of gene flow. The Tajima's neutrality values were negative for all populations, with a notable emphasis in the Southern population. Negative Tajima's D values can suggest population expansions after selective sweep and bottleneck (Galtier et al., 2000). Due to the loss of genetic variation after spatial isolation, the new population can become genetically distinct from the original population (Arenas et al., 2012), which could explain the structure of four populations here observed in *B*. *actaeus*. Further, studies will be necessary to investigate demographic history and evaluate differences in timing and intensity of bottlenecks in *B*. *actaeus* populations. In addition, the fixation of rare alleles in the Southern population (CEPA and SAI) might be an outcome of smaller effective population size during spatial isolation (Pabijan et al., 2012), suggesting a recent contact with CAS from Center population.

The morphometric analysis revealed that both head length and width made a substantial contribution to individual differences. The observed overlap between color morphs led us to interpret this outcome as a reflection of intraspecific variability among individuals within same sampled localities. Additionally, no differences in body size were detected. Aposematic coloration is known to function as an effective warning signal, typically favoring larger-sized individuals

(Hagman & Forsman, 2003). Contrary to the predictions presented for the general body size shifts within the genus *Brachycephalus* (Condez et al., 2020), we found no evidence supporting positive selection pressures favoring larger body size in the orange morph of *B. actaeus*. Although this phenomenon has been documented in amphibians, such as *Oophaga granulifera* (Brusa et al., 2013), *O. pumilio* (Rudh, 2013), or *Ambystoma* (Winebarger et al., 2018), it is possible that certain species, as observed in *Plethodon* (Winebarger et al., 2018), are too small to derive advantages from conspicuous coloration in larger bodies.

In the osteological comparison of *B. actaeus*, we identified prominent disparities, underscoring the importance of evaluating intraspecific characteristics. Predominantly, these differences were related to specific details in bone structures, such as variations in the length and orientation of transverse processes of vertebrae, fusion in manus bones, the shape of the fingertips, and pes' phalangeal formula. The intraspecific variability observed in the phalangeal formula agrees with previous remarks observed in miniaturized species, suggesting a potential outcome of miniaturization (Yeh, 2002). Notably, the fusion of centra and the transverse processes in the anomalous vertebrae column of the CFBH 39872 specimen aligns with conditions observed in other *Brachycephalus* species, such as those with bony plates (i.e., *B. ephippium* and *B. rotenbergae*; Campos et al., 2010). This discovery, tied to the fact that structural modifications, like bone fusions and bone plates, are shared between all *Brachycephalus* relatives, reinforces that the genes responsible for structural modifications may be present but inactive in some species. Similarly, substantial osteological variations in diagnostic traits have been documented in *Brachycephalus* species when the intraspecific sample size is expanded (Folly et al., 2021). Combined with existing literature, these intraspecific variations support the idea that increased intraspecific variability in adults of miniaturized species may result as a by-product of size reduction (Hanken, 1993; Hanken & Wake, 1993; Yeh, 2002).

Furthermore, our bioacoustics approach revealed the influence of the Center population (comprising CAG and CAS localities, represented by orange and gray morphs, respectively) and geographic distances on call variation. Male calls from these localities exhibited predominantly three pulses per call (one call-note), a pattern uncommon in all other localities where calls regularly consist of two pulses per note. This distinctive acoustic characteristic suggests population specificity in the communication patterns of *B. actaeus*. The conspicuous orange coloration and acoustic distinctions in CAG perhaps can contribute to multimodal signaling, potentially

influencing local female mate choice preferences (Dreher & Pröhl, 2014; Rojas et al., 2018), which was supported by low genetic admixture among other populations. On the other hand, the similar call characteristics amid CAS and CAG, coupled with color variation and clearly genetic admixture between the CAS and Southern population, indicate CAS as a potential recent transition zone among color morphs.

Diversification in acoustic signals in polymorphic/polytypic poison frogs has been proposed as a consequence of the aposematism, aiding in partner recognition while employing a color strategy to avoid predation (Dreher et al., 2015; Rojas et al., 2018; Santos et al., 2014). Also, numerous studies have linked call variation to factors like geographic variation or/and genetic structure (Brusa et al., 2013; González-Acosta et al., 2023; Twomey et al., 2015). Within *Brachycephalus* species, there is a noteworthy absence of studies that assess intraspecific acoustic variation across the geographic distribution of species. The puzzle deepens when considering the presumed deafness of *Brachycephalus* species (Goutte et al., 2017). The fact that males of different species of *Brachycephalus* emit conspicuous vocalizations (authors personal observations; e.g. Condez et al., 2021) and antiphonal calls (Oliveira & Haddad, 2017; C.F.B. Haddad, personal observations for *B. ephippium*, *B. pitanga*, *B. rotenbergae*, and *B. toby*; J.P.C. Monteiro observations for all species of *B. pernix* group), which presuppose acoustic synchronization with neighboring males, shows that they have the ability to perceive sounds. In an evolutionary context, we argue that acoustics signals in *Brachycephalus* have a sensory function, potentially being received through an alternative pathway. Our findings still suggest that intraspecific acoustic variation in *B. actaeus* may be influenced by sexual selection and geographic distance. It is, however, crucial to acknowledge the limitation of our data, which warrant further research to improve sample size and incorporate important variables, such as male body size, environmental conditions, and behavior, to improve statistical robustness and to test alternative explanations.

Until recently, color variation in *Brachycephalus* was often overlooked as an intraspecific characteristic. Instead, the attribution of high numbers of newly identified microendemic species has been linked to color differences, helping as a diagnostic character indicative of rapid diversification (e. g. Pie et al., 2018; Ribeiro et al., 2015, 2017). The inclusion of more samples offers a greater understanding of intraspecific variation and could help signal possible paraphylies as exemplified in our phylogenetic reconstruction. While the mechanisms underlying phenotypic diversity in *Brachycephalus* are unknown, our results confirm that certain characters, such as

coloration, osteology, and bioacoustics, frequently used to define taxa, do not always reflect evolutionary divergence.

Thus, an alternative evolutionary interpretation among *Brachycephalus* species predicts intriguing scenarios where color diversity within species evolves from cryptic or aposematic phenotypes multiple times, a pattern common in dendrobatids (Grant et al., 2017). Undoubtedly, researchers must make effort to reassess the described species by identifying intraspecific morphological features and patterns in genetic lineages. This step will be crucial to important advances in understanding evolution in *Brachycephalus*, resulting in appropriated conservations measures. Many of these species and/or color morphs are limited to specific conditions at higher elevation locations in the Atlantic Forest remnants, making them vulnerable to climate change and habitat disturbance. The future direction for conservation should be carefully reconsidered, considering a broad understanding to preserve the evolutionary history of each lineage.

Altogether, our evidence provides a significant contribution to evolutionary scenario in *Brachycephalus*, highlighting the challenges in the taxonomy and systematics of these cryptic, aposematic, and miniaturize species – these last two phenomena contributing to high intraspecific variation (Briolat et al., 2019; Hanken & Wake, 1993; Paluh et al., 2020). The gradient from crypsis to aposematism in *B. actaeus* represents possible predator avoidance strategies (Monteiro et al., unpublished), reflecting opposing solutions to the trade-off between the costs of detection by predators and the benefits of learned aversion (Willink et al., 2013). However, nothing is known about whether female mate preferences play a role in selecting color morphs or if there is epigenetic regulation influenced by environmental conditions (Caballero et al., 2012; Gao et al., 2022). An intriguing avenue for future research on color morph selection will be to assess (1) the geographic variation in predator identity; (2) frequency-dependent sexual selection due to females' mate preferences; (3) how environmental variables (e.g., climate, resource availability, luminance) affect microhabitat; and (4) the variation of chemical defences among color morphs.

In conclusion, this study underscores the urgent need for targeted conservation efforts, particularly for the vulnerable Island population of *B. actaeus*. The imminent threats posed by urbanization and pollution stemming from the nearby port region place this population at significant risk, exacerbated by its location outside of conservation areas and confined to a limited space. On the other hand, mainland populations face a similar alert level for threats, mainly associated with urbanization. However, the prospect of future protection within the conservation

area “Refúgio da Vida Silvestre das Nascentes do Saí” provides a promising path for its populations.

References

Arcanjo, D. D. R., Vasconcelos, A. G., Comerma-Steffensen, S. G., Jesus, J. R., Silva, L. P., Pires, O. R., Costa-Neto, C. M., Oliveira, E. B., Migliolo, L., Franco, O. L., Restini, C. B. A., Paulo, M., Bendhack, L. M., Bemquerer, M. P., Oliveira, A. P., Simonsen, U., & De Almeida Leite, J. R. D. S. (2015). A novel vasoactive proline-rich oligopeptide from the skin secretion of the frog *Brachycephalus ephippium*. *PLoS ONE*, *10*(12), 1–19. https://doi.org/10.1371/journal.pone.0145071

Arenas, M., Ray, N., Currat, M., & Excoffier, L. (2012). Consequences of range contractions and range shifts on molecular diversity. *Molecular Biology and Evolution*, *29*(1), 207–218. https://doi.org/10.1093/molbev/msr187

Baden, T., & Osorio, D. (2019). The retinal basis of vertebrate color vision. *Annual Review of Vision Science*, *5*, 177–200. https://doi.org/10.1146/annurev-vision-091718

Bandelt, H.-J., Forster, P., & Röhl, A. (1999). Median-Joining networks for inferring intraspecific phylogenies. *Molecular Biology and Evolution*, *16*(1), 37–48. https://academic.oup.com/mbe/article/16/1/37/993192

Borcard, D., Gillet, F., & Legendre, P. (2018). *Numerical ecology with R* (Second Edition). Springer International Publishing AG. https://doi.org/https://doi.org/10.1007/978-3-319-71404-2

Borcard, D., & Legendre, P. (2002). All-scale spatial analysis of ecological data by means of principal coordinates of neighbour matrices. *Ecological Modelling*, *153*, 51–68. www.elsevier.com/locate/ecolmodel

Bornschein, M. R., Pie, M. R., & Teixeira, L. (2019). Conservation status of *Brachycephalus* toadlets (Anura: Brachycephalidae) from the Brazilian Atlantic rainforest. *Diversity*, *11*(9), 9–11. https://doi.org/10.3390/d11090150

Boul, K. E., Funk, W. C., Darst, C. R., Cannatella, D. C., & Ryan, M. J. (2007). Sexual selection drives speciation in an Amazonian frog. *Proceedings of the Royal Society B: Biological Sciences*, *274*(1608), 399–406. https://doi.org/10.1098/rspb.2006.3736

Briolat, E. S., Burdfield-Steel, E. R., Paul, S. C., Rönkä, K. H., Seymoure, B. M., Stankowich, T., & Stuckert, A. M. M. (2019). Diversity in warning coloration: selective paradox or the norm? *Biological Reviews*, *94*(2), 388–414. https://doi.org/10.1111/brv.12460

Brusa, O., Bellati, A., Meuche, I., Mundy, N. I., & Pröhl, H. (2013). Divergent evolution in the polymorphic granular poison-dart frog, *Oophaga granulifera*: genetics, coloration, advertisement calls and morphology. *Journal of Biogeography*, *40*(2), 394–408. https://doi.org/10.1111/j.1365-2699.2012.02786.x

Caballero, L., Benítez, M., Alvarez-Buylla, E. R., Hernández, S., Arzola, A. V, & Cocho, G. (2012). An epigenetic model for pigment patterning based on mechanical and cellular interactions. *Journal of Experimental Zoology Part B: Molecular and Developmental Evolution*, *318*, 209–223. https://doi.org/10.1002/jez.22007

Camargo, A. (2022). PCAtest: testing the statistical significance of Principal Component Analysis in R. *PeerJ*, *10*. https://doi.org/10.7717/peerj.12967

Campos, L. A., Ricardo, H., Silva, D. A., & Sebben, A. (2010). Morphology and development of additional bony elements in the genus *Brachycephalus* (Anura: Brachycephalidae). *Biological Journal of the Linnean Society*, *99*, 752–767. https://academic.oup.com/biolinnean/article-abstract/99/4/752/2448033

Caro, T. (2017). Wallace on coloration: contemporary perspective and unresolved insights. *Trends in Ecology and Evolution*, *32*(1), 23–30. https://doi.org/10.1016/j.tree.2016.10.003

Caro, T., & Ruxton, G. (2019). Aposematism: unpacking the defences. *Trends in Ecology and Evolution*, *34*(7), 595–604. https://doi.org/10.1016/j.tree.2019.02.015

Catchen, J., Hohenlohe, P. A., Bassham, S., Amores, A., & Cresko, W. A. (2013). Stacks: an analysis tool set for population genomics. *Molecular Ecology*, *22*(11), 3124–3140. https://doi.org/10.1111/mec.12354

Chimetto Tonon, L. A., Rua, C., Crnkovic, C. M., Bernardi, D. I., Pires Junior, O. R., Haddad, C. F. B., Pedrosa, C. S. G., Souza, L. R. Q., Rehen, S. K., de Azevedo, G. P. R., Thompson, C. C., Thompson, F. L., & Berlinck, R. G. S. (2021). Microbiome associated with the tetrodotoxin-bearing anuran *Brachycephalus pitanga*. *Toxicon*, *203*, 139–146. https://doi.org/10.1016/j.toxicon.2021.10.002

Condez, T. H., Haddad, C. F. B., & Zamudio, K. R. (2020). Historical biogeography and multi-trait evolution in miniature toadlets of the genus *Brachycephalus* (Anura: Brachycephalidae). *Biological Journal of the Linnean Society*, *129*(3), 664–686. https://doi.org/10.1093/biolinnean/blz200

Condez, T. H., Monteiro, J. P. C., Malagoli, L. R., Trevine, V. C., Schunck, F., Garcia, P. C. A., & Haddad, C. F. B. (2021). Notes on the hyperossified pumpkin toadlets of the genus Brachycephalus (Anura: Brachycephalidae) with the description of a new species. *Herpetologica*, *77*(2), 176–194. https://doi.org/10.1655/HERPETOLOGICA-D-20-00031

Cruickshank, T. E., & Hahn, M. W. (2014). Reanalysis suggests that genomic islands of speciation are due to reduced diversity, not reduced gene flow. *Molecular Ecology*, *23*(13), 3133–3157. https://doi.org/10.1111/mec.12796

Cummings, M. E., & Endler, J. A. (2018). 25 Years of sensory drive: the evidence and its watery bias. *Current Zoology*, *64*(4), 471–484. https://doi.org/10.1093/cz/zoy043

de Jong, M. J., de Jong, J. F., Hoelzel, A. R., & Janke, A. (2021). SambaR: an R package for fast, easy and reproducible population-genetic analyses of biallelic SNP data sets. *Molecular Ecology Resources*, *21*(4), 1369–1379. https://doi.org/10.1111/1755-0998.13339

de Medeiros, B. A. S., & Farrell, B. D. (2018). Whole-genome amplification in double digest RADseq results in adequate libraries but fewer sequenced loci. *PeerJ*, *7*(e5089), 1–27. https://doi.org/10.7717/peerj.5089

Danecek, P., Auton, A., Abecasis, G., Albers, C. A., Banks, E., DePristo, M. A., Handsaker, R. E., Lunter, G., Marth, G. T., Sherry, S. T., McVean, G., & Durbin, R. (2011). The variant call format and VCFtools. *Bioinformatics*, *27*(15), 2156–2158. https://doi.org/10.1093/bioinformatics/btr330

Dorigo, T. A., Siqueira, C. C., Vrcibradic, D., Maia-Carneiro, T., Almeida-Santos, M., & Rocha, C. F. D. (2012). Ecological aspects of the pumpkin toadlet, *Brachycephalus garbeanus* Miranda-Ribeiro, 1920 (Anura: Neobatrachia: Brachycephalidae), in a highland forest of southeastern Brazil. *Journal of Natural History*, *46*(39–40), 2497–2507. https://doi.org/10.1080/00222933.2012.713525

Dray, S., Pélissier, R., Couteron, P., Fortin, M. J., Legendre, P., Peres-Neto, P. R., Bellier, E., Bivand, R., Blanchet, F. G., De Cáceres, M., Dufour, A. B., Heegaard, E., Jombart, T., Munoz, F., Oksanen, J., Thioulouse, J., & Wagner, H. H. (2012). Community ecology in the age of multivariate multiscale spatial analysis. In *Ecological Monographs* (Vol. 82, Issue 3, pp. 257–275). https://doi.org/10.1890/11-1183.1

Dreher, C. E., Cummings, M. E., & Pröhl, H. (2015). An analysis of predator selection to affect aposematic coloration in a poison frog species. *PLoS ONE*, *10*(6), 1–18. https://doi.org/10.1371/journal.pone.0130571

Dreher, C. E., & Pröhl, H. (2014). Multiple sexual signals: calls over colors for mate attraction in an aposematic, color-diverse poison frog. *Frontiers in Ecology and Evolution*, *2*(22), 1–10. https://doi.org/10.3389/fevo.2014.00022

Duellman, W. E. (2015) *Marsupial frogs:* Gastrotheca *& allied genera*. Johns Hopkins University Press, Baltimore, Maryland.

Eaton, D. A. R., & Overcast, I. (2020). Ipyrad: Interactive assembly and analysis of RADseq datasets. *Bioinformatics*, *36*(8), 2592–2594. https://doi.org/10.1093/bioinformatics/btz966

Emberts, Z., & Wiens, J. J. (2022). Why are animals conspicuously colored? Evolution of sexual versus warning signals in land vertebrates. *Evolution*, *76*(12), 2879–2892. https://doi.org/10.1111/evo.14636

Endler, J. A. (1991). Variation in the appearance of guppy color patterns to guppies and their predators under different visual conditions. *Vision Research*, *31*(3), 587–608.

Endler, J. A. (1992). Signals, signal conditions, and the direction of evolution. *The American Naturalist*, *139*, 125–153.

Endler, J. A. (1993). The color of light in forests and its implications. *Ecological Monographs*, *63*(1), 1–27.

Falush, D., Stephens, M., & Pritchard, J. K. (2007). Inference of population structure using multilocus genotype data: dominant markers and null alleles. *Molecular Ecology Notes*, *7*(4), 574–578. https://doi.org/10.1111/j.1471-8286.2007.01758.x

Folly, M., de Luna-Dias, C., Miguel, I. R., Ferreira, J. C., Machado, A., Tadeu Lopes, R., & Pombal, J. P. (2021). Tiny steps towards greater knowledge: an osteological review with novel data on the Atlantic Forest toadlets of the *Brachycephalus ephippium* species group . *Acta Zoologica*, *December 2020*, 1–35. https://doi.org/10.1111/azo.12398

Ford, E. B. (1945). Polymorphism. *Biological Reviews of the Cambridge Philosophical Society*, *20*, 73–88.

Frichot, E., & François, O. (2015). LEA: An R package for landscape and ecological association studies. *Methods in Ecology and Evolution*, *6*(8), 925–929. https://doi.org/10.1111/2041-210X.12382

Frichot, E., Mathieu, F., Trouillon, T., Bouchard, G., & François, O. (2014). Fast and efficient estimation of individual ancestry coefficients. *Genetics*, *196*(4), 973–983. https://doi.org/10.1534/genetics.113.160572

Galtier, N., Depaulis, F., & Barton, N. H. (2000). Detecting bottlenecks and selective sweeps from DNA sequence polymorphism. *Genetics*, *155*, 981–987.

Gao, Y., Chen, Y., Li, S., Huang, X., Hu, J., Bock, D. G., MacIsaac, H. J., & Zhan, A. (2022). Complementary genomic and epigenomic adaptation to environmental heterogeneity. *Molecular Ecology*, *31*, 3598–3612. https://doi.org/10.1111/mec.16500

Gerhardt, H. C., & Huber, F. (2002) *Acoustic communication in insects and anurans: common problems and diverse solutions*. Chicago and London, University of Chicago Press.

González-Acosta, C., Amézquita, A., & Vargas-Salinas, F. (2023). Variation in the advertisement call of the poison frog *Andinobates bombetes* relates to geographic distance between populations, but not to divergence in warning coloration. *Studies on Neotropical Fauna and Environment*, 1–13. https://doi.org/10.1080/01650521.2023.2238560

Gotelli, N. J., & Ellison, A. M. -S, F. (2011). *Princípios de estatística em ecologia*. Artmed, Porto Alegre

Goutte, S., Mason, M. J., Christensen-Dalsgaard, J., Montealegre-Z, F., Chivers, B. D., Sarria-S, F. A., Antoniazzi, M. M., Jared, C., Almeida Sato, L., & Felipe Toledo, L. (2017). Evidence of auditory insensitivity to vocalization frequencies in two frogs. *Scientific Reports*, *7*(1), 1–9. https://doi.org/10.1038/s41598-017-12145-5

Grant, T., Rada, M., Anganoy-Criollo, M., Batista, A., Dias, P. H., Jeckel, A. M., MacHado, D. J., & Rueda-Almonacid, J. V. (2017). Phylogenetic systematics of dart-poison frogs and their

relatives revisited (Anura: Dendrobatoidea). *South American Journal of Herpetology*, *12*(s1), S1–S90. https://doi.org/10.2994/SAJH-D-17-00017.1

Hagman, M., & Forsman, A. (2003). Correlated evolution of conspicuous coloration and body size in poison frogs (Dendrobatidae). *Evolution*, *57*(12), 2904–2910.

Hanken, J. (1993). Adaptation of bone growth to miniaturization of body size. *CRC Press*, *7*, 79–104.

Hanken, J., & Wake, D. B. (1993). Miniaturization of body size: organismal consequences and evolutionary significance. *Annual Review of Ecology and Systematics*, *24*, 501–519. www.annualreviews.org

Heyer, W. R., Rand, A. S., Da Cruz, C. A. G., Peixoto, O. L., Nelson, C. E. 1990. Frogs of Boracéia. *Arquivos de Zoologia*, *31*, 231–410.

Hoffman, E. A., & Blouin, M. S. (2000). A review of colour and pattern polymorphisms in anurans. *Biological Journal of the Linnean Spciety*, *70*, 633–665. https://doi.org/10.1006/bijl.1999.0421

Hugall, A. F., & Stuart-Fox, D. (2012). Accelerated speciation in colour-polymorphic birds. *Nature*, *485*(7400), 631–634. https://doi.org/10.1038/nature11050

Hutton, P., Seymoure, B. M., McGraw, K. J., Ligon, R. A., & Simpson, R. K. (2015). Dynamic color communication. *Current Opinion in Behavioral Sciences*, *6*, 41–49. https://doi.org/10.1016/j.cobeha.2015.08.007

Jombart T., Kamvar Z. N., Collins C., Lustrik R., Beugin M. P., Knaus B. J., …, Dimens, P. (2018). Adegenet: exploratory analysis of genetic and genomic data. Available online at: https://cran.r-project.org/web/packages/adegenet/index.html (Accessed August 15, 2023).

Jombart, T. (2008). Adegenet: a R package for the multivariate analysis of genetic markers. *Bioinformatics*, *24*(11), 1403–1405. https://doi.org/10.1093/bioinformatics/btn129

Katoh, K., Rozewicki, J. & Yamada, K. D. 2019. MAFFT online service: multiple sequence alignment, interactive sequence choice and visualization. *Briefings in Bioinformatics*, *20*(4), 1160–1166.

Köhler, J., Jansen, M., Rodríguez, A., Kok, P. J. R., Toledo, L. F., Emmrich, M., Glaw, F., Haddad, C. F. B., Rödel, M. O., &Vences, M. 2017. The use of bioacoustics in anuran taxonomy: theory, terminology, methods and recommendations for best practice. *Zootaxa*, *4251*(1), 001–124. https://doi.org/10.11646/zootaxa.4251.1.1

Kruskal, W. H., & Wallis, W. A. (1952). Use of ranks in one-criterion variance analysis. *Journal of the American Statistical Association*, *47*(260), 583–621.

Lawrence, J. P., Rojas, B., Blanchette, A., Saporito, R. A., Mappes, J., Fouquet, A., & Noonan, B. P. (2023). Linking predator responses to alkaloid variability in poison frogs. *Journal of Chemical Ecology*, *49*(3–4), 195–204. https://doi.org/10.1007/s10886-023-01412-7

Legendre, P. and L. Legendre. 2012. *Numerical ecology*, 3rd English edition. Elsevier Science BV, Amsterdam.

Legendre, P., Oksanen, J., & ter Braak, C. J. F. (2011). Testing the significance of canonical axes in redundancy analysis. *Methods in Ecology and Evolution*, *2*(3), 269–277. https://doi.org/10.1111/j.2041-210X.2010.00078.x

Leigh, J. W., & Bryant, D. (2015). POPART: Full-feature software for haplotype network construction. *Methods in Ecology and Evolution*, *6*(9), 1110–1116. https://doi.org/10.1111/2041-210X.12410

Lima, M. S. C. S., Pederassi, J., & Souza, C. A. dos S. (2013). Habitat use by the pumpkin toadlet, *Brachycephalus ephippium* (Anura, Brachycephalidae), in the Atlantic Rain Forest of Brazil. *Boletín de La Asociación Herpetológica Española*, *24*(2), 11–15.

Lorioux-Chevalier, U., Tuanama Valles, M., Gallusser, S., Mori Pezo, R., & Chouteau, M. (2023). Unexpected colour pattern variation in mimetic frogs: implication for the diversification of warning signals in the genus *Ranitomeya*. *Royal Society Open Science*, *10*, 1–13. https://doi.org/10.1098/rsos.230354

Lyra, M. L., Monteiro, J. P. C., Rancilhac, L., Irisarri, I., Künzel, S., Sanchez, E., Condez, T. H., Rojas-Padilla, O., Solé, M., Toledo, L. F., Haddad, C. F. B., & Vences, M. (2021). Initial phylotranscriptomic confirmation of homoplastic evolution of the conspicuous coloration and bufoniform morphology of pumpkin-toadlets in the genus *Brachycephalus*. *Toxins*, *13*(816), 1–16. https://doi.org/10.3390/toxins13110816

Maniatis, T., Fritsch, E. F. & Sambrook, J. (1982) *Molecular Cloning: A Laboratory Manual*. Cold Spring Harbor Laboratory Press, New York.

Mappes, J., Marples, N., & Endler, J. A. (2005). The complex business of survival by aposematism. *Trends in Ecology and Evolution*, *20*(11), 598–603. https://doi.org/10.1016/j.tree.2005.07.011

Mayr, E. (1963). *Animal species and evolution* (3rd ed.). Harvard University Press.

Mclean, C. A., Moussalli, A., & Stuart-Fox, D. (2014). Local adaptation and divergence in colour signal conspicuousness between monomorphic and polymorphic lineages in a lizard. *Journal of Evolutionary Biology*, *27*(12), 2654–2664. https://doi.org/10.1111/jeb.12521

Mclean, C. A., & Stuart-Fox, D. (2014). Geographic variation in animal colour polymorphisms and its role in speciation. *Biological Reviews*, *89*(4), 860–873. https://doi.org/10.1111/brv.12083

Miller, M. A., Pfeiffer, W. & Schwartz, T. (2010) Creating the CIPRES Science Gateway for inference of large phylogenetic trees. *Proceedings of the Gateway Computing Environments Workshop*, 1–8. https://doi.org/10.1109/GCE.2010.5676129

Monteiro, J. P. C., Pröhl, H., Lyra, M. L., Brunetti, A. E., Nardin, E. C., Condez, T. H., Haddad, C. F. B., & Rodríguez, A. (unpublished) Expression patterns of melanin-related genes are linked to crypsis and aposematism in a pumpkin toadlet. Submitted to Molecular Ecology.

Monteiro, J. P. C., Condez, T. H., Garcia, P. C. D. A., Comitti, E. J., Amaral, I. B., & Haddad, C. F. B. (2018). A new species of *Brachycephalus* (Anura, Brachycephalidae) from the coast of Santa Catarina State, Southern Atlantic Forest, Brazil. *Zootaxa*, *4407*(4), 483–505. https://doi.org/10.11646/zootaxa.4407.4.2

Nei, M. (1987) *Molecular Evolutionary Genetics*. Columbia University Press, New York.

Nei, M., & Li, W.-H. (1979). Mathematical model for studying genetic variation in terms of restriction endonucleases (molecular evolution/mitochondrial DNA/nucleotide diversity). *Genetics*, *76*(10), 5269–5273.

Oliveira, E. G., & Haddad, C. F. B. (2017). Activity, acoustic repertoire and social interactions of the red toadlet, *Brachycephalus pitanga* (Anura: Brachycephalidae). *Salamandra*, *53*(4), 501–506. http://www.salamandra-journal.com

Oksanen J., Blanchet F. G., Kindt R., Legendre P., Minchin P. R., O'Hara R. B., ..., Weedon, J. (2022). vegan: Community Ecology Package. R package version 2.6.4

Osorio, D., & Vorobyev, M. (2008). A review of the evolution of animal colour vision and visual communication signals. *Vision Research*, *48*(20), 2042–2051. https://doi.org/10.1016/j.visres.2008.06.018

Pabijan, M., Wollenberg, K. C., & Vences, M. (2012). Small body size increases the regional differentiation of populations of tropical mantellid frogs (Anura: Mantellidae). *Journal of Evolutionary Biology*, *25*(11), 2310–2324. https://doi.org/10.1111/j.1420-9101.2012.02613.x

Padial, J. M., Grant, T., & Frost, D. R. (2014). Molecular systematics of terraranas (Anura: Brachycephaloidea) with an assessment of the effects of alignment and optimality criteria. *Zootaxa*, *3825*(1), 1–132. https://doi.org/10.11646/zootaxa.3825.1.1

Paluh, D. J., Stanley, E. L., & Blackburn, D. C. (2020). Evolution of hyperossification expands skull diversity in frogs. *Proceedings of the National Academy of Sciences of the United States of America*, *117*(15), 8554–8562. https://doi.org/10.1073/pnas.2000872117

Palumbi, S. R., Martin, A. P., Kessing, B. D. & McMillan, W. O. (1991) Detecting population structure using mitochondrial DNA. In: Hoelzel, A. R. (Ed.), *Genetic Ecology of Whales and Dolphins*. International Whaling Commission, Cambridge, pp. 271–278.

Peterson, B. K., Weber, J. N., Kay, E. H., Fisher, H. S., & Hoekstra, H. E. (2012). Double digest RADseq: an inexpensive method for de novo SNP discovery and genotyping in model and non-model species. *PLoS ONE*, *7*(5), 1–11. https://doi.org/10.1371/journal.pone.0037135

Pie, M. R., Faircloth, B. C., Ribeiro, L. F., Bornschein, M. R., & Mccormack, J. E. (2018). Phylogenomics of montane frogs of the Brazilian Atlantic Forest is consistent with isolation in sky islands followed by climatic stability. *Biological Journal of the Linnean Society*, *125*, 72–82. https://doi.org/10.1093/biolinnean/bly093

Pie, M. R., Meyer, A. L. S., Firkowski, C. R., Ribeiro, L. F., & Bornschein, M. R. (2013). Understanding the mechanisms underlying the distribution of microendemic montane frogs

(*Brachycephalus* spp., Terrarana: Brachycephalidae) in the Brazilian Atlantic Rainforest. *Ecological Modelling*, *250*, 165–176. https://doi.org/10.1016/j.ecolmodel.2012.10.019

Pires, O. R., Sebben, A., Schwartz, E. F., Morales, R. A. V., Bloch, C., & Schwartz, C. A. (2005). Further report of the occurrence of tetrodotoxin and new analogues in the anuran family Brachycephalidae. *Toxicon*, *45*(1), 73–79. https://doi.org/10.1016/j.toxicon.2004.09.016

Pombal Jr, J. P. (1999). Oviposição e desenvolvimento de *Brachycephalus ephippium* (Spix) (Anura, Brachycephalidae). *Revista Brasileira de Zoologia*, *16*(4), 967–976.

Pombal Jr., J. P., Sazima, I., & Haddad, C. F. B. (1994). Breeding behavior of the pumpkin toadlet, *Brachycephalus ephippium* (Brachycephalidae). *Journal of Herpetology*, *28*(4), 516–519.

Pröhl, H., & Ostrowski, T. (2011). Behavioural elements reflect phenotypic colour divergence in a poison frog. *Evolutionary Ecology*, *25*(5), 993–1015. https://doi.org/10.1007/s10682-010-9455-5

Purcell, S., Neale, B., Todd-Brown, K., Thomas, L., Ferreira, M. A. R., Bender, D., Maller, J., Sklar, P., De Bakker, P. I. W., Daly, M. J., & Sham, P. C. (2007). PLINK: A tool set for whole-genome association and population-based linkage analyses. *American Journal of Human Genetics*, *81*(3), 559–575. https://doi.org/10.1086/519795

Rebouças, R., Carollo, A. B., Freitas, M. de O., Lambertini, C., Dos Santos, R. M. N., & Toledo, L. F. (2019). Is the conspicuous dorsal coloration of the Atlantic Forest pumpkin toadlets aposematic? *Salamandra*, *55*(1), 39–47.

Ribeiro, L. F., Blackburn, D. C., Stanley, E. L., Pie, M. R., & Bornschein, M. R. (2017). Two new species of the *Brachycephalus pernix* group (Anura: Brachycephalidae) from the state of Paraná, Southern Brazil. *PeerJ*, *5*(e3603), 1–28. https://doi.org/10.7717/peerj.3603

Ribeiro, L. F., Bornschein, M. R., Belmonte-Lopes, R., Firkowski, C. R., Morato, S. A. A., & Pie, M. R. (2015). Seven new microendemic species of *Brachycephalus* (Anura: Brachycephalidae) from Southern Brazil. *PeerJ*, *3*(e1011), 1–36. https://doi.org/10.7717/peerj.1011

Rodríguez, A., Mundy, N. I., Ibáñez, R., & Pröhl, H. (2020). Being red, blue and green: the genetic basis of coloration differences in the strawberry poison frog (*Oophaga pumilio*). *BMC Genomics*, *21*(1), 1–16. https://doi.org/10.1186/s12864-020-6719-5

Rojas, B. (2017). Behavioural, ecological, and evolutionary aspects of diversity in frog colour patterns. *Biological Reviews*, *92*(2), 1059–1080. https://doi.org/10.1111/brv.12269

Rojas, B., Burdfield-Steel, E., De Pasqual, C., Gordon, S., Hernández, L., Mappes, J., Nokelainen, O., Rönkä, K., & Lindstedt, C. (2018). Multimodal aposematic signals and their emerging role in mate attraction. *Frontiers in Ecology and Evolution*, *6*(93), 1–24. https://doi.org/10.3389/fevo.2018.00093

Rojas, B., Valkonen, J., & Nokelainen, O. (2015). Aposematism. *Current Biology*, *25*(9), R350–R351. https://doi.org/10.1016/j.cub.2015.02.015

Rößler, D. C., Lötters, S., Mappes, J., Valkonen, J. K., Menin, M., Lima, A. P., & Pröhl, H. (2019). Sole coloration as an unusual aposematic signal in a Neotropical toad. *Scientific Reports*, *9*(1). https://doi.org/10.1038/s41598-018-37705-1

Rudh, A. (2013). Loss of conspicuous coloration has co-evolved with decreased body size in populations of poison dart frogs. *Evolutionary Ecology*, *27*(4), 755–767. https://doi.org/10.1007/s10682-013-9649-8

Santos, J. C., Baquero, M., Barrio-Amorós, C., Coloma, L. A., Erdtmann, L. K., Lima, A. P., & Cannatella, D. C. (2014). Aposematism increases acoustic diversification and speciation in poison frogs. *Proceedings of the Royal Society B: Biological Sciences*, *281*(20141761), 1–9. https://doi.org/10.1098/rspb.2014.1761

Saporito, R. A., Donnelly, M. A., Jain, P., Martin Garraffo, H., Spande, T. F., & Daly, J. W. (2007). Spatial and temporal patterns of alkaloid variation in the poison frog *Oophaga pumilio* in Costa Rica and Panama over 30 years. *Toxicon*, *50*(6), 757–778. https://doi.org/10.1016/j.toxicon.2007.06.022

Stamatakis, A. (2014). RAxML version 8: A tool for phylogenetic analysis and post-analysis of large phylogenies. *Bioinformatics*, *30*(9), 1312–1313. https://doi.org/10.1093/bioinformatics/btu033

Tajima, F. (1989). Statistical method for testing the neutral mutation hypothesis by DNA polymorphism. *Genetics*, *123*, 585–595.

Twomey, E., Kain, M., Claeys, M., Summers, K., Castroviejo-Fisher, S., & Van Bocxlaer, I. (2020). Mechanisms for color convergence in a mimetic radiation of poison frogs. *American Naturalist*, *195*(5), E132–E149. https://doi.org/10.1086/708157

Twomey, E., Mayer, M., & Summers, K. (2015). Intraspecific call variation in the mimic poison frog *Ranitomeya imitator*. *Herpetologica*, *71*(4), 252–259. https://doi.org/10.1655/HERPETOLOGICA-D-15-00004

Vargas-Salinas, F., & Amézquita, A. (2013). Stream noise, hybridization, and uncoupled evolution of call traits in two lineages of poison frogs: *Oophaga histrionica* and *Oophaga lehmanni*. *PLoS ONE*, *8*(10). https://doi.org/10.1371/journal.pone.0077545

Verdade, V. K., Rodrigues, M. T., Cassimiro, J., Pavan, D., Liou, N., & Lange, M. C. (2008). Advertisement call, vocal activity, and geographic distribution of *Brachycephalus hermogenesi* (Giaretta and Sawaya, 1998) (Anura, Brachycephalidae). *Journal of Herpetology*, *42*(3), 542–549. https://doi.org/10.1670/07-287.1

Wang, I. J. (2011). Inversely related aposematic traits: reduced conspicuousness evolves with increased toxicity in a polymorphic poison-dart frog. *Evolution*, *65*(6), 1637–1649. https://doi.org/10.1111/j.1558-5646.2011.01257.x

Watterson, G. A. (1975). On the number of segregating sites in genetical models without recombination. *Theoretical Population Biology*, *7*, 256–276.

Wickham, H., Averick, M., Bryan, J., Chang, W., McGowan, L., François, R., Grolemund, G., Hayes, A., Henry, L., Hester, J., Kuhn, M., Pedersen, T., Miller, E., Bache, S., Müller, K., Ooms, J., Robinson, D., Seidel, D., Spinu, V., … Yutani, H. (2019). Welcome to the Tidyverse. *Journal of Open Source Software*, *4*(43), 1686. https://doi.org/10.21105/joss.01686

Willink, B., Brenes-Mora, E., Bolaños, F., & Pröhl, H. (2013). Not everything is black and white: Color and behavioral variation reveal a continuum between cryptic and aposematic strategies in a polymorphic poison frog. *Evolution*, *67*(10), 2783–2794. https://doi.org/10.1111/evo.12153

Winebarger, M. M., Pugh, M. W., Gangloff, M. M., Osbourn, M. S., & Siefferman, L. (2018). Body size is positively correlated with conspicuous coloration in *Ambystoma* salamanders, but negatively correlated with conspicuous coloration in *Plethodon* salamanders. *Frontiers in Ecology and Evolution*, *6*(143), 1–8. https://doi.org/10.3389/fevo.2018.00143

Write, S. (1943) Isolation by distance. *Genetics*, *28*: 114-138.

Yeh, J. (2002). The effect of miniaturized body size on skeletal morphology in frogs. *Evolution*, *56*(3), 628–641. www.geocities.com/jyevolution/miniat.html

Yewers, M. S. C., Stuart-Fox, D., & McLean, C. A. (2019). Space use and genetic structure do not maintain color polymorphism in a species with alternative behavioral strategies. *Ecology and Evolution*, *9*(1), 295–306. https://doi.org/10.1002/ece3.4729

Zhang, C., Dong, S. S., Xu, J. Y., He, W. M., & Yang, T. L. (2019). PopLDdecay: a fast and effective tool for linkage disequilibrium decay analysis based on variant call format files. *Bioinformatics*, *35*(10), 1786–1788. https://doi.org/10.1093/bioinformatics/bty875

Appendix I. Details of *Brachycephalus actaeus* samples used in the present study. Abbreviations: m. = measurements and SFS = São Francisco do Sul. Acronyms: CFBH = Célio F. B. Haddad amphibian collection; JPCM = Juliane Petry de Carli Monteiro; TC = Thais Condez; UFMG = amphibian collection of Centro de Coleções Taxonômicas do Instituto de Ciências Biológicas da Universidade Federal de Minas Gerais, and UNIVILLE = Universidade da Região de Joinville.

Field code	Voucher	Morph	Population	Local code	ddRAD matrix	Call matrix	Measu. matrix	Locality	Municipality	Latitude (S)	Longitude (W)	Elevation (meters)
JPCM400		Brown	Northern	BFb	x*		x	Alto Bom Futuro	Garuva	-26.1128	-48.7449	339
JPCM401		Brown	Northern	BFb	x*		x	Alto Bom Futuro	Garuva	-26.1128	-48.7449	339
JPCM402		Green	Northern	BFg	x*		x	Baixo Bom Futuro	Garuva	-26.1106	-48.7405	282
JPCM403		Green	Northern	BFg			x	Baixo Bom Futuro	Garuva	-26.1106	-48.7405	282
JPCM390		Brown	Northern	BNb	x**		x	Morro da Antena, Alto Braço do Norte	Itapoá	-26.1225	-48.7396	452
JPCM391		Brown	Northern	BNb	x*		x	Morro da Antena, Alto Braço do Norte	Itapoá	-26.1225	-48.7396	452
JPCM392		Brown	Northern	BNb	x*		x	Morro da Antena, Alto Braço do Norte	Itapoá	-26.1225	-48.7396	452
JPCM393		Brown	Northern	BNb	x*		x	Morro da Antena, Alto Braço do Norte	Itapoá	-26.1225	-48.7396	452
JPCM394		Brown	Northern	BNb	x*		x	Morro da Antena, Alto Braço do Norte	Itapoá	-26.1225	-48.7396	452
JPCM409		Brown	Northern	BNb	x*		x	Morro da Antena, Alto Braço do Norte	Itapoá	-26.1287	-48.7417	521
JPCM410		Brown	Northern	BNb	x*		x	Morro da Antena, Alto Braço do Norte	Itapoá	-26.1211	-48.7356	464
JPCM411		Brown	Northern	BNb	x*		x	Morro da Antena, Alto Braço do Norte	Itapoá	-26.1211	-48.7356	464
JPCM707		Brown	Northern	BNb		x		Morro da Antena, Alto Braço do Norte	Itapoá	-26.1225	-48.7396	452
JPCM708		Brown	Northern	BNb		x		Morro da Antena, Alto Braço do Norte	Itapoá	-26.1225	-48.7396	452
JPCM708		Brown	Northern	BNb		x		Morro da Antena, Alto Braço do Norte	Itapoá	-26.1225	-48.7396	452

JPCM361	CFBH 39863	Green	Northern	BNg	x*	x	Estrada para Morro da Antena, Baixo Braço do Norte	Itapoá	-26.1248	-48.7300	236
JPCM362	CFBH 39864	Green	Northern	BNg	x*	x	Estrada para Morro da Antena, Baixo Braço do Norte	Itapoá	-26.1248	-48.7300	236
JPCM363	CFBH 39865	Green	Northern	BNg	x*	x	Estrada para Morro da Antena, Baixo Braço do Norte	Itapoá	-26.1248	-48.7300	236
JPCM364	UFMG18972	Green	Northern	BNg	x*	x	Estrada para Morro da Antena, Baixo Braço do Norte	Itapoá	-26.1248	-48.7300	236
JPCM365	CFBH 39867	Green	Northern	BNg		x	Estrada para Morro da Antena, Baixo Braço do Norte	Itapoá	-26.1248	-48.7300	236
JPCM366	CFBH 39868	Green	Northern	BNg	x*	x	Estrada para Morro da Antena, Baixo Braço do Norte	Itapoá	-26.1248	-48.7300	236
JPCM367	CFBH 39869	Green	Northern	BNg	x*		Estrada para Morro da Antena, Baixo Braço do Norte	Itapoá	-26.1248	-48.7300	236
JPCM368	CFBH 39870	Green	Northern	BNg	x*	x	Estrada para Morro da Antena, Baixo Braço do Norte	Itapoá	-26.1248	-48.7300	236
JPCM369	CFBH 39871	Green	Northern	BNg	x*		Estrada para Morro da Antena, Baixo Braço do Norte	Itapoá	-26.1248	-48.7300	236
JPCM387	CFBH 30875	Green	Northern	BNg	x*	x	Estrada para Morro da Antena, Baixo Braço do Norte	Itapoá	-26.1248	-48.7300	236
JPCM702		Green	Northern	BNg		x	Estrada para Morro da Antena, Baixo Braço do Norte	Itapoá	-26.1248	-48.7300	236
JPCM703		Green	Northern	BNg		x	Estrada para Morro da Antena, Baixo Braço do Norte	Itapoá	-26.1248	-48.7300	236
JPCM706		Green	Northern	BNg		x	Estrada para Morro da Antena, Baixo Braço do Norte	Itapoá	-26.1218	-48.7323	346

JPCM265	UFMG18970	Green	Southern	CEPA		x	Trilha da captação, Centro de Estudos e Pesquisas Ambientais UNIVILLE	SFS	-26.2233	-48.6886	138
JPCM313	UFMG18971	Green	Southern	CEPA		x	Trilha da captação, Centro de Estudos e Pesquisas Ambientais UNIVILLE	SFS	-26.2233	-48.6886	138
JPCM356	CFBH 39855	Green	Southern	CEPA	x*	x	Trilha da captação, Centro de Estudos e Pesquisas Ambientais UNIVILLE	SFS	-26.2233	-48.6886	138
JPCM357	CFBH 39856	Green	Southern	CEPA	x**	x	Trilha da captação, Centro de Estudos e Pesquisas Ambientais UNIVILLE	SFS	-26.2233	-48.6886	138
JPCM358	CFBH 39857	Green	Southern	CEPA	x*	x	Trilha da captação, Centro de Estudos e Pesquisas Ambientais UNIVILLE	SFS	-26.2233	-48.6886	138
JPCM359	CFBH 39858	Green	Southern	CEPA	x*	x	Trilha da captação, Centro de Estudos e Pesquisas Ambientais UNIVILLE	SFS	-26.2233	-48.6886	138
JPCM360	CFBH 39859	Green	Southern	CEPA		x	Trilha da captação, Centro de Estudos e Pesquisas Ambientais UNIVILLE	SFS	-26.2233	-48.6886	138
JPCM374	UFMG18973	Green	Southern	CEPA	x*	x	Trilha da captação, Centro de Estudos e Pesquisas Ambientais UNIVILLE	SFS	-26.2233	-48.6886	138
JPCM375	CFBH 39561	Green	Southern	CEPA	x*	x	Trilha da captação, Centro de Estudos e Pesquisas Ambientais UNIVILLE	SFS	-26.2233	-48.6886	138
JPCM599		Green	Southern	CEPA		x	Trilha da captação, Centro de Estudos e Pesquisas Ambientais UNIVILLE	SFS	-26.2233	-48.6886	138

TC269	CFBH 39847	Green	Southern	CEPA	x*		x	Trilha da captação, Centro de Estudos e Pesquisas Ambientais UNIVILLE	SFS	-26.2232	-48.6886	138
TC288	CFBH 39848	Green	Southern	CEPA	x*	x		Trilha da captação, Centro de Estudos e Pesquisas Ambientais UNIVILLE	SFS	-26.2233	-48.6886	138
JPCM259		Orange	Center	CAG			x	Morro Cantagalo	SFS	-26.1893	-48.7323	237
JPCM341		Orange	Center	CAG	x*		x	Morro Cantagalo	SFS	-26.1893	-48.7323	237
JPCM342		Orange	Center	CAG	x*		x	Morro Cantagalo	SFS	-26.1893	-48.7323	237
JPCM343		Orange	Center	CAG	x*		x	Morro Cantagalo	SFS	-26.1893	-48.7323	237
JPCM344		Orange	Center	CAG	x*		x	Morro Cantagalo	SFS	-26.1893	-48.7323	237
JPCM345		Orange	Center	CAG	x**	x	x	Morro Cantagalo	SFS	-26.1893	-48.7323	237
JPCM346		Orange	Center	CAG	x**		x	Morro Cantagalo	SFS	-26.1893	-48.7323	237
JPCM347		Orange	Center	CAG	x*		x	Morro Cantagalo	SFS	-26.1893	-48.7323	237
JPCM348		Orange	Center	CAG	x*		x	Morro Cantagalo	SFS	-26.1893	-48.7323	237
JPCM349		Orange	Center	CAG	x*		x	Morro Cantagalo	SFS	-26.1893	-48.7323	237
JPCM350		Orange	Center	CAG	x*		x	Morro Cantagalo	SFS	-26.1893	-48.7323	237
JPCM351		Orange	Center	CAG	x**		x	Morro Cantagalo	SFS	-26.1893	-48.7323	237
JPCM352		Orange	Center	CAG			x	Morro Cantagalo	SFS	-26.1893	-48.7323	237
JPCM353		Orange	Center	CAG	x**		x	Morro Cantagalo	SFS	-26.1893	-48.7323	237
JPCM354		Orange	Center	CAG	x*		x	Morro Cantagalo	SFS	-26.1893	-48.7323	237
JPCM677		Orange	Center	CAG		x		Morro Cantagalo	SFS	-26.1893	-48.7323	237
JPCM678		Orange	Center	CAG		x		Morro Cantagalo	SFS	-26.1893	-48.7323	237
TC278		Orange	Center	CAG				Morro Cantagalo	SFS	-26.1893	-48.7323	237
TC279		Orange	Center	CAG				Morro Cantagalo	SFS	-26.1892	-48.7310	237
TC280		Orange	Center	CAG	x*		x	Morro Cantagalo	SFS	-26.1892	-48.7310	237
TC281		Orange	Center	CAG	x*		x	Morro Cantagalo	SFS	-26.1892	-48.7310	237
TC282		Orange	Center	CAG			x	Morro Cantagalo	SFS	-26.1893	-48.7323	237
TC283		Orange	Center	CAG	x*		x	Morro Cantagalo	SFS	-26.1893	-48.7323	237
TC284		Orange	Center	CAG	x*		x	Morro Cantagalo	SFS	-26.1892	-48.7310	237
TC285		Orange	Center	CAG	x*		x	Morro Cantagalo	SFS	-26.1892	-48.7310	237
TC286		Orange	Center	CAG	x**		x	Morro Cantagalo	SFS	-26.1893	-48.7323	237
JPCM355		Gray	Center	CAS	x*		x	Casarão Backmeyer	SFS	-26.1753	-48.7125	129

JPCM675		Gray	Center	CAS		x		Casarão Backmeyer	SFS	-26.1753	-48.7125	129
TC232		Gray	Center	CAS			x	Casarão Backmeyer	SFS	-26.1753	-48.7125	129
TC233		Gray	Center	CAS	x**		x	Casarão Backmeyer	SFS	-26.1753	-48.7125	129
TC253		Gray	Center	CAS	x**		x	Casarão Backmeyer	SFS	-26.1753	-48.7125	129
TC254		Gray	Center	CAS			x	Casarão Backmeyer	SFS	-26.1753	-48.7125	129
TC255		Gray	Center	CAS	x*		x	Casarão Backmeyer	SFS	-26.1753	-48.7125	129
TC256		Gray	Center	CAS	x*		x	Casarão Backmeyer	SFS	-26.1753	-48.7125	129
TC257		Gray	Center	CAS	x*		x	Casarão Backmeyer	SFS	-26.1753	-48.7125	129
TC258		Gray	Center	CAS	x**		x	Casarão Backmeyer	SFS	-26.1753	-48.7125	129
TC259		Gray	Center	CAS			x	Casarão Backmeyer	SFS	-26.1753	-48.7125	129
TC260		Gray	Center	CAS	x*		x	Casarão Backmeyer	SFS	-26.1753	-48.7125	129
TC261		Gray	Center	CAS	x*			Casarão Backmeyer	SFS	-26.1753	-48.7125	129
TC262		Gray	Center	CAS	x*		x	Casarão Backmeyer	SFS	-26.1753	-48.7125	129
TC267	CFBH 39846	Green	Island	MOG	x*			Morro Grande	SFS	-26.2964	-48.6194	40
JPCM294	CFBH 39850	Green	Island	SPA			x	Serra da Palha	SFS	-26.2949	-48.6738	80
JPCM295	CFBH 39851	Green	Island	SPA	x*		x	Serra da Palha	SFS	-26.2949	-48.6738	80
JPCM371	CFBH 39872	Green	Island	SPA	x*		x	Serra da Palha	SFS	-26.2949	-48.6738	80
JPCM372	CFBH 39873	Green	Island	SPA	x*		x	Serra da Palha	SFS	-26.2949	-48.6738	80
JPCM373	UFMG18973	Green	Island	SPA	x*		x	Serra da Palha	SFS	-26.2949	-48.6738	80
JPCM396	CFBH 39876	Green	Island	SPA	x*		x	Serra da Palha	SFS	-26.2949	-48.6738	80
JPCM397	CFBH 39877	Green	Island	SPA	x*		x	Serra da Palha	SFS	-26.2949	-48.6738	80
JPCM670		Green	Island	SPA		x		Serra da Palha	SFS	-26.2949	-48.6738	80
JPCM671		Green	Island	SPA		x		Serra da Palha	SFS	-26.2949	-48.6738	80
JPCM412	CFBH 42005	Green	Northern	PAJ	x*		x	Fazenda Palmito Juriti	SFS	-26.1359	-48.7316	125
JPCM413	CFBH 42006	Green	Northern	PAJ	x*		x	Fazenda Palmito Juriti	SFS	-26.1367	-48.7354	170
JPCM414	CFBH 42007	Green	Northern	PAJ	x*		x	Fazenda Palmito Juriti	SFS	-26.1367	-48.7354	170
JPCM415	CFBH 42008	Green	Northern	PAJ	x**		x	Fazenda Palmito Juriti	SFS	-26.1367	-48.7354	170
JPCM320	CFBH 39853	Green	Southern	SAI			x	Estrada do Saí	SFS	-26.2020	-48.6935	81
JPCM321	CFBH 39854	Green	Southern	SAI	x**		x	Estrada do Saí	SFS	-26.2020	-48.6935	81
JPCM370	CFBH 39862	Green	Southern	SAI	x*		x	Estrada do Saí	SFS	-26.2020	-48.6935	81
JPCM642		Green	Southern	SAI		x		Estrada do Saí	SFS	-26.2020	-48.6935	81

*Final samples used in ddRAD dataset; **Samples excluded from ddRAD dataset by filter criterium.

SUPPLEMENTARY INFORMATION

Aposematism and miniaturization: the evolutionary miscellany in *Brachycephalus* taxonomy

Juliane P. C. Monteiro, Mariana L. Lyra, Thais H. Condez, Thiago R. Carvalho, Kelly R. Zamudio, and Célio F. B. Haddad

Supplementary tables and figures

Table S1. Final statistics summary provided by ipyrad for the 57 samples of *Brachycaphalus actaeus* in this study. Raw reads refer to the total reads produced during Illumina sequencing; post-processing reads are those that remained after filtering for quality, adaptor contamination, ambiguous barcodes, and mitochondrial sequences; total clusters are the number of homologous sequences clusters created with the post-processing reads; mean depth is the mean depth of coverage of a cluster. Estimated heterozygosity (H) and error rate (E) were calculated across clusters, and consensus sequences were created for each cluster (Consens. reads). Consensus sequences were clustered across specimens and loci that passed filtering parameters were included in the final data matrix (Loci in assembly).

Sample	Raw reads	Reads passing filter	Total clusters	Hidepth clusters	H	E	Consens. reads	Loci in assembly
JPCM295	1951114	1946077	74292	22890	0.037	0.014	15624	12946
JPCM341	1575692	1561278	70826	19966	0.041	0.015	12977	11051
JPCM342	3215533	3184815	126761	32324	0.048	0.012	22326	18822
JPCM343	2238591	2219328	93241	24984	0.040	0.013	16311	13758
JPCM344	1596301	1579478	80158	20220	0.044	0.015	13007	10927
JPCM347	1985728	1972641	71940	24398	0.044	0.013	16547	14155
JPCM348	2576760	2557619	101286	29825	0.042	0.013	20827	17705
JPCM349	1462280	1449819	66997	18419	0.045	0.015	11671	9922
JPCM350	3996285	3956628	105973	37699	0.038	0.011	27470	23196
JPCM354	2823155	2798005	89425	32068	0.036	0.013	22708	19428
JPCM356	3652663	3630861	104886	34383	0.039	0.011	24346	20372
JPCM358	3878013	3845068	108851	37745	0.038	0.011	27455	23594
JPCM359	4713738	4683344	130420	40102	0.041	0.011	28345	24187
JPCM361	2093264	2075110	80319	24244	0.043	0.014	16373	13816
JPCM362	4148700	4109081	119402	39394	0.043	0.011	28527	23908
JPCM363	2691700	2669147	92429	30434	0.039	0.013	21150	17938
JPCM364	4009418	3999969	127001	42478	0.035	0.012	30876	23452
JPCM366	3919415	3886611	118091	37679	0.045	0.011	27004	22780
JPCM367	3991387	3962514	110875	38628	0.038	0.011	28043	23445
JPCM368	2534070	2511957	89194	29486	0.041	0.012	20535	17434
JPCM369	2089057	2066583	81766	26074	0.041	0.014	17606	15066
JPCM370	4100141	4070688	112553	38832	0.041	0.011	28711	24243

Sample	Raw reads	Reads passing filter	Total clusters	Hidepth clusters	H	E	Consens. reads	Loci in assembly
JPCM371	4397722	4370389	119118	39034	0.040	0.010	28819	24223
JPCM372	2591300	2572741	91339	29571	0.039	0.012	21116	17992
JPCM373	1984082	1967586	77366	24508	0.039	0.013	16985	14524
JPCM374	3187307	3158534	89785	33754	0.038	0.011	24603	21053
JPCM375	3386293	3355111	97737	35135	0.038	0.012	25327	21755
JPCM387	2633979	2614252	87641	28240	0.039	0.013	19588	16518
JPCM391	1976171	1955064	75265	23904	0.040	0.015	15965	13552
JPCM392	1639193	1625013	70574	19795	0.042	0.015	12709	10735
JPCM393	2497142	2470101	85772	27736	0.041	0.014	19178	16283
JPCM394	2867686	2843574	92432	30612	0.039	0.013	21543	18079
JPCM396	2828084	2815293	86561	32889	0.038	0.012	24157	20470
JPCM397	6080752	6029167	138109	44958	0.043	0.010	33647	27461
JPCM400	4077148	4045504	157241	41086	0.041	0.011	29636	21998
JPCM401	1998520	1994061	80282	23806	0.040	0.014	15738	12693
JPCM402	2056271	2039400	78091	24998	0.041	0.013	16957	14099
JPCM409	3240430	3214037	117001	33992	0.043	0.013	23938	20131
JPCM410	3470655	3456832	130151	38729	0.039	0.013	27374	21906
JPCM411	2601947	2583714	87504	29915	0.036	0.013	20796	17592
JPCM412	2773838	2747267	97366	30401	0.040	0.013	21341	18095
JPCM413	2911583	2879820	96998	29994	0.040	0.013	20860	17613
JPCM414	3164487	3139076	94415	33503	0.038	0.011	23994	20280
TC255	3816275	3791587	107019	36699	0.045	0.011	26815	22501
TC256	2311918	2294766	84714	26301	0.044	0.013	17276	14976
TC257	3126042	3104947	104384	32245	0.046	0.012	22907	19427
TC260	1835325	1821198	75477	22451	0.043	0.015	14944	12736
TC261	3194804	3170705	106999	32818	0.047	0.012	23229	19707
TC262	2176088	2158194	79599	26141	0.042	0.013	17905	15202
TC267	3111359	3100443	115856	35125	0.040	0.013	25437	20731
TC269	4103791	4090638	115999	42259	0.036	0.012	31351	24357
TC280	2475773	2451375	89408	28608	0.042	0.013	20002	17111
TC281	2439268	2418838	111773	27255	0.046	0.013	18212	15267
TC283	1741995	1722328	93553	21634	0.046	0.015	13907	11697
TC284	3494578	3466808	132218	33665	0.049	0.012	23413	19758
TC285	2758053	2729336	112020	30471	0.045	0.013	21154	17692
TC288	4015382	3987452	114462	38119	0.042	0.010	28001	23897

Table S2. Summary statistics for two filters parameters used for SNPs dataset performed in SambaR v1.0.9 package. Before filtering refers to file generated by VCFtools.

	Before filtering	After filtering*	After filtering**
Number of individuals	57	57	39
Number of SNPs	228403	5039	21545
Percentage of SNPs with maf >= 0.05	57.36	31.59	52.21
Mean proportion of missing data per individual	0.56	0.56	0.51
GC content	0.61	0.66	0.64
Transition vs transversion ratio	1.30	1.31	1.29

Filter parameters: *indmiss=0.95; snpmiss = 0.05; MAC = 2; dohefilter = TRUE;
**indmiss=0.6; snpmiss = 0.15; MAC = 2; dohefilter = TRUE.

Table S3. Information on sound recordings from *Brachycephalus actaeus*. For abbreviations of local code see Appendix I.

Sound file	Voucher	Morph	Local code	Population	Air (°C)	UR (%)	Date
JPCM086	unvouched	brown	BNb	Northern	25	70	8/10/2019
JPCM087	JPCM707	brown	BNb	Northern	23	70	8/10/2019
JPCM088	unvouched	brown	BNb	Northern	22	75	8/10/2019
JPCM089	unvouched	brown	BNb	Northern	22	75	8/10/2019
JPCM090	unvouched	brown	BNb	Northern	22	75	8/10/2019
JPCM091	unvouched	brown	BNb	Northern	22	75	8/10/2019
JPCM092	unvouched	brown	BNb	Northern	19	80	8/10/2019
JPCM093	JPCM708	brown	BNb	Northern	19	89	8/10/2019
JPCM094	JPCM708	brown	BNb	Northern	19	89	8/10/2019
JPCM095	unvouched	brown	BNb	Northern	19	85	8/9/2019
JPCM098	unvouched	brown	BNb	Northern	19	85	8/9/2019
JPCM001	CFBH 39848	green	CEPA	Southern	25	95	23/10/2014
JPCM002	unvouched	green	CEPA	Southern	19	95	23/10/2014
JPCM015	unvouched	green	CEPA	Southern	23	85	15/9/2014
JPCM035	JPCM599	green	CEPA	Southern	21	95	16/9/2018
JPCM037	unvouched	green	CEPA	Southern	21	95	16/9/2018
JPCM050	unvouched	green	SAI	Southern	28	90	28/1/2019
JPCM051	JPCM642	green	SAI	Southern	28	90	28/1/2019
JPCM052	unvouched	green	SAI	Southern	28	90	28/1/2019
JPCM085	JPCM706	green	BNg	Northern	23	80	8/10/2019
JPCM005	unvouched	green	BNg	Northern	17	100	23/11/2015
JPCM006	unvouched	green	BNg	Northern	16	100	23/11/2015
JPCM074	JPCM702	green	BNg	Northern	23	85	8/10/2019
JPCM076	unvouched	green	BNg	Northern	23	85	8/10/2019
JPCM077	JPCM703	green	BNg	Northern	23	85	8/10/2019
JPCM078	unvouched	green	BNg	Northern	23	85	8/10/2019
JPCM082	unvouched	green	BNg	Northern	24	85	8/10/2019
JPCM083	unvouched	green	BNg	Northern	24	85	8/10/2019
JPCM003	unvouched	green	SPA	Island	24	80	20/11/2015
JPCM004	unvouched	green	SPA	Island	24	80	20/11/2015
JPCM053	JPCM671	green	SPA	Island	21	80	30/9/2019
JPCM054	JPCM670	green	SPA	Island	21	80	30/9/2019
JPCM056	unvouched	green	SPA	Island	20	90	30/9/2019
JPCM057	unvouched	green	SPA	Island	20	90	30/9/2019
JPCM058	unvouched	green	SPA	Island	20	90	30/9/2019
JPCM060	unvouched	gray	CAS	Center	23	80	1/9/2019
JPCM061	unvouched	gray	CAS	Center	21	84	1/9/2019
JPCM062	unvouched	gray	CAS	Center	21	85	1/9/2019
JPCM063	unvouched	gray	CAS	Center	21	85	1/9/2019
JPCM064ind1	unvouched	gray	CAS	Center	21	85	1/9/2019
JPCM064ind2	unvouched	gray	CAS	Center	21	85	1/9/2019
JPCM065	unvouched	gray	CAS	Center	20	85	1/9/2019
JPCM066	JPCM675	gray	CAS	Center	20	85	1/9/2019
JPCM016	JPCM345	orange	CAG	Center	17	91	29/8/2015
JPCM067	unvouched	orange	CAG	Center	22	78	2/10/2019
JPCM068	unvouched	orange	CAG	Center	22	78	2/10/2019

Sound file	Voucher	Morph	Local code	Population	Air (°C)	UR (%)	Date
JPCM069	JPCM677	orange	CAG	Center	21	80	2/10/2019
JPCM070	unvouched	orange	CAG	Center	22	80	2/10/2019
JPCM071	unvouched	orange	CAG	Center	21	80	2/10/2019
JPCM072	JPCM678	orange	CAG	Center	21	80	2/10/2019
JPCM073	unvouched	orange	CAG	Center	21	88	2/10/2019

Table S4. GenBank accession numbers of 16S mtDNA sequences of *Brachycephalus* and outgroups (*Haddadus* and *Ischnocnema*) used in this study. All *Brachycephalus actaeus* sequences in the present study where generate from ddRAD extractions. New sequences are highlighted in bold. Brazilian States (UF): BA = Bahia; ES = Espírito Santo; MG = Minas Gerais; PR = Paraná; RJ = Rio de Janeiro; SC = Santa Catarina; and SP = São Paulo.

Species	Voucher	Field Voucher	Locality	Municipality	UF	GenBank	Observation
Brachycephalus actaeus		JPCM400	Alto Bom Futuro	Garuva	SC	**This study**	
Brachycephalus actaeus		JPCM401	Alto Bom Futuro	Garuva	SC	**This study**	
Brachycephalus actaeus		TC255	Casarão Backmeyer	São Francisco do Sul	SC	**This study**	
Brachycephalus actaeus		TC256	Casarão Backmeyer	São Francisco do Sul	SC	**This study**	
Brachycephalus actaeus		TC257	Casarão Backmeyer	São Francisco do Sul	SC	**This study**	
Brachycephalus actaeus		TC260	Casarão Backmeyer	São Francisco do Sul	SC	**This study**	
Brachycephalus actaeus		TC261	Casarão Backmeyer	São Francisco do Sul	SC	**This study**	
Brachycephalus actaeus		TC262	Casarão Backmeyer	São Francisco do Sul	SC	**This study**	
Brachycephalus actaeus	CFBH 39862	JPCM370	Estrada do Saí	São Francisco do Sul	SC	**This study**	paratype
Brachycephalus actaeus	CFBH 39863	JPCM361	Estrada para Morro da Antena, Baixo Braço do Norte	Itapoá	SC	**This study**	paratype
Brachycephalus actaeus	CFBH 39864	JPCM362	Estrada para Morro da Antena, Baixo Braço do Norte	Itapoá	SC	**This study**	paratype
Brachycephalus actaeus	CFBH 39865	JPCM363	Estrada para Morro da Antena, Baixo Braço do Norte	Itapoá	SC	**This study**	paratype
Brachycephalus actaeus	CFBH 39868	JPCM366	Estrada para Morro da Antena, Baixo Braço do Norte	Itapoá	SC	**This study**	paratype
Brachycephalus actaeus	CFBH 39869	JPCM367	Estrada para Morro da Antena, Baixo Braço do Norte	Itapoá	SC	**This study**	paratype
Brachycephalus actaeus	CFBH 39870	JPCM368	Estrada para Morro da Antena, Baixo Braço do Norte	Itapoá	SC	**This study**	paratype
Brachycephalus actaeus	UFMG 18972	JPCM364	Estrada para Morro da Antena, Baixo Braço do Norte	Itapoá	SC	**This study**	paratype
Brachycephalus actaeus	CFBH 42005	JPCM412	Fazenda Palmito Juriti	São Francisco do Sul	SC	**This study**	
Brachycephalus actaeus	CFBH 42006	JPCM413	Fazenda Palmito Juriti	São Francisco do Sul	SC	**This study**	
Brachycephalus actaeus	CFBH 42007	JPCM414	Fazenda Palmito Juriti	São Francisco do Sul	SC	**This study**	
Brachycephalus actaeus		JPCM341	Morro Cantagalo	São Francisco do Sul	SC	**This study**	
Brachycephalus actaeus		JPCM342	Morro Cantagalo	São Francisco do Sul	SC	**This study**	
Brachycephalus actaeus		JPCM343	Morro Cantagalo	São Francisco do Sul	SC	**This study**	
Brachycephalus actaeus		JPCM347	Morro Cantagalo	São Francisco do Sul	SC	**This study**	
Brachycephalus actaeus		JPCM348	Morro Cantagalo	São Francisco do Sul	SC	**This study**	

Species	Voucher	Field Voucher	Locality	Municipality	UF	GenBank	Observation
Brachycephalus actaeus		JPCM350	Morro Cantagalo	São Francisco do Sul	SC	**This study**	
Brachycephalus actaeus		JPCM352	Morro Cantagalo	São Francisco do Sul	SC	**This study**	
Brachycephalus actaeus		JPCM354	Morro Cantagalo	São Francisco do Sul	SC	**This study**	
Brachycephalus actaeus		TC278	Morro Cantagalo	São Francisco do Sul	SC	**This study**	
Brachycephalus actaeus		TC280	Morro Cantagalo	São Francisco do Sul	SC	**This study**	
Brachycephalus actaeus		TC281	Morro Cantagalo	São Francisco do Sul	SC	**This study**	
Brachycephalus actaeus		TC285	Morro Cantagalo	São Francisco do Sul	SC	**This study**	
Brachycephalus actaeus		JPCM391	Morro da Antena, Alto Braço do Norte	Itapoá	SC	**This study**	
Brachycephalus actaeus		JPCM392	Morro da Antena, Alto Braço do Norte	Itapoá	SC	**This study**	
Brachycephalus actaeus		JPCM393	Morro da Antena, Alto Braço do Norte	Itapoá	SC	**This study**	
Brachycephalus actaeus		JPCM409	Morro da Antena, Alto Braço do Norte	Itapoá	SC	**This study**	
Brachycephalus actaeus		JPCM410	Morro da Antena, Alto Braço do Norte	Itapoá	SC	**This study**	
Brachycephalus actaeus		JPCM411	Morro da Antena, Alto Braço do Norte	Itapoá	SC	**This study**	
Brachycephalus actaeus	CFBH 39846	TC267	Morro Grande	São Francisco do Sul	SC	**This study**	paratype
Brachycephalus actaeus	CFBH 39851	JPCM295	Serra da Palha	São Francisco do Sul	SC	**This study**	paratopotype
Brachycephalus actaeus	CFBH 39872	JPCM371	Serra da Palha	São Francisco do Sul	SC	**This study**	paratopotype
Brachycephalus actaeus	CFBH 39873	JPCM372	Serra da Palha	São Francisco do Sul	SC	**This study**	paratopotype
Brachycephalus actaeus	CFBH 39877	JPCM397	Serra da Palha	São Francisco do Sul	SC	**This study**	paratopotype
Brachycephalus actaeus	CFBH 39561	JPCM375	Centro de Estudos e Pesquisas Ambientais UNIVILLE	São Francisco do Sul	SC	**This study**	paratype
Brachycephalus actaeus	CFBH 39847	TC269	Centro de Estudos e Pesquisas Ambientais UNIVILLE	São Francisco do Sul	SC	**This study**	paratype
Brachycephalus actaeus	CFBH 39848	TC288	Centro de Estudos e Pesquisas Ambientais UNIVILLE	São Francisco do Sul	SC	**This study**	paratype
Brachycephalus actaeus	CFBH 39855	JPCM356	Centro de Estudos e Pesquisas Ambientais UNIVILLE	São Francisco do Sul	SC	**This study**	paratype
Brachycephalus actaeus	CFBH 39858	JPCM359	Centro de Estudos e Pesquisas Ambientais UNIVILLE	São Francisco do Sul	SC	**This study**	paratype
Brachycephalus actaeus	UFMG 18970	JPCM265	Centro de Estudos e Pesquisas Ambientais UNIVILLE	São Francisco do Sul	SC	**This study**	paratype
Brachycephalus actaeus	UFMG 18973	JPCM374	Centro de Estudos e Pesquisas Ambientais UNIVILLE	São Francisco do Sul	SC	**This study**	paratype

Species	Voucher	Field Voucher	Locality	Municipality	UF	GenBank	Observation
Brachycephalus albolineatus	CFBH 41754	CHCpo701	Morro Boa Vista	Jaraguá do Sul	SC	MG889434	topotype
Brachycephalus albolineatus		JPCM729	Morro Boa Vista	Jaraguá do Sul	SC	**This study**	topotype
Brachycephalus albolineatus		JPCM730	Morro Boa Vista	Jaraguá do Sul	SC	**This study**	topotype
Brachycephalus albolineatus		Feb2017-RNA02	Morro Boa Vista	Jaraguá do Sul	SC	MZ770738	topotype
Brachycephalus alipioi		CFBH3566		Vargem Alta	ES	HQ435690	
Brachycephalus auroguttatus		JPCM597	Pedra da Tartaruga	Garuva	SC	MZ770739	topotype
Brachycephalus auroguttatus		JPCM560	Campos do Quiriri	Garuva	SC	**This study**	
Brachycephalus auroguttatus		JPCM561	Campos do Quiriri	Garuva	SC	**This study**	
Brachycephalus auroguttatus		JPCM571	Campos do Quiriri	Garuva	SC	**This study**	
Brachycephalus auroguttatus		JPCM573	Campos do Quiriri	Garuva	SC	**This study**	
Brachycephalus auroguttatus		JPCM576	Pedra da Tartaruga	Garuva	SC	MZ770739	topotype
Brachycephalus auroguttatus		JPCM577	Pedra da Tartaruga	Garuva	SC	**This study**	topotype
Brachycephalus auroguttatus		JPCM587	Campos do Quiriri	Garuva	SC	**This study**	
Brachycephalus auroguttatus		JPCM594	Campos do Quiriri	Garuva	SC	**This study**	
Brachycephalus auroguttatus		JPCM595	Campos do Quiriri	Garuva	SC	**This study**	
Brachycephalus auroguttatus		JPCM596	Pedra da Tartaruga	Garuva	SC	**This study**	topotype
Brachycephalus boticario		JPCM867	Morro do Cachorro	Blumenau	SC	**This study**	topotype
Brachycephalus boticario		JPCM868	Morro do Cachorro	Blumenau	SC	**This study**	topotype
Brachycephalus boticario		JPCM869	Morro do Cachorro	Blumenau	SC	**This study**	topotype
Brachycephalus brunneus		JPCM777	Caratuva, Parque Estadual Pico Paraná	Campina Grande do Sul	PR	**This study**	topotype
Brachycephalus brunneus		JPCM781	Pico Caratuva	Campina Grande do Sul	PR	**This study**	topotype
Brachycephalus brunneus		JPCM785	Pico Caratuva	Campina Grande do Sul	PR	**This study**	topotype
Brachycephalus brunneus		JPCM787	Próximo ao Pico Paraná	Antonina	PR	**This study**	
Brachycephalus brunneus		JPCM788	Próximo ao grampo, Pico Paraná	Antonina	PR	**This study**	
Brachycephalus brunneus		JPCM790	Próximo ao grampo, Pico Paraná	Antonina	PR	**This study**	
Brachycephalus brunneus		JPCM897	Parque Nacional Guaricana	Morretes	PR	**This study**	

Species	Voucher	Field Voucher	Locality	Municipality	UF	GenBank	Observation
Brachycephalus brunneus		JPCM854	Parque Nacional Guaricana	Morretes	PR	**This study**	
Brachycephalus brunneus		JPCM855	Parque Nacional Guaricana	Morretes	PR	**This study**	
Brachycephalus brunneus		JUM28	Pedra Branca do Araraquara	Guaratuba	PR	**This study**	
Brachycephalus bufonoides	ZUFRJ 15424		Serra Queimada trail, APA de Macaé de Cima, Lumiar	Nova Friburgo	RJ	MH259790	topotype
Brachycephalus clarissae	MNRJ 56504			Cachoeiras de Macacu	RJ	**This study**	paratype
Brachycephalus coloratus	MHNCI 11566		Recreio da Serra, Mananciais da Serra	Piraquara	PR	MT928335	
Brachycephalus coloratus			Recreio da Serra, Mananciais da Serra	Piraquara	PR	MT928334	
Brachycephalus coloratus			Recreio da Serra, Mananciais da Serra	Piraquara	PR	MT928336	
Brachycephalus crispus	CFBH 44400	TC146	Trilha do cedro grande	Cunha	SP	**This study**	
Brachycephalus curupira		JPCM791	Distrito Malhada - Serro e Gemido	São José dos Pinhais	PR	**This study**	topotype
Brachycephalus curupira		JPCM792	Distrito Malhada - Serro e Gemido	São José dos Pinhais	PR	**This study**	topotype
Brachycephalus curupira		JPCM794	Distrito Malhada - Serro e Gemido	São José dos Pinhais	PR	**This study**	topotype
Brachycephalus darkside	PPGT602		Parque Estadual da Serra do Brigadeiro	Ervália	MG	**This study**	topotype
Brachycephalus didactylus	CFBH T11506		Vale da Revolta	Teresópolis	RJ	MG889427	
Brachycephalus ferruginus	CFBH 40436	TC142	Parque Estadual Pico do Marumbi - Trilha Abrolhos	Morretes	PR	MG889438	topotype
Brachycephalus ferruginus		JPCM841	Parque Estadual Pico do Marimbi	Morretes	PR	**This study**	topotype
Brachycephalus ferruginus		JPCM842	Parque Estadual Pico do Marumbi - Trilha Branca	Morretes	PR	**This study**	topotype
Brachycephalus ferruginus		JPCM848	Parque Estadual Pico do Marimbi	Morretes	PR	**This study**	topotype
Brachycephalus ferruginus		TC142	Parque Estadual Pico do Marimbi	Morretes	PR	MG889438	topotype
Brachycephalus fuscolineatus		JPCM600	Morro do Baú	Ilhota	SC	**This study**	topotype
Brachycephalus fuscolineatus		JPCM870	Morro do Baú	Ilhota	SC	**This study**	topotype
Brachycephalus fuscolineatus		JPCM871	Morro do Baú	Ilhota	SC	**This study**	topotype
Brachycephalus fuscolineatus		JPCM872	Morro do Baú	Ilhota	SC	**This study**	topotype
Brachycephalus garbeanus	CFBH 16800		Sítio de Davi Miler	Macaé de Cima	RJ	HQ435694	
Brachycephalus guarani	CFBH 12997		Morro Prumirim	Ubatuba	SP	MK697371	paratopotype
Brachycephalus hermogenesi		TC129		Salesópolis	SP	MG889426	
Brachycephalus ibitinga	CFBH 44448	TC410	Parque das Neblinas	Bertioga	SP	**This study**	paratype

Species	Voucher	Field Voucher	Locality	Municipality	UF	GenBank	Observation
Brachycephalus izecksohni		JPCM919	Parque Nacional de Saint Hilaire-Lange	Guaratuba	PR	**This study**	topotype
Brachycephalus izecksohni		JPCM919	Pico Torre da Prata	Guaratuba	PR	**This study**	topotype
Brachycephalus izecksohni		JPCM921	Pico Torre da Prata	Guaratuba	PR	**This study**	topotype
Brachycephalus izecksohni		JPCM927	Pico Torre da Prata	Guaratuba	PR	**This study**	topotype
Brachycephalus leopardus		JPCM799	Pico do Araçatuba	Tijucas do Sul	PR	**This study**	topotype
Brachycephalus leopardus		JPCM800	Pico do Araçatuba	Tijucas do Sul	PR	**This study**	topotype
Brachycephalus leopardus		JPCM801	Pico do Araçatuba	Tijucas do Sul	PR	**This study**	topotype
Brachycephalus margaritatus	CFBH 2420		Castelo Country Club	Petrópolis	RJ	MK697377	
Brachycephalus mariaterezae		JPCM684	Serra Queimada	Joinville	SC	**This study**	topotype
Brachycephalus mariaterezae		JPCM685	Serra Queimada	Joinville	SC	**This study**	topotype
Brachycephalus mariaterezae		JPCM686	Serra Queimada	Joinville	SC	**This study**	topotype
Brachycephalus mariaterezae		JPCM692	Serra Queimada	Joinville	SC	**This study**	
Brachycephalus mariaterezae		JPCM693	Serra Queimada	Joinville	SC	**This study**	
Brachycephalus mariaterezae		JPCM720	Serra Queimada	Joinville	SC	**This study**	
Brachycephalus mirissimus		JPCM743	Morro Santo Anjo	Massaranduba	SC	**This study**	topotype
Brachycephalus mirissimus	Not given	MP-2018	Morro Santo Anjo	Massaranduba	SC	MH136570	
Brachycephalus mirissimus		JPCM743	Morro Santo Anjo	Massaranduba	SC	**This study**	topotype
Brachycephalus mirissimus		JPCM744	Morro Santo Anjo	Massaranduba	SC	**This study**	topotype
Brachycephalus mirissimus		JPCM745	Morro Santo Anjo	Massaranduba	SC	**This study**	topotype
Brachycephalus nodoterga	CFBH T2226	CFBH9606		Santana do Parnaiba	SP	MG889425	
Brachycephalus olivaceus	CFBH 40440	TC236	Castelo dos Bugres	Joinville	SC	MG889435	
Brachycephalus olivaceus		TC241	Castelo dos Bugres	Joinville	SC	**This study**	
Brachycephalus olivaceus		TC243	Castelo dos Bugres	Joinville	SC	**This study**	
Brachycephalus olivaceus		TC246	Morro do Boi	Corupá	SC	MG889436	
Brachycephalus olivaceus		JPCM699	Serra Queimada	Joinville	SC	**This study**	topotype
Brachycephalus olivaceus		JPCM700	Serra Queimada	Joinville	SC	**This study**	topotype
Brachycephalus olivaceus		JPCM701	Serra Queimada	Joinville	SC	**This study**	topotype
Brachycephalus pernix		JPCM856	Morro do Anhangava	Quatro Barras	PR	**This study**	topotype

Species	Voucher	Field Voucher	Locality	Municipality	UF	GenBank	Observation
Brachycephalus pernix		JPCM857	Morro do Anhangava	Quatro Barras	PR	**This study**	topotype
Brachycephalus pernix		JPCM862	Morro do Anhangava	Quatro Barras	PR	**This study**	topotype
Brachycephalus pitanga	CFBH 16746		Núcleo Santa Virgínia PESM	São Luiz do Paraitinga	SP	HQ435699	holotype
Brachycephalus pitanga		MVTIS3205	Núcleo Santa Virgínia PESM	São Luiz do Paraitinga	SP	MZ770741	topotype
Brachycephalus pombali		JPCM898	PARNA Guaricana - Serra das Canasvieiras	Morretes	PR	**This study**	topotype
Brachycephalus pombali		JPCM899	PARNA Guaricana - Serra das Canasvieiras	Morretes	PR	**This study**	topotype
Brachycephalus pombali		JPCM900	PARNA Guaricana - Serra das Canasvieiras	Morretes	PR	**This study**	topotype
Brachycephalus pulex		TC184		Camacan	BA	MK697385	topotype
Brachycephalus pulex		MVTIS3204	Parque Nacional Serra das Lontras	Arataca	BA	MZ770742	
Brachycephalus puri	MZUSP 139152		Parque Nacional do Caparaó	Ibitirama	ES	OK298954	paratype
Brachycephalus puri	ZUFABC039		Parque Nacional do Caparaó	Ibitirama	ES	OK298956	topotype
Brachycephalus quiririensis	CFBH 40406	TC202	Campos do Quiriri	Campo Alegre	SC	MG889437	
Brachycephalus quiririensis		Feb2017-RNA-D	Campos do Quiriri	Campo Alegre	SC	MZ770743	
Brachycephalus quiririensis		Feb2017-RNA-C	Campos do Quiriri	Campo Alegre	SC	MZ770744	
Brachycephalus rotenbergae	CFBH 16854		Serra do Japi	Jundiaí	SP	HM216361	
Brachycephalus rotenbergae	CFBH 16809			Atibaia	SP	HM208306	
Brachycephalus rotenbergae	HCLP-A78			São Francisco Xavier	SP	MT396579	paratype
Brachycephalus sulfuratus	CFBH 39146	TC244	Castelo dos Bugres	Joinville	SP	MG889429	paratype
Brachycephalus sulfuratus		JPCM389	Morro da Antena, Alto Braço do Norte	Itapoá	SC	MG889430	
Brachycephalus sulfuratus	CFBH 39150	TC141	Morro do Anhangava	Quatro Barras	SP	MG889428	paratype
Brachycephalus sulfuratus		Feb2017-RNA44	Casarão Backmeyer	São Francisco do Sul	SC	MZ770751	
Brachycephalus tabuleiro	MNRJ 93858		Serra do Tabuleiro	São Bonifácio	SC	OR116969	paratype
Brachycephalus tabuleiro	UNIFESSPA 112		Serra do Tabuleiro	São Bonifácio	SC	OR116970	paratype
Brachycephalus tabuleiro	ZUFMS-AMP 14532		Serra do Tabuleiro	São Bonifácio	SC	OR116971	paratype
Brachycephalus toby	CFBH 23002		Morro do Corcovado	Ubatuba	SP	HQ435701	paratype

Species	Voucher	Field Voucher	Locality	Municipality	UF	GenBank	Observation
Brachycephalus tridactylus	CFBH 43888	TRID5	Reserva Natural Salto Morato	Guaraqueçaba	PR	MG889432	topotype
Brachycephalus tridactylus	CFBH 43889	TRID6	Reserva Natural Salto Morato	Guaraqueçaba	PR	MG889433	topotype
Brachycephalus tridactylus	MHNCI 10294	TRID1	Reserva Natural Salto Morato	Guaraqueçaba	PR	MG889431	topotype
Brachycephalus tridactylus	JPCM449	JPCM449	Parque Estadual do Rio Turvo	Barra do Turvo	SP	**This study**	
Brachycephalus tridactylus	JPCM450	JPCM450	Parque Estadual do Rio Turvo	Barra do Turvo	SP	**This study**	
Brachycephalus tridactylus	JPCM451	JPCM451	Parque Estadual do Rio Turvo	Barra do Turvo	SP	**This study**	
Brachycephalus tridactylus	TC341	TC341	Ilha do Cardoso	Cananéia	SP	**This study**	
Brachycephalus tridactylus	TC348	TC348	Ilha do Cardoso	Cananéia	SP	**This study**	
Brachycephalus tridactylus	TC363	TC363	Ilha do Cardoso	Cananéia	SP	**This study**	
Brachycephalus vertebralis	CFBH 7907		Sopé do Morro Cuzcuzeiro	Picinguaba	SP	HQ435702	
Brachycephalus verurcosus	CFBH 42072	JPCM467	Morro da Tromba	Joinville	SC	**This study**	topotype
Brachycephalus verurcosus	CFBH 42073	JPCM468	Morro da Tromba	Joinville	SC	**This study**	topotype
Brachycephalus verurcosus	CFBH 42080	JPCM475	Morro da Tromba	Joinville	SC	**This study**	topotype
Brachycephalus verurcosus	CFBH 42093	JPCM490	Morro da Tromba	Joinville	SC	**This study**	topotype
Haddadus binottatus	CFBH T16973	CFBH34398	Floresta Nacional da Tijuca	Rio de Janeiro	RJ	MG889423	
Ischnocnema colibri	CFBH 41809	PPGT653	Reserva Biológica Augusto Ruschi	Santa Teresa	ES	MH538419	paratype
Ischnocnema juipoca	CFBH 9904		Retiro	Campos do Jordão	SP	JX267349	
Ischnocnema nasuta	CFBH 24782	JLG90084	Reserva Biológica Augusto Ruschi	Santa Teresa	ES	JX267520	
Ischnocnema parnaso	CFBH 41812	LOD1385	Pedra do Sino, Parque Nacional da Serra dos Órgãos	Guapimirim	RJ	MH538421	holotype
Ischnocnema venancioi	MNRJ 53932			Teresópolis	RJ	KC468531	

Table S5. Measurements of females and males of *Brachycephalus actaeus* from the eight localities northern of the State of Santa Catarina. Values are given as mean ± SD (min – max). Abbreviations: BNb, Braço do Norte brown morph; BNg, Braço do Norte green morph; CEPA, Centro de Estudos e Pesquisas Ambientais da Univille; CAG, Morro Cantagalo; CAS, Casarão Backmeyer; PAJ, Fazenda Palmito Juriti; SPA, Serra da Palha (Island); and SAI, Estrada do Saí.

	Females (N = 31)							
Trait	BNb (N = 1)	BNg (N = 6)	CEPA (N = 3)	CAG (N = 11)	CAS (N = 3)	PAJ (N = 4)	SAI (N = 1)	SPA (N = 2)
SVL	11.94	11.77 ± 0.23 (11.45 – 12.10)	11.24 ± 0.49 (10.81 – 11.77)	11.47 ± 0.63 (10.00 – 12.26)	12.85 ± 0.38 (12.42 – 13.07)	11.57 ± 0.38 (11.29 – 12.10)	12.42	11.69 ± 0.11 (11.61 – 11.77)
HL	2.48	2.22 ± 0.09 (2.10 – 2.33)	2.16 ± 0.09 (2.06 – 2.21)	2.19 ± 0.08 (2.06 – 2.29)	2.37 ± 0.07 (2.29 – 2.41)	2.48 ± 0.19 (2.25 – 2.72)	2.29	2.16 ± 0.13 (2.06 – 2.25)
HW	4.15	3.94 ± 0.14 (3.81 – 4.15)	3.94 ± 0.28 (3.71 – 4.25)	3.99 ± 0.26 (3.42 – 4.39)	4.03 ± 0.15 (3.90 – 4.20)	4.03 ± 0.32 (3.66 – 4.39)	4.10	3.74 ± 0.04 (3.71 – 3.76)
ND	0.26	0.37 ± 0.01 (0.36 – 0.38)	0.36 ± 0 (0.36 – 0.36)	0.38 ± 0.03 (0.33 – 0.43)	0.38 ± 0.09 (0.28 – 0.43)	0.28 ± 0.02 (0.26 – 0.31)	0.36	0.40 ± 0.05 (0.36 – 0.43)
IND	1.40	1.33 ± 0.05 (1.26 – 1.38)	1.27 ± 0.01 (1.26 – 1.28)	1.28 ± 0.08 (1.11 – 1.40)	1.46 ± 0.09 (1.38 – 1.55)	1.32 ± 0.04 (1.26 – 1.36)	1.4	1.26 ± 0 (1.26 – 1.26)
ED	1.41	1.40 ± 0.05 (1.33 – 1.45)	1.38 ± 0.03 (1.35 – 1.41)	1.35 ± 0.07 (1.22 – 1.47)	1.51 ± 0.10 (1.45 – 1.62)	1.39 ± 0.04 (1.33 – 1.41)	1.35	1.38 ± 0.07 (1.33 – 1.43)
IOD	2.52	2.31 ± 0.07 (2.21 – 2.41)	2.29 ± 0.07 (2.21 – 2.33)	2.28 ± 0.15 (2.02 – 2.60)	2.62 ± 0.15 (2.52 – 2.79)	2.45 ± 0.09 (2.33 – 2.52)	2.60	2.33 ± 0.06 (2.29 – 2.37)
END	0.84	0.69 ± 0.02 (0.67 – 0.71)	0.66 ± 0.01 (0.65 – 0.67)	0.68 ± 0.05 (0.62 – 0.78)	0.64 ± 0.06 (0.57 – 0.67)	0.75 ± 0.05 (0.71 – 0.81)	0.64	0.70 ± 0.02 (0.68 – 0.71)
AL	2.29	2.42 ± 0.26 (1.98 – 2.75)	2.24 ± 0.23 (1.98 – 2.44)	2.32 ± 0.12 (2.14 – 2.59)	2.44 ± 0.27 (2.29 – 2.75)	2.20 ± 0.19 (1.98 – 2.44)	2.29	2.44 ± 0 (2.44 – 2.44)
FAL	2.44	2.25 ± 0.14 (2.10 – 2.44)	2.38 ± 0.05 (2.33 – 2.41)	2.33 ± 0.14 (2.06 – 2.48)	2.55 ± 0.15 (2.44 – 2.72)	2.18 ± 0.13 (2.06 – 2.37)	2.25	2.47 ± 0.08 (2.41 – 2.52)
HAL	2.14	1.87 ± 0.09 (1.80 – 2.04)	1.87 ± 0.07 (1.83 – 1.95)	1.94 ± 0.09 (1.80 – 2.04)	2.10 ± 0.09 (2.04 – 2.20)	2.02 ± 0.08 (1.98 – 2.14)	1.92	1.70 ± 0.23 (1.53 – 1.86)
THL	5.00	4.51 ± 0.20 (4.17 – 4.7)	4.22 ± 0.37 (3.79 – 4.47)	4.48 ± 0.18 (4.09 – 4.70)	4.68 ± 0.12 (4.55 – 4.78)	4.55 ± 0 (4.55 – 4.55)	4.78	4.51 ± 0.06 (4.47 – 4.55)
TIBL	3.79	3.70 ± 0.21 (3.41 – 3.94)	3.72 ± 0.27 (3.49 – 4.02)	3.72 ± 0.23 (3.26 – 4.02)	3.89 ± 0.19 (3.71 – 4.09)	3.93 ± 0.07 (3.87 – 4.02)	4.09	3.87 ± 0.11 (3.79 – 3.94)
FL	5.76	5.37 ± 0.21 (5.08 – 5.61)	5.13 ± 0.19 (4.93 – 5.31)	5.31 ± 0.27 (4.85 – 5.69)	5.51 ± 0.35 (5.15 – 5.84)	5.27 ± 0.26 (5.00 – 5.61)	5.84	5.54 ± 0.22 (5.38 – 5.69)

	Males (N = 39)						
	BNb (N = 6)	BNg (N = 2)	CEPA (N = 6)	CAG (N = 9)	CAS (N = 9)	SAI (N = 2)	SPA (N = 5)
SVL	10.03 ± 0.23 (9.84 – 10.48)	9.36 ± 0.39 (8.55 – 10.65)	10.11 ± 0.65 (9.84 – 10.16)	9.84 ± 0.26 (10.00 – 10.32)	10.2 ± 0.11 (9.36 – 13.07)	10.08 ± 0.42 (10.48 – 12.10)	10.10 ± 9.68 (9.52 – 12.42)
HL	2.06 ± 0.06 (1.78 – 2.21)	2.02 ± 0.13 (1.78 – 2.29)	1.99 ± 0.13 (1.90 – 2.02)	1.95 ± 0.14 (1.94 – 2.13)	2.01 ± 0.06 (1.78 – 2.41)	1.98 ± 0.14 (2.21 – 2.72)	2.02 ± 1.94 (2.06 – 2.29)
HW	3.62 ± 0.13 (3.37 – 3.66)	3.42 ± 0.20 (3.12 – 3.71)	3.53 ± 0.20 (3.37 – 3.66)	3.45 ± 0.14 (3.42 – 3.56)	3.57 ± 0.17 (3.03 – 4.20)	3.54 ± 0.20 (3.76 – 4.39)	3.35 ± 3.42 (3.51 – 4.15)
ND	0.24 ± 0 (0.33 – 0.36)	0.36 ± 0.04 (0.33 – 0.43)	0.37 ± 0.01 (0.33 – 0.36)	0.35 ± 0.03 (0.34 – 0.37)	0.37 ± 0.01 (0.28 – 0.43)	0.35 ± 0.04 (0.31 – 0.31)	0.34 ± 0.17 (0.36 – 0.36)
IND	1.19 ± 0.04 (1.11 – 1.26)	1.17 ± 0.06 (1.06 – 1.33)	1.18 ± 0.07 (1.14 – 1.28)	1.17 ± 0.07 (1.21 – 1.19)	1.23 ± 0.05 (1.06 – 1.55)	1.25 ± 0.06 (1.23 – 1.36)	1.11 ± 1.14 (1.19 – 1.40)
ED	1.27 ± 0.06 (1.24 – 1.32)	1.26 ± 0.03 (1.18 – 1.39)	1.30 ± 0.05 (1.17 – 1.28)	1.25 ± 0.07 (1.22 – 1.39)	1.31 ± 0.04 (1.24 – 1.62)	1.25 ± 0.06 (1.32 – 1.41)	1.31 ± 1.17 (1.30 – 1.35)
IOD	2.09 ± 0.08 (1.98 – 2.17)	2.08 ± 0.10 (1.90 – 2.29)	2.10 ± 0.10 (2.02 – 2.25)	2.05 ± 0.09 (2.13 – 2.17)	2.17 ± 0.08 (2.06 – 2.79)	2.19 ± 0.06 (2.13 – 2.52)	2.12 ± 2.02 (2.13 – 2.6)
END	0.59 ± 0.04 (0.55 – 0.64)	0.63 ± 0.04 (0.57 – 0.67)	0.60 ± 0.02 (0.57 – 0.67)	0.62 ± 0.04 (0.65 – 0.68)	0.64 ± 0.01 (0.60 – 0.67)	0.66 ± 0.03 (0.68 – 0.81)	0.65 ± 0.47 (0.65 – 0.67)
AL	2.04 ± 0.11 (1.86 – 2.20)	2.06 ± 0.17 (1.92 – 2.17)	2.08 ± 0.10 (1.68 – 2.14)	2.05 ± 0.15 (1.98 – 2.35)	1.96 ± 0.11 (1.83 – 2.75)	2.06 ± 0.22 (2.35 – 2.44)	2.03 ± 1.83 (2.14 – 2.29)
FAL	1.98 ± 0.20 (1.90 – 2.25)	1.96 ± 0.11 (1.82 – 2.29)	2.08 ± 0.16 (2.06 – 1.98)	2.07 ± 0.09 (1.98 – 2.17)	2.19 ± 0 (2.06 – 2.72)	1.98 ± 0.04 (2.13 – 2.37)	2.12 ± 1.78 (2.10 – 2.25)
HAL	1.67 ± 0 (1.68 – 1.86)	1.62 ± 0.06 (1.40 – 1.92)	1.72 ± 0.17 (1.71 – 1.80)	1.69 ± 0.08 (1.74 – 1.74)	1.81 ± 0.04 (1.43 – 2.20)	1.77 ± 0.13 (1.83 – 2.14)	1.64 ± 1.53 (1.62 – 1.92)
THL	3.87 ± 0.06 (3.79 – 4.47)	3.83 ± 0.21 (3.64 – 4.32)	4.02 ± 0.24 (3.79 – 4.17)	4.18 ± 0.18 (4.17 – 4.24)	4.03 ± 0 (3.79 – 4.78)	4.17 ± 0.21 (4.17 – 4.55)	3.99 ± 3.71 (3.87 – 4.78)
TIBL	3.41 ± 0.16 (3.18 – 3.49)	3.3 ± 0.14 (3.03 – 4.32)	3.41 ± 0.19 (3.34 – 3.41)	3.29 ± 0.3 (3.18 – 3.41)	3.57 ± 0.16 (3.18 – 4.32)	3.30 ± 0.08 (3.56 – 4.02)	3.27 ± 3.11 (3.41 – 4.09)
FL	4.69 ± 0 (4.55 – 5.15)	4.62 ± 0.18 (4.55 – 5.08)	4.78 ± 0.22 (4.47 – 4.78)	4.84 ± 0.2 (4.62 – 4.93)	4.81 ± 0.11 (4.24 – 5.84)	4.70 ± 0.27 (4.93 – 5.61)	4.67 ± 4.32 (4.62 – 5.84)

*Abbreviation: AL, upper arm length; FAL, forearm length; ED, eye diameter; END, eye-nostril distance; FL, foot length; HAL, hand length; IND, internarial distance; IOD, interorbital distance; HL, head length; HW, head width; ND, nostril diameter; SVL, snout-vent length; TIBL, tibia length; and THL, thigh length.

Table S6. Component loadings, eigenvalues, and variance explained of principal component analyses of the first five axes based on the morphometric traits for *Brachycephalus actaeus*. In bold, the highest loadings (P-value < 0.05) of significative axes (PC1 and PC2 for males).

Morphometric variable	Females (n =31)					Males (n = 39)				
	PC1	PC2	PC3	PC4	PC5	**PC1**	**PC2**	PC3	PC4	PC5
Head length	-0.73	0.41	-0.09	0.19	-0.05	-0.08	0.16	-0.73	0.24	-0.09
Head width	-0.31	-0.05	0.16	-0.71	0.14	**0.65**	0.40	0.17	-0.17	-0.14
Eye diameter	0.06	0.08	-0.40	0.02	0.78	0.39	-0.42	0.28	0.22	-0.32
Interorbital distance	-0.15	-0.38	0.52	-0.23	0.36	**0.64**	-0.09	-0.18	0.27	-0.30
Eye-nostril distance	0.00	0.32	0.47	0.64	0.04	0.32	-0.02	-0.17	0.72	0.27
Internarial distance	-0.24	0.24	0.68	0.13	0.23	**0.73**	0.23	-0.38	0.01	-0.20
Interorbital distance	-0.69	0.37	-0.17	-0.06	0.29	0.08	-0.04	-0.64	-0.57	-0.04
Upper arm length	0.09	-0.68	0.00	0.17	0.18	-0.23	**-0.68**	-0.19	-0.02	-0.31
Forearm length	-0.12	-0.66	0.32	0.12	0.01	0.28	-0.44	0.14	0.15	0.38
Hand length	-0.54	0.02	0.16	-0.31	-0.28	**0.72**	0.03	0.33	-0.31	-0.15
Thigh length	-0.66	-0.20	-0.09	0.24	0.17	0.11	**-0.79**	-0.23	-0.09	0.04
Tibia length	-0.65	-0.29	-0.11	0.06	-0.34	0.41	0.18	-0.19	-0.14	0.71
Foot length	-0.39	-0.52	-0.34	0.27	0.01	0.33	**-0.65**	0.02	-0.24	0.27
Eigenvalue	2.52	1.92	1.43	1.30	1.16	2.57	2.16	1.51	1.25	1.17
% of variance explained	19.40	14.76	11.02	10.02	8.93	19.80	16.61	11.62	9.61	9.00

Table S7. Advertisement call of *Brachycephalus actaeus* from the seven localities from northern of the State of Santa Catarina. Values are given as mean ± SD (min – max). Abbreviations: BNb = Braço do Norte brown morph; BNg = Braço do Norte green morph; CEPA = Centro de Estudos e Pesquisas Ambientais da Univille; CAG = Morro Cantagalo; CAS = Casarão Backmeyer; SPA= Serra da Palha (Island); and SAI = Estrada do Saí.

Trait*	BNb (N = 11)	BNg (N = 9)	CEPA (N = 5)	CAG (N = 8)	CAS (N = 8)	SPA (N = 7)	SAI (N = 3)
CD	0.05 ± 0.01 (0.04 – 0.07)	0.04 ± 0.01 (0.03 – 0.06)	0.04 ± 0.00 (0.03 – 0.04)	0.04 ± 0.01 (0.03 – 0.05)	0.05 ± 0.01 (0.04 – 0.06)	0.04 ± 0.00 (0.04 – 0.05)	0.05 ± 0.01 (0.04 – 0.06)
CR	13 ± 2 (11 – 16)	13 ± 3 (8 – 19)	14 ± 4 (9 – 19)	16 ± 2 (11 – 19)	14 ± 2 (12 – 18)	10 ± 2 (7 – 13)	18 ± 3 (16 – 22)
CI	4.50 ± 0.76 (3.41 – 5.63)	4.66 ± 1.60 (2.70 – 7.68)	4.78 ± 1.60 (3.10 – 6.80)	3.92 ± 0.68 (3.20 – 5.41)	4.20 ± 0.48 (3.67 – 4.83)	5.85 ± 1.22 (4.49 – 8.22)	3.34 ± 0.59 (2.68 – 3.82)
NP	2 ± 1 (2 – 3)	2 ± 1 (2 – 4)	2 ± 0 (2 – 2)	3 ± 0 (2 – 3)	3 ± 1 (2 – 4)	2 ± 0 (2 – 3)	1 ± 1 (1 – 2)
PR	32 ± 9 (22 – 48)	33 ± 16 (16 – 63)	29 ± 11 (19 – 46)	42 ± 7 (31 – 52)	41 ± 17 (23 – 70)	24 ± 7 (11 – 32)	24 ± 3 (22 – 28)
LF	6234.9 ± 337.6 (5625 – 6750)	6577.6 ± 366.8 (5881.5 – 7020.8)	6218.8 ± 153.6 (5986.3 – 6405.6)	5839.7 ± 628.3 (5250.0 – 7008.9)	6388.3 ± 280.8 (6009.6 – 6833.4)	6238.0 ± 612.9 (5233.5 – 7087.5)	6417.5 ± 262.7 (6114.6 – 6583.3)
UF	7169.0 ± 151.4 (6953.1 – 7406.2)	7446.1 ± 306.9 (6981.9 – 7925.8)	7100.0 ± 142.9 (6916.5 – 7304.2)	6762.5 ± 509.3 (6328.1 – 7700.9)	7135.2 ± 296.5 (6776.8 – 7653.4)	7328.4 ± 410.5 (6676.3 – 7900.0)	7512.2 ± 625.9 (6791.7 – 7921.9)
DF	6722.8 ± 210.7 (6454.3 – 7031.2)	7074.6 ± 262.3 (6663.7 – 7395.8)	6695.7 ± 67.1 (6612.1 – 6791.3)	6313.4 ± 611.6 (5653.1 – 7366.0)	6821.0 ± 281.5 (6413.5 – 7321.0)	6960.5 ± 441.2 (6308.0 – 7543.8)	7096.4 ± 521.1 (6510.4 – 7507.9)
FBW	934.1 ± 270.8 (536.9 – 1481.2)	868.5 ± 173.3 (630.2 – 1100.3)	881.2 ± 141.3 (670.9 – 1023.0)	922.8 ± 139 (691.9 – 1081.2)	746.9 ± 217.5 (339.3 – 980.1)	1090.4 ± 503.1 (728.2 – 2134.2)	1094.6 ± 367.2 (677.1 – 1367.2)
RT	12 ± 4 (1 – 2)	14 ± 5 (1 – 2)	16 ± 5 (1 – 2)	13 ± 5 (1 – 2)	11 ± 4 (1 – 2)	16 ± 5 (1 – 2)	17 ± 6 (1 – 2)

*CD, call duration (s); CI, inter-call interval; CR, call rate/min; DF, dominant frequency (Hz); FBW, frequency bandwidth (Hz); LF, lower frequency (Hz); NP, number of pulses; RT, call rise time (%); PR, pulse rate/min; UF, upper frequency (Hz).

Table S8. Component loadings, eigenvalues, and variance explained of the first five axes of principal component analyses based on acoustic traits from 51 males of *Brachycephalus actaeus*. In bold, the highest loadings (P-value < 0.05) of significative axes (PC1 and PC2).

Acoustic traits	PC1	PC2	PC3	PC4	PC5
Call repetition rate	**-0.65**	0.41	-0.60	0.03	-0.12
Pulse repetition rate	**-0.77**	0.47	0.08	0.24	0.30
Number of Pulses	**-0.53**	0.29	0.54	0.24	0.50
Call duration	-0.39	0.27	0.40	-0.25	-0.61
Lower frequency	**0.64**	**0.71**	0.00	-0.25	0.09
Upper frequency	**0.75**	**0.56**	0.00	0.33	-0.11
Dominant frequency	**0.69**	**0.64**	-0.02	0.27	-0.02
Frequency bandwidth	0.00	-0.39	0.00	0.87	-0.31
Call rise time	0.41	-0.37	-0.57	0.00	0.34
Inter-call interval	**0.64**	-0.45	0.56	-0.06	0.13
Eigenvalue	3.41	2.21	1.42	1.15	0.96
Percentage of variance	34.80	22.54	14.46	11.75	9.75

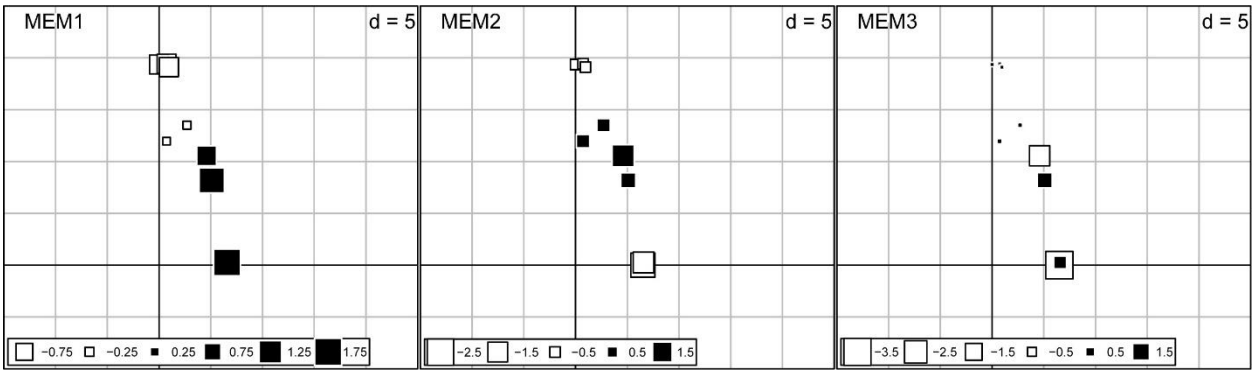


Figure S1. Moran's eigenvectors maps (MEMs) attributed to each site. Eigenvalue scores are proportional to the size of the squares (black = negative, white = positive). MEM1 was significantly correlated with acoustic parameters matrix. (dbMEM1: broad-scale variable; 2 medium scale; 3 fine-scale).

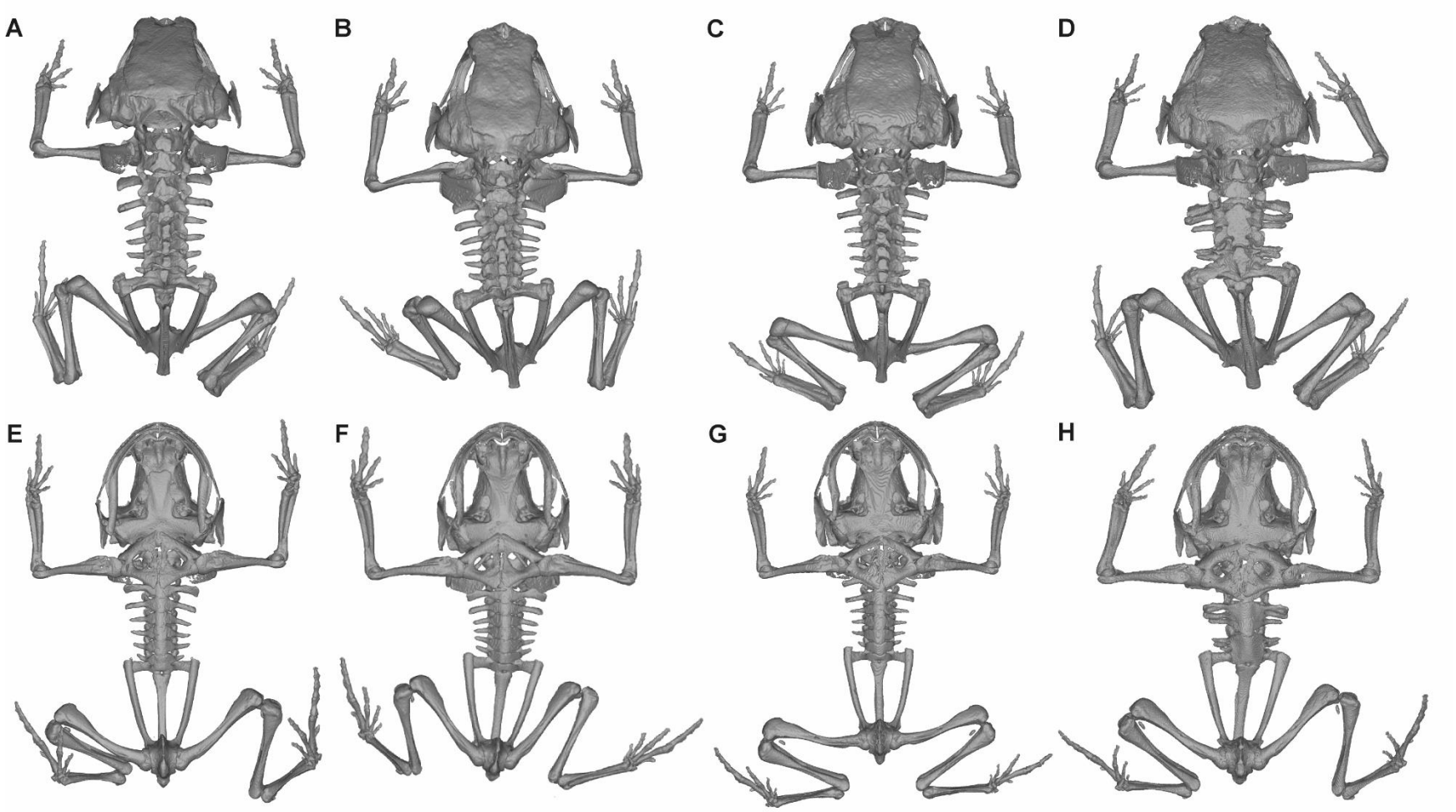


Figure S2. High-resolution computed tomography (Micro-CT) scans of *Brachycephalus actaeus* body. A and E: gray morph (TC256); B and F: orange morph (JPCM351); C and G: brown morph (JPCM410); and D and H: green morph (CFBH 39872). Above, dorsal view. Below, ventral view.

CONCLUSÕES GERAIS

i) O gênero *Brachycephalus* representa um modelo promissor para compreender a evolução da coloração, defesa química, plano corporal e hiperossificação do esqueleto.

ii) As translocações encontradas no genoma mitocondrial da espécie de sapo-pulga, *B. hermogenesi*, e das espécies do grupo de *B. ephippium*, destacam a necessidade de um amplo estudo evolutivo para entender os prováveis eventos de introgressão e as implicações funcionais derivadas dessa nova ordenação gênica nas espécies.

iii) *Brachycephalus actaeus* é apresentado como mais uma evidência evolutiva em anfíbios onde o aposematismo em espécies diurnas e tóxicas pode ser precursor do polimorfismo/politipismo de cor. Além, outras espécies descritas para o gênero são potenciais candidatas para representar esse fenômeno.

iv) A regulação gênica entre os diferentes morfos de coloração de *Brachycephalus actaeus* é poligênica e principalmente regulada pelos genes relacionados à síntese de melanina. Não foi encontrada expressão dos genes que regulam pigmentos de carotenoides e pteridinas na pele do morfo laranja. Assim, as espécies de *Brachycephalus* podem ser interessantes modelo para investigar os perfis gênicos associados a coloração da pele, podendo revelar novas vias na aquisição de cor.

v) Diante de um predador visualmente orientado, os morfos de *Brachycephalus actaeus* foram percebidos diferentemente, sugerindo uma potencial função ecológica. Até então, nenhum estudo focou na variação intraespecífica de coloração como uma estratégia antipredatória no gênero. Estudos *in situ* são fortemente necessários para identificar a pressão de seleção de cor local pelos predadores.

vi) A miniaturização promove intensa variação na morfologia. O aposematismo promove intensa variação de coloração e pode influenciar diferenças bioacústicas. Em *Brachycephalus actaeus* exemplificamos essa problemática e lançamos luz sobre as dificuldades taxonômicas e sistemáticas que refletem diretamente em como as descrições de espécies estão sendo conduzidas atualmente.

vii) Os padrões de isolamento tipicamente observados na diversificação das espécies de *Brachycephalus* em conjunto com os padrões de cores nem sempre corroboram como divergência evolutiva. De fato, essas espécies representam complexos evolutivos ao

longo de cadeias de montanhas da Mata Atlântica, apresentando alta variação de coloração em um sistema ainda pouco compreendido, pois não foi estudado.

viii) Este estudo fornece diversas evidências para do polimorfismo de cor em *Brachycephalus* abrindo caminho para novas perguntas sobre a diversificação da coloração aposemática e o uso de estratégias de cor nesse interessante modelo de espécies aposemáticas e miniaturizadas.

APÊNDICE I

Monteiro, J. P. C., Ibáñez, R., Mantzana-Oikonomaki, V., Pröhl, H., & Rodríguez, A. (2023) Genetic diversity of *Oophaga vicentei* (Anura: Dendrobatidae) and taxonomic position of a remarkable color morph from Panama. Salamandra, 59(4): 347–351.

"Diversidade genética de *Oophaga vicentei* (Anura: Dendrobatidae) e posição taxonômica de um notável morfo de cor do Panamá"

Resumo

Apesar de ser um dos grupos de anuros Neotropicais mais estudados, as relações filogenéticas, o status taxonômico e os limites das espécies das rãs do gênero *Oophaga* permanecem pouco claros. Neste estudo, combinamos novas sequências de DNA mitocondrial de duas localidades no noroeste do Panamá com dados pré-existentes para reconstruir uma filogenia de Máxima Verossimilhança das *Oophaga* Mesoamericanas. Nossos resultados fornecem as primeiras evidências genéticas sobre a monofilia de *Oophaga vicentei* e esclarecem a posição taxonômica de uma morfologia de cor distinta. Nosso trabalho destaca a importância de estudos adicionais sobre a diversidade fenotípica e genotípica de *O. vicentei* como um sistema modelo contrastante para estudos comparativos de aposematismo.

SALAMANDRA **59**(4): 347–351
30 October 2023 | ISSN 0036–3375

SALAMANDRA
German Journal of Herpetology

Correspondence

Genetic diversity of *Oophaga vicentei* (Anura: Dendrobatidae) and taxonomic position of a remarkable color morph from Panama

Juliane P. C. Monteiro[1], Roberto Ibáñez[3,4], Vasiliki Mantzana-Oikonomaki[2], Heike Pröhl[2] & Ariel Rodríguez[2]

[1] Universidade Estadual Paulista (UNESP), Instituto de Biociências, Departamento de Biodiversidade e Centro de Aquicultura (CAUNESP), 13506-900, Rio Claro, São Paulo, Brazil

[2] Institute of Zoology, University of Veterinary Medicine Hannover, 30559 Hannover, Germany

[3] Smithsonian Tropical Research Institute, Apartado Postal 0843-03092, Panamá, República de Panamá

[4] Sistema Nacional de Investigación, Secretaría Nacional de Ciencia, Tecnología e Innovación, Apartado 0816-02852, Panamá, República de Panamá

Corresponding author: Ariel Rodríguez, ORCID: 0000-0003-1936-793X, e-mail: ariel.rodriguez@tiho-hannover.de

Manuscript received: 8 June 2023
Accepted: 25 July 2023 by Stefan Lötters

The genus *Oophaga* Bauer, 1994 comprises 12 species and is harbored among Neotropical poison frogs of the Dendrobatidae family (Frost 2023). These species are distributed throughout Central America and northwestern South America (Grant et al. 2017). Despite being one of the most studied Neotropical anuran groups, the phylogenetic relationships, taxonomic status and species boundaries of this genus remain unclear. The known color polymorphism within and across species poses challenges for accurate taxa identification, emphasizing the importance of integrative taxonomic tools (Brown et al. 2011).

Oophaga vicentei (Jungfer, Weygoldt & Juraske, 1996) is distributed in the forested areas of the Coclé and Veraguas provinces in the central region and the Caribbean of Panama. It inhabits altitudes ranging from sea level up to approximately 900 meters above sea level (m a.s.l.) and is exclusively found on epiphyte-laden trees within preserved forests (Lötters et al. 2007). Several color morphs have been described for this species, including green, blue, and bright red, with patterns of dorsal dark markings including bands, spots, and vermiculations (Lötters et al. 2007). Until the study conducted by Flores et al. (2019), the field ecology of this species was basically unknown. Their research provided valuable insights into the calling activity, bioacoustics and diet of males from three different populations in Central Panama.

During fieldwork surveys on June 2022 in Panama, aimed at identifying divergent color morphs of *Oophaga vicentei*, three of us (RI, VMO, AR) visited two localities in the Colón and Veraguas provinces. In one of them, we observed individuals displaying a unique color pattern characterized by pale yellow dots distributed on a dark brown background in the dorsal region (Fig. 1). This color pattern bears a resemblance to *Oophaga arborea* (Myers, Daly & Martínez, 1984), another endemic species from Panama. Around 2004, specimens of this dotted morph were smuggled into the European pet trade market and sold as *O. arborea* but later classified as *O.* cf. *vicentei* (Ostrowski & Mahn 2023). In order to elucidate the taxonomic position of this population, as well as the other collected samples, herein we use DNA sequence information to determine their phylogenetic relationships and provide insights into the genetic diversity and ecology of this population.

We sampled frogs at the locality of La Empalizada, Provincia de Veraguas, Panamá (8°45'40" N, 81°12'50" W, 82 m a.s.l.) and at the surroundings of La Ceiba, Área de Uso Múltiple Donoso, Distrito Especial Omar Torrijos Herrera, Provincia de Colón, Panamá (8°48'30" N, 80°36'24" W, 100 m a.s.l.) (Fig. 1A). We searched for frogs in the leaf litter, trunks, vines and leaves aided by their vocalizations and captured individuals by hand. We photographed the collected individuals in the field and later euthanized them by immersion in 5% MS-222. We subsequently extracted thigh muscle tissue and stored it in 96% ethanol vials.

Once in the lab, we extracted total DNA from the tissues using Qiagen DNeasy® Blood and Tissue kit (Qiagen, Hilden, Germany) and PCR amplified two commonly used mitochondrial markers in amphibians, the 16S rRNA (16S)

© 2023 Deutsche Gesellschaft für Herpetologie und Terrarienkunde e.V. (DGHT), Germany
Open access at https://www.salamandra-journal.com

and the protein-coding cytochrome b gene (COB). We performed the PCRs with a final volume of 11 µl using: 7 µl sterile H_2O, 2.5 µl GoTaq Reaction buffer (Promega), 0.3 µl each primer, 0.25 µl dNTP (10 mM), and 0.08 µl GoTaq® DNA polymerase (Promega). For 16S amplification, we used the primers 16Sar-L and 16Sbr-H (Palumbi et al. 1991; respectively 5'-CGCCTGTTTATCAAAAACAT-3' and 5'-CCGGTCTGAACTCAGATCACGT-3'). The PCR program included an initial denaturing step of 3 min at 95°C followed by 35 cycles of amplification (95°C for 20 s; 50°C for 20 s of annealing temperature; and 65°C for 1 min for extension), with a final extension step at 65°C for 3 min. Additionally, for COB amplification, we used the primers cytbA and cytbC (Bossuyt & Milinkovitch 2000; respectively 5'-CCATGAGGACAAATATCATTYTGRGG-3' and 5'-CTACTGGTTGTCCTCCGATTCATGT-3'). The PCR cycling was identical except for the 38 cycles of amplification (95°C for 20 s; 52°C for 20 s of annealing temperature; and 68°C for 50 s for extension) and the final extension step at 72°C for 3 min. Sanger sequencing in both directions was performed by Eurofins Genomics Europe Sequencing GmbH (Köln, Germany). We inspected and edited the chromatograms for quality and assembled the sequences using Geneious software (v.10.3, Biommaters). The newly obtained sequences were deposited in GenBank (NCBI accession numbers: OR133808-15 and OR271415-22).

For each of the two loci, we constructed multiple sequence alignments including the newly obtained sequences plus homologous sequences available on NCBI GenBank. Our compilation included DNA sequences from eight *Oophaga* species from Central (*O. arborea*, *O. granulifera*, *O. pumilio*, *O. speciosa*, *O. vicentei*) and South America (*O. histrionica*, *O. lehmanni*, *O. sylvatica*). Due to the unavailability of homologous 16S and COB sequences, *O. anchicayensis*, *O. andresi*, *O. occultator*, and *O. solanensis* could not be included in the alignments. In accordance with recent phylogenetic reconstructions (Guillory et al.

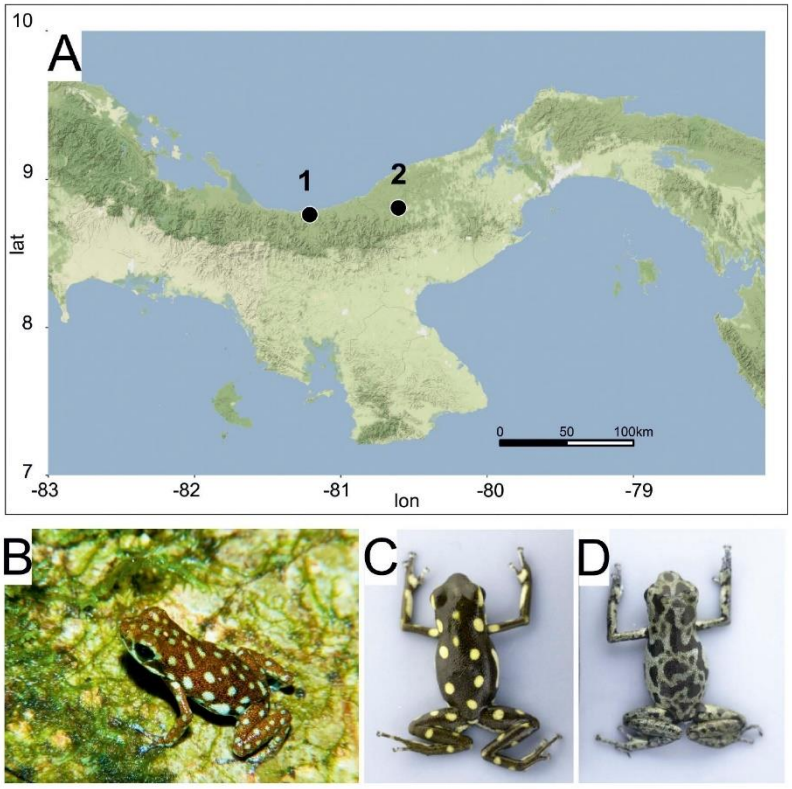


Figure 1. Geographic location and representative photographs of the study populations of *Oophaga vicentei*. (A) Map of Western Panama identifying the study sites: (1) La Empalizada, Veraguas; (2) La Ceiba, Área de Uso Múltiple Donoso, Colón. (B) Male of *O. vicentei* from La Empalizada photographed in situ by AR; (C) dorsal view of *O. vicentei* male from La Empalizada, photographed by VMO; and (D) dorsal view of *O. vicentei* male from La Ceiba, photographed by VMO.

2019, Jetz & Pyron 2018), sequences from three *Dendrobates* species (*D. auratus*, *D. leucomelas*, *D. tinctorius*) were included as outgroups (GenBank accession numbers are provided in Appendix 1). Alignments of the 16S and COB sequence sets were conducted in Mega using default settings (v.5.0, Tamura et al. 2011) and later concatenated using the R package concatipede (v.1.0.0, Vecci & Bruneaux 2021). We inferred the phylogenetic relationships of the samples in the concatenated alignment using iQTree (v.1.6.12, Nguyen et al. 2015). We implemented four data partitions (16S, and each of the three COB codon positions) and searched for the best-fit models of sequence evolution and partition scheme with the Model Finder algorithm of iQTree. The model fit results (16S and all COB codons together: TPM2+G4) were used in the final maximum likelihood (ML) tree reconstruction. Node support was assessed by an ultrafast bootstrap with 1000 pseudoreplicates.

We observed approximately a dozen active individuals at La Empalizada site, only five of these were collected. Most individuals we were able to locate were active calling males, perching on tree trunks, vines, rocks, and the leaf litter, from the ground to 3 m high. All observed individuals exhibited a distinctive dorsal color pattern with pale yellow to light green spots over a dark background (Fig. 1B, C). The ventral color was pale yellow to light green with no distinctive markings or dark areas in the gular region. At La Ceiba, the understory vegetation had been partially removed. However, active frogs including calling males were similarly seen (from the ground to 3 m high), on the leaf litter and on superficial roots, trunks and low branches of trees. Further, some males were heard calling from perches above 3 m. In total, eight males were collected at this locality. The individuals displayed dark brown and blueish green color with vermiculation pattern on the dorsal area (Fig. 1D). The ventral area was light blueish green without patterns. As our sampling protocol included dissection and extraction of multiple organs, no voucher specimens were obtained.

The concatenated alignment of 16S and COB DNA sequences measured 1,515 bp in length and included 42 terminals (eight obtained in this study; Appendix 1). The reconstructed ML phylogeny displayed a strongly supported (100% ultrafast bootstrap value) *O. vicentei* as monophyletic clade encompassing all newly obtained sequences from La Empalizada and La Ceiba plus the previously existing GenBank record of *O. vicentei* from El Copé (Grant et

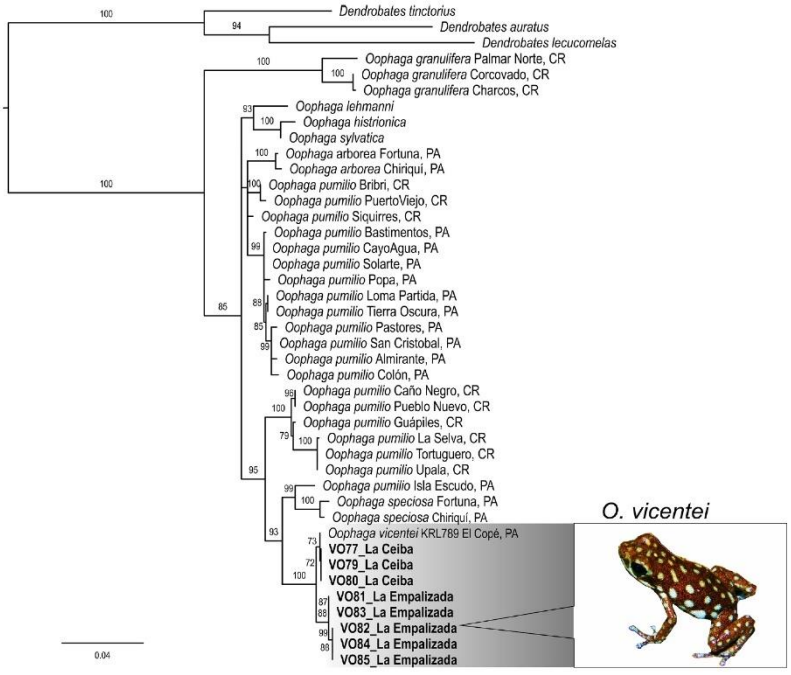


Figure 2. Maximum likelihood phylogenetic tree obtained from a matrix of 1,515 bp of mitochondrial DNA sequences of 42 terminals of *Oophaga* and *Dendrobates* (outgroup) frogs. Ultrafast bootstrap support values above 70% are presented on the tree branches. The *O. vicentei* clade is highlighted in gray, with the newly obtained sequences in bold. The inset shows a photograph of a male with the dotted pattern observed at La Empalizada locality. Abbreviations: CR = Costa Rica, PA = Panama. Sequence accession numbers are provided in Appendix 1.

al. 2006). This clade clustered within a strongly supported clade including northern Costa Rica and Isla Escudo de Veraguas samples of *O. pumilio* and *O. speciosa*. Interestingly, the geographically proximal GenBank accessions of *O. pumilio* from Bocas del Toro region were not in this clade and their phylogenetic position, as well as those of *O. pumilio* terminals from Southern Costa Rica, *O. arborea*, and the South American *Oophaga* were not resolved in the ML tree (Fig. 2).

The genus *Oophaga* has been one of the most studied amphibian groups in terms of behavior, ecology, evolutionary biology and aposematism (e.g. Wang & Shaffer 2008, Brown et al. 2010, Yang et al. 2019). Despite this, the phylogenetic relationships, taxonomic status, and species boundaries remain unclear, resulting in the grouping into species complexes. By including sequences from multiple samples, our phylogenetic analysis provides the first molecular evidence for the monophyly of *O. vicentei* and its close relationship with *O. speciosa* and the *O.* cf. *pumilio* from Isla Escudo de Veraguas. Additionally, our mitochondrial phylogeny corroborates the notion that *O. pumilio* is a paraphyletic taxon comprising distinct mitochondrial lineages some of which show uncertainties in their phylogenetic relationships. Similar inconsistencies in mitochondrial phylogenies have been previously reported by multiple authors (Hagemann & Pröhl 2007, Hauswaldt et al. 2011, Grant et al. 2017), and reinforce the need for taxonomic reassessment of this species complex. It is also worth noting that our taxa and loci sampling was geared towards the elucidation of the relationship of *O. vicentei* samples. In order to reconstruct the phylogeny of this genus a more extensive sampling, of loci and taxa, will be required.

The pronounced variations in coloration observed among the localities with available DNA sequences and herein studied (La Empalizada: dark with light dots, La Ceiba: bluish green with dark vermiculations, and El Copé: yellowish green with variable spotting) (Jungfer et al. 1996), in complement with the existence of other less known localities where red, green and blue color morphs have been documented (AmphibiaWeb 2023, Ostrowski & Mahn 2023) underscore the potential of this species for future investigations into the evolution of color polymorphism. A comprehensive characterization of the phenotypic and genotypic diversity of *O. vicentei* in mainland Panama will also allow for additional testing of the existing hypothesis for the evolution of the polytypic *O. pumilio* in the Bocas del Toro archipelago.

Apart from elucidating the phylogenetic position of a unique color morph of *O. vicentei*, our field-based behavioral observations contribute further insights into the ecology of this species. Typically, *O. vicentei* is considered an exclusive tree-dweller associated with bromeliads in the arboreal stratum (Lötters et al. 2007), spending most of the time high in the upper canopy (Flores et al. 2019). However, at the La Empalizada and La Ceiba localities, we observed active males of this species calling from the leaf litter and perches in the lower stratum of the forest understory. These observations, together with the Peña et al. (2016) report, who found a female in the forest floor in another locality within the Santa Fe area, suggest that microhabitat preferences in *O. vicentei* may exhibit plasticity and be locality-specific across the range of occurrence.

Acknowledgements

Our field collection, euthanasia and sampling protocol (SI-21017) was approved by the Animal Care and Use Committee (IACUC) of the Smithsonian Tropical Research Institute (STRI). Collecting permit ARBG-0027-2022 was kindly provided by the Ministerio de Ambiente de la República de Panamá. We thank Edgar and Luis Sánchez, who guided us in the regions of La Ceiba and Santa Fe. We are particularly grateful to Orelis Arosemena, Lil Camacho, and other STRI staff members who greatly facilitated our work in Panama and the exportation of samples. We also thank the Institut für Zoologie at TiHo for providing molecular laboratory facilities and Sebastian Wöhle for assistance in the laboratory. This work was partially funded by a DFG grant to A. Rodríguez (RO5508/2-1) and Heike Pröhl (PR 626/10-1). J.P.C. Monteiro was supported by São Paulo Research Foundation (#2018/09691-0 and #2021/08799-4) and R. Ibáñez by the Panama Amphibian Rescue and Conservation project.

References

AmphibiaWeb. (2023): AmphibiaWeb: information on amphibian biology and conservation. – AmphibiaWeb, Berkeley. Available at: https://amphibiaweb.org, accessed 30 May 2023.

Bossuyt F. & M. C. Milinkovitch (2000): Convergent adaptive radiations in Madagascan and Asian ranid frogs reveal covariation between larval and adult traits. – Proceedings of the National Academy of Sciences, **97**: 6585–6590.

Brown, J. L., E. Twomey, A. Amézquita, M. B. Souza, J. P. Caldwell, S. Lötters, R. von May, P. R. Melo-Sampaio, D. Mejía-Vargas, P. Perez-Peña, M. Pepper, E. H. Poelman, M. Sanchez-Rodriguez & K. Summers (2011): A taxonomic revision of the Neotropical poison frog genus *Ranitomeya* (Amphibia: Dendrobatidae). – Zootaxa, **3083**: 1–120.

Brown, J. L., M. E. Maan, M. E. Cummings & K. Summers (2010): Evidence for selection on coloration in a Panamanian poison frog: a coalescent-based approach. – Journal of Biogeography, **37**: 891–901.

Flores, E. E., A. Batista, V. Rodríguez & R. A. Page (2019): Vicente´s poison frog (*Oophaga vicentei*) in the wild: calling activity, bioacoustics and diet. – The Herpetological Bulletin, **149**: 11–17.

Frost, D. R. (2023): Amphibian species of the world: an online reference. Version 6.1. – American Museum of Natural History, New York, USA. Available at: http://research.amnh.org/herpetology/amphibia/index.html, accessed 09 June 2023.

Guillory, W. X., M. R. Muell, K. Summers & J. L. Brown (2019): Phylogenomic reconstruction of the Neotropical poison frogs (Dendrobatidae) and their conservation. – Diversity, **11**: 1–14.

Grant, T., M. Rada, M. Anganoy-Criollo, A. Batista, P. H. Dias, A. M. Jeckel, D. J. Machado & J. V. Rueda-Almonacid (2017): Phylogenetic systematics of dart-poison frogs and their relatives revisited (Anura: Dendrobatoidea). – South American Journal of Herpetology, **12**: S1–S90.

Grant, T., D. R. Frost, J. P. Caldwell, R. Gagliardo, C. F. B. Haddad, P. J. R. Kok, D. B. Means, B. P. Noonan, W. E Schargel & W. C.Wheeler (2006): Phylogenetic systematics of dart-poison frogs and their relatives (Amphibia: Athesphatanura: Dendrobatidae). – Bulletin of the American Museum of Natural History, **299**: 1–261.

Jetz, W. & R. A. Pyron (2018): The interplay of past diversification and evolutionary isolation with present imperilment across the amphibian tree of life. – Nature Ecology and Evolution, **2**: 850–858.

Hagemann, S. & H. Pröhl (2007): Mitochondrial paraphyly in a polymorphic poison frog species (Dendrobatidae; *D. pumilio*). – Molecular Phylogenetics and Evolution, **45**: 740–747.

Hauswaldt, J. S., A. K. Ludewig, M. Vences & H. Pröhl (2011): Widespread co-occurrence of divergent mitochondrial haplotype lineages in a Central American species of poison frog (*Oophaga pumilio*). – Journal of Biogeography, **38**: 711–726.

Jungfer, K.-H., P. Weygoldt & N. Juraske (1996): *Dendrobates vicentei*, ein neuer Pfeilgiftfrosch aus Zentral-Panama. – Herpetofauna, **18**: 17–26.

Lötters, S., K.-H. Jungfer, W. Schmidt & F. W. Henkel (2007): Poison frogs: Biology, species and captive husbandry. – Edition Chimaira, Frankfurt.

Nguyen, L. T., H. A. Schmidt, A. v. Haeseler & B. Q. Minh (2015): IQ-TREE: A fast and effective stochastic algorithm for estimating maximum-likelihood phylogenies. – Molecular Biology and Evolution, **32**: 268–274.

Ostrowski, T. & T. Mahn (2023): Artbeschreibung *Oophaga vicentei*. Dendrobase.de – Datenbank für der Überfamilie Dendrobatoidea. Available at: https://dendrobase.de, accessed 30 May 2023.

Palumbi, S., A. Martin, S. Romano, W. O. McMillan, L. Stice & G. Grabowski (1991): The simple fool's guide to PCR. – Second version. Honolulu, HI.

Peña, B., V. D. Gracia & E. E. Flores (2016): *Oophaga vicentei* (Vicente's poison frog): Habitat use. – Herpetological Review, **47**: 114.

Tamura, K., D. Peterson, N. Peterson, G. Stecher, M. Nei & S. Kumar (2011): MEGA5: Molecular evolutionary genetics analysis using Maximum Likelihood, Evolutionary Distance, and Maximum Parsimony methods. – Molecular Biology and Evolution, **28**: 2731–2739.

Vecci, M. & M. Bruneaux (2021): Concatipede: an R package to concatenate fasta sequences easily. – Available at: http://doi.org/10.5281/zenodo.5130603, accessed 25 May 2023.

Wang, I. J., & H. B. Shaffer (2008): Rapid color evolution in an aposematic species: a phylogenetic analysis of color variation in the strikingly polymorphic strawberry poison-dart frog. – Evolution, **62**: 2742–2759.

Yang, Y., M. R. Servedio & C. L. Richards-Zawacki (2019): Imprinting sets the stage for speciation. – Nature, **574**: 99–102.

Appendix 1

GenBank accession numbers of DNA sequences of *Oophaga* and *Dendrobates* used in this study with newly obtained sequences highlighted in bold. Abbreviations: CO = Colombia, CR = Costa Rica, EC = Ecuador, and PA = Panama.

Species	sample	16S	COB
O. vicentei	VO77_La Ceiba	**OR133808**	**OR271415**
O. vicentei	VO79_La Ceiba	**OR133809**	**OR271416**
O. vicentei	VO80_La Ceiba	**OR133810**	**OR271417**
O. vicentei	VO81_La Empalizada	**OR133811**	**OR271418**
O. vicentei	VO82_La Empalizada	**OR133812**	**OR271419**
O. vicentei	VO83_La Empalizada	**OR133813**	**OR271420**
O. vicentei	VO84_La Empalizada	**OR133814**	**OR271421**
O. vicentei	VO85_La Empalizada	**OR133815**	**OR271422**
O. vicentei	KRL789_El Cope, PA	DQ502167	DQ502602
O. speciosa	Fortuna, PA	AF098747	AF120014
O. speciosa	Chiriquí, PA	DQ502037	DQ502468
O. arborea	Fortuna, PA	AF098748	AF120015
O. arborea	Chiriquí, PA	DQ502036	DQ502467
O. pumilio	Bribri, CR	EF597161	EF597201
O. pumilio	Cano Negro, CR	EF597162	EF597202
O. pumilio	Guapiles, CR	EF597163	EF597203
O. pumilio	La Selva, CR	EF597164	EF597204
O. pumilio	Pueblo Nuevo, CR	EF597165	EF597205
O. pumilio	Puerto Viejo, CR	EF597166	EF597206
O. pumilio	Siquirres, CR	EF597167	EF597207
O. pumilio	Tortuguero, CR	EF597168	EF597208
O. pumilio	Upala, CR	EF597169	EF597209
O. pumilio	Almirante, PA	EF597170	EF597210
O. pumilio	Bastimentos, PA	EF597171	EF597211
O. pumilio	Colón, PA	EF597172	EF597212
O. pumilio	Cayo Agua, PA	EF597173	EF597213
O. pumilio	Escudo, PA	EF597174	EF597214
O. pumilio	Loma Partida, PA	EF597175	EF597215
O. pumilio	Pastores, PA	EF597176	EF597216
O. pumilio	Popa, PA	EF597177	EF597217
O. pumilio	San Cristobal, PA	EF597178	EF597218
O. pumilio	Solarte, PA	EF597179	EF597219
O. pumilio	Tierra Oscura, PA	EF597180	EF597220
O. granulifera	Corcovado, CR	AF098749	AF120016
O. granulifera	Charcos, CR	HE804764	HE775251
O. granulifera	Palmar Norte, CR	HE804766	HE775254
O. histrionica	unknown	AF098742	AF120009
O. lehmanni	Valle del Cauca, CO	DQ502034	DQ502465
O. sylvatica	Santo Domingo, EC	DQ502059	DQ502490
D. auratus	unknown	MF069434	MF069434
D. leucomelas	unknown	MF069435	MF069435
D. tinctorius	unknown	MF069437	MF069437

APÊNDICE II

Condez, T. H., **Monteiro, J. P. C.**, Malagoli, L. R., Trevine, V. C., Schunck, S., Garcia, P. C. A., & Haddad, C. F. B. 2021. Notes on the hyperossified pumpkin toadlets of the genus *Brachycephalus* (Anura: Brachycephalidae) with the description of a new species. *Herpetologica*, *77*(2): 176–194

"Notas sobre os sapinhos-pingo-de-ouro hiperossificados do gênero *Brachycephalus* (Anura: Brachycephalidae) com a descrição de uma nova espécie"

Resumo

Atualmente, quatro espécies de sapinhos-pingo-de-ouro são reconhecidas pelo extremo grau de hiperossificação no crânio e coluna vertebral dentro do gênero *Brachycephalus*. Além de seu tamanho corporal maior em comparação com outras espécies do gênero, *B*. *darkside*, *B*. *ephippium*, *B*. *garbeanus* e *B*. *margaritatus* compartilham características osteológicas notáveis, como as grandes placas paravertebrais que formam um escudo ósseo dorsal ornamentado, visível através do tegumento. Contribuímos para o conhecimento atual desse grupo ao analisar sua diversidade e descrever uma nova espécie hiperossificada proveniente de importantes remanescentes de Mata Atlântica no sudeste do Brasil, incluindo aqueles que fazem fronteira com São Paulo, a maior e mais populosa cidade da América do Sul. A nova espécie é diagnosticada por uma combinação de caracteres morfológicos, osteológicos e bioacústicos, com evidências adicionais de sequências de mtDNA para confirmar seu posicionamento filogenético. As placas ósseas paróticas e paravertebrais externamente delimitadas por uma borda áspera e clara podem prontamente distinguir a nova espécie das outras espécies hiperossificadas dentro de *Brachycephalus*. A nova espécie está amplamente distribuída ao longo da Serra do Mar, incluindo a região da Serra de Paranapiacaba, em altitudes de 700 a 1000 metros acima do nível do mar, na costa central do estado de São Paulo, sudeste do Brasil. Discutimos caracteres morfológicos valiosos dentro desse grupo de espécies, reforçamos a necessidade de estudos adicionais e destacamos a relevância de áreas protegidas para a conservação da biodiversidade em regiões metropolitanas.

Herpetologica, 77(2), 2021, 176–194
© 2021 by The Herpetologists' League, Inc.

Notes on the Hyperossified Pumpkin Toadlets of the Genus *Brachycephalus* (Anura: Brachycephalidae) with the Description of a New Species

Thais H. Condez[1,8], Juliane P.C. Monteiro[2,3], Leo R. Malagoli[4], Vivian C. Trevine[5], Fabio Schunck[6], Paulo C.A. Garcia[7], and Célio F.B. Haddad[2,3]

[1] Instituto Nacional da Mata Atlântica (INMA), 29.650–000, Santa Teresa, Espírito Santo, Brazil
[2] Programa de Pós-Graduação em Zoologia, Instituto de Biociências, Universidade Estadual Paulista (UNESP), 13506–900, Rio Claro, São Paulo, Brazil
[3] Universidade Estadual Paulista (UNESP), Instituto de Biociências, Departamento de Biodiversidade e Centro de Aquicultura (CAUNESP), 13506–900, Rio Claro, São Paulo, Brazil
[4] Fundação para a Conservação e a Produção Florestal do Estado de São Paulo, Parque Estadual da Serra do Mar, Núcleo São Sebastião, 11600–000, São Sebastião, São Paulo, Brazil
[5] Laboratório de Coleções Zoológicas, Instituto Butantan, 05503–900, São Paulo, São Paulo, Brazil
[6] Comitê Brasileiro de Registros Ornitológicos, www.cbro.org.br, 04785–040, São Paulo, São Paulo, Brazil
[7] Universidade Federal de Minas Gerais, Instituto de Ciências Biológicas, Departamento de Zoologia, Laboratório de Herpetologia, 31270–910, Belo Horizonte, Minas Gerais, Brazil

Abstract: Four species of pumpkin toadlets are currently recognized by the extreme condition of hyperossification in the skull and vertebral column within the genus *Brachycephalus*. In addition to their larger body size, relative to other congeneric species, *Brachycephalus darkside*, *Brachycephalus ephippium*, *Brachycephalus garbeanus*, and *Brachycephalus margaritatus* share remarkable osteological features, such as the large paravertebral plates forming an ornamented dorsal bone shield, visible through the integument. We add to the current knowledge of this group by analyzing its diversity and describing a new hyperossified species from some important Atlantic Forest remnants in southeastern Brazil, including those bordering São Paulo, the largest and most populous city in South America. The new species is diagnosed by a combination of morphological, osteological, and bioacoustic characters, with further evidence of mtDNA sequences to confirm its distinction from the other congeners. The parotic and paravertebral bone plates externally bordered with a rough and pale contour can readily distinguish the new species from the other hyperossified species within *Brachycephalus*. The new species is widely distributed along the Serra do Mar mountain range, including the regionally named Serra de Paranapiacaba, in elevations from 700 to 1000 m above sea level (a.s.l.), in the central coast of the state of São Paulo, southeastern Brazil. We discuss valuable morphological characters within this group of species, reinforce the need for further studies, and highlight the relevance of protected areas for biodiversity conservation in metropolitan regions.

Key words: Bone shield; Brachycephaloidea; Hyperossification; Miniaturization

The genus *Brachycephalus* Fitzinger 1826 currently consists of 36 species of miniaturized leaf-litter–dwelling toadlets endemic to the Atlantic Forest domain (Frost 2020). Despite their occurrence in a wide elevational range from sea level to more than 1500 m a.s.l., the impressive diversity of the genus is still associated with moderate- and high-elevation areas, generally occurring above 700 m of elevation (Bornschein et al. 2019a). Recent studies in remote mountain ranges revealed several new species of *Brachycephalus* that supported a relatively high and steady rate of species description in the past few years. Moreover, these studies have revealed species complexes and potentially new species across the distribution of the genus (Bornschein et al. 2019a; Condez et al. 2020).

Brachycephalus currently includes the pumpkin toadlets, which are the majority of the species, and the poorly known flea-toads (Condez et al. 2016). The popular name "pumpkin toadlet" was attributed to the bright-colored type species *Brachycephalus ephippium* (Pombal et al. 1994). The bufoniform body aspect (Miranda-Ribeiro 1920), and the general conspicuous orange body color, which can be associated with the presence of toxic tetrodotoxin-like substances and oligopeptides on their skin (Pires et al. 2005; Arcanjo et al. 2015), is shared among 32 pumpkin toadlets species within *Brachycephalus*. However, the four cryptic colored flea-toad species (*Brachycephalus didactylus*, *Brachycephalus hermogenesi*, *Brachycephalus pulex*, and *Brachycephalus sulfuratus*) embedded within the pumpkin toadlets (Condez et al. 2020) prevent the broad use of the popular term "pumpkin toadlet" for the genus (i.e., because of its nonmonophyly). In the first molecular phylogenetic analysis of *Brachycephalus*, Clemente-Carvalho et al. (2011a) recovered pumpkin toadlets living in latitudes between 20°S to 24°S in the Brazilian states of Espírito Santo, Rio de Janeiro, and São Paulo as a monophyletic group, clearly distinct from those living in higher latitudes. At that time, within *Brachycephalus* two distinct clades were already recognized based on molecular information and osteological features (Clemente-Carvalho et al. 2009, 2011a; Campos et al. 2010). Recently, Condez et al. (2020), based on an extensive taxon sampling, recovered and explicitly named these pumpkin toadlet clades. The *B. ephippium* clade is represented by the largest species within the genus, with the extreme condition of hyperossification of the skin, skull, and vertebral column, externally identified and diagnosed by the presence of a dorsal bone shield. This clade includes *B. ephippium* (Spix 1824), *Brachycephalus garbeanus* Miranda-Ribeiro 1920, and *Brachycephalus margaritatus* Pombal and Izecksohn 2011 (Condez et al. 2020), together with the recently described *Brachycephalus darkside* Guimarães, Luz, Rocha and Feio 2017, which was never formally included in molecular studies but referred to this clade according to the original publication (Guimarães et al. 2017). The *Brachycephalus vertebralis* clade is repre-

[8] Correspondence: e-mail, thacondez@gmail.com

sented by pumpkin toadlets with variable conditions of hyperossification of the skin, skull, and vertebral column, but lacking the dorsal bone shield, including *Brachycephalus alipioi* Pombal and Gasparini 2006; *Brachycephalus bufonoides* Miranda-Ribeiro 1920 (see also Folly et al. 2020); *Brachycephalus crispus* Condez, Clemente-Carvalho, Haddad and Reis 2014; *Brachycephalus guarani* Clemente-Carvalho, Giaretta, Condez, Haddad and Reis 2012; *Brachycephalus nodoterga* Miranda-Ribeiro 1920; *Brachycephalus pitanga* Alves, Sawaya, Reis and Haddad 2009; *Brachycephalus toby* Haddad, Alves, Clemente-Carvalho and Reis 2010; and *B. vertebralis* Pombal 2001. A single exception, not formally included in this clade, but probably referred to it, is *Brachycephalus atelopoide* Miranda-Ribeiro 1920, a poorly known species from the state of São Paulo whose holotype is lost (Pombal 2010).

The extreme condition of hyperossification exhibited by the four species within the *Brachycephalus ephippium* clade (Condez et al. 2020) is distinct from all the other congeners, with large additional bone elements in the skull and vertebral column, generally ornamented and visible through the integument (Campos et al. 2010). *Brachycephalus darkside*, *B. ephippium*, *B. garbeanus*, and *B. margaritatus* share remarkable osteological features, such as (1) the presence of large parotic plates covering the squamosal, pro-otics, and auditory capsule, (2) spinal plates associated with presacral vertebrae, and (3) large paravertebral plates forming a dorsal bone shield (Miranda-Ribeiro 1920; Clemente-Carvalho et al. 2009; Campos et al. 2010; Pombal and Izecksohn 2011). Herein, we contribute to the knowledge of the genus *Brachycephalus* by describing a new hyperossified species in the *Brachycephalus ephippium* clade from the state of São Paulo, Brazil. We based our results on a set of morphological, osteological, and bioacoustic characters, with further evidence from mtDNA sequences to confirm the new species designation.

Material and Methods

Specimens

Specimens were collected during several expeditions to the municipalities of Bertioga, Itanhaém, Juquitiba, Santo André, São Bernardo do Campo, São Paulo, and São Vicente, all in the state of São Paulo, southeastern Brazil. All geographic coordinates are in the datum WGS84. The expeditions were mainly performed in the rainy seasons between 2005 and 2017. After being photographed, live specimens were euthanized in 5% lidocaine, fixed in 10% formalin, and preserved in 70% ethanol. Tissue samples were taken from liver or hind limb muscle and preserved in absolute ethanol for molecular analysis. The collected specimens and tissue samples are deposited in Célio F.B. Haddad Amphibian Collection (CFBH), Departamento de Biodiversidade, Instituto de Biociências, Universidade Estadual Paulista, Rio Claro, São Paulo, Brazil; Amphibian Collection of Museu de Zoologia da USP (MZUSP), Universidade de São Paulo, São Paulo, Brazil; and Amphibian Collection of Centro de Coleções Taxonômicas, Universidade Federal de Minas Gerais (UFMG), Minas Gerais, Brazil. Sound recordings are deposited in Coleção Bioacústica da Universidade Federal de Minas Gerais, Minas Gerais, Brazil (CBUFMG), and Macaulay Library, The Cornell Lab of Ornithology, Cornell University, NY, USA (ML).

External Morphology and Osteology

Preserved specimens were measured by a single person (T.H. Condez) with a graduated micrometric ocular fitted to a Zeiss Stemi SV11 stereomicroscope. The abbreviations for the 14 measurements adopted are SVL (snout–vent length); HL (head length; from the tip of snout to the angle of the jaw); HW (head width; greatest width of head located between the angle of the jaw); ND (nostril diameter); IND (internostril distance; between inner margins of nostrils); ED (eye diameter); IOD (interorbital distance; between anterior corners of eyes); END (eye–nostril distance; from the anterior corner of the eye to posterior margin of the nostril); THL (thigh length); TBL (tibia length); FL (foot and tarsus length; from the longest toe to the plantar plus tarsus length); UAL (upper arm length); FAL (forearm length); and HAL (hand length; between the palmar and the longest finger). Except for FL, which is modified to include tarsus length, and ND (Condez et al. 2016), the measurements follow Duellman (1970; SVL, HL, HW, ED, and TBL), Cei (1980; IOD, IND, and END), and Heyer et al. (1990; UAL, FAL, HAL, and THL). Sex of specimens was determined by the presence of vocal slits in adult males and the presence of mature oocytes in adult females. To evaluate sexual dimorphism in size we tested differences between measurements of males and females, considering different sample sizes and heteroscedasticity of the data, with the Welch's *t*-test in the R environment (R Core Team 2020). For osteological descriptions we prepared two cleared and double-stained specimens from the municipalities of Bertioga (MZUSP 135753) and Santo André (CFBH 27188), and also a single specimen scanned for high-resolution microtomography (micro CT) collected at municipality of Santo André (CFBH 42337). The skin of cleared and double-stained material was preserved to search for small dotted osteoderms and, after careful removal of eyes and internal content (such as gonads and digestive tract), the specimen was immersed in absolute ethanol for 24 h. The specimen was transferred to a solution of 80% absolute ethanol, 20% acetic acid, and 0.1 g alcian blue for 1 h and neutralized in 1% KOH solution for 20 h. The digestion occurred in a solution of 70% water, 30% borax, and 0.1 g trypsin for approximately 4 h and then the specimen was washed in a solution of 1% KOH for 10 min. The specimen was stained in a solution of 1% KOH and 0.1 g alizarin red for 10 min, then washed in a solution of 1% KOH, and immersed in a series of glycerin solutions, with increasing glycerin concentration every 24 h (40%, 70%, and 90%). It was permanently stored in 90% glycerin and 10% KOH. This clearing and double-staining protocol was modified from Taylor and Van Dyke (1985). The osteological description based on cleared and double-stained specimens was made using a Zeiss SteREO Discovery V20 stereomicroscope (Zeiss Group) with motorized 20×-zoom. The micro CT was made on Phoenix v|tome|xs240 (General Electric Company) at Universidade de São Paulo, Ribeirão Preto, Brazil. The preserved specimen was fitted in a small plastic tube, supported by low-density foam soaked in 70% ethanol to avoid dehydration on the procedure of scanning. During a single scan rotation we took 1300 x-ray images of 990 × 1000

pixels using an exposure time 0.33 s, voltage of 50 KV, and amperage of 150 mA. The same projection view was created three times and then averaged; the final volume had 0.018955 mm of resolution (for x, y, and z). The DICOM data was reconstructed using 3D Slicer v4.10 (Fedorov et al. 2012). The micro CT reconstruction was segmented using threshold values adjusted manually to include the desired proportion of bones. The surface model was generated using 3D Slicer's Segment Editor Module. Background artifacts were manually cropped and the model was smoothed by a factor of 0.1 before being exported to 3D Mesh (Standard Tessellation Language File; STL). Final STL is available online at https://www.morphosource.org/Detail/MediaDetail/Show/media_id/85738. Prepared specimens were then compared to other species within the *B. ephippium* clade: *B. ephippium* (UF72725, a micro CT specimen available online at https://www.morphosource.org/Detail/SpecimenDetail/Show/specimen_id/3735), *Brachycephalus garbeanus* (CFBH 16806, a cleared and double-stained specimen), and *Brachycephalus* sp. (aff. *ephippium*) (three cleared and double-stained specimens not deposited in scientific collections obtained from municipality of Atibaia [AT025], municipality of São José dos Campos [SFX004], and municipality of Jundiaí [SJ004]). Comparisons with *B. darkside* and *B. margaritatus* follow the original species descriptions (Pombal and Izecksohn 2011; Guimarães et al. 2017). The terminology of osteological structures follows Trewavas (1932) for hyoid and laryngeal skeleton; Trueb (1993, 2015), Pugener and Maglia (1997), and Campos et al. (2010) for cranial bones; and Trueb (1973), Campos et al. (2010), and Fabrezi (1992, 1993, 2001) for axial and appendicular skeleton. Specimens examined are presented in Appendix I and the museum acronyms follow Sabaj (2016), except for the Herpetology Collection of Florida Museum of Natural History, University of Florida, USA (UF).

Acoustic Analysis

Calling males were recorded with a tape recorder Marantz PMD 222 coupled with an Audio-Technica AT835 unidirectional microphone by P.C.A. Garcia at the municipality of Bertioga, state of São Paulo, Brazil, and with a digital recorder Marantz PMD 660 (Marantz Corp.) coupled with a Sennheiser ME66/K6 (Sennheiser electronic GmbH & Co.) unidirectional microphone by F. Schunck and K. Evangelista at the municipality of Santo André, state of São Paulo, Brazil. Recordings were made at 44.1-kHz sampling rate and sample size of 16 bit. We applied a 500-Hz high-pass filter to sound files in Audacity v2.1.1 (Audacity Team 2017) before conducting the acoustic analysis to reduce background noise. Spectral and temporal parameters were measured using Raven Pro v1.5 (Bioacoustics Research Program 2014) directly from spectrograms and oscillograms. Spectrograms were produced with a Hann window type, window size 512 samples, overlap 90% (locked), hop size 51 samples, DFT size 1024 samples (locked), grid spacing 43.1 Hz, brightness and contrast in default, and color map Cool. We used a note-centered approach and 10 advertisement call parameters were obtained following the definitions provided by Köhler et al. (2017): (1) call duration (s), (2) intercall interval (s), (3) number of notes per call (notes/call), (4) note repetition rate (notes/s), (5) number of pulses per note (pulses/note), (6) dominant frequency (defined as peak frequency in Raven Pro v1.5), (7) lower and (8) upper frequencies (kHz; defined as frequency 5% and frequency 95% in Raven Pro 1.5, respectively), (9) 5%–95% frequency bandwidth (kHz), and (10) rise time (%, defined as peak time relative in Raven Pro 1.5). Sound parameters are presented as the range (mean ± standard deviation). The sound graphics were prepared in R v4.0.1 (R Core Team 2020) using the package Seewave v2.1.0 (Sueur et al. 2008), with the spectrogram settings Hann window, 90% overlap, 256 samples resolution, and a color scale defined by 30 relative dB.

Molecular Phylogenetics

We analyzed genetic samples from 20 specimens of the new species and also from a recently available sample of *Brachycephalus darkside*. For these samples, total DNA was extracted from ethanol-preserved muscle or liver tissues using DNeasy Tissue Kits (Qiagen Inc.). We performed polymerase chain reactions (PCRs) for the amplification of two fragments of the mitochondrial 16S rRNA gene (694 + 521 base pairs [bp]), using two distinct pairs of primers: 12SM (GGCAAGTCGTAACATGGTAAG; Darst and Cannatella 2004) and 16SA (ATGTTTTTGGTAAACAGGCG; Palumbi et al. 1991), and 16SAR-L (CGCCTGTTTAT CAAAAACAT) and 16SBR-H (CCGGTCTGAACTCAGAT CACGT) (Palumbi et al. 1991). We carried out DNA amplification in a 20-µL-volume reaction using each specific pair of primers and PCR Master Mix (Taq Polymerase 0.05 U/µL, PCR reaction buffer with 4 mM $MgCl_2$, 0.4 mM of each dNTP; MBI Fermentas, USA). Thermocycling conditions for amplification of 12SM-16SA began with denaturation at 94°C (3 min), followed by 35 cycles each of 1-min denaturation at 94°C, 1-min annealing at 52°C, and 1-min extension at 72°C, followed by a single final 5-min extension at 72°C. The amplification of 16Sar-16Sbr began with denaturation at 94°C (3 min), followed by 37 cycles each of 20-s denaturation at 94°C, 20-s annealing at 50°C, 45-s extension at 68°C, and a final step of 5-min at 68°C. PCR products were purified using Exonuclease and Shrimp Alkaline Phosphatase (Affimetrix/USB, Thermo Fisher Scientific). Samples were sequenced in both directions by Macrogen Inc. (Seoul, Republic of Korea). Chromatograms were manually inspected and the consensus sequences were assembled with CodonCode Aligner v3.5 (Codon Code Corp., Centerville, MA).

We complemented our sampling with sequences available from GenBank, considering all known species within *Brachycephalus*. Although we only sequenced 16S rRNA fragments for the new species and *B. darkside*, we included in our data set the sequences of two other mitochondrial fragments: 12S rRNA (792 bp) and Cytochrome-b (694 bp), aiming to have a better resolution in our topology. In total, our data set included molecular data for 80 individuals, with 1–4 sequences for each of the 36 known species of *Brachycephalus*. We also included *Haddadus binotatus* (to root the trees) and *Ischnocnema parva* as the outgroup taxon, based on their close phylogenetic relationships with *Brachycephalus* (Heinicke et al. 2018). Newly generated sequences were submitted to GenBank and the list of material included in the molecular analysis is available in Supplemental Table S1, available online.

Sequences were aligned with MAFFT v7.402 (Katoh and Standley 2013), using the Q-INS-i strategy that considers RNA secondary structure (Katoh and Toh 2008) for the 12S rRNA and 16S rRNA fragments, the default strategy for Cytochrome-b, and default transition/transversion cost ratio and gap opening penalty for all fragments. Alignments were then concatenated using Sequence Matrix v1.0 (Vaidya et al. 2011), resulting in a final file of 2701 bp. We used PartitionFinder v2.1.1 (Lanfear et al. 2017) to select the optimal partition scheme and nucleotide substitution models for each data block based on all search algorithms, linked model of branch lengths, and the corrected Akaike Information Criterion (AIC_c). For Cytochrome-b we considered each codon position as a possible partition. The best model was GTR+I+G for all data blocks (16S rRNA, 12S rRNA, and the tree independent partitions of Cytochrome-b). Phylogenetic trees were then obtained using Bayesian phylogenetic inference and maximum parsimony. We use MrBayes v3.2.6. (Ronquist et al. 2012), implemented in the online CIPRES Science Gateway Portal (Miller et al. 2010), for running two independent runs, of four chains for 100 million generations, sampling each 10,000 generations, and discarding 25% of trees as burn-in. We assumed convergence by checking the standard deviation of split frequencies ($P < 0.01$) and the estimated sample sizes of parameters (ESS > 200) in Tracer v1.6 (Rambaut et al. 2014). The remaining trees were summarized in a majority-rule consensus tree and used to calculate the Bayesian posterior probabilities (BPP), as the node support values. For the maximum parsimony we used TNT v1.5 (Goloboff and Catalano 2016) with the New Technology search option, search level 50, sectorial searches, tree drift, and tree fusing included, hitting the best length 100 times. We estimated the jackknife absolute frequency (Farris et al. 1996) with 1000 replicates using New Technology search, driven searches, and checking level every 10 hits in the strict consensus tree. We plotted both the BPP and the jackknife absolute frequencies the in the 50% majority-rule consensus tree resulting from the Bayesian analysis. Topology was edited using FigTree v1.4.3 (Rambaut 2016). Additionally, we calculated the uncorrected pairwise genetic distances (*p*-distance) among individuals of the new species and related congeners, considering the concatenated sequences of 16S rRNA. The number of base differences between sequences was calculated considering 331 sites, after the complete deletion of gaps, and ambiguous sites/missing data, using Mega X (Kumar et al. 2018; Stecher et al. 2020).

SPECIES DESCRIPTION

Brachycephalus ***ibitinga*** sp. nov.
(Table 1; Figs. 1–6)

Brachycephalus cf. *nodoterga*: Pie et al. (2013:167), in part
Brachycephalus sp.: Trevine et al. (2014:129), in part; Bornschein et al. (2019a:16), in part
Brachycephalus sp. 4: Condez et al. (2020:671), in part

Holotype.—CFBH 44449, adult male, collected at Trilha do Mirante, Parque das Neblinas, municipality of Bertioga, state of São Paulo, Brazil (23°44′31″S, 46°08′20″W, 750 m a.s.l.), on 12 December 2017, by T.H. Condez, J.P.C. Monteiro, E.C. Nardin, and M.T.T. Santos (Figs. 1, 2).

TABLE 1.—Measurements in millimeters of the adults included in the type series of *Brachycephalus* ***ibitinga*** sp. nov.[a]

	Females (n = 15)			Males (n = 10)		
	Mean	SD	Range	Mean	SD	Range
SVL	14.6	1.0	13.1–16.9	12.2	0.4	11.5–12.7
HL	3.4	0.2	3.0–3.7	3.0	0.1	2.8–3.2
HW	4.3	0.2	3.8–4.6	3.8	0.1	3.6–4.0
ND	0.5	0.0	0.4–0.5	0.4	0.0	0.4–0.5
IND	1.9	0.1	1.7–2.1	1.7	0.0	1.6–1.7
ED	1.6	0.1	1.5–1.8	1.5	0.1	1.3–1.6
IOD	3.2	0.2	2.8–3.6	2.8	0.1	2.7–3.0
END	1.0	0.1	0.9–1.2	0.9	0.0	0.9–1.0
THL	5.9	0.3	5.3–6.4	5.2	0.2	4.9–5.7
TBL	5.3	0.4	4.5–5.9	4.6	0.2	4.3–4.9
FL	8.2	0.6	7.2–9.2	7.2	0.4	6.4–7.7
UAL	2.7	0.2	2.3–3.1	2.4	0.1	2.3–2.6
FAL	3.3	0.3	2.7–3.6	2.8	0.2	2.6–3.1
HAL	2.9	0.1	2.6–3.1	2.5	0.2	2.2–2.9

[a] SVL (snout–vent length); HL (head length; from the tip of snout to the angle of the jaw); HW (head width; greatest width of head located between the angle of the jaw); ND (nostril diameter); IND (internostril distance; between inner margins of nostrils); ED (eye diameter); IOD (interorbital distance; between anterior corners of eyes); END (eye–nostril distance; from the anterior corner of the eye to posterior margin of the nostril); THL (thigh length); TBL (tibia length); FL (foot and tarsus length; from the longest toe to the plantar plus tarsus length); UAL (upper arm length); FAL (forearm length); and HAL (hand length; between the palmar and the longest finger).

Paratopotypes.—CFBH 44451 and 44452, adult males, CFBH 44448 and 44450 adult females, collected with the holotype.

Paratypes.—MZUSP 135753, cleared and double-stained adult male, collected on 24 September 2005 by R.S. Cordeiro, B.V.M. Berneck, and M.V. Segalla; UFMG 0007, adult male, collected on 12 October 2009 by P.C.A. Garcia, J. Thompson, P.P.G. Taucce, and B. Fehlberg; UFMG 21557 and 21558, adult females, collected, respectively, on 3 November 2006, by P.C.A. Garcia and M. Forlani, and 1 November 2005, by P.C.A. Garcia, all at Parque das Neblinas, municipality of Bertioga, state of São Paulo, Brazil (23°44′49″S, 46°07′42″W, 790 m a.s.l.). MZUSP 136870, adult male, and MZUSP 136871, adult female, collected on 9 December 2005, by P.C.A. Garcia; MZUSP 136872, adult female and 136873 juvenile, collected respectively on 14



FIG. 1.—*Brachycephalus* ***ibitinga*** sp. nov. in life (CFBH 44449; adult male; holotype). Photo by T.H. Condez. A color version of this figure is available online.

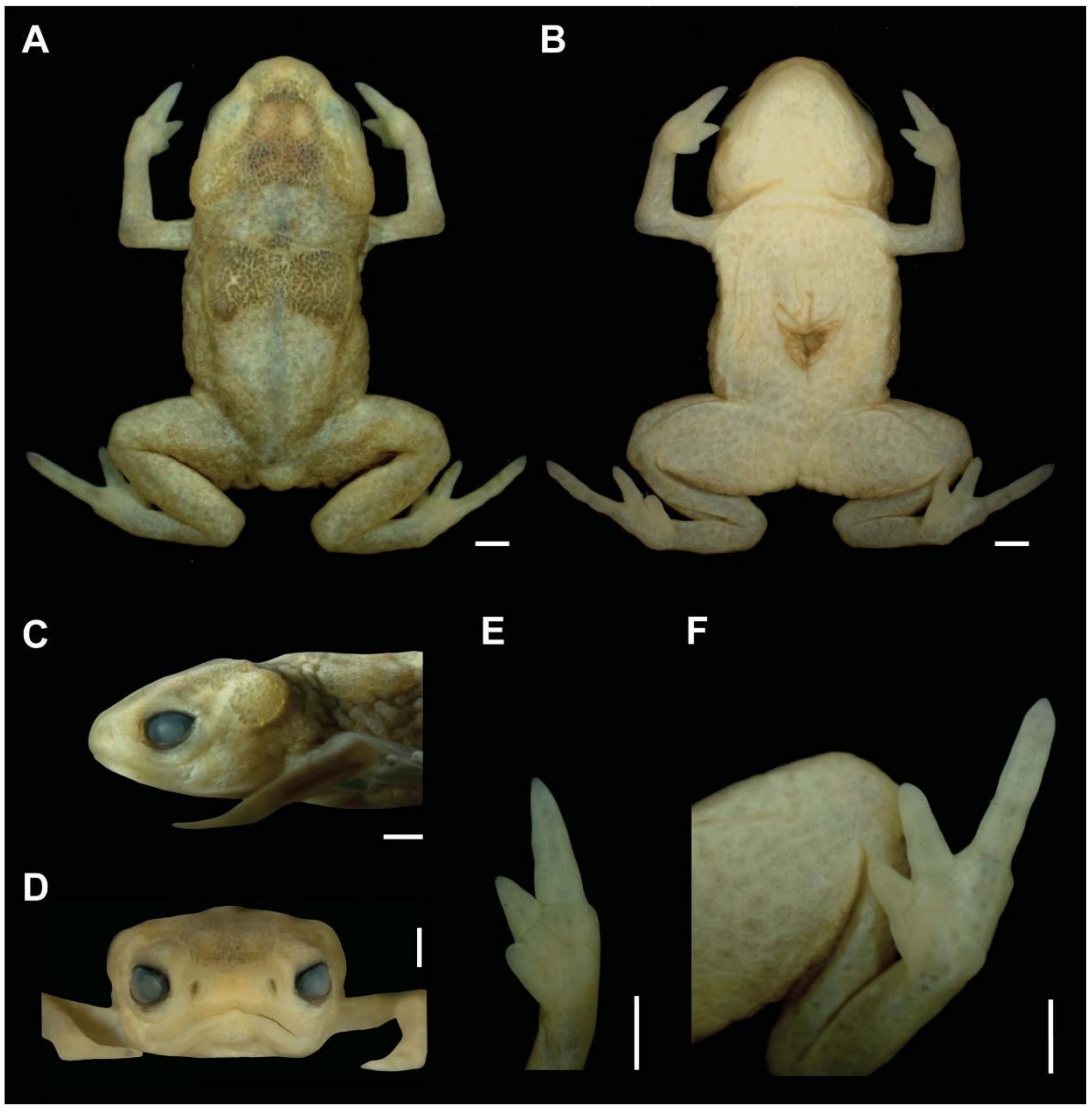


FIG. 2.—*Brachycephalus* ***ibitinga*** sp. nov. in preservative (CFBH 44449; adult male; holotype). Dorsal view of the body (A); ventral view of the body (B); lateral view of the head (C); frontal view of the head (D); ventral view of the left hand (E); and ventral view of the left foot (F). Scale bars = 1 mm. A color version of this figure is available online.

December 2004, and 24 February 2005, by S.E.X.F. Souza; MZUSP 136877 and 136879 adult females, MZUSP 136874–136876, and 136878, juveniles, collected on 19 November 2005, by C.O.R. Costa and collaborators, all at Parque das Neblinas, municipality of Bertioga, state of São Paulo, Brazil (23°43′60″S, 46°08′60″W, 740 m a.s.l.). CFBH 27188, cleared and double-stained adult male, CFBH 27189 and 27190, adult males, CFBH 27187, adult female, collected at Parque Natural Municipal das Nascentes de Paranapiacaba, municipality of Santo André, state of São Paulo, Brazil (23°46′46″S, 46°17′42″W, 920 m a.s.l.), on 20 October 2010, by V.C. Trevine and T.H. Condez. CFBH 28168, adult female, collected at Parque Natural Municipal das Nascentes de Paranapiacaba, municipality of Santo André, state of São Paulo, Brazil (23°46′55″S, 46°17′42″W, 975 m a.s.l.), on 16 October 2010, by V.C. Trevine and T.H. Condez. Four adult females CFBH 28206 (collected on 24 February 2010), CFBH 28207 (collected on 4 December 2009), CFBH 28208

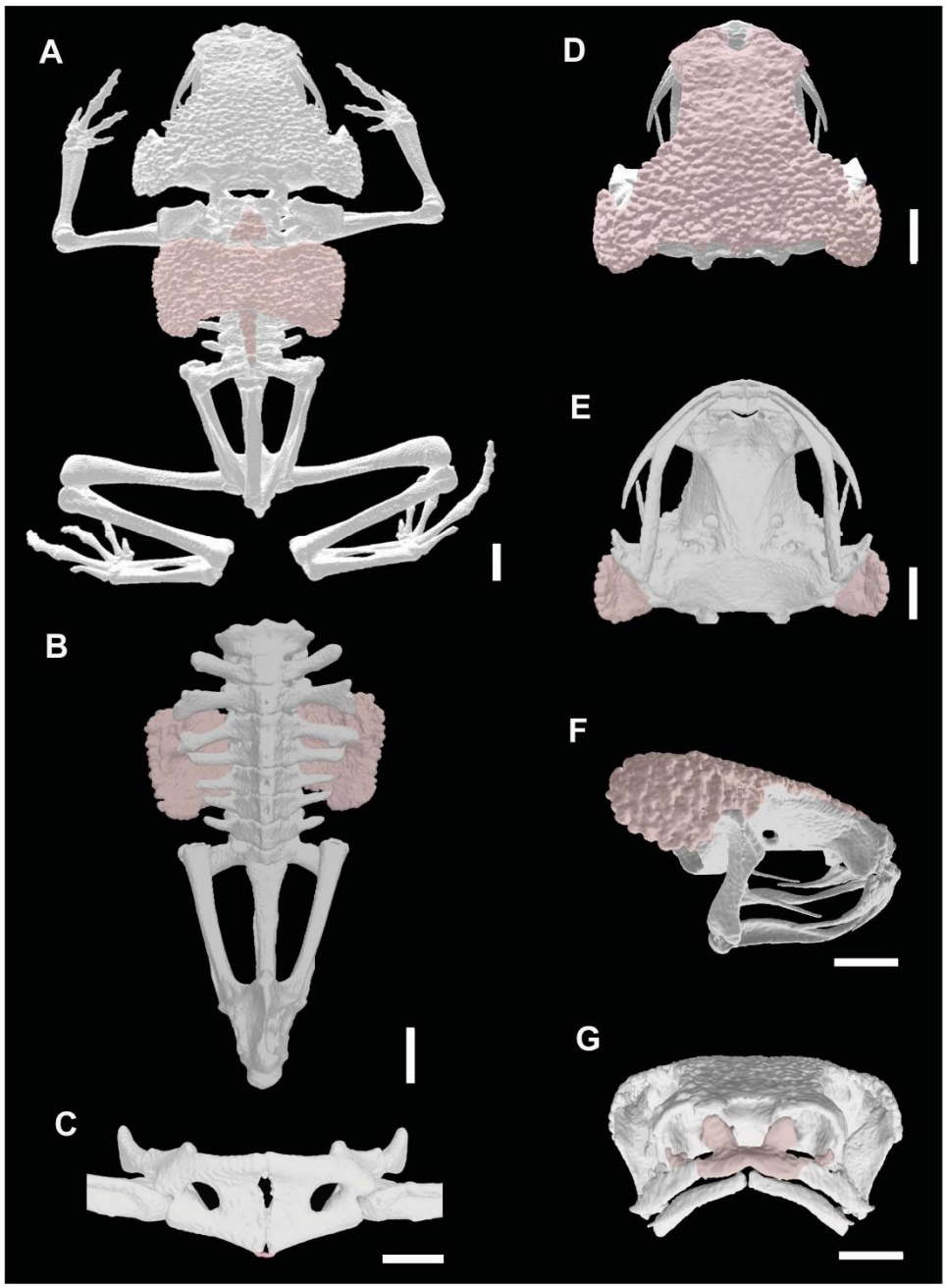


Fig. 3.—Osteological images of *Brachycephalus* ***ibitinga*** sp. nov. obtained from high-resolution microtomography (CFBH 42337; adult male). Skeleton in dorsal (A) and ventral (B) views, with the ornamented dermal bones represented by the spinal and paravertebral plates (in red); pectoral girdle in ventral view (C), showing the sternum (in red); skull in (D) dorsal, (E) ventral, and (F) lateral views, with the dermal bones represented by the ornamented skull and parotic plates (in red); skull in frontal view (G), with premaxillae and septomaxillae (in red). Nomenclature for additional bone elements follows Campos et al. (2011). Scale bars = 1 mm. A color version of this figure is available online.

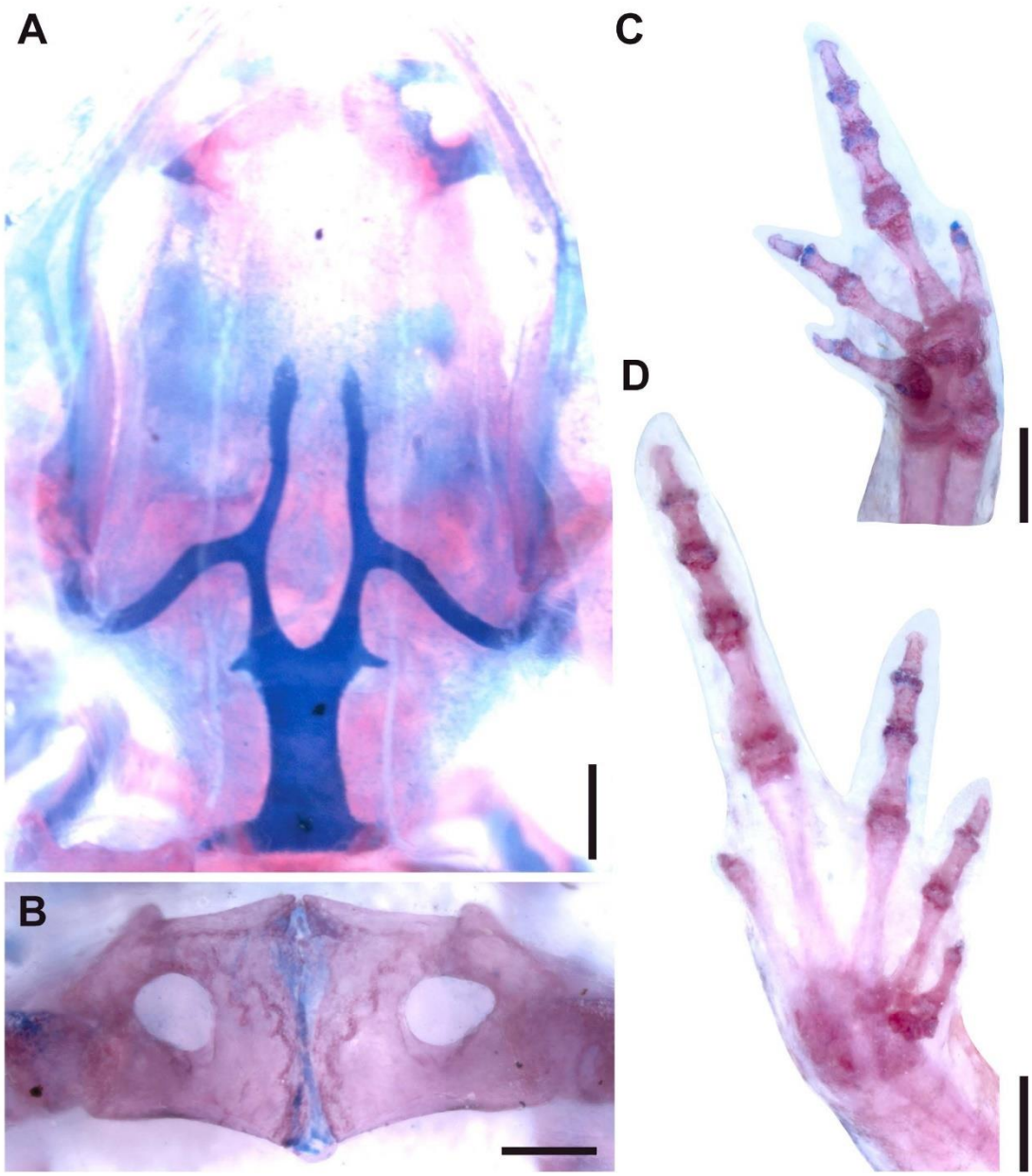


FIG. 4.—Details of the hyoid plate (A), pectoral girdle (B), left hand (C), and right foot (D) of *Brachycephalus* ***ibitinga*** sp. nov. obtained from pictures of a cleared and double-stained specimen (MZUSP 135743; adult male). Bones in gray, cartilage in blue. Scale bars = 1 mm. A color version of this figure is available online.

(collected on 6 December 2009), CFBH 28209 (collected on 6 November 2009), and a juvenile CFBH 28210 (collected on 5 May 2010), at Parque Natural Municipal das Nascentes de Paranapiacaba, municipality of Santo André, state of São Paulo, Brazil (23°46′55″S, 46°17′42″W, 975 m a.s.l.) by V.C. Trevine and collaborators. CFBH 37864, adult female, collected at Parque Natural Municipal das Nascentes de Paranapiacaba, municipality of Santo André, state of São

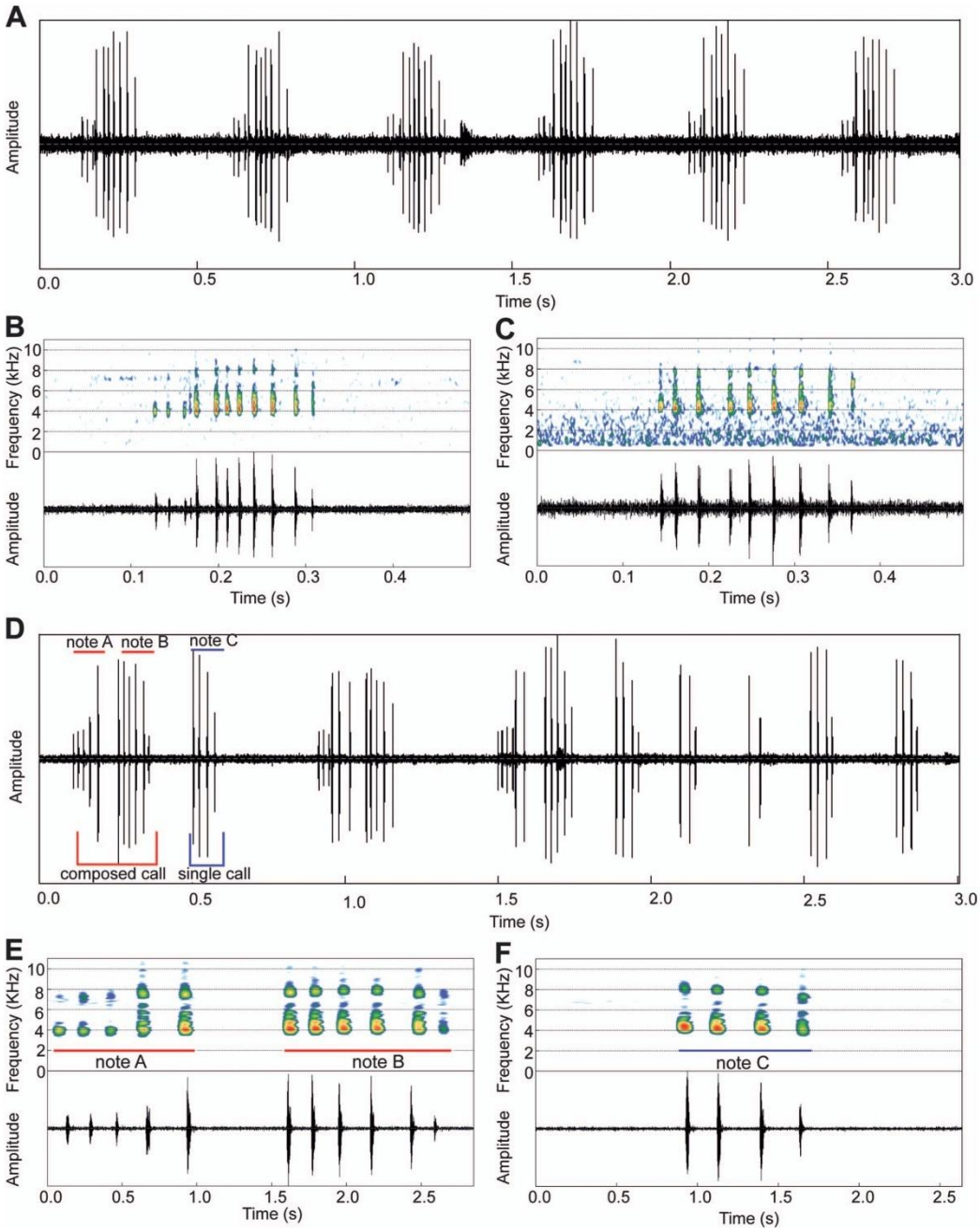


Fig. 5.—Advertisement and aggressive calls of *Brachycephalus* ***ibitinga*** sp. nov. (A) Oscillogram of six advertisement calls (unvouchered; recording CBUFMG 1077); detailed spectrograms (above) and oscillograms (below) of a single advertisement call from (B) the type locality (unvouchered; recording CBUFMG 1077) and (C) from the municipality of Santo André (CFBH 42337; recording ML 273937); (D) oscillogram of nine aggressive calls; detailed spectrogram (above) and oscillogram (bellow) of (E) the composite aggressive call and (F) the single aggressive call (unvouchered; recording CBUFMG 1078). A color version of this figure is available online.

Paulo, Brazil (23°46′41″S, 46°17′39″W, 912 m a.s.l.), on 28 February 2011, by V.C. Trevine, P. Machado, B.V.M. Berneck, and C.S. Cassini. CFBH 42337, adult male, collected at Picada Washington Luís, Reserva Biológica do Alto da Serra de Paranapiacaba (REBio Paranapiacaba), municipality of Santo André, state of São Paulo, Brazil (23°46′53″S, 46°18′48″W, 780 m a.s.l.), on 4 October 2017, by F. Schunck and K.E. Rodrigues.

Referred specimens.—CFBH 19348, adult female, collected at Parque Estadual da Serra do Mar, Núcleo Curucutu, municipality of Itanhaém, state of São Paulo, Brazil (24°00′36″S, 46°46′57″W, 720 m a.s.l.), on 17 November 2007, by L.R. Malagoli, F. Schunck, and A.S. Monteiro. CFBH 25809 and 25816, adult females, collected at Parque Estadual da Serra do Mar, Núcleo Curucutu, municipality of Itanhaém, state of São Paulo, Brazil (24°00′36″S, 46°46′57″W, 720 m a.s.l.), respectively on 11 and 12 January 2009, by L.R. Malagoli and F. Schunck. CFBH 32311, adult female, collected at Parque Estadual da Serra do Mar, Núcleo Curucutu, municipality of Juquitiba, state of São Paulo, Brazil (24°02′07″S, 46°55′45″W, 750 m a.s.l.), on 7 December 2010, by L.R. Malagoli and F. Schunck. CFBH 44436, adult male, collected at Parque Estadual da Serra do Mar, Núcleo Itutinga-Pilões, municipality of São Vicente, state of São Paulo, Brazil (23°58′56″S, 46°35′35″W, 800 m a.s.l.), on 2 December 2015, by L.R. Malagoli, D. Baêta, and F. Schunck. CFBH 44437 and 44438, juveniles, collected at Caminhos do Mar, Parque Estadual da Serra do Mar, Núcleo Itutinga-Pilões, municipality of São Bernardo do Campo, state of São Paulo, Brazil (23°51′23″S, 46°27′27″W, 753 m a.s.l.), on 11 January 2017, by L.R. Malagoli and B. Rocha. CFBH 38013, adult male, collected at Pousada dos Pescadores, municipality of São Bernardo do Campo, state of São Paulo, Brazil (23°48′28″S, 46°28′54″W, 770 m a.s.l.), on 24 September 2014, by L.B.S. Arruba. CFBH 11623, adult female, collected at Parque Natural Municipal Varginha, Peninsula do Bororé, left bank of the Represa Billings, municipality of São Paulo, state of São Paulo, Brazil (23°47′49″S, 46°40′17″W, 795 m a.s.l.), on 31 March 2006, by L.R. Malagoli. MNRJ 42873, juvenile, collected at Alto da Serra de Cubatão, state of São Paulo, Brazil (nongeoreferenced data), on 31 October 1940, by B. Lutz and J. Venâncio. MZUSP 8858, sex undetermined, collected at REBio Paranapiacaba, municipality of Santo André, state of São Paulo, Brazil (nongeoreferenced data), on 10 October 1951, by P.E. Vanzolini and W.C.A. Bokermann. MZUSP 93350 and 93351, sex undetermined, collected at Paranapiacaba, state of São Paulo, Brazil (nongeoreferenced data), on 25–26 January 1997, by P. Rocha and Casari. Ten specimens, sex undetermined, MZUSP 143856–143858 (collected on 15 September 2009, by P. Bernardo and collaborators), MZUSP 143859–143862 (collected on 11 December 2010 to 6 November 2010, by V.C. Trevine), MZUSP 143863–143865 (collected on 6–7 December 2009, by P. Bernardo), at Parque Natural Municipal das Nascentes de Paranapiacaba, municipality of Santo André, state of São Paulo, Brazil (23°46′10″S, 46°17′05″W, 940 m a.s.l.). MNRJ 25367, juvenile, collected at Paranapiacaba, state of São Paulo, Brazil (nongeoreferenced data), on October 1983, by A.J. Cardoso and C.F.B. Haddad.

Diagnosis.—The new species is distinguished from all of its congeners by the combination of the following characters: (1) presence of cranial and postcranial ornamented bone plates; (2) parotic plates covering the squamosal and pro-otics, and also the auditory capsule in lateral view; (3) paravertebral plates heavily developed and ornamented, forming the dorsal bone shield; (4) small body size in adult males (11.5–12.7 mm of SVL; in average 12.2 ± 0.4 mm); (5) parotic and paravertebral bone plates externally bordered with a rough pale contour; (6) paravertebral plates slightly convex with rounded lateral edges and not expanded to the lateral surface of the body; (7) transverse processes of vertebrae IV and V distally fused and associated to paravertebral plates; (8) absence of small dotted osteoderms; (9) discrete spinal plates along the main spinal axis; (10) fingertip I pointed, II and III arrow-shaped, and IV reduced and rounded; (11) toetips I and V with small terminal phalangeal elements rounded in shape, toetip II pointed, and toetips III and IV arrow-shaped; (12) deep hyoglossal sinus and absence of postero-lateral processes at the hyoid plate; and (13) advertisement call characterized by one note repeated in sequence, commonly comprised of 8–12 pulses.

Comparisons.—The presence of cranial and postcranial ornamented bone plates distinguishes the new species from the species lacking these traits: *Brachycephalus actaeus* (Monteiro et al. 2018a), *Brachycephalus albolineatus* (Bornschein et al. 2016), *Brachycephalus auroguttatus* (Ribeiro et al. 2015), *Brachycephalus boticario* (Ribeiro et al. 2015), *Brachycephalus brunneus* (Ribeiro et al. 2005), *Brachycephalus coloratus* (Ribeiro et al. 2017), *Brachycephalus curupira* (Ribeiro et al. 2017), *B. didactylus* (Izecksohn 1971), *Brachycephalus ferruginus* (Alves et al. 2006), *Brachycephalus fuscolineatus* (Ribeiro et al. 2015), *Brachycephalus hermogenesi* (Giaretta and Sawaya 1998), *Brachycephalus izecksohni* (Ribeiro et al. 2005), *Brachycephalus leopardus* (Ribeiro et al. 2015), *Brachycephalus mariaeterezae* (Ribeiro et al. 2015), *Brachycephalus mirissimus* (Pie et al. 2018), *Brachycephalus olivaceus* (Ribeiro et al. 2015), *Brachycephalus pernix* (Pombal et al. 1998), *Brachycephalus pombali* (Alves et al. 2006), *B. pulex* (Napoli et al. 2011), *Brachycephalus quiririensis* (Pie and Ribeiro 2015), *B. sulfuratus* (Condez et al. 2016), *Brachycephalus tridactylus* (Garey et al. 2012), and *Brachycephalus verrucosus* (Ribeiro et al. 2015). The parotic plates, covering the squamosal and pro-otics, and also the auditory capsule in lateral view, distinguishes the new species from other species that have relatively small parotic plates (in which the plates do not cover the articulation between squamosal and pro-otics, and also the auditory capsule): *B. alipioi* (Pombal and Gasparini 2006), *B. atelopoide* (Miranda-Ribeiro 1920), *B. bufonoides* (Folly et al. 2020), *B. crispus* (Condez et al. 2014; see the specimen identified as *Brachycephalus* sp. 3 in Campos et al. 2010), *B. guarani* (Clemente-Carvalho et al. 2012), *B. nodoterga* (Miranda-Ribeiro 1920; see the specimen identified as *Brachycephalus* sp. 1 in Campos et al. 2010), *B. pitanga* (Alves et al. 2009; see the specimen identified as *Brachycephalus* sp. 2 in Campos et al. 2010), *B. toby* (Haddad et al. 2010), and *B. vertebralis* (Pombal 2001; Campos et al. 2010). Additionally, in *B.* ***ibitinga*** sp. nov. the dorsal bone shield formed by the paravertebral plates is heavily developed and ornamented, differing from *B. alipioi*, *B. atelopoide*, *B. bufonoides*, *B. crispus*, *B. guarani*, *B.*

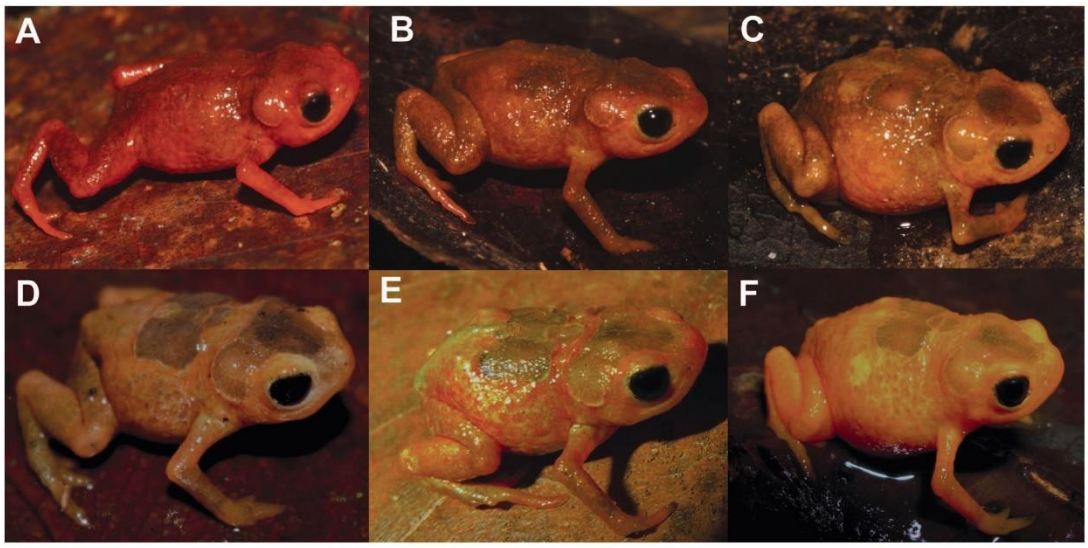


FIG. 6.—Variation of *Brachycephalus* ***ibitinga*** sp. nov. in life. CFBH 44450, adult female, Parque das Neblinas, municipality of Bertioga (A); CFBH 42337, adult male, Reserva Biológica de Paranapiacaba, municipality of Santo André (B); CFBH 28209, adult female, Parque Natural Municipal das Nascentes de Paranapiacaba, municipality of Santo André (C); CFBH 44436, adult male, Parque Estadual da Serra do Mar, Núcleo Itutinga-Pilões, municipality of São Vicente (D); CFBH 32311, adult female, Parque Estadual da Serra do Mar, Núcleo Curucutu, municipality of Juquitiba (E); CFBH 19348, adult female, Parque Estadual da Serra do Mar, Núcleo Curucutu, municipality of Itanhaém (F). Photos (A)–(C) by T.H. Condez; photos (D)–(F) by L.R. Malagoli.

nodoterga, *B. pitanga*, *B. toby*, and *B. vertebralis*, in which it is absent. Considering the group of species with the bone shield, the small body size in adult males (SVL = 11.5–12.7 mm; mean 12.2 ± 0.4 mm) distinguish the new species from *B. margaritatus* (described as a large species within the genus; SVL = 15.0–18.9 mm, adult males mean = 14.5 mm; Pombal and Izecksohn 2011; Condez et al. 2020), *B. darkside* (SVL = 14.8–18.5 mm, and the holotype, an adult male exhibits 17.9 mm; Guimarães et al. 2017), *B. garbeanus* (SVL = 14.3–17.3 mm, adult males mean = 15.2 mm; Pombal 2010, Condez et al. 2020), and *B. ephippium* (SVL = 13.0–22.0 mm, adult males mean = 14.8 mm; Condez et al. 2020). The parotic and paravertebral bone plates externally bordered with a rough pale contour distinguishes the new species from *B. darkside*, *B. ephippium*, *B. garbeanus*, and *B. margaritatus* in which the borders of the bone plates are not ornamented. The paravertebral plates slightly convex with rounded lateral edges and not expanded to the lateral surface of the body, also distinguish the new species from *B. garbeanus* and *B. margaritatus*. In *B. garbeanus* the paravertebral plates are large, and its lateral edges pointed and curved ventrally (Pombal 2010), and in *B. margaritatus* the lateral edges are curved ventrally (Pombal and Izecksohn 2011). Additionally, the transverse processes of vertebrae IV and V fused and associated to paravertebral plates in the new species is distinct from the condition of *B. garbeanus*, in which the transverse processes of vertebrae IV–VII are fused and associated to the larger paravertebral plates (see the specimen identified as *B. ephippium* from Nova Friburgo, RJ, in Campos et al. 2010). The absence of small dotted osteoderms distinguishes the new species from *B. margaritatus*, in which the dorsal skin exhibits well-developed and sparse dotted osteoderms (Pombal and Izecksohn 2011; Condez et al. 2014). The discrete spinal plates along the main spinal axis distinguish the new species from *B. darkside*, in which the ornamentation on vertebrae VII and VIII are well developed and clearly visible externally (Guimarães et al. 2017). The tips of the terminal phalangeal elements of fingers and toes in the new species (fingertip I pointed, II and III arrow-shaped, and IV reduced and rounded; toetips I and V with small terminal phalangeal elements rounded in shape, toetip II pointed, and toetips III and IV arrow-shaped) distinguishes the new species from *B. ephippium* (fingertips I and IV pointed; toetip I with terminal phalangeal element small and rounded in shape, toetips II–IV arrow-shaped, and V pointed; Campos et al. 2010); and also from *B. darkside* (fingertips I–IV and toetip II arrow-shaped; Guimarães et al. 2017). The deep hyoglossal sinus and the absence of posterolateral processes at the hyoid plate also distinguish the new species from *B. ephippium* (posterolateral processes much reduced; Trewavas 1932), and from *B. garbeanus* (shallower hyoglossal sinus and alary and posterolateral processes about the same size; this study). Finally, the main structure of the advertisement call of the new species, characterized by one note repeated in sequence, commonly comprised of 8–12 pulses, distinguishes it from the advertisement call of *B. actaeus*, *B. albolineatus*, *B. hermogenesi*, *B. mirissimus*, *B. olivaceus*, *B. pernix*, *B. quiririensis*, and *B. tridactylus* (in which the number of pulses per notes varies from 1 to 4; Bornschein et al. 2018; Monteiro et al. 2018a,b; Pie et al. 2018; Bornschein et al. 2019b), and also from *B. darkside* (notes comprised of

6–8 pulses; Guimarães et al. 2017). Additionally, the dominant frequency of the advertisement call ranging from 4.0 to 4.3 kHz (in average 4.1 ± 0.06) in new species is also distinct from the described for *B. darkside*: 2.8–3.7 kHz (in average 3.4 ± 1.8; Guimarães et al. 2017) and *B. sulfuratus*: 6.2–7.2 kHz (in average 6.7 ± 0.3 kHz; Condez et al. 2016).

Description of holotype.—Adult male, SVL = 12.5 mm, body robust, bufoniform; head wider than long (HL/HW = 0.72); head length is 23% of SVL; snout short, rounded in dorsal, ventral, and lateral views (Fig. 2A–E). Nostril slightly protuberant and anterolaterally directed; canthus rostralis indistinct; loreal region slightly concave; eye protruding laterally and dorsally; eye diameter 48% of head length; tympanic annulus absent; lips nearly sigmoid (Fig. 2C,D). Vocal sac not expanded externally; vocal slits present; tongue longer than wide, with the posterior half not adherent to floor of mouth; vomerine teeth absent; choanae small and ovoid, anterior to eyes. A cranial ornamented bone plate, the parotic plate, is externally visible from the tip of the snout to the end of the skull, being expanded laterally. In lateral view, this plate is large and rounded, about the same size of the eye; parotic plate length does not trespass the inferior border of the eye (Fig. 2C). Dorsum covered by ornamented postcranial bone plates. The spinal plates in the main vertebral axis are represented by discrete rounded-shaped ornamentation; paravertebral plates are heavily developed and ornamented, forming the dorsal bone shield that is observed medially as a narrowed and distally expanded structure; bone shield is wider than longer (width 4.3 mm and length 2.3 mm), representing 18% of the SVL (Fig. 2A). Arm and forearm moderately slender; hand with fingers I and IV reduced; finger II short but distinct; finger III large and robust; fingertips I and IV rounded, fingertips II and III pointed; finger lengths IV < I < II < III; subarticular tubercles absent; inner and outer metacarpal tubercles absent (Fig. 2E). Leg relatively short, moderately robust; thigh length 38% of SVL; tibia length 82% of thigh length; foot with toes I and V reduced; toe II short and distinct; toes III and IV large and robust; toe lengths I < V < II < III < IV; tips of toes I, II, III, and V rounded, tip of toe IV pointed; subarticular tubercles absent; inner and outer metatarsal tubercles absent (Fig. 2F). General dorsum smooth, except for the rough top of the head and bone shield, clearly distinct due to the ornamented surface of skull and postcranial plates (Fig. 2A). Skin on arm, leg, dorsum, and venter with small granules; lateral surface of the belly and area around the cloacal opening slightly rough (Fig. 2B).

Measurements of holotype (in mm).—SVL 12.5; HL 2.9; HW 4.0; ND 0.4; IND 1.7; ED 1.4; IOD 2.9; END 1.0; THL 5.7; TBL 4.7; FL 7.5; AL 2.6; FAL 2.9; HAL 2.4.

Color of holotype in life and preservative.—In life, general background color orange, dorsum covered by brownish blotches; cranial and postcranial bone plates bordered with a pale contour, almost white; medial skull and paravertebral plates greenish and slightly darker than the overall body color; iris black (Fig. 1). In preservative, general background body color is cream; dorsum covered by dark brown blotches; cranial and postcranial bone plates grayish (Fig. 2).

Osteology.—The cleared and double-stained and micro CT scanned specimens revealed that *Brachycephalus* ***ibitinga*** sp. nov. has ornamented dermal bones in skull and vertebral column (Fig. 3). Skull bones completely ornamented; nasals, sphenethmoid, frontoparietals, pro-otics, and exoccipitals fused (Fig. 3D,E). Nasal sculptured; the process maxillaris of the nasal in contact with the preorbital process of the maxilla (Fig. 3F,G). Cranial ornamentation expanded laterally composing the parotic plates; the plates cover the squamosal, pro-otics, and also the auditory capsule (Fig. 3F). Premaxillae broad, fused medially; alary processes of premaxillae distinct and widely separated from each other, being longer than larger, slightly separated from the nasal (Fig. 3G). Maxillae arched, odontoids absent. Septomaxillae are cylindrical paired bones in L shape, fused at the maxillae (Fig. 3G). Squamosal elongated in lateral view; anterior zygomatic ramus very reduced, not ornamented; posterior optic ramus not ornamented and partially allocated behind the parotic plate (Fig. 3F). In lateral view, quadratojugal absent; pterygoid elongated and not in contact with the maxillary arch (Fig. 3F). In ventral view, parasphenoid and sphenethmoid fused and robust; palatine absent; vomers fused, dentigerous process absent (Fig. 3E). Tympanic annulus absent; fenestra ovalis completely covered by the operculum; operculum circular and cartilaginous, bearing small bony processes. We were not able to identify the collumela. Mandible edentate; paired mentomekelian bones clearly separated from each other and fused to dentary; posterior end of angulosplenial bones expanded. Hyoid plate longer than wide, lateral slightly concave; alary processes reduced, posterolateral processes absent (Fig. 4A). Hyale projections long and curved in the posterior end; anterior processes of hyale long and straight, slightly expanded on its distal half; anterior processes of hyale about the same size of hyoid plate, forming a deep hyoglossal sinus. Posteromedial processes of the hyoid cylindrical and completely mineralized. Pectoral girdle arciferal and robust (Fig. 3C); procoracoid and epicoracoid fused with clavicle, coracoid, and scapula; clavicle separated from the coracoid by an ovoid fenestra; epicoracoid cartilaginous (Fig. 4B); cartilaginous omosternum undistinguishable; reduced cartilaginous sternum with the distal portion calcified (Fig. 4B); supraescapula expanded, its anterior half ossified as cleithrum. Vertebral column well developed and ornamented with dermal bones, covered by small spinal plates associated to the dorsal main vertebral axis, and large paravertebral plates, associated to the transverse processes of vertebrae (Fig. 3A,B). Eight presacral and nonimbricate vertebrae form the vertebral column; in ventral view, presacral vertebrae IV and V fused. First presacral vertebra with transverse processes indistinguishable; presacral vertebrae II and VI–VIII with slender unornamented transverse processes; extremities of transverse processes of vertebra III expanded but not forked; transverse processes of vertebrae IV and V associated to the paravertebral plates; lengths of transverse processes of presacrals: VIII ~ VII < VI < II < V < IV < III (Fig. 3B). Two trapezoidal and large paravertebral plates, disposed at each side of the vertebral column, compose the conspicuous dorsal bone shield (Fig. 3A); the paravertebral plates are heavily developed and ornamented, and cover completely the transverse processes of vertebrae IV–VII, and partially the transverse processes of vertebrae III; paravertebral plates are slightly convex, but not expanded to the lateral surface of the body; lateral edges rounded. In dorsal

view, spinal plates in vertebrae I and II resemble together a triangle-shaped ornamentation not clearly distinguished externally; in vertebra III the spinal process joints the paravertebral plates; the paravertebral plates cover the spinal processes of vertebrae IV–VI; vertebrae VII and VIII have discrete ornamentation, not visible externally. Sacral diapophyses expanded; urostyle length slightly larger than the set of presacral vertebrae. Humerus about the same size of forearm; radius and ulna completely fused but distinguishable (Fig. 3A). Manus with radiale and ulnare about the same size; distal carpals (II–IV) fused; a large element y; a single prepollical element present; palmar sesamoid elements present; phalangeal formula 1–2–3–1; tip of the terminal phalangeal element of finger I pointed, tips of fingers II and III arrow-shaped, tip of the terminal phalangeal element of finger IV reduced and rounded (Fig. 4C). Hindlimb with tibia and fibula completely fused but distinguishable, forming the tibiafibula; tibiafibula and femur about the same size; tibiale and fibulare fused at their distal and proximal ends (medially not fused); a single sesamoid element present in knee joint (Fig. 3A). Pes with distal tarsal element I, II, III, and IV present and V absent; element y and plantar sesamoid elements present. One very reduced prehallical element; phalangeal formula 1–2–3–4–1; toes I and V with small terminal phalangeal element rounded in shape, tip of Toe II pointed, tips of toes III and IV arrow-shaped (Fig. 4D).

Advertisement and aggressive calls.—One calling male was recorded twice at Parque das Neblinas, municipality of Bertioga, state of São Paulo, Brazil (23°44′49″S, 46°07′42″W, 790 m a.s.l.), on 25 October 2006, respectively 1043 h and 1110 h, air temperature 19°C (unvouchered, recordings CBUFMG 1077–1078). A second calling male was recorded at Reserva Biológica do Alto da Serra de Paranapiacaba (23°46′53″S, 46°18′48″W, 780 m a.s.l.), municipality of Santo André, state of São Paulo, Brazil, on 4 October 2017, 0720 h, air temperature 21°C, air relative humidity 100%, weather with windy conditions (voucher specimen CFBH 42337, recording ML 273937; https://macaulaylibrary.org/asset/273937). Recordings from the type locality have 80 advertisement calls and 93 aggressive calls (sensu Toledo et al. 2015), whereas the recording from the municipality of Santo André only has 37 advertisement calls. We evaluated the best calls for the advertisement call description, so it was based on 25 calls from the first recording and 23 from the second recording ($n = 48$). The advertisement call of *Brachycephalus* ***ibitinga*** sp. nov. is characterized by one note repeated in sequence, at a rate of 1.85 notes/s ($n = 48$; Fig. 5A). Both recorded males repeated the call several times uninterrupted, evidencing a long calling activity. The call (or note) lasts 0.18–0.25 s (0.22 ± 0.02; $n = 48$) and the intercall (or internote) interval is 0.28–0.37 s (0.32 ± 0.03; $n = 46$; Fig. 5B,C). Notes are comprised of 8–12 pulses (10 ± 1; $n = 48$; Fig. 5B,C). The notes in the advertisement call from the type locality exhibit increasing amplitude modulations (Fig. 5B), which was not observed in the advertisement call from the municipality of Santo André (Fig. 5C). The lower frequency is 3.0–3.9 kHz (3.7 ± 0.20; $n = 48$), the upper frequency is 6.0–7.7 kHz (7.0 ± 0.55; $n = 48$), and the dominant frequency is 4.0–4.3 kHz (4.1 ± 0.06; $n = 48$; Fig. 5B, C). Most of the energy (90%) is concentrated within 1.1–4.7 kHz (2.4 ± 1.41; $n = 48$) and the highest energy concentration throughout the entire call was variable, with rise time ranging from 2% to 71% of call length (39 ± 19; $n = 48$; Fig. 5B,C). Except for the temporal parameters, the general structure of the advertisement calls of *B.* ***ibitinga*** sp. nov. overlaps those described for *B. crispus* and *B. pitanga* (Condez et al. 2014; Oliveira and Haddad 2017).

We identified two distinct aggressive calls in *Brachycephalus* ***ibitinga*** sp. nov. (Fig. 5D). The first call, composed by Note A and Note B, lasts 0.22–0.29 s (0.25 ± 0.02; $n = 25$). When repeated in sequence the repetition rate is 0.33 calls/s ($n = 10$). Note A is comprised of 5–6 pulses (6 ± 0; $n = 25$), lasts 0.08–0.14 s (0.11 ± 0.02; $n = 25$), and exhibits increasing amplitude modulations (Fig. 5E). Its lower frequency is 3.6–3.9 kHz (3.7 ± 0.06; $n = 25$), the upper frequency is 5.4–7.7 kHz (7.1 ± 0.68; $n = 25$), and the dominant frequency is 3.9–4.3 kHz (4.0 ± 0.09; $n = 25$). Note B is comprised of 4–7 pulses (6 ± 1; $n = 25$), lasts 0.08–0.14 s (0.11 ± 0.01; $n = 25$), and exhibits decreasing amplitude modulations (Fig. 5E). Its lower frequency is 3.8–4.0 kHz (3.9 ± 0.04; $n = 25$), the upper frequency is 5.4–7.8 kHz (6.8 ± 0.75; $n = 25$), and the dominant frequency is 3.9–4.4 kHz (4.1 ± 0.11; $n = 25$). The internote interval is 0.01–0.05 s (0.03 ± 0.01; $n = 25$; Fig. 5E). The second call is characterized by a single note (note C) and lasts 0.02–0.12 s (0.09 ± 0.02; $n = 50$). The note C is comprised of 1–7 pulses (4 ± 1; $n = 50$), the lower frequency is 3.6–4.0 kHz (3.9 ± 0.07; $n = 50$), the upper frequency is 4.7–7.8 kHz (6.5 ± 0.94; $n = 50$), and the dominant frequency is 4.0–5.5 kHz (4.3 ± 0.23; $n = 50$; Fig. 5F). This note (or call) repetition rate is 0.22 calls/s ($n = 15$). Our recordings suggest *B.* ***ibitinga*** sp. nov. probably combine these calls in distinct aggressive contexts. Definitely, the low intensity of the calls and the cryptic activity of calling males, make recording this species and studying natural history a challenge. Further studies are necessary to investigate the social context of aggressive calls.

Variation.—Type series of *Brachycephalus* ***ibitinga*** sp. nov. is composed of 10 adult males, 15 adult females, and six juveniles. Morphometric variation in adults is given in Table 1. In our sample, females are larger than males (mean SVL of females = 14.6 ± 1.0 mm; mean SVL of males = 12.2 ± 0.4 mm, Welch's t-test $t = 7.8$, df = 18.9, $P < 0.01$). We found no significant variation in body size across the geographic range of the new species. The greatest variation in *B.* ***ibitinga*** sp. nov. refers to the general body color, in which the background color varies from completely orange (Fig. 6A) to predominantly yellow (Fig. 6F). Additionally, the distinctiveness of the bone ornamentation, externally revealed by the color, size, and shape of cranial and postcranial bone plates, also contributes to the variation in the new species. The parotic and paravertebral bone plates of *B.* ***ibitinga*** sp. nov. are always bordered with a pale contour, while the color contrast with the background varies. The bone plates can be similar to the background color (Fig. 6A,C), or contrast in dark brown and green (Fig. 6B,D–F). The combination of the background and the bone plates colors are responsible for the general brownish (Fig. 6B), pallid (Fig. 6D), or greenish (Fig. 6E) aspect of some specimens. According to Campos et al. (2010), bone ornamentation is defined considering the amount of mineralized spicules in cranial and postcranial bones that project to the dermis, a process related to heterochrony

(Trueb and Alberch 1985). The size and shape of cranial and postcranial bone plates are variable ontogenetically in the new species, similar to what was described for *B. ephippium* (Campos et al. 2010). The parotic and paravertebral plates of juveniles are poorly developed, smaller, or less distinct than observed in the adult specimens.

Etymology.—The specific epithet *ibitinga* is a Portuguese noun derived from the indigenous Tupi-Guarani words yby + tinga. These words mean respectively "land" and "white," which together compose a name applied to describe the fog, or mist condition characteristic from the mountains at the Atlantic Forest, where the new species occurs. In Portuguese, the translation for this weather condition is "Neblina": the whitish perception and limited visibility typically caused by fine water droplets suspended in the atmosphere. The type locality "Parque das Neblinas" is also named after this atmospheric condition.

Natural history.—*Brachycephalus* ***ibitinga*** sp. nov. is a ground-dwelling species, living amidst the leaf-litter in preserved Dense Ombrophilous Atlantic Forest remnants. Individuals are rarely observed walking on the leaf-litter, being usually found during the day, underneath tangled roots, below fallen trunks, inside fallen bromeliads and other ground shelters, or directly sitting on the ground under deep layers of leaf litter. Males are not exposed during the calling activity, which is diurnal and concentrated in cloudy and rainy days with temperatures around 20°C during the rainy season (from September to March). In September 2009 an amplected pair was found hidden under the leaf litter at the municipality of Santo André.

Geographic distribution.—*Brachycephalus* ***ibitinga*** sp. nov. is known from distinct localities at the Serra do Mar mountain range, including the regionally named Serra de Paranapiacaba, in the central coast of the state of São Paulo, southeastern Brazil (Fig. 7). Its occurrence extends from the escarpments through the continental Atlantic Plateau in moderate to high elevation areas (from 700 to 1000 m a.s.l.), at the municipalities of Bertioga, Cubatão, Itanhaém, Juquitiba, Santo André, São Bernardo do Campo, São Paulo, and São Vicente. From the type locality, at the municipality of Bertioga, the occurrence of *B.* ***ibitinga*** sp. nov. extends about 90 km southward, to the municipality of Juquitiba. Populations of the new species were mostly found inside legally protected areas at the Atlantic Forest domain. However, the geographic range of the new species encompasses the southern borders of São Paulo, the largest and most populous city of South America. Together with São Paulo, the municipalities of Santo André, São Bernardo, and Juquitiba, where the new species occurs, are included in the São Paulo metropolitan region, which currently harbors more than 21.5 million people (IBGE 2018). Additionally, the municipalities of Bertioga, Cubatão, Itanhaém, and São Vicente are also part of the Baixada Santista metropolitan region (which currently harbors 1.8 million people; IBGE 2018).

Molecular phylogenetics.—The new species was recovered as a monophyletic and well-supported clade in both the Bayesian phylogenetic inference and the maximum parsimony reconstructions (BPP = 1; jackknife absolute frequency = 98; Fig. 8). Its position was recovered within the extreme hyperossified species of pumpkin toadlets with bone shield (*Brachycephalus garbeanus*, *B. ephippium*, *B. darkside*, and *B. margaritatus*). Additionally, our results confirm the phylogenetic position of *B. darkside* within this clade. In this hyperossified clade, *B. ephippium* from Vale da Revolta, Parque Nacional da Serra dos Órgãos, and Reserva Ecológica de Guapiaçu, state of Rio de Janeiro, were paraphyletic with respect to other sampled populations of the same species. We then attributed the name *Brachycephalus* sp. (aff. *ephippium*) for the populations from Serra do Japi (municipality of Jundiaí), Serra do Itapeti (municipality of Mogi das Cruzes), state of São Paulo, and Serra do Alambari (municipality of Resende), state of Rio de Janeiro, for further taxonomic evaluation (Fig. 8). According to our results, the relationships between *Brachycephalus* sp. (aff. *ephippium*), *B. darkside,* and *B. margaritatus* must be also further investigated.

Based on the genetic distances for the partial 16S rRNA gene the new species differs from *Brachycephalus* sp. (aff. *ephippium*) by 2.2%, from *B. margaritatus* by 2.5%, from *B. darkside* by 3.1%, from *B. ephippium* by 3.3%, and from *B. garbeanus* by 4.5% (Table 2). The highest divergence within the extreme hyperossified species of *Brachycephalus* is found between *B. garbeanus* and all other species, except *B. margaritatus* (5.7%–7.4%; Table 2). *B. margaritatus* only differs 0.2% from *Brachycephalus* sp. (aff. *ephippium*), and 1.0% from *B. darkside*, which is equivalent to the observed intraspecific divergences. The genetic divergence within the populations of *B.* ***ibitinga*** sp. nov. varies from 0% to 1.5%, similar to other species within this group (up to 1.2% in specimens of *B. garbeanus* and 1.3% in specimens of *Brachycephalus* sp. [aff. *ephippium*]; Table 2). The distance between specimens of *B.* ***ibitinga*** sp. nov. from the municipality of Santo André varies from 0% to 0.2%, and specimens from the type locality vary from 0% to 1.1%. Specimens from Bertioga and Santo André municipalities also differ 0%–1.1%, and the geographic distance between these localities do not exceed 17 km in a straight line. The specimens from São Paulo and São Vicente municipalities differ 0.6% from each other, and both populations essentially differ from the other specimens examined in 0.2%–1.4%. The specimens from Juquitiba differ 0.4%–1.2% from the other specimens examined, and the highest genetic divergence within *B.* ***ibitinga*** sp. nov. (1.5%) is found between the type specimens and the specimens from Itanhaém municipality. Unfortunately, we were not able to include any DNA sample from São Bernardo do Campo municipality in our analyses because of the low quality of the genetic material.

Our main results corroborate the previously published phylogenetic hypothesis and also reinforce the relatively low genetic divergence within clades (Condez et al. 2020). The Bayesian phylogenetic inference and the maximum parsimony reconstructions showed concordant topologies, diverging only in the position of the flea-toads *Brachycephalus hermogenesi* and *B. pulex*, in addition to the poorly supported internal relationships within *B. pernix* group (Fig. 8, see also Supplemental Fig. S1, available online). The incongruences among the most parsimonious trees involve the flea-toads *B. pulex* and *B. hermogenesi*, which are the sister taxon to the remaining *Brachycephalus* species or were recovered embedded within the main group; and seven species terminals in the *B. pernix* group: *B. boticario*, *B. brunneus*, *B. coloratus*, *B. fuscolineatus*, *B. izecksohni*, *B*

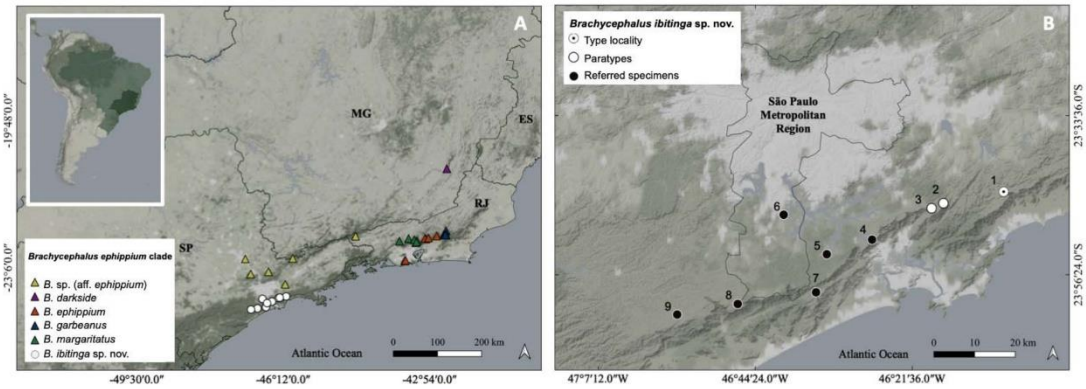


Fig. 7.—Geographic distribution of the hyperossified species within the *Brachycephalus ephippium* clade (A), and occurrence of *Brachycephalus* ***ibitinga*** sp. nov. in the state of São Paulo, southeastern Brazil (B). (1) Parque das Neblinas, municipality of Bertioga; (2) Parque Natural Municipal Nascentes de Paranapiacaba, and (3) Reserva Biológica de Paranapiacaba, both at municipality of Santo André; (4) Parque Estadual da Serra do Mar, Núcleo Itutinga-Pilões, municipality of São Bernardo do Campo; (5) Alto da Serra (approximated coordinates), municipality of Cubatão; (6) Parque Natural Municipal Varginha, municipality of São Paulo; (7) Parque Estadual da Serra do Mar, Núcleo Itutinga-Pilões, municipality of São Vicente; (8) Parque Estadual da Serra do Mar, Núcleo Curucutu, municipality of Itanhaém; and (9) Parque Estadual da Serra do Mar, Núcleo Curucutu, municipality of Juquitiba. Stamen Terrain was used as the background image, obtained with the Quick Map Services Complement in QGIS v3.12 (QGIS Development Team 2020). Light-colored areas on the detailed map represent the metropolitan regions of São Paulo (at the Atlantic Plateau) and Baixada Santista (at the coastal lowlands); the polygon represents the municipality of São Paulo. A color version of this figure is available online.

mariaeterezae, and *B. olivaceus*. Our results support the sister position of the flea-toads *B. didactylus* (related to the *B. ephippium* and *B. vertebralis* clades), and *B. sulfuratus* (related to the *B. pernix* clade). However, the deepest divergences within *Brachycephalus*, especially regarding the position of *B. pulex*, remain unresolved. The inclusion of other molecular markers might contribute to solving poorly supported relationships in *Brachycephalus*, especially those within the *B. pernix* species group, which is mainly evaluated based on a single small fragment of the 16S rRNA gene.

Discussion

The genus *Brachycephalus* was considered monotypic for more than a century (Fitzinger 1826; Miranda-Ribeiro 1920). The hyperossified pumpkin toadlet *B. ephippium* was the earliest described species in the genus, and in the original description, both the cranial and postcranial bone plates were already highlighted (Spix 1824). The type locality of *B. ephippium* was originally designated as "Provincia Bahiae," and later attributed to the municipality of Ilhéus, state of Bahia, northeastern Brazil (Bokermann 1966), probably because of a labeling error (Pombal et al. 1998). However, until recently there was no evidence for the occurrence of this species in northeastern Brazil. The type locality is consensually assumed to be in the city of Rio de Janeiro or surroundings, localities visited by Spix and Martius during their field expeditions, and where *B. ephippium* is still locally abundant (Pombal et al. 1998). Using only the presence of a dorsal bone shield as diagnosis, several populations under the name *B. ephippium* are currently found in the states of São Paulo, Rio de Janeiro, and Minas Gerais (Bornschein et al. 2019a; Condez et al. 2020). The resurrection of *B. garbeanus* (Pombal 2010) and the description of *B. margaritatus* (Pombal and Izecksohn 2011) began to reveal the diversity within this extremely hyperossified group of species. Clemente-Carvalho et al. (2011b) described some osteological and molecular divergences between *B. ephippium* from the municipality of Nova Friburgo, state of Rio de Janeiro (thereafter named *B. garbeanus*), and some populations of *B. ephippium* from the state of São Paulo (municipalities of Atibaia, Jundiaí, and São José dos Campos, state of São Paulo; herein identified as *Brachycephalus* sp. (aff. *ephippium*). Even considering the recent description of *B. darkside* (Guimarães et al. 2017), several divergent populations under the name *B. ephippium* remain poorly studied across its distribution and deserve further attention.

Hyperossification has evolved independently several times in phylogenetically and ecologically diverse anuran lineages (Blotto et al. 2020; Paluh et al. 2020). So, distinct explanatory hypotheses regarding its function might arise, such as the correlation with shifts in body size and specialized ecology, particularly regarding the morphological changes into multiple novel shapes and functions (Paluh et al. 2020). The extremely hyperossified species of the *Brachycephalus ephippium* clade also have the largest body sizes within the genus, a very distinct group when compared to the plesiomorphic condition of small-bodied species that lack bone ornamentation (Condez et al. 2020). Despite never being functionally tested, the presence of additional bones and the excessive mineralization of the skull and vertebral column in *Brachycephalus* might be related to water conservation, defense against predators, or mechanical protection for living amidst the leaf litter, which clearly deserves further investigation (Condez et al. 2020). Additionally, the skull and bone shields of *B.* ***ibitinga*** sp. nov. and *B. ephippium* are fluorescent under ultraviolet light (E.C. Nardin, personal communication; Goutte et al. 2019). The fluorescent contrast to the main orange or yellow background color of *B. ephippium* was recently suggested as having a potential role in intraspecific communication (Rebouças et al. 2019). Complementary studies are neces-

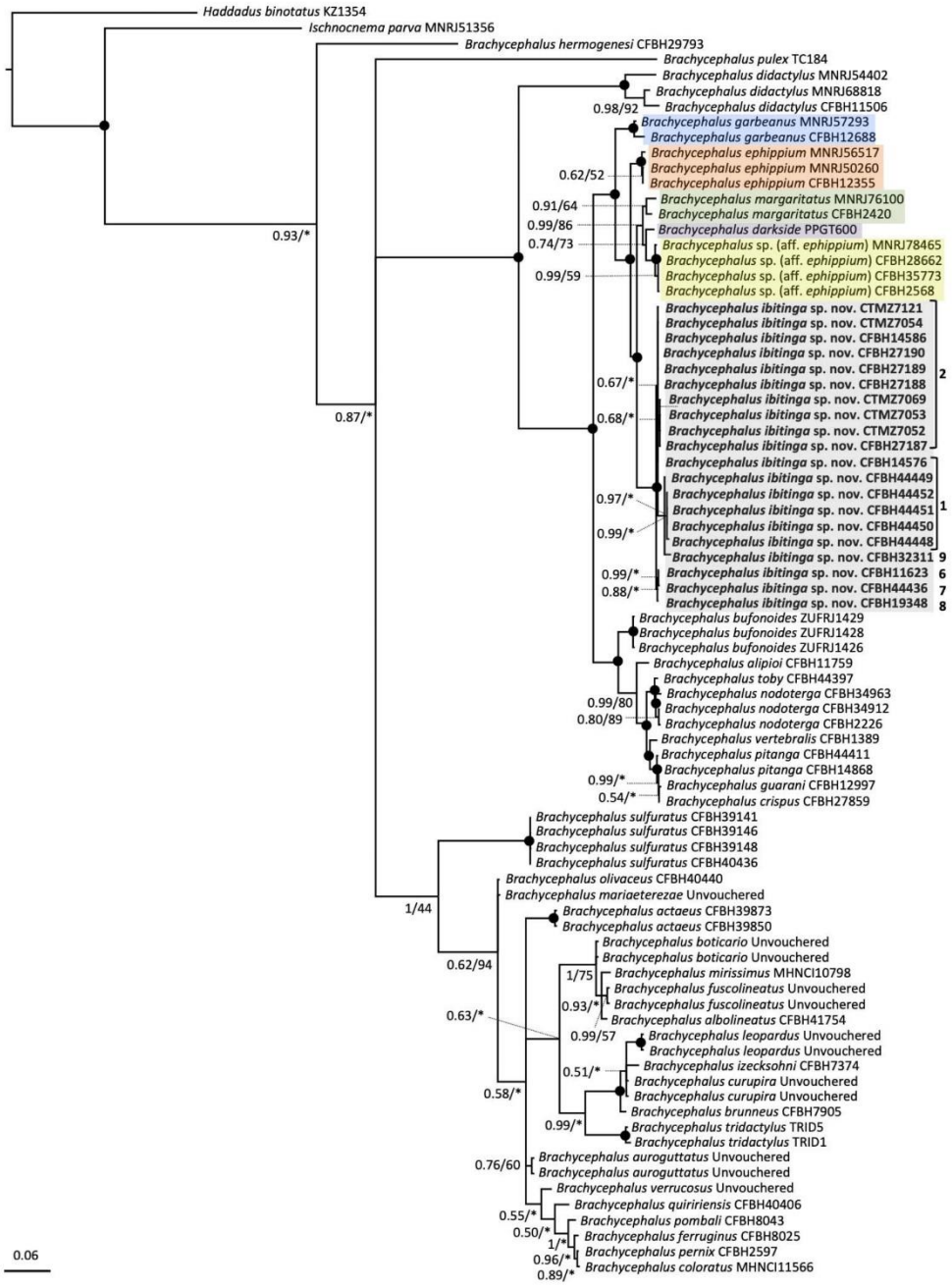


FIG. 8.—The majority rule consensus tree resulting from the Bayesian phylogenetic inference based on the alignment of 2701 bp (12S rRNA, 16S rRNA, and Cytochrome-b) showing the relationships within the genus *Brachycephalus*. Numbers below nodes represent Bayesian posterior probabilities (BPP)/ jackknife absolute frequencies (calculated on the strict consensus of the 286 most parsimonious trees of 3211 steps each; Supplemental Fig. S1). Asterisks (*) mean that the specific clade was not recovered. Black circles (•) on nodes represent BPP > 0.99 and jackknife > 90. The hyperossified species within the *B. ephippium* clade are highlighted in colors. Sequences of the new species (in bold) are from: (1) municipality of Bertioga; (2) municipality of Santo André; (6) municipality of São Paulo; (7) municipality of São Vicente; (8) municipality of Itanhaém; and (9) municipality of Juquitiba. See Supplemental Table S1 for the GenBank accession numbers. A color version of this figure is available online.

TABLE 2.—Interspecific uncorrected *p* distances based on 331 sites of the 16S rRNA gene for the pumpkin toadlets within the *B. ephippium* clade. Minimum and maximum values are reported in percentage (%). In bold, the number of analyzed individuals for each species (in parentheses), followed by the intraspecific distances.

	1	2	3	4	5	6
1 *Brachycephalus* ***ibitinga*** sp. nov.	**(20) 0–1.5**					
2 *Brachycephalus* sp. (aff. *ephippium*)	2.2–5.9	**(4) 0.5–1.3**				
3 *Brachycephalus darkside*	3.1–4.0	1.7–3.0	**(1) NA**			
4 *Brachycephalus margaritatus*	2.5–4.2	0.2–1.9	1.0–1.5	**(2) 0.4**		
5 *Brachycephalus ephippium*	3.3–5.6	2.8–4.7	3.7–3.9	1.0–2.8	**(3) 0–0.6**	
6 *Brachycephalus garbeanus*	4.5–7.4	3.7–4.7	5.4–5.7	1.0–3.7	4.0–5.8	**(2) 1.2**

sary to investigate the fluorescence within the *B. ephippium* clade and its evolutionary significance.

Our research suggests that some morphological characters must be carefully investigated within the *Brachycephalus ephippium* clade. The omosternum, an anteroventral element of the pectoral girdle, was first considered absent in *B. ephippium* (Trueb 1973; Duellman and Trueb 1986; Pombal et al. 1998), but further described as short and cartilaginous (Kaplan 2002). Despite the reported absence in *B. darkside* (Guimarães et al. 2017), this structure is probably very reduced and undistinguishable from the epicoracoid in all *Brachycephalus* species, being only visible through histological sections or even not easily preserved (Kaplan 2002; Robovská-Havelková 2010). Until today the presence of the omosternum is considered a singular characteristic for the genus *Brachycephalus* (Kaplan 2002; Padial et al. 2014). In the same way, the absence of sternum, at the posterior end of the epicoracoid cartilage, has been considered among the putative characteristics for this taxon definition (Izecksohn 1971; Hedges et al. 2008). However, we herein reported for *B.* ***ibitinga*** sp. nov. the presence of a reduced cartilaginous sternum with a calcified distal portion, a new condition for the genus *Brachycephalus*, possibly found in other hyperossified congeners. Additionally, the black epimysium in the dorsal muscles of *B. darkside* is also weakly present in some preserved individuals of *B. garbeanus* and *B. margaritatus* (exhibiting few scattered areas with dark pigmentation), whereas no dark pigmentation was observed in preserved individuals of *B. ephippium*, *Brachycephalus* sp. (aff. *ephippium*), and *B.* ***ibitinga*** sp. nov. We therefore identified this dark pigmentation as a variable condition of the preserved specimens and suggest further analysis using fresh material, such as was done for *B. darkside* (Guimarães et al. 2017).

The distribution range of the extremely hyperossified species of *Brachycephalus* generally overlaps protected areas (Bornschein et al. 2019a). An exception is *B. margaritatus*, a vulnerable species found outside formally protected areas in a severely fragmented landscape (Pombal and Izecksohn 2011; T. Condez personal observation). Fortunately, during the 1980s, the occurrence of the flea-toad *B. didactylus* in Sacra Família do Tinguá, municipality of Engenheiro Paulo de Frontin, state of Rio de Janeiro, which is also the type locality of *B. margaritatus*, motivated the creation of the Reserva Biológica do Tinguá, a large original forested area bordering the populous city of Rio de Janeiro (Carvalho-e-Silva and Carvalho-e-Silva 2013). Nowadays, the conservation of both species is likely assured by such area protection. All the distribution records of *Brachycephalus* ***ibitinga*** sp. nov. are located inside legally protected areas under Category II of the International Union for Conservation of Nature (Dudley 2008). However, despite being not apparently threatened, the new species distribution limit is bounded by the metropolitan region of São Paulo, which is exposed to intensive pressures resulting from deforestation, pollution, and general changes in land use. In the last 5 yr, these threats are devastating the Atlantic Forest remnants in the south of the municipality of São Paulo at alarming rates, highlighting the importance of the nearest protected areas (Natalini 2020). As one of the most effective tools for conserving species and natural habitats, the protected areas that encompass the Atlantic Forest remnants near the metropolitan region of São Paulo support a huge diversity of amphibians (Malagoli 2008; Lourenço-de-Moraes et al. 2018), including some recently discovered species (e.g., Malagoli et al. 2017; this study), and a new recently described reproductive mode for frogs (Malagoli et al. 2021).

Acknowledgments.—We are indebted to E.C. Nardin, M.T.T. Santos, D. Baêta, B. Rocha, and B.V.M. Berneck for the valuable help during fieldwork. We also thank M. Alonso, T. Schimidt, V.S. Nascimento, and M.J. Gonçalves for logistical support at Parque Estadual da Serra do Mar, Núcleo Curucutu, and surrounding areas. For providing the collecting permits we thank Ministério do Meio Ambiente (MMA/ICMBio/IBAMA; 019/07, 16350-1, 23501-1, 45665-1, 45665-2, 45665-3, 49587-4), Comissão Técnico-Científica do Instituto Florestal (COTEC/IF; 40.452/2004, 40.574/2006, 260108-011.074/2010, 260108-003.523/2014), Instituto Ecofuturo, Suzano Papel e Celulose S/A, and Prefeitura Municipal de Santo André. We thank the Centro de Estudos de Insetos Sociais (CEIS/UNESP/Rio Claro) for providing molecular laboratory facilities. We also thank the Centro para Documentação da Biodiversidade at Universidade de São Paulo, Faculdade de Filosofia, Ciências e Letras de Ribeirão Preto (CDB/FFCLRP) for the micro CT scan imaging. We are also grateful to H. Zaher, J.P. Pombal, Jr., R.N. Feio, and C.S. Guimarães for providing access to specimens and tissues under their care and to reviewers for the valuable suggestions on the earliest versions of this manuscript. The authors thank the São Paulo Research Foundation (FAPESP 2013/50741–7, 2014/23677-9, 2014/50342-8, 2015/00461-1, 2017/26281-7, 2018/09691-0), Conselho Nacional de Desenvolvimento Científico e Tecnológico (CNPq 141716/2010-0, 141259/2014-0, 372165/2017-6, 371993/2018-0, 302308/2019-9, 301381/2020-8), Higher Education Improvement Coordination (CAPES 131947/2015-0) and Fundação Grupo Boticário de Proteção à Natureza for the financial support. CFBH and PCAG also thank CNPq for their productivity fellowship.

SUPPLEMENTAL MATERIAL

Supplemental material associated with this article can be found online at https://doi.org/10.1655/Herpetologica-D-20-00031.F1 and https://doi.org/10.1655/Herpetologica-D-20-00031.T1

LITERATURE CITED

Alves, A.C.R., L.F. Ribeiro, C.F.B. Haddad, and S.F. Reis. 2006. Two new species of *Brachycephalus* (Anura: Brachycephalidae) from the Atlantic

Forest in Paraná state, southern Brazil. Herpetologica 62:221–233. DOI: https://doi.org/10.1655/05-41.1

Alves, A.C.R., R.J.S. Sawaya, S.F. Reis, and C.F.B. Haddad. 2009. New species of *Brachycephalus* (Anura: Brachycephalidae) from the Atlantic Rain Forest in São Paulo State, Southeastern Brazil. Journal of Herpetology 43:212–219. DOI: https://doi.org/10.1670/0022-1511-43.2.212

Arcanjo, D.D.R., A.G. Vasconcelos, S.G. Comerma-Steffensen, ..., J.R. Leite. 2015. A novel vasoactive proline-rich oligopeptide from the skin secretion of the frog *Brachycephalus ephippium*. PLoS One 10 e0145071. DOI: https://doi.org/10.1371/journal.pone.0145071

Audacity Team. 2017. Audacity®: Free Audio Editor and Recorder, Version 2.2.1. Available at https://www.audacityteam.org/. Carnegie Mellon University, USA.

Bioacoustics Research Program. 2014. Raven Pro: Interactive Sound Analysis Software, Version 1.5. Available at https://ravensoundsoftware.com/. The Cornell Lab of Ornithology, USA.

Blotto, B.L., M.L. Lyra, M.C.S. Cardoso, ..., J. Faivovich. 2020. The phylogeny of the Casque-headed Treefrogs (Hylidae: Hylinae: Lophyohylini). Cladistics 37:36–72. DOI: https://doi.org/10.1111/cla.12409

Bokermann, W.C.A. 1966. Lista Anotada das Localidades Tipo de Anfíbios Brasileiros. RUSP, Brazil.

Bornschein, M.R., L.F. Ribeiro, D.C. Blackburn, E.L. Stanley, and M.R. Pie. 2016. A new species of *Brachycephalus* (Anura: Brachycephalidae) from Santa Catarina, southern Brazil. PeerJ 4:e2629. DOI: https://doi.org/10.7717/peerj.2629

Bornschein, M.R., L.F. Ribeiro, M.M. Rollo, A.E. Confetti, and M.R. Pie. 2018. Advertisement call of *Brachycephalus albolineatus* (Anura: Brachycephalidae). PeerJ 6:e5273. DOI: https://doi.org/10.7717/peerj.5273

Bornschein, M.R., M.R. Pie, and L. Teixeira. 2019a. Conservation status of *Brachycephalus* toadlets (Anura: Brachycephalidae) from the Brazilian Atlantic Rainforest. Diversity 11:1–29. DOI: https://doi.org/10.3390/d11090150

Bornschein, M.R., M.M. Rollo, M.R. Pie, A.E. Confetti, and L.F. Ribeiro. 2019b. Redescription of the advertisement call of *Brachycephalus tridactylus* (Anura: Brachycephalidae). Phyllomedusa 18:3–12. DOI: https://doi.org/10.11606/issn.2316-9079.v18i1p3-12

Campos, L.A., H.R. Silva, and A. Sebben. 2010. Morphology and development of additional bony elements in genus *Brachycephalus* (Anura: Brachycephalidae). Biological Journal of the Linnean Society 99:752–767. DOI: https://doi.org/10.1111/j.1095-8312.2010.01375.x

Carvalho-e-Silva, A.M.P.T., and S.P. Carvalho-e-Silva. 2013. Obituários: Eugênio Izecksohn (14/05/1932–03/06/2013). Herpetologia Brasileira 2:66–70.

Cei, J.M. 1980. Amphibians of Argentina. Monitore Zoologico Italiano. Nuova Serie, Monographs 2. Universita degli studi di Firenze, Italia.

Clemente-Carvalho, R.B.G., M.M. Antoniazzi, C. Jared, C.F.B. Haddad, A.C.R. Alves, H.S. Rocha, G.R. Pereira, D.F. Oliveira, R.T. Lopes, and S.F. Reis. 2009. Hyperossification in miniaturized toadlets of the genus *Brachycephalus* (Amphibia: Anura: Brachycephalidae): Microscopic structure and macroscopic patterns of variation. Journal of Morphology 270:1285–1295. DOI: https://doi.org/10.1002/jmor.10755

Clemente-Carvalho, R.G.B., J. Klaczo, I. Perez, A.C.R. Alves, C.F.B. Haddad, and S.F. Reis. 2011a. Molecular phylogenetic relationships and phenotypic diversity in miniaturized toadlets genus *Brachycephalus* (Amphibia: Anura: Brachycephalidae). Molecular Phylogenetics and Evolution 61:79–89. DOI: https://doi.org/10.1016/j.ympev. 2011.05.017

Clemente-Carvalho, R.G.B., A.C.R. Alves, S.I. Perez, and C.F.B. Haddad. 2011b. Morphological and molecular variation in the pumpkin toadlet, *Brachycephalus ephippium* (Anura: Brachycephalidae). Journal of Herpetology 45:94–99. DOI: https://doi.org /10.1670/09-164.1

Clemente-Carvalho, R.B.G., A.A. Giaretta, T.H. Condez, C.F.B. Haddad, and Reis, S.F. 2012. A new species of miniaturized toadlet, genus *Brachycephalus* (Anura: Brachycephalidae), from the Atlantic Forest of southeastern Brazil. Herpetologica 68:365–374. DOI: https://doi.org/10.1655/HERPETOLOGICA-D-11-00085.1

Condez, T.H., R.B.G. Clemente-Carvalho, C.F.B. Haddad, and S.F. Reis. 2014. A new species of *Brachycephalus* (Anura: Brachycephalidae) from the highlands of the Atlantic Forest, southeastern Brazil. Herpetologica 70:89–99. DOI: https://doi.org/10.1655/HERPETOLOGICA-D-13-00044

Condez, T.H., J.P.C. Monteiro, E.J. Comitti, P.C.A. Garcia, I.B. Amaral, and C.F.B. Haddad. 2016. A new species of flea-toad (Anura: Brachycephalidae) from southern Atlantic Forest, Brazil. Zootaxa 4083:40–56. DOI: https://doi.org/10.11646/zootaxa.4083.1.2

Condez, T.H., C.F.B. Haddad, and K.R. Zamudio. 2020. Historical biogeography and multi-trait evolution in miniature toadlets of the genus *Brachycephalus* (Anura: Brachycephalidae). Biological Journal of the Linnean Society 129:664–686. DOI: https://doi.org/10.1093/biolinnean/blz200

Darst, C.R., and D.C. Cannatella. 2004. Novel relationships among hyloid frogs inferred from 12S and 16S mitochondrial DNA sequences. Molecular Phylogenetics and Evolution 31:462–475. https://doi.org/10.1016/j.ympev.2003.09.003

Dudley, N. 2008. Guidelines for applying protected area management categories. International Union for the Conservation of Nature (IUCN), Switzerland.

Duellman, W.E. 1970. Hylid frogs of Middle America. Monograph of the Museum of Natural History. The University of Kansas, USA.

Duellman, W.E., and L. Trueb. 1986. Biology of Amphibians. McGraw-Hill, USA.

Fabrezi, M. 1992. El carpo de los anuros. Alytes 10:1–36.

Fabrezi, M. 1993. The anuran tarsus. Alytes 11:47–63.

Fabrezi, M. 2001. A survey of prepollex and prehallux variation in anuran limbs. Zoological Journal of the Linnean Society 131:227–248. DOI: https://doi.org/10.1111/j.1096-3642.2001.tb01316.x

Farris, J.S., V.A. Albert, M. Källersjö, D. Lipscomb, and A.G. Kluge. 1996. Parsimony jackknifing outperforms neighbor joining. Cladistics 12:99–124. DOI: https://doi.org/10.1006/clad.1996.0008

Fedorov, A., R. Beichel, J. Kalpathy-Cramer, ..., R. Kikinis. 2012. 3D slicer as an image computing platform for the quantitative imaging network. Magnetic Resonance Imaging 30:1323–1341. DOI: https://doi.org/10.1016/j.mri.2012.05.001

Fitzinger, L.J. 1826. Neue Classification der Reptilien nach ihren Natürlichen Verwandtschaften nebst einer Verwandtschafts-Tafel und einem Verzeichnisse der Reptilien-Sammlung des K.K. Zoologisch Museums zu Wien. K.K. Hof-Naturalien-Cabinet, Austria.

Folly, M., L.C. Amaral, S.P. Carvalho-e-Silva, and J.P. Pombal. 2020. Rediscovery of the toadlet *Brachycephalus bufonoides* Miranda-Ribeiro, 1920 (Anura: Brachycephalidae) with osteological and acoustic descriptions. Zootaxa 4819:265–294. DOI: https://doi.org/10.11646/zootaxa.4819.2.3

Frost, D.R. 2020. Amphibian Species of the World: An Online Reference, Version 6.0. Available at http://research.amnh.org/herpetology/amphibia/index.html. American Museum of Natural History, USA. Archived by WebCite at http://www.webcitation.org/6qp8hUYGQ on 29 May 2017.

Garey, M.V., A.M.X. Lima, M.T. Hartmann, and C.F.B. Haddad. 2012. A new species of miniaturized toadlet, genus *Brachycephalus* (Anura: Brachycephalidae), from southern Brazil. Herpetologica 68:266–271. DOI: https://doi.org/10.1655/HERPETOLOGICA-D-11-00074.1

Giaretta, A.A., and R.J. Sawaya. 1998. Second species of *Psyllophryne* (Anura: Brachycephalidae). Copeia 1998:985–987. DOI: https://doi.org 10.2307/1447345

Goloboff, P.A., and S.A. Catalano. 2016. TNT Version 1.5, including a full implementation of phylogenetic morphometrics. Cladistics 32:221–238. DOI: https://doi.org/10.1111/cla.12160

Goutte, S., M.J. Mason, M.M. Antoniazzi, ..., M. Thoury. 2019. Intense bone fluorescence reveals hidden patterns in pumpkin toadlets. Scientific Reports 9:5388. DOI: https://doi.org/10.1038/s41598-019-41959-8

Guimarães, C.S., S. Luz, P.C. Rocha, and R.N. Feio. 2017. The dark side of pumpkin toadlet: A new species of *Brachycephalus* (Anura: Brachycephalidae) from Serra do Brigadeiro, southeastern Brazil. Zootaxa 4258:327–344. DOI: https://doi.org/10.11646/zootaxa.4258.4.2

Haddad, C.F.B., A.C.R. Alves, R.B.G. Clemente-Carvalho, and S.F. Reis. 2010. A new species of *Brachycephalus* from the Atlantic Rain Forest in São Paulo state, southeastern Brazil (Amphibia: Anura: Brachycephalidae). Copeia 2010:410–420. DOI: https://doi.org/10.1643/CH-09-102

Hedges, S.B., W.E. Duellman, and M.P. Heinicke. 2008. New World direct-developing frogs (Anura: Terrarana): Molecular phylogeny, classification, biogeography, and conservation. Zootaxa 1737:1–182. DOI: https://doi.org/10.11646/zootaxa.1737.1.1

Heinicke, M.P., A.R. Lemmon, E.M. Lemmon, K. McGrath, and S.B. Hedges. 2018. Phylogenomic support for evolutionary relationships of New World direct-developing frogs (Anura: Terraranae). Molecular Phylogenetics and Evolution 118:145–155. DOI: https://doi.org/10.1016/j.ympev.2017.09.021

Heyer, W.R., A.S. Rand, C.A.G. Cruz, O.L. Peixoto, and C.E. Nelson. 1990.

Frogs of Boracéia. Arquivos de Zoologia 31:231–410. DOI: https://doi.org/10.11606/issn.2176-7793.v31i4p231-410

IBGE (Instituto Brasileiro de Geografia e Estatistica). 2018. Instituto Brasileiro de Geografia e Estatística: Estimativas da população residente para os municípios e para as unidades da federação com data de referência em 1° de julho de 2018. Ministério do Planejamento, Desenvolvimento e Gestão. Distrito Federal, Brasil.

Izecksohn, E. 1971. Novo gênero e nova espécie de Brachycephalidae do estado do Rio de Janeiro, Brasil. Boletim do Museu Nacional, Zoologia 280:1–12.

Kaplan, M. 2002. Histology of the anteroventral part of the breast-shoulder apparatus of *Brachycephalus ephippium* (Brachycephalidae) with comments on the validity of the genus *Psyllophryne* (Brachycephalidae). Amphibia-Reptilia 23:225–227. DOI: https://doi.org/10.1163/156853802760061840

Katoh, K., and H. Toh. 2008. Improved accuracy of multiple ncRNA alignment by incorporating structural information into a MAFFT-based framework. BMC Bioinformatics 9:212. DOI: https://doi.org/10.1186/1471-2105-9-212

Katoh, K., and D.M. Standley. 2013. MAFFT multiple sequence alignment software version 7: Improvements in performance and usability. Molecular Biology and Evolution 30:772–780. DOI: https://doi.org/10.1093/molbev/mst010

Köhler, J., M. Jansen, A. Rodríguez, P.J.R. Kok, L.F. Toledo, M. Emmrich, F. Glaw, C.F.B. Haddad, M.O. Rödel, and M. Vences. 2017. The use of bioacoustics in anuran taxonomy: Theory, terminology, methods and recommendations for best practice. Zootaxa 4251:001–124. DOI: http://dx.doi.org/10.11646/zootaxa.4251.1.1

Kumar, S., G. Stecher, M. Li, C. Knyaz and K. Tamura. 2018. MEGA X: Molecular Evolutionary Genetics Analysis across computing platforms. Molecular Biology and Evolution 35:1547–1549. DOI: https://doi.org/10.1093/molbev/msy096

Lanfear, R., P.B. Frandsen, A.M. Wright, T. Senfeld, and B. Calcott. 2017. Partitionfinder 2: New methods for selecting partitioned models of evolution for molecular and morphological phylogenetic analyses. Molecular Biology and Evolution 34:772–773. DOI: https://doi.org/10.1093/molbev/msw260

Lourenço-de-Moraes, R., L.R. Malagoli, V.B. Guerra, R.B. Ferreira, I.P. Affonso, C.F.B. Haddad, R.J. Sawaya, and R.P Bastos. 2018. Nesting patterns between Neotropical species assemblages: Can reserves in urban areas be failing to protect anurans? Urban Ecosystems 21:933–942. DOI: https://doi.org/10.1007/s11252-018-0767-5

Malagoli, L.R. 2008. Anfíbios do município de São Paulo: Histórico, conhecimento atual e desafios para a conservação. Pp. 204–233 in Além do concreto: Contribuições para a proteção da biodiversidade paulistana (L.R. Malagoli, F.B. Bajesteiro and M. Whately, orgs.). Instituto Socioambiental, Brazil.

Malagoli, L.R., F.P. de Sá, C. Canedo, and C.F.B. Haddad. 2017. A new species of *Hylodes* (Anura, Hylodidae) from Serra do Mar, Southeastern Brazil: The fourth with nuptial thumb tubercles. Herpetologica 73:136–147. DOI: https://doi.org/10.1655/HERPETOLOGICA-D-16-00069

Malagoli, L.R., T.L. Pezzuti, D.L. Bang, J. Faivovich, M.L. Lyra, J.G.R. Giovanelli, P.C.A. Garcia, R.J. Sawaya, and C.F.B. Haddad. 2021. A new reproductive mode in anurans: Natural history of *Bokermannohyla astartea* (Anura: Hylidae) with the description of its tadpole and vocal repertoire. PLoS One 16:e0246401. DOI: https://doi.org/10.1371/journal.pone.0246401

Miller, M.A., W. Pfeiffer, and T. Schwartz. 2010. Creating the CIPRES Science Gateway for Inference of Large Phylogenetic Trees. Proceedings of the Gateway Computing Environments Workshop 2010:1–8. DOI: https://doi.org/10.1109/GCE.2010.5676129

Miranda-Ribeiro, A. 1920. Os brachycephalídeos do Museu Paulista (com três espécies novas). Revista do Museu Paulista 12:307–315.

Monteiro, J.P.C., T.H. Condez, P.C.A. Garcia, E.J. Comitti, I.B. Amaral, and C.F.B. Haddad. 2018a. A new species of *Brachycephalus* (Anura, Brachycephalidae) from the coast of Santa Catarina State, southern Atlantic Forest, Brazil. Zootaxa 4407:483–505. DOI: https://doi.org/10.11646/zootaxa.4407.4.2

Monteiro, J.P.C., T.H. Condez, P.C.A. Garcia, and C.F.B. Haddad. 2018b. The advertisement calls of two species of *Brachycephalus* (Anura: Brachycephalidae) from southern Atlantic Forest, Brazil. Zootaxa 4415:183–188. DOI: https://doi.org/10.11646/zootaxa.4415.1.10

Napoli, M.F., U. Caramaschi, C.A.G. Cruz, and I.R. Dias. 2011. A new species of flea-toad, genus *Brachycephalus* Fitzinger (Amphibia: Anura: Brachycephalidae), from the Atlantic rainforest of southern Bahia, Brazil. Zootaxa 2739:33–40. DOI: https://doi.org/10.11646/zootaxa.2739.1.3

Natalini, G. 2020. Dossiê: A devastação da Mata Atlântica no município de São Paulo. Segunda Edição. Câmara Municipal de São Paulo, Brasil.

Oliveira, E.G., and C.F.B. Haddad. 2017. Activity, acoustic repertoire and social interactions of the Red Toadlet, *Brachycephalus pitanga* (Anura: Brachycephalidae). Salamandra 53:501–506.

Padial, J.M., T. Grant, and D.R. Frost. 2014. Molecular systematics of terraranas (Anura: Brachycephaloidea) with an assessment of the effects of alignment and optimality criteria. Zootaxa 3825:1–132. DOI: https://doi.org/10.11646/zootaxa.3825.1.1

Paluh, D.J., E.L. Stanley, and D.C. Blackburn. 2020. Evolution of hyperossification expands skull diversity in frogs. Proceedings of the National Academy of Sciences of the United States of America 117:8554–8562. DOI: https://doi.org/10.1073/pnas.2000872117

Palumbi, S., A. Martin, S. Romano, W.O. McMillan, L. Stice, and G. Grabowski. 1991. The simple fool's guide to PCR. Version 2. Privately published, Honolulu, Hawaii.

Pie, M.R., and L.F. Ribeiro. 2015. A new species of *Brachycephalus* (Anura: Brachycephalidae) from the Quiriri mountain range of southern Brazil. PeerJ 3:e1179. DOI: https://doi.org/10.7717/peerj.1179

Pie, M.R., A.L.S. Meyer, C.R. Firkowski, L.F. Ribeiro, and M.R. Bornschein. 2013. Understanding the mechanisms underlying the distribution of microendemic montane frogs (*Brachycephalus* spp., Terrarana: Brachycephalidae) in the Brazilian Atlantic Rainforest. Ecological Modelling 250:165–176. DOI: https://doi.org/10.1016/j.ecolmodel.2012.10.019

Pie, M.R., L.F. Ribeiro, A.E. Confetti, M.J. Nadaline, and M.R. Bornschein. 2018. A new species of *Brachycephalus* (Anura: Brachycephalidae) from southern Brazil. PeerJ 6:e5683. DOI: https://doi.org/10.7717/peerj.5683

Pires, O.R., A. Sebben, E.F. Schwartz, R.A.V. Morales, C. Bloch, and C.A. Schwartz. 2005. Further report of the occurrence of tetrodotoxin and new analogues in the anuran family Brachycephalidae. Toxicon 45:73–79. DOI: https://doi.org/10.1016/j.toxicon.2004.09.016

Pombal, J.P. 2001. A new species of *Brachycephalus* (Anura: Brachycephalidae) from Atlantic Rain Forest of Southeastern Brazil. Amphibia-Reptilia 22:179–185. DOI: https://doi.org/10.1163/156853801752030409

Pombal, J.P. 2010. A posição taxonômica das "variedades" de *Brachycephalus ephippium* (Spix, 1824) descritas por Miranda-Ribeiro, 1920 (Amphibia, Anura, Brachycephalidae). Boletim do Museu Nacional, Zoologia 526:1–12.

Pombal, J.P., and J.L. Gasparini. 2006. A new *Brachycephalus* (Anura: Brachycephalidae) from the Atlantic Rainforest of Espírito Santo, southeastern Brazil. South American Journal of Herpetology 1:87–93. DOI: https://doi.org/10.2994/1808-9798

Pombal, J.P., and E. Izecksohn. 2011. Uma nova espécie de *Brachycephalus* (Anura: Brachycephalidae) do estado do Rio de Janeiro. Papéis Avulsos de Zoologia 51:443–451. DOI: https://doi.org/10.1590/S0031-10492011002800001

Pombal, J.P., I. Sazima, and C.F.B. Haddad. 1994. Breeding behavior of the pumpkin toadlet, *Brachycephalus ephippium* (Brachycephalidae). Journal of Herpetology 28:516–519. DOI: https://doi.org/10.2307/1564972

Pombal, J.P., E.M. Wistuba, and M.R. Bornschein. 1998. A new species of Brachycephalid (Anura) from the Atlantic rain forest of Brazil. Journal of Herpetology 32:70–74. DOI: https://doi.org/10.2307/1565481

Pugener, L.A., and A.M. Maglia.1997. Osteology and skeletal development of *Discoglossus sardus* (Anura: Discoglossidae). Journal of Morphology 233:267–286. DOI: https://doi.org/10.1002/(SICI)1097-4687(199709)233:3<267::AID-JMOR6>3.0.CO;2-0

QGIS Development Team. 2020. QGIS Geographic Information System, Version 3.12. Available at https://www.qgis.org. Accessed on 12 December 2020. Open Source Geospatial Foundation, USA.

R Core Team. 2020. R: A Language and Environment for Statistical Computing, Version 4.0.1. Available at https://www.r-project.org/. R Foundation for Statistical Computing, Austria.

Rambaut, A. 2016. FigTree, Version1.4.3: Tree Figure Drawing Tool. Available at https://tree.bio.ed.ac.uk/software/figtree/. University of Edinburgh, UK.

Rambaut, A., M.A. Suchard, D. Xie, and A.J. Drummond. 2014. Tracer v1.6. University of Edinburgh, UK.

Rebouças, R., A.B. Carollo, M.O. Freitas, C. Lambertini, R.M.N. Santos, and L.F. Toledo. 2019. Is the conspicuous dorsal coloration of the Atlantic forest pumpkin toadlets aposematic? Salamandra 55:39–47.

Ribeiro, L.F., A.C.R. Alves, C.F.B. Haddad, and S.F. Reis. 2005. Two new species of Brachycephalus Günther, 1985 from the state of Paraná,

southern Brazil (Amphibia, Anura, Brachycephalidae). Boletim do Museu Nacional (Zoologia) 519:1–18.
Ribeiro, L.F., M.R. Bornschein, R. Belmonte-Lopes, C.R. Firkowski, S.A.A. Morato, and M.R. Pie. 2015. Seven new microendemic species of Brachycephalus (Anura: Brachycephalidae) from southern Brazil. PeerJ 3:e1011. DOI: https://doi.org/10.7717/peerj.1011
Ribeiro, L.F., D.C. Blackburn, E.L. Stanley, M.R. Pie, and M.R. Bornschein. 2017. Two new species of the Brachycephalus pernix group (Anura: Brachycephalidae) from the state of Paraná, southern Brazil. PeerJ 5:e3603. DOI: https://doi.org/10.7717/peerj.3603
Robovská-Havelková, P. 2010. How can ontogeny help us to understand the morphology of anuran pectoral girdle? Zoomorphology 129:121–132. DOI: https://doi.org/10.1007/s00435-010-0105-9
Ronquist, F., M. Teslenko, P. Van Der Mark, D.L. Ayres, A. Darling, S. Höhna, B. Larget, L. Liu, M.A Suchard, and J.P. Huelsenbeck. 2012. Mrbayes 3.2: Efficient Bayesian phylogenetic inference and model choice across a large model space. Systematic Biology 61:539–542. DOI: https://doi.org/10.1093/sysbio/sys029
Sabaj, M.H. 2016. Standard Symbolic Codes for Institutional Resource Collections in Herpetology and Ichthyology: An Online Reference, Version 6.5. Available at https://www.asih.org/. American Society of Ichthyologists and Herpetologists, USA. Archived by WebCite at https://www.webcitation.org/6qpZPWPt3 on 29 May 2017.
Spix, J.B. 1824. Animalia nova sive species novae testudinum et ranarum, quas in itinere per Brasiliam annis MDCCCXVII-MDCCCXX jussu et auspiciis Maximiliani Josephi I Bavariae Regis suscepto collegit et descripsit. Monachii, Typis Francisci Seraphi Hybschmanni 22:1–29.
Stecher, G., K. Tamura, and S. Kumar. 2020. Molecular Evolutionary Genetics Analysis (MEGA) for macOS. Molecular Biology and Evolution 37:1237–1239. DOI: https://doi.org/10.1093/molbev/msz312
Sueur, J., T. Aubin, and C. Simonis. 2008. Seewave, a free modular tool for sound analysis and synthesis. Bioacoustics The International Journal of Animal Sound and Its Recording 18:213–226. DOI: https://doi.org/10.1080/09524622.2008.9753600
Taylor, W.R., and G.C. Van Dyke. 1985. Revised procedures for staining and clearing small fishes and other vertebrates for bone and cartilage study. Cybium 9:107–119.
Toledo, L.F., I.A. Martins, D.P. Bruschi, M.A. Passos, C. Alexandre, and C.F.B. Haddad. 2015. The anuran calling repertoire in the light of social context. Acta Ethologica 18:87–99. DOI: https://doi.org/10.1007/s10211-014-0194-4
Trevine, V., M.C. Forlani, C.F.B. Haddad, and H.E.D. Zaher. 2014. Herpetofauna of Paranapiacaba: Expanding our knowledge on a historical region in the Atlantic forest of southeastern Brazil. Zoologia 31:126–146. DOI: https://doi.org/10.1590/S1984-46702014000200004.
Trewavas, E. 1932. The hyoid and larynx of the Anura. Philosophical Transactions of the Royal Society of London Series B 222:483–493. DOI: https://doi.org/10.1098/rstb.1932.0020
Trueb, L. 1973. Bones, frogs, and evolution. Pp. 65–132 in Evolutionary Biology of the Anurans: Contemporary Research on Major Problems (J.L. Vial, ed.). University of Missouri Press, USA.
Trueb, L. 1993. Patterns of cranial diversity among the Lissamphibia. Pp. 255–343 in The Skull Volume 2 (J. Hanken and B.K. Hall, eds.). The University of Chicago Press, USA.
Trueb, L. 2015. Osteology. Pp. 31–51 in Marsupial Frog: Gastrotheca and Allied Genera (W.E. Duellman, ed.). Johns Hopkins University Press, USA.
Trueb, L., and P. Alberch. 1985. Miniaturization and the anuran skull: A case study of heterochrony. Pp. 113–121 in Functional Morphology of Vertebrates (H.R. Duncker and G. Fleischer, eds.). Gustav Fisher VerJag, Germany.
Vaidya, G., D.J. Lohman, and R. Meier. 2011. SequenceMatrix: Concatenation software for the fast assembly of multi-gene datasets with character set and codon information. Cladistics 27:171–180. DOI: https://doi.org/10.1111/j.1096-0031.2010.00329.x

Accepted on 3 March 2021
ZooBank.org registration LSID: A14DE043-26B2-4AD2-88CC-95EF2B6E4A6C
Published on 8 June 2021
Associate Editor: Julian Faivovich

Appendix I

Specimens Examined in Morphological Comparisons

Asterisks denote (*) cleared and double-stained and (**) micro CT specimens.

Brachycephalus ephippium.—State of Rio de Janeiro: municipality of Cachoeiras de Macacu, Reserva Ecológica do Guapiaçu (MNRJ 38104, 56517, 56518, 59946); municipality of Rio de Janeiro, Pedra Branca, Jacarepaguá (MNRJ 3327, 13818, 13819, 27577–25579); municipality of Rio de Janeiro, Represa Rio Grande (MZUSP 9031, 100277, 100281, 100283, 100285, 100286, 100342–100344, 100346, 100349, 100356); municipality of Teresópolis, Alto do Soberbo (MZUSP 49991, 49996, 50008, 50009, 50011, 50014, 50022, 50023, 50028, 50032, 50039, 50043, 50051, 50054, 50055), Parque Nacional da Serra dos Órgaos (CFBH 22013–22015, 24763, 24764, 32569, 32570; MZUSP 11205, 34646, 71707, 71708; MNRJ 17438, 17439, 17450, 51580–51583), Vale da Revolta (MNRJ 50260, 50261, 70580; UF 72725**).

Brachycephalus sp. (aff. *ephippium*).—State of São Paulo: municipality of Atibaia (MZUSP 104203, 104204; CFBH 16807–16811, 16813, 16815, 16817, 16818, 16820, 16821, 16824, 16826; Not Deposited Specimen AT025*); municipality of Campinas, Joaquim Egídio (CFBH 994, 996, 1343, 2565, 2566, 2568, 2569, 4259, 4260; MNRJ 25347–25352); municipality of Jundiaí, Serra do Japi (CFBH 9431, 16837, 16839, 16857, 16859, 16864, 16870, 30834, 30835, 30842; Not Deposited Specimen SJ004*); municipality of Mogi das Cruzes (CFBH 28658, 28659, 28663, 28664, 28667, 28668, 28670; MZUSP 104208–104210, 136758, 136762, 136764, 136787, 137319, 138775, 138776); municipality of São José dos Campos, São Francisco Xavier (CFBH 16827–34; MNRJ 70619, 70623–70625; MZUSP 2761, 2762; Not Deposited Specimen SFX013*); state of Rio de Janeiro: municipality of Resende (MNRJ 73096–73099, 78465).

Brachycephalus darkside.—State of Minas Gerais: municipalities of Ervália and Miradouro, Parque Estadual da Serra do Brigadeiro (MZUFV 16636 [holotype], MZUFV 2897, 6658–6660, 15557–15561, 15565–15571, 15716–15721, 16491, 16579, 16627, 16628, 16631, 16632, 16780; MNRJ 91327; UFMG 19522 [paratypes]).

Brachycephalus garbeanus.—State of Rio de Janeiro: municipality of Nova Friburgo (MZUSP 811 [lectotype], MZUSP 1460, 1461 [paralectotypes], MNRJ 17433, 27008, 27009), Alto Caledônia (MNRJ 39585, 39602, 67498), Baixo Caledônia (MNRJ 57124, 57293), Alto de Macaé (CFBH 16806*, 23564–23567, 23569–23571, 23574, 23576, 23577; MNRJ 17440, 17441, 25391, 25398, 39617), Serra Nevada (MNRJ 39342, 39343), Theodoro de Oliveira (MNRJ 51472, 51473).

Brachycephalus margaritatus.—State of Rio de Janeiro: municipality of Engenheiro Paulo de Frontin, Sacra Família do Tinguá (MNRJ 39312 [holotype], MNRJ 21675, 25373–25376, 25385, 25387–25389, 25401 [paratypes]); municipality of Paty do Alferes (MNRJ 76100, 76101); municipality of Petrópolis (MNRJ 60869, 60870, 60891, 62976–62984), Castelo Country Club (MNRJ 73700–73702), Castelo Monte Belo (MNRJ 70428, 70429), Quitandinha (MNRJ 75174).